AALBORG UNIVERSITY

DENMARK

Sub-sampling Receivers for Wireless Communications

Behjou, Nastaran

Publication date:
2008

Document Version
Peer reviewed version

[Link to publication from Aalborg University](#)

Citation for published version (APA):
Behjou, N. (2008). Sub-sampling Receivers for Wireless Communications. Aalborg: Department of Electronic Systems, Aalborg University.

Sub-sampling Receivers for Wireless Communications

Nastaran Behjou

Dissertation submitted to the Faculty of the Aalborg University
in partial fulfillment of the requirements for the degree of

DOCTOR OF PHILOSOPHY

in Electrical Engineering

Printed and bound in Aalborg, Denmark, by Uniprint.

This thesis was typeset with LATEX.

To my Alborz···
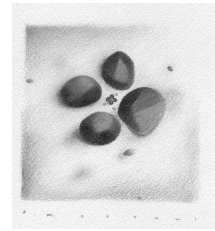
Preface

The dissertation is submitted to the Faculty of Technology and Science at Aalborg University, Denmark as a consequence of accomplishment of the requirements for the Doctor of Philosophy in Electrical Engineering degree (Ph.D. E.E.). The project was carried out in the department of Electronic Systems, within the Technology Platforms Section during the period October 2004 to 2007.

The rapid development of portable devices, and the increasing trend toward a single device integrating several features, encourage the companies and research centers to develop the multi-standard front-ends. This research is an effort to develop a multi-standard multi-mode receiver by employing RF sub-sampling receiver architecture. This PhD project is part of danish ministry of science, technology and innovation (VTU) supported project WANDA (Wireless Access Network Devices & Applications). The WANDA project is a joint research activity in a consortium consisting of Texas Instruments, Motorola (former Siemens and BenQ), RF Micro devices, BLIP Systems, Technological Institute, and Aalborg University.

The overall goal of the project was to develop techniques to efficient, robust, and flexible multi-band receiver architecture. The application area was the battery-powered mobile devices. The trend in modern wireless communication systems is to have several communication links integrated in a single user equipment [1]. For the portable battery-powered receivers, high level of integration, high flexibility, and low power dissipation are precedence objectives. Thus it is required to avoid expensive and power hungry parallel transceivers by employing more integrated and flexible devices in multi-band applications. To accomplish this, the system level investigation of the promising wireless RF receiver for multi-band application has been done. It is concluded that for the receiver part, the sampling receiver [2], [3] is a viable solution. This is one step toward the software defined radio vision with the majority of processing being done in the digital domain [4]. It provides the ability of processing several different signals in a single receiving chain. The verification of the theoretic studies is done through an experimental test set up. The key parts of the receiver such as sampler block and RF filters and amplifiers are implemented using off the shelf components. The soundness of the proposed ideas is acquired through experimental proof by considering the limitations of commercially developed components. This part of the work was done in a close cooperation with Motorola A/S, one of the project partners. At the company, the work was carried out in RF department especially in the RF labs. Including this preface and the publications at the end, the dissertation form a 180 pages extended summary of the work done in the period of this Ph.D. research. The organiza-

tion of the thesis, the list of the publications resulted from this work and a short description of each are presented in the following parts of the preface.

Organization of the Thesis

This dissertation is divided into 5 main Chapters. Each chapter contains an abstract, an extended summary and a brief discussion and conclusion at the end.

Chapter 1 provides an introduction to the whole work. The required background knowledge to create a common understanding ground for the dissertation is presented in this chapter. The scopes of the thesis are set by providing an overview to the wireless multi-band systems for mobile communications and the challenges in the field. The state of the art RF receivers for multi-band applications is presented in this chapter to fundament the selected RF sub-sampling architecture for the further investigation. A comparison of the architectures are made with respect to their multi-band capabilities. A description of the signals used for the current research, the methodology and the simulation environment is explained.

Chapter 2 describes in detail the proposed receiver architecture of the thesis — RF sub-sampling receiver. The basic principles of the architecture are presented. Thermal noise and jitter are considered as the important noise sources of the proposed architecture. Thus, to model the receiver precisely, they are involved. Moreover, an overview of the RF requirements for this receiver architecture is presented. The receiver must be able to maintain the adequate performance by preserving the bit error rate (BER) below a certain value even in the existence of noise and undesired signals from different sources.

Chapter 3 includes the frequency planning of the receiver and the required knowledge to select the best possible sampling frequency. First an exposition of the sampling frequency and its important role in RF sub-sampling receiver is given. It follows by the different methodologies for calculation of sampling frequency in terms of the Nyquist criteria, image noise and improving the signal to noise ratio based on pursuing the environment. Summing up all the techniques, a complete flow is achieved to calculate the most optimum sampling frequency for the receiver. The proposed concepts are supported by simulations and measurements on the specific sub-sampling receiver defined in the thesis.

Chapter 4 concerns RF requirements of the receiver to ensure the proper functionality of the RF Sub-sampling architecture in the multi-band applications. The RF requirements of a multi-standard receiver in the presence of the noise and nonlinear distortions are investigated in this chapter. The necessary design constrains are also derived. The sensitivity, linearity and selectivity issues are investigated for the multi-band applications. The derived constrains for selectivity and linearity are not dependent on any specific receiver architecture and are applicable for all types of receivers. The special selectivity requirements in accordance with the RF sub-sampling receivers are derived consequently. That is due to the indispensable role of filtering in sampling techniques to prevent the folding of noise along with desired signal to the band of interest. A technique on how to calculate the needed front-end selectivity to obtain a specified SNR at the output of the sampler is presented. This procedure combines

blocking tests of the relevant communication standard with the special image properties of the sub-sampling receiver. Moreover, the filter specifications based on out-of-band blocking requirements is discussed. The correct filtering in sampling based architecture improves the final performance of the receiver significantly. The derived specifications are verified by simulations and measurements on the specific sub-sampling receiver.

Chapter 5 is dedicated to the design issues of an RF sub-sampling architecture for target signals. The novel idea of selecting this architecture for multi-band application provides more flexibility and integration level by realizing most of the receiver functionality in digital domain. In the defined scenario of this study, the RF front-end is operating for the WLAN and UMTS signals at the same time with a single user equipment (UE) by employing RF sub-sampling architecture. The example for using these standards are when the user is downloading or transferring the information from the net while talking with the UMTS mobile phone simultaneously. The best sampling frequency is found by employing the method introduced in chapter 3. Moreover, the technique of chapter 4 is employed to define the RF requirements of the receiver. The simulation environment and methodology of receiver modeling are explained. The proposed concepts are supported by simulations of the target sub-sampling receiver.

Several experiments is presented in Chapter 6 to verify the theoretical and simulation results presented in subsequent chapters. An experimental sub-sampling receiver with the commercially available components is developed. The proposed concepts of the thesis are supported by measurements on the sub-sampling receiver.

Publications

Several publications has been resulted from the work done in this Ph.D which are listed below:

1. N. Behjou, B. E. Priyanto, O. K. Jensen and, T. Larsen, "Interference Issues between UMTS & WLAN in a Multi-Standard RF Receiver," *IST Mobile Wireless Comms Summit*, Mykonos, Greece, June. 2006.

2. N. Behjou, B. E. Priyanto, O. K. Jensen and, T. Larsen, "RF Sub-system Design for a Multi-standard Digital-IF Receiver," *Symposium on Wireless Personal Multimedia Communications (WPMC)* , Sept. 2006, Hyatt Regency, La Jolla, California.

3. N. Behjou, T. Larsen and O. K. Jensen,"RF Sub-sampling Receiver Architecture based on Milieu Adapting Techniques," *Submitted to the IEEE Signal Processing letters.*

4. M. R. Awan, M. M. Alam, P. Koch and N. Behjou,"Design and Implementation of an FPGA-based Multi-Standard Software Radio Receiver," *25th Norchip Conference*, November 2007, Aalborg, Danmark. Forskning: Konferenceartikel, peer reviewed

5. N. Behjou, T. Larsen and Morten Hoegdal, "Design of a Simultaneous Multi-Band RF Sub-Sampling Receiver," *IEEE MTT-S International Microwave Symposium*, June. 2008, Atlanta, US.

6. M. R. Awan, M. M. Alam, P. Koch and N. Behjou, "Area Efficient Implementation of Polyphase Channelizer for Multi-Standard Software Radio Receiver," *WSR08 conferance - 5th Karlsruhe Workshop on Software Radios*, Mar. 2008, Karlsruhe, Germany.

7. N. Behjou and T. Larsen ,"Design and Implementation of a Concurrent Multi-Band RF Sub-Sampling Receiver," *Submitted to the transactions on microwave theory and techniques.*

8. N. Behjou and T. Larsen ,"Image Distortion in Sub-Sampling Receivers," *Under internal review process.*

Résumé of Publications

In the following part, a brief summary of the papers including the motivation, the addressed problems and the major results is presented.

1. **Interference Issues between UMTS & WLAN in a Multi-Standard RF Receiver**

   This paper investigates one of the issues in multi-band receiver design which is the signal interference between UMTS and WLAN. There is an increasing demand for single user equipment (UE) supporting multi standards in third generation communication systems and beyond. Nevertheless, integrating several standards in one UE increases the front-end design complexity due to the coexistence of several systems. This paper investigates one of these issues which is the signal interference between UMTS and WLAN applications. By considering the system issues, multi-standard operation and interfering effects in a multi-standard transceiver supporting UMTS and WLAN, the receiver requirements have been derived based on the existing 3GPP specifications. The derived constrains are generally valid for all types of receiver architectures. Therefore, they are applicable for selection of components such as LNAs and filters in a multi-standard receiver front-end regardless of the chosen architecture.

2. **RF Sub-system Design for a Multi-standard Digital-IF Receiver**

   This paper presents the requirements for a multi-band RF transceiver. The RF receiver sub-system design is done according to the derived requirements. The introduction of multi-standard compatible user equipment (UE) elaborates some complication in the existing transceiver design platforms due to concurrent coexistence of several standards. The transceiver RF requirements must be calculated according to multi-standard operation, especially the interference issues. It is important to note that in a multi-frequency application, each received signal may appear as interference for other signals. Thus, to comply with the existing requirements for each standard the interfering power of other signals in the desired receive-band should be controlled. Consequently, the RF receiver sub-system

design requires modifications according to the stringent requirements. The RF budget-analysis for the sub-system blocks and ADC requirements for a multi-standard digital-IF receiver are presented with respect to the overall receiver requirements. The obtained results shows that the implementation of the proposed architecture is more feasible and realistic.

3. **RF Sub-sampling Receiver Architecture based on Milieu Adapting Techniques**

A new sub-sampling based architecture is proposed in this letter. The main intention of introducing this architecture is to reduce the problem of image distortion in sub-sampling receivers. Consequently, the signal to noise ratio may improve significantly. The technique is based on sensing the environment and adapting the sampling rate of the receiver to the best possible selection. The enabling components of such an architecture are a programmable clock generator, and tunable image rejection and IF filters. The proposed technique is applied to an RF sub-sampling receiver and has revealed great improvements in the signal to noise level (SNR) of the receiver. Measurements on an experimental sub-sampling receiver show that the presented method provides 85.9 dB improvements in the SNR of the receiver when comparing SNR for best and worst choice of the sampling rate (including the milieu adapting technique and excluding this method).

4. **Design and Implementation of an FPGA-based Multi-Standard Software Radio Receiver**

The aim of this work is to design and implement an FPGA-based Multi-Standard Software Radio Receiver. WLAN and UMTS are taken as the case study. Xilinx FPGA Virtex- IV is the target platform. Bandpass sampling technique at 840MHz is used to alias the combined band of WLAN and UMTS. In the channelization process, in contrast to conventional channelizer, polyphase channelizer is employed. The designed prototype filter for WLAN has 50 taps, partitioned into 5 polyphase sub-filters whereas for the UMTS the prototype filter has 2520 taps, partitioned into 210 polyphase sub-filters. In the implementation, serial polyphase structure with parallel MAC is selected. An implementation analysis based on the area requirements for multipliers, adders and registers for different structures is performed. For 16-tap filter, the structures for Parallel-Multiply and Accumulate, DA, Fast FIR, and Frequency domain filtering require 2896 (without adders), 3072, 4064, and 5572 slices, respectively. The DA is found to be suitable for the implementation due to being resource efficient. Polyphase sub filter is implemented with Distributed Arithmetic structure and also with Xilinx-DSP48 slices for improved performance.

5. **Design of a Simultaneous Multi-Band RF Sub-Sampling Receiver**

This paper addresses the practical design issues of a multi-standard RF sub-sampling front-end. The system level design flow of a dual-standard sub-sampling receiver is provided with focus on two important design issues. The first critical design issue is the

careful selection of the sampling rate and consequently the frequency plan of the receiver. This is done in this paper based on a novel proposed interfering profile. The second issue relates to the RF requirements of the sub-sampling receiver. By considering the system issues, multi-standard operation and interfering effects in a RF sub-sampling receiver supporting UMTS and WLAN, the receiver requirements have been derived based on the existing specifications. The proposed issues are theoretically analyzed and simulated. Furthermore, measurements are made on a designed and implemented sub-sampling receiver. The experimental results agree fully with theory and simulations.

6. **Area Efficient Implementation of Polyphase Channelizer for Multi-Standard Software Radio Receiver**

Software Defined Radio architectures for multi-standard receiver i.e. UMTS and WLAN are proposed in this work. To extract the 12 and 3 channels of UMTS and WLAN respectively, we propose Polyphase techniques being used in the channelizer. This is a resource efficient way of implementing the multi-rate filters and further to extract the channels. The aim of this paper is to illustrate an area efficient implementation of the Polyphase channelizer, where the target chip is a Virtex IV FPGA from Xilinx. In the implementation, different structures for Polyphase channelizer are considered, such as standard structure, symmetric property based structure with shared adders and multipliers structure and serial Polyphase structure with serial and parallel Multiplier and Accumulator (MAC). The complexity analysis (in terms of hardware resources and operating frequency) of these structures is conducted. The Serial Polyphase structure with parallel MAC is selected since it requires fewer resources and also operates at the same rate, in which the input data is supplied. In the individual sub-filter implementation of the Polyphase channelizer, different implementation structures are considered. These being Parallel Multipliers and Accumulate, Distributed Arithmetic (DA), Fast FIR, Frequency domain filtering and Multiplier- Less filtering techniques. An analysis based on the approximations for the area requirements for multipliers, adders and registers for these structures is performed.

7. **Design and Implementation of a Concurrent Multi-Band RF Sub-Sampling Receiver**

This paper addresses the practical design of a multi-standard RF sub-sampling front-end. The system level design flow of a dual-standard sub-sampling receiver is provided with focus on two important design issues. The first critical design issue is selection of the sampling rate, and consequently the frequency plan of the receiver. This is done in this paper based on a novel proposed interfering profile. The second issue relates to the RF requirements of the sub-sampling receiver. By considering the system issues, multi-standard operation and interfering effects in an RF sub-sampling receiver supporting UMTS and WLAN, the receiver requirements have been derived based on the existing specifications. The proposed issues are theoretically analyzed and simulated. Furthermore, measurements are made on a designed and implemented sub-sampling receiver. The experimental

results agree fully with theory and simulations.

8. **Image Distortion in Sub-Sampling Receivers**

Sub-sampling techniques are attractive for flexible and reconfigurable receivers for wireless communications. One thing which is problematic with the sub-sampling receiver is that it besides the desired frequency band also down-converts numerous image bands image bands being frequency bands other than the desired but which at least partly gets down-converted to the desired intermediate frequency band. The present paper addresses two issues related to image problems in sub-sampling receivers. These issues provide a complete overview of the sampling frequency and selectivity requirements of the sub-sampling architecture to deal with the image distortion. The proposed concepts are supported by simulations and measurements on a sub-sampling receiver. Measurements show that taking the presented issues in the current paper into account can provide 70% improvements in the normalized cross-correlation of the signal.

Scientific Contributions

This thesis is based on investigation of sub-sampling technique as an attractive choice for flexible and reconfigurable receivers for wireless communications. The major contributions that are listed below:

- Methods are proposed for calculating the key parameters of the receiver such as sensitivity, linearity and selectivity for a multi-standard application supporting several desired bands. By considering the system issues, multi-standard operation and interfering effects in a multi-standard transceiver, the receiver RF requirements have been derived.

- New technique is presented on how to calculate the needed front-end selectivity to obtain a specified SNR at the output of the sampler. This procedure combines blocking tests of the relevant communication standard with the special image properties of the sub-sampling receiver. The proper filtering enhances the functionality of the sampling receiver extensively by preventing the folding of noise along with the desired signal.

- The new procedure for how to select the best sampling rates is addressed which is an extension to the well known methods of calculating the sampling frequency. It is based on two novel proposed techniques:

  1. The first technique is focused on making an interference profile from the impending frequency bands distance to the desired signal. It indicates which bands that are expected to be most likely to cause interference including desired and undesired signals of the scenario. Combining this with the image properties of the sub-sampling receiver provides a technique for how to select the best possible sampling rate.

2. The second technique is based on pursuing the environment and adapting the sample rate according to that. Thus by sensing the environment and controlling the SNR, the best selection of sampling frequency is viable.

Acknowledgments

The accomplishment of this dissertation would not be possible without the love and support of Alborz, my husband- my true friend. To him I dedicated this dissertation although I know that he deserves much more. I would never be what I am without having him as my foot hold, my soul mate and my love. His love, patience and unconditional support flattened this tough rough route.

My appreciation also goes to my grandmother, Maman joon, for teaching me the love, inner peace, desire to explore and eagerness to learn. Although physically she can not walk, she has definitely been my guidance to achieve the highest summits of my life.

I am immensely indebted to my supervisor Professor Dr. Techn. Torben Larsen for the three years of appreciable academic guidance at AAU, and for his encouragements and motivations that has spurred me to achieve unreachable goals. Without his support and concern, this job could not be accomplished.

My thanks go to the Faculty and students of the Technology Platforms Section (former risk), for providing a superb atmosphere at University. I would like to thank all of my fellows/colleagues and all of my friends at technology platforms and outside for enriching my life during the last couple of years. I would especially like to thank Basuki Endah Priyanto, Svetoslav Gueorguiev, Huseyin Aniktar, Bulent Sen, Michael Nielsen, Jan H. Mikkelsen, Daniel Sira, Lei zou, Mehmood-ur-Rehman Awan, Muhammad Mahtab Alam, Yonghui Huang, Tian Tong and Peter Koch. I would like to thank the secretaries of our department particularly Eva Hanssen and Rikke D. Klemmensen for their assistance all the time.

My sincere thanks go to Ole Kiel Jensen for providing numerous fruitful technical discussions. Ole is one of the rare people in the world that you should be delightful to know one: always ready to help. He surprised me once while we were discussing about gallbladder by bringing an anatomy book and start describing about human body!

My friend, Jorge Martires deserves to receive my special gratitude. He is the true meaning of a great friend, always ready to help me in need, motivate me to continue and refresh me with a lot of useful cheering up discussions about many things in the world.

My sincere thanks go to the people participating in Wanda consortium for following up on my project and providing good input to improve it accordingly during our regular meetings.

In the Motorla company I got the chance to know a lot of nice people. Particularly, I am indebted to the RF group manager, Per Dahlgaard Pedersen, for providing me the opportunity to work with the Motorola Labs and supporting me from all aspects. I would like to thank

Contents

Chapter 1

Introduction

The aim of this chapter is to provide the reader the necessary background knowledge over the field, its potential problems and challenges. The chapter starts with an introduction to the problem. The case study is introduced and the initial problem is defined. The useful funda- mental concepts are discussed briefly. The section is continued by introducing the promising state-of-the art receiver architectures, related to the problem of the current investigations. The architectures are summarized according to their multi-band capabilities, and the chosen architec- ture or sub-sampling architecture is introduced. The challenges with the sampling architecture are mentioned. Finally, the section is pursued by describing what research methodology is picked to form the ground of the research.

1.1 Introduction

The trend in modern communication systems is to have several communication links integrated in a single device. The key challenges in transceiver design are to provide enormous services in a heterogeneous wireless infrastructure and higher bandwidth, all in one user equipment (UE). The trend toward bandwidth revolution along with wider coverage and mobility is illustrated in Fig. 1.1. Thus to achieve the goal, the front-end with multi-band reception capability is required. This can be realized through multiple front-ends targeting to receive each standard separately. Nevertheless, this is not a good solution due to its high power consumption and price. To avoid the expensive and power hungry parallel transceivers, it is vital to find more efficient and flexible solutions. The software defined radio (SDR) and Software Radio (SR) have been attractive concepts since many years with the aim of majority of processing being done in the digital domain. This makes it feasible to have the reconfigurable and flexible piece of hardware supporting a variety of technologies such as universal mobile telecommunications system (UMTS) [5] and [6], wireless local area network (WLAN) [7], global system for mobile telecommunications (GSM) [8], digital video broadcasting (DVB) [9], digital video broadcasting - handheld (DVB-H) [10], digital audio broadcasting (DAB) [11] and worldwide interoperability for microwave access (WIMAX) [12] by allocating the software resources. Having most of the process in digital domain is along with several advantages: (i) it introduces high level

1
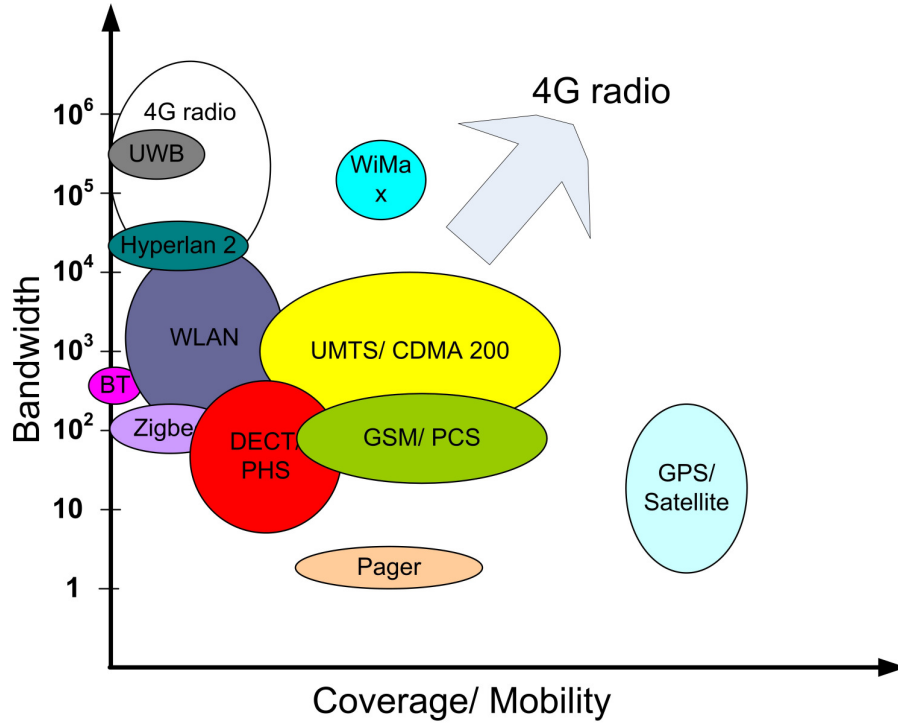
Figure 1.1: Coverage versus bandwidth

of integration in a single user equipment. In the digital domain, the unique functionalities of each standard can be set in the digital signal processing (DSP) part by employing SDR. Consequently, it is more feasible to have several parallel communication links integrated in a device. (ii) It is more robust to have most of the procedure in digital domain. For the companies, it is much easier to change the supplier and moving the digital design to the new platform. Besides, the normal small errors causing the failure of the analogue design is alleviated in digital design.

Thus, SDR ambitiously is pursued as a generic hardware analog circuit under a flexible programmable software for many years. However, although it has been a very tempting concept for designers since 1990 (when it was first time introduced by John Mitola [4]), it was not practically employed in the design of transceivers. The main reason has been the shortcoming of the existing technologies to serve in such an architectures. One of the key bottle necks in the mobile industry has been the appropriate Analog to digital converter (ADC) [1]. Realizing the SDR is along with shifting the ADC closer to the antenna. Thus for GHz mobile applications, a high speed, high dynamic range and low power ADC is the fundamental enabling factor. However with the available technologies, direct digitization of RF signals at more than twice the bandwidth sets very tough requirements on ADC especially in the high frequency ranges. Thus, this architecture has not been achievable for many years. A practical way of realizing SDR is developing high speed low power ADC. Especially implementing the software defined

---

[1]Since the focus of the thesis is on the receivers, the emphasis is on the ADCs. Similar discussion is applicable to the digital to analog converter (DAC)s in the transmitter chain.

radio in battery-powered devices requires the ADCs with very high data rates and resolution but consuming very low power. With the given discussion, it is concluded that there is still room for improvement in the electronic world to reach to the pure SDR hand held devices. In the meantime, the designers and researchers have been explored the alternative methods that lead us closer to the SDR vision.

One alternative way is to shift the digitization process to lower frequency by moving the analog to digital converter to the intermediate frequency (IF). Thus, the digitizing is done on a high-IF instead of radio frequency (RF) signal. In other words, the ADC is placed in a more reasonable frequency seen from today's developed technologies point of view. The frequency translations to IF is feasible in several ways. It can be done through more traditional approaches such as mixing and analog multiplying. Another approach is to do the frequency translation through sampling the signal instead of employing the analog multipliers. This is again one step closer to the SDR vision since the signal is sampled soon in the receiver chain and the rest of the signal processing is the discrete time processing.

Due to its indispensable advantages for multi-band applications, the RF sub-sampling architecture is proposed as a proper architecture in modern developed transceivers. In this architecture, the desired RF signals are sampled and aliased down intentionally without using conventional analog multipliers. The receiver samples the data at the rate greater than twice the cumulated information bandwidth around carrier frequencies instead of twice the total bandwidth which is desirable for high frequency applications. By transferring the data to discrete time and employing RF sub-sampling, the requirements of sampling rate and dynamic range is relaxed since it is done in much lower frequencies. The RF sub-sampling receiver has several advantages for multi-standard applications such as high level of integration by the ability of processing several input RF signals in a single front-end. By appropriate choice of sampling frequency, the RF signals can be aliased down to the Nyquist band from DC to half the sampling frequency without overlapping. This dissertation focuses on this architecture. The feasibility of realizing the multi-band RF receiver with this architecture is investigated. The receiver is simulated and implemented for a dual-band scenario supporting the UMTS and IEEE 802.11g.

1.1.1 Case study

The intention of this Ph.D. research was to to develop techniques to efficient, robust, and flexible multi-band receiver architecture. The system level study of the RF sub-sampling architecture is done for a generic RF receiver regardless of the selected standard. However, a specific case-study is used to further support the concepts and derive the experimental data. according to the defined scenario of this case-study, the UE enables both the WLAN and UMTS to operate concurrently. Since UMTS is a frequency Division Duplex (FDD) operating standard, both the UMTS uplink (UL) and UMTS downlink (DL) signals may exist at the same time with the separation in frequency domain. The duplexer is responsible of isolating these two signals in the 3G transceiver. However, the WLAN UL and WLAN DL are operating in different time periods due to the time division duplex (TDD) capability of the IEEE 802.11 standard.
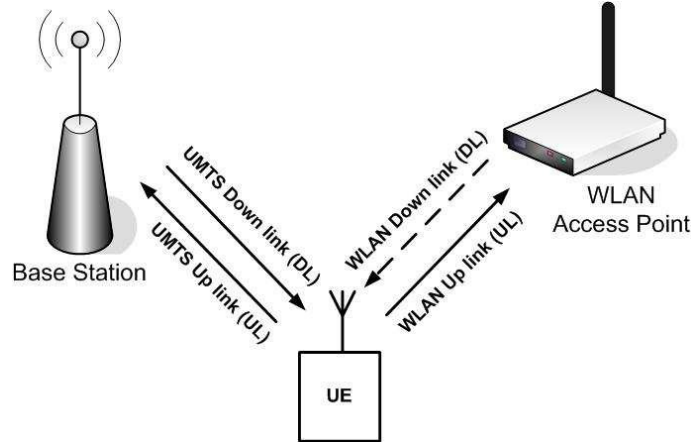
Figure 1.2: Illustration of multi-standard user equipment supporting UMTS and WLAN standards.

Therefore in each moment, only one of the WLAN UL or DL may exist in the user equipment. The scenario of the WLAN and UMTS signals operating simultaneously at the same transceiver is shown in Fig. 1.2.

The UMTS UL from the UE is operating at the transmit maximum average power of 24 dBm (power class 3). The WLAN UL signal is a 20 dBm signal. The UMTS and WLAN main specifications are presented in Table 1.1.

Table 1.1: UMTS and WLAN Specifications for UE [5], [7].

	IEEE 802.11g	UMTS
Duplexing	TDD	FDD
Frequency	2.4 - 2.4835 GHz	1920 - 1980 MHz: UL
		2110 - 2170 MHz: DL
Receiver Sensitivity	-82 to -65 dBm	-117 dBm
Channel Bandwidth	16.6 MHz	3.84 MHz
Transmitter Power Level	20 dBm (Europe)	24 dBm (Class 3)

1.1.2   Standards under consideration

IEEE 802.11g (WLAN)

The IEEE 802.11g which is an orthogonal frequency division multiplexing (OFDM) signal is used as one of the desired signals of the current research. The IEEE 802.11g is an extension of IEEE 802.11b with addition of OFDM modulation of IEEE 802.11a. The executive summary of this standard is presented in Table. 1.2. OFDM is a modulation technique with great potential of using the frequency spectrum. Each communications channel consists of several

Table 1.2: Key RF specifications for WLAN standard [5].

General Req.	Frequency band	2.4 2.4835 GHz
	Bandwidth	83.5 MHZ (3 non-overlapping Channels)
	Data rate	1-54 Mbit/s
Tx Req.	Power Level	20 dBm (Europe) 30 dBm (USA)
	PAR	17 dB (maximum theoretical value)
	EVM	5.9 % for 64-QAM%
Rx Req.	Sensitivity	-82 to -65 dBm (Data rate dependent)
	Adjacent Channel Rejection	35 to -1 dB (Data rate dependent)

sub-carriers which are orthogonal to each other. Thus, they can be placed close to each other in the frequency spectrum without any interference as illustrated in Fig. 1.3.
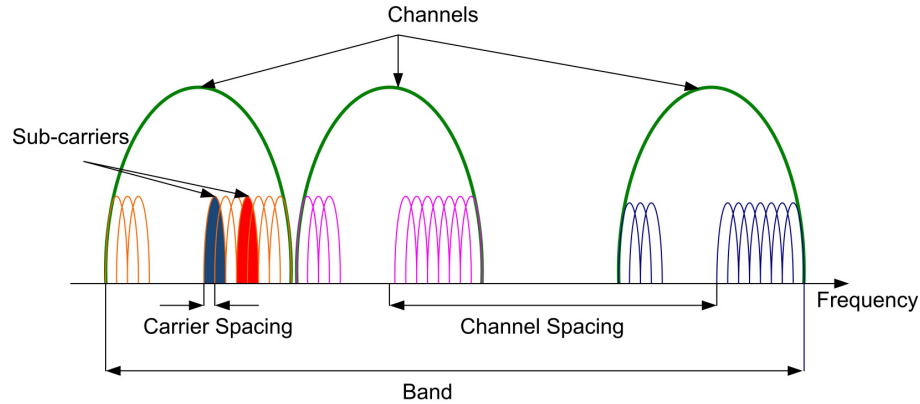
Figure 1.3: The OFDM channel and carrier definition.

The signal used for this research contains 52 sub-carriers operating at the data rate of 54 Mbps available from [13]— hereafter called WLAN signal for simplicity. Except 4 of the sub-carriers which are modulated with binary phase shift keying (BPSK), the rest are modulated with 64 quadrature amplitude modulation (QAM). Each channel of the WLAN signal has a bandwidth of 20 MHz with the channel bandwidth of 16.6 MHz[2]. The maximum transmit power is 20 dBm. The receiver sensitivity without adjacent channel interference (ACI) and minimum signal to noise ratio (SNR) is specified in the standard to reach to the bit error rate (BER)s less than 10^{-5} as outlined in Table 1.3. As it is shown, these numbers depend on the modulation scheme and data rates. The sensitivity including the ACI is 3 dB higher than without ACI.

---

[2]This is calculated from the fact that the sub-carriers except the DC are exploiting $((54 - 1)/64) * 20$ MHz effectively.

Table 1.3: Performance requirements of WLAN for UE [7].

Rates (Mbps)	Sensitivity without ACI (dBm)	SNR (dB)	EVM (dB)
6	-82	6.02	-5
9	-81	7.78	-8
12	-79	9.03	-10
18	-77	10.79	-13
24	-74	17.04	-16
36	-70	18.80	-19
48	-66	24.05	-22
54	-65	24.56	-25

The emitted power of the WLAN standard should be within the mask shown in Fig. 1.4. The illustrated mask is valid for data rates of 6, 9, 12, 18, 24, 36, 48 and 54 Mbps [7].
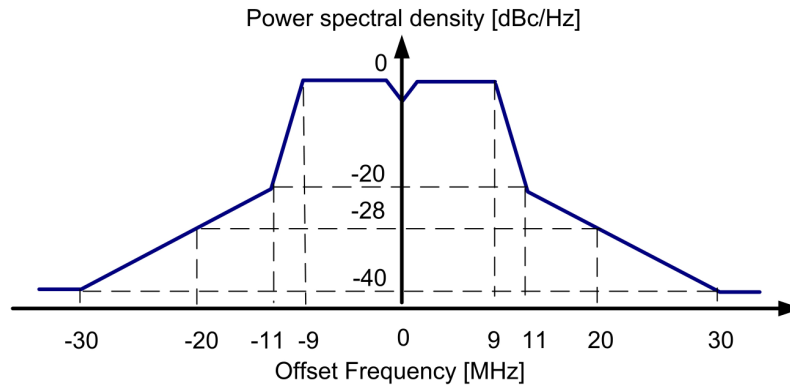
Figure 1.4: Transmitter spectrum mask of IEEE 802.11g for data rates 6, 9, 12, 18, 24, 36, 48 and 54 Mbps [7].

UMTS

UMTS is the 3rd generation of mobile communication standard which is available in two options: TDD and FDD. The focus of this research is on the FDD option. The summary of the key specification of the UMTS standard is presented in Table. 1.4. The Code division multiple access (CDMA) technique is employed for the UMTS signal. Many users may use the whole spectrum simultaneously in CDMA technique. The distinction among different users is made by allocating different spreading code to each user. In the receiver side, only the user with the correct code can de-spread and reach the information as illustrated in Fig. 1.5.

The data rates may vary between 12.2 and 768 kbps for DL and between 12.2 and 384

Table 1.4: Key RF specifications for UMTS standard [5].

General Req.	Frequency (Band 1)	1920 - 1980 MHz: UL 2110 - 2170 MHz: DL
	Bandwidth (Band 1)	60 MHZ (12 Channels)
	Chip rate	3.84 Mcps
	Data rate	12.2 kbs 384 kbs :UL 12.2 kbs 768 kbs :DL
Tx Req.	Power Level Class (1-4)	33, 27, 24 and 21 dBm
	PAR	3.5 dB
	EVM	17.5 %
Rx Req.	Sensitivity	-117 dBm (while transmitting)
	Adjacent Channel Rejection	33 dB
	Alternate Channel Rejection	49 dB
	Noise figure	7 dB

kbps for UL. The chip sequence multiplied by the data for spreading and de-spreading is 3.84 Mchip/s. The modulation of the UMTS is quadrature phase shift keying (QPSK) for both DL and UL. The specified EVM_{rms} for the UMTS standard is below 17.5 %.
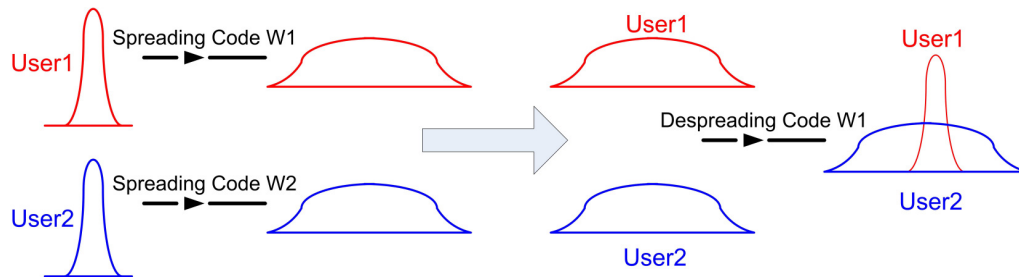
Figure 1.5: Illustration of the CDMA spectrum: spreading and de-spreading the data.

The frequency allocation of different bands are summarized in Table 1.5.

The selected band of this research is the band 1. The transmission mask of the UMTS signal must be within the mask illustrated in Fig. 1.6.

1.2 Background

The general task of the RF receiver is to convert incoming RF signals to the corresponding digital bit streams. There are a number of challenges and trade-offs during the design of a radio

Table 1.5: UTRA/FDD WCDMA Transmit Bands [5].

	UL	DL
Band 1	1920 - 1980 MHz	2110 - 2170 MHz
Band 2	1850 - 1910 MHz	1930 - 1990 MHz
Band 3	1710 - 1785 MHz	1805 - 1880 MHz
Band 4	1710 - 1755 MHz	2110 - 2155 MHz
Band 5	824 - 849 MHz	869 - 894 MHz
Band 6	830 - 840 MHz	875 - 885 MHz
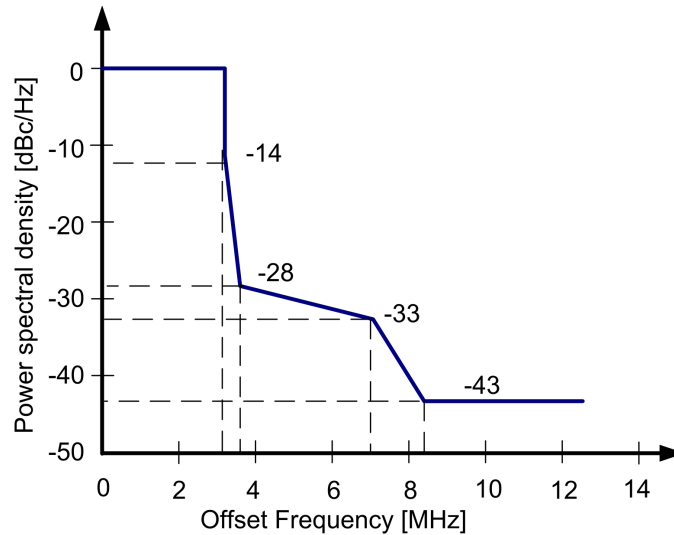
Figure 1.6: Illustration of the spectrum emission mask for the UMTS standard.

receiver. Several fundamental concepts are required to understand these challenges and trade-offs. The basic concepts which are frequently used in the thesis are defined in this sub-section. The deeper discussion is provided in the following sections.

1.2.1   Noise figure and sensitivity

The sensitivity is defined as the minimum level of the input signal that can provide the required SNR at the output of the receiver. There is no universal method for measuring the sensitivity. It depends on the receiver demodulation scheme and measures according to the signal characteristics [14]. One way to measure the sensitivity is to know the overall noise figure of the receiver.

The noise figure is defined as the ratio of the SNR of the input signal to the SNR of the output of the receiver:

$$NF = \frac{SNR_{in}}{SNR_{out}} \tag{1.1}$$

where k is Boltzmann's constant, T is the noise temperature, Δf_n is the signal bandwidth and NF is the noise figure of the receiver. The input/output signal to noise ratios are expressed in the linear units (not decibles). The term $10log(NF)$ is expressed the noise figure contribution in dB. $10log(kT)$ equates to -174 dBm at room temperature ($T = 290K$), and presents a typical resolution limit for measurement equipments. The relationship between sensitivity and noise figure is:

$$S_{i,min} = (kT)_{dB} + log(\Delta f_n) + NF_{dB} + SNR_{Req} \quad \text{[dBm]} \tag{1.2}$$

The sensitivity is determined from the overall noise figure of the receiver (NF_T). If the input and output signal-to-noise ratios are identical, then the system element has added no noise to the input signal. Thus its noise factor is unity. All practical elements contribute to the noise of the total receiver chain and hence provide $NF > 1$. Since noise figure is meaningful for every single block of the receiver, the NF_T for the cascaded receiver blocks is calculated from Friis equation:

$$NF_T = NF_1 + \frac{NF_2 - 1}{k_1} + \frac{NF_3 - 1}{k_1 \cdot k_2} \ldots + \frac{NF_n - 1}{k_1 \ldots k_{n-1}} \tag{1.3}$$

where NF_n is the noise figure of each component and k_n is the power gain of nth block illustrated in Fig. 1.7. Eq. (1.3) indicates that the noise figure (NF) of the first few blocks has very critical role in setting the total NF of the receiver.
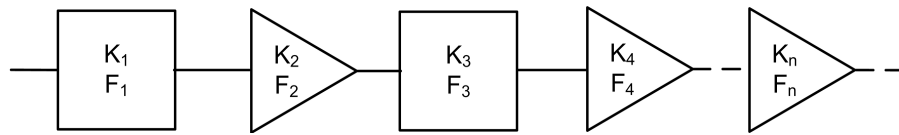
Figure 1.7: Illustration of the cascaded noise figure.

1.2.2 Linearity and intermodulation distortion

Although the components can be modeled linearly in less power levels, all practical components are nonlinear at high power levels. The nonlinearity is modeled with power series such as Taylor series:

$$v_o = a_1 v_i + a_2 v_i^2 + a_3 v_i^3 + \ldots = v_i(0) + (\frac{dv_o}{dv_i}) \cdot v_i + (\frac{d^2 v_o}{dv_i^2}) \cdot v_i^2 + \ldots \tag{1.4}$$

where v_i is the input and v_o is the output signals. It should be noted that Eq. (1.4) could be used for modeling the behavior of non-linear products in a small operating zone in the proximity

of the DC operating point. It is only useful for analyzing the weakly nonlinear systems due to its limitations. One of the limitations is that Eq. (1.4) does not include the phase components of the system. However in a real system, the output voltage is dependent to both the amplitude and the phase of the input. The other limitation is that the a_n coefficients are not constant during the input and output tuning. They are also sensitive to the bias levels at the input and output [15].

It can be seen from Eq. (1.4) that infinite number of terms is required to completely model the nonlinear effects of the device. However, in most cases the 5th to 7th order is enough to have a good model. The distortion product related to each order of intercept point will dominant when the input or output signals reach to the corresponding value. Especially, the third-order distortion should be taken into account since it has dominant role even in the weakly nonlinear systems. The third order distortion may exist in the pass-band of the desired signal and deteriorate the signal significantly. The output third-order intercept point (oIP_3) is defined as the point at which the extrapolated power curves of the signal and the third-order intermodulation distortion would intersect [16] as shown in Fig. 1.8. The iIP_3 is the
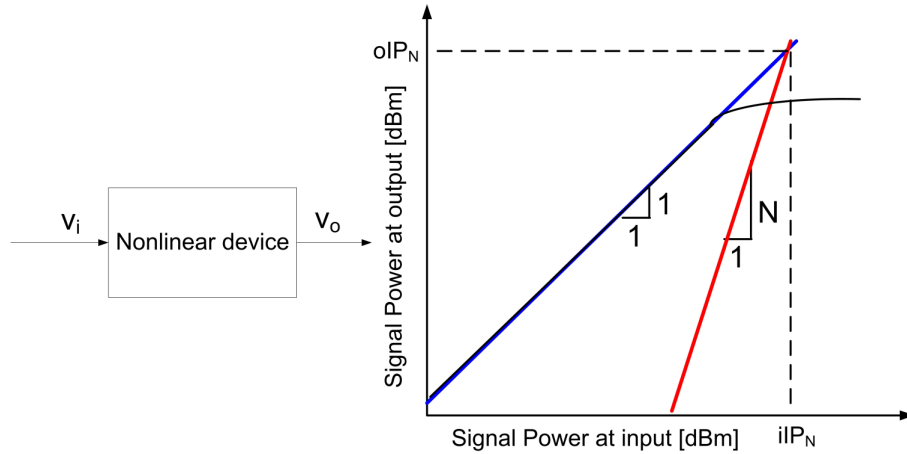
Figure 1.8: Graphical plot of intercept point.

corresponding input third-order intercept point:

$$iIP_3 = oIP_3 - k_T \quad [\text{dB}] \tag{1.5}$$

where k_T is the total power gain. To calculate the overall IP_3 of the receiver, the following formula could be used:

$$\frac{1}{IP_3^2} = \frac{1}{IP_{3,1}^2} + \frac{k_1}{IP_{3,2}^2} \cdot + \frac{k_1 \cdots k_{n-1}}{IP_{3,n}^2} \tag{1.6}$$

where $IP_{3,n}$ is the third-order intercept point of the nth component.

1.2.3   Dynamic range

Dynamic range is defined as the range between the maximum input level to minimum input level in which the device has desirable performance:

$$DR_{ADC} \; = \; P_{max} - P_{min} \quad \text{[dB]} \qquad\qquad (1.7)$$

In other words, it is the useful signal level range which the receiver can process the data with a particular BER. This term is defined in different application differently. For RF applications, the minimum signal is usually considered as the sensitivity level of the input signal. However, the maximum signal level in the dynamic range is not necessarily correspond to the maximum level of the desired signal itself. It could be a strong blocker level or the maximum input level of the two-tone test for which the distortion is still below the noise floor. Specifically for the ADC as a focal component, the P_{min} is the input noise level of the ADC. The P_{max} is determined from the maximum mean power level specified in each standard. The effective number of bits (ENOB) is calculated based on the dynamic range of the ADC (DR_{ADC}) if the input is a full-scale signal:

$$ENOB \; = \; \frac{DR_{ADC} - 1.76}{6.02} \qquad\qquad (1.8)$$

1.3   Multi-band state-of-the art receiver architectures

The aim of this section is to provide an overview to the existing receiver architectures and their performance in the multi-standard applications. This will clarify the advantages of the selected architecture for further investigations. A wide overview of the detailed performance of each architecture is not in the scope of the current thesis and can be found in famous literature in the field such as [17].

     The trend in transceiver design is to reach to an omni-purpose piece of hardware capable of supporting different technologies such as UMTS, WLAN, global positioning system (GPS), DVB-H, DAB and WIMAX. It is not so far from now to employ multi-service UEs capable of downloading all type of features from the net. Thus, it is mandatory to find solutions to implement the multi-standard transceiver in the most optimum way.

     The simplest way of reaching to this goal is to use multiple parallel transceivers to process each standard separately. The first circuit for multi-mode receiver was published in the year 99 with the parallel circuits [18] and designed for receiving two bands [19]. However this is not an optimum solution for manufacturing since it has very high power consumption and requires plenty of space. Thus, this is required to find solutions to realize the multi-standard UE with maximum hardware reuse, small size and low power consumption. These precedence objectives are especially very important in the design of battery-powered hand held devices. The multi-standard transceiver's flexible blocks must be defined to operate under wide range of specifications from different standards. This will bring up real challenges on the selection of the architecture and definition of the blocks. The design specification from different technologies

form a trade off among several factors such as flexibility, reconfigurability, cost, maximum hardware reuse, and power consumption. This section presents a discussion on the ability of the existing multi-band receivers in multi-standard applications with respect to the mentioned goals. Their suitability for employment in wireless battery-powered transceiver is argued. This discussion is not possible without an extensive knowledge of the state-of-the art receivers. Thus a review of the state-of-the art receivers employed in the multi-standard application is presented. The section has three main sub-sections. The first sub-section 1.3.1 focuses on the traditional radio receiver architectures such as "Heterodyne", "Homodyne" and "Image-reject" Receiver architectures. The second sub-secion 1.3.2 discusses the alternative approaches close to the SDR. This consists of the digital IF and sub-sampling receiver architectures. The last group of receiver architectures is the SDR. It should be noted that the portioning of the analog and digital circuitry or the placement of ADC has an eminent role in this categorization. It effects all the important receiver factors such as the configurability, integrability, complexity, power consumption, and the price of the receiver [20].

1.3.1   Traditional radio receivers

The main functionality of the receiver is frequency translation while performing the level adjustment and filtering all the undesired signals. An abstracted model of the radio receiver is shown in Fig. 1.9. It consists of several stages of mixing, level adjustment and filtering. As
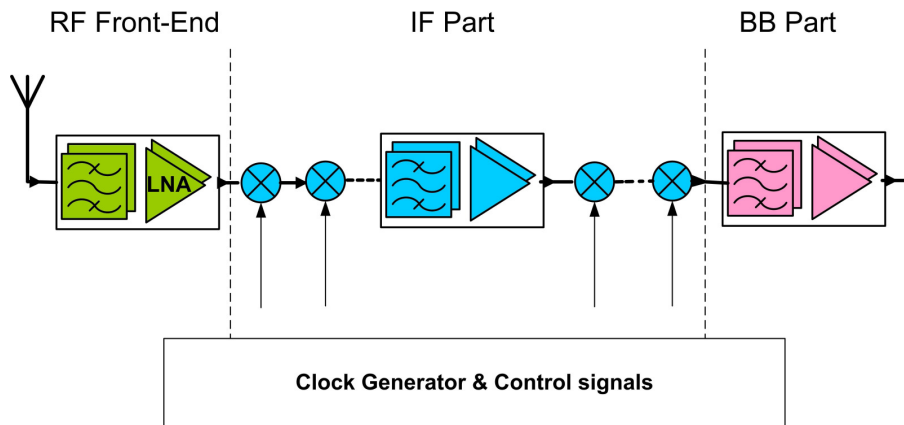
Figure 1.9: An abstracted model of the radio receivers.

mentioned, the portioning of the analog and digital circuitry has an important role. All the mentioned functionalities of the receiver can be performed in digital domain by moving the ADC closer to the antenna. The place of ADC has direct impact on the complexity, power consumption, configurability, integration level and cost of the receiver [20].

Heterodyne receiver

The Heterodyne receivers stay the receiver of the choice for decades. The reason has been its ability to select narrow band high-frequency signals from the noisy environment while sup-

pressing the interferes to a great extent. The generic block diagram of this receiver is shown in Fig. 1.10. The chain starts with an RF band-select filter aiming to reject the out-of-band
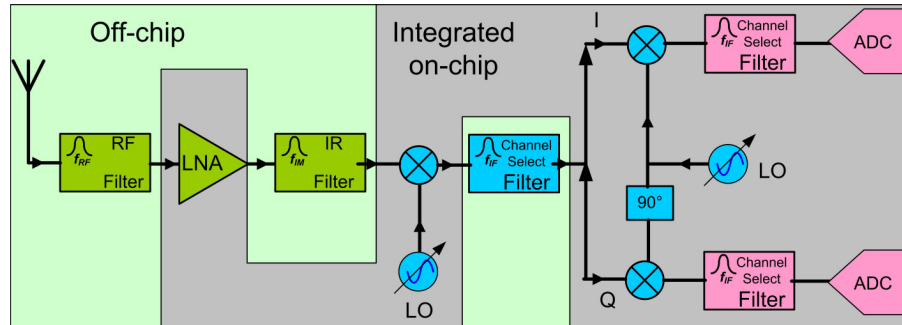
Figure 1.10: Heterodyne Receiver Architecture.

undesired signals and deliver the RF signal to the low noise amplifier (LNA) for amplification. Subsequently, the signal is passed through a high-Q off-chip image-rejection (IR) filter to prevent the image noise to be down-converted along with the desired signal. The IR filter is usually implemented with physically large surface acoustic wave (SAW) to provide high-Q filter transfer function in high frequency. The signal is then mixed down with the local oscillator frequency and translated to lower intermediate frequency. Then, it is delivered to the next consequent block which is the IF channel select filter. The quadrature down conversion (QDC) is done from the IF to baseband (BB). Thus the ADC is operated on the in/quadrature phase (IQ) signals in low frequencies such as IF or BB signals. It may be required to place a programmable-gain amplifier (PGA) prior to IF quadrature down-conversion to adjust the gain [21].

One of the important issues in this receiver is the selection of the IF. According to the selected IF, a trade-off exists between the IR capability and the channel selection. A higher IF results in easier IR since a wider bandwidth filter could be employed for IR. However this provides more difficulty in channel selection procedure since more interferes are down-converted to the IF along with the signal. On the contrary if a lower IF is selected, the image rejection is more difficult which leads to a more relaxed channel selection later in the receiver chain. The trade-off between RF filtering and image suppression is shown in Fig. 1.11. To make the best compromise between the filtering and down-conversion, several stages of down-conversion may be employed. The Heterodyne receiver has several advantages and disadvantages which are described below and also outlined in Table 1.7. The pros of this architecture could be listed:

- It has the very reliable performance from both the selectivity and sensitivity point of view. The High-Q IR filter provides high selectivity.

- The signal processing is done in IF stages. Thus the BB-originated problems such as flicker noise and DC block is not an issue for this receiver.

- The IQ matching is quite good. The reason is the quadrature down-conversion is performed in lower frequencies.
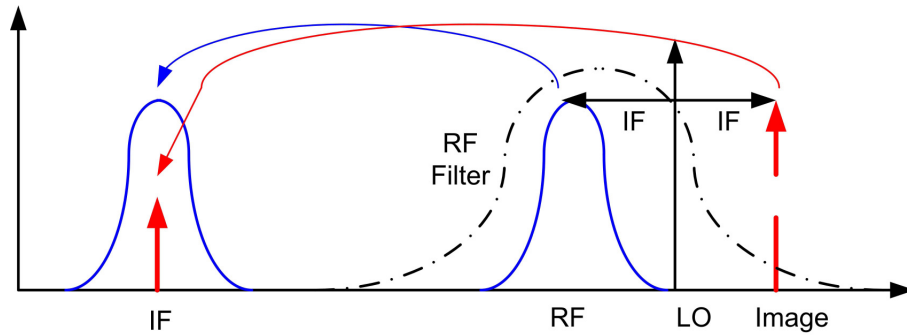
Figure 1.11: The trade-off between RF filtering and the image signal.

The cons of the architecture are outlined below:

- Very little flexibility is provided with this architecture. The architecture depends on the hardware for each individual standard. Thus, it has low-integration capabilities. Operating with several standards requires several multiple external SAW and channel-select filters. So it is not feasible to use them in integrated multi-band applications.

- Using the large off-chip SAW filters brings some extra matching requirements. The LNA should be driven by a 50 Ω. Thus, this makes the receiver very sensitive to the derivations of 50 Ω load external buffering.

- The power consumption is high in this type of receiver. The buffering along with the external components is increasing the power consumption.

- The complexity and size is increased due to employing the external components.

Although this architecture is very popular for single frequency applications, it is not vastly employed in multi-standard application. The reason is its drawbacks such as high power consumption, increased complexity and large size which are contradicting the precedence objectives of mobile wireless terminals. However [22] and [23] are few examples of multi-standard applications implemented with heterodyne receiver architecture.

Image-reject receiver

To overcome the problems of using the bulky off-chip IR filters in heterodyne receivers, the image rejection techniques are proposed. In this technique, the image and signal are being processed differently. The image is alleviated by the help of its negative replica or signal cancellation. There are two famous image-rejection receiver architectures: Hartley [24] and Weaver

Hartley Architecture This architecture is originated from an idea represented by Hartley in 1928 [24]. The block diagram of this architecture proposed by Hartley is shown in Fig. 1.12.

The input RF signal is splat to in-phase (I) and quadrature phase (Q) components by employing quadrature down-conversion. The result I and Q signals are then low-pass filtered.
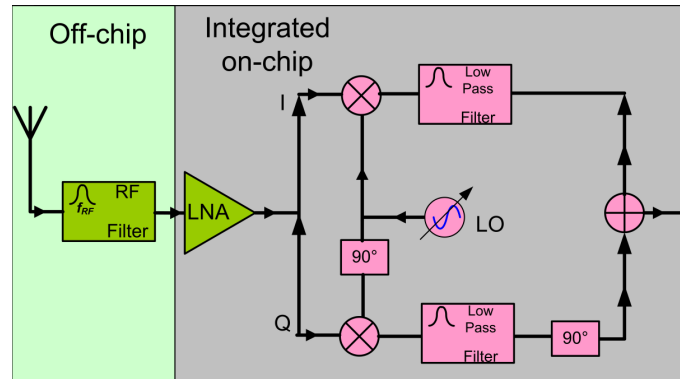
Figure 1.12: Hartley IR receiver architecture.

The Q is added to a 90°-phase-shifter. The image signal is removed by the summation of I and Q signals. It is concluded that this architecture is introducing higher level of integration by employing signal cancellation technique instead of bulky off-chip IR filter. So the pros of this architecture are outlined:

- The integrability of this architecture is higher due to elimination of bulky external IR filters. Consequently the cost, area and power are reduced.

- The BB-originated problems such as flicker noise and DC block are still not a problem for this receiver architecture.

The cons of the architecture are listed below:

- This architecture is very sensitive to mismatches in I and Q paths. If the phase difference in QDC is not exactly 90° or there is a gain or phase mismatch in I and Q paths, the IR is not done completely. The image will be partly down-converted to the band of interest.

- The noise and interference in the neighboring channels is not completely suppressed by low pass filter (LPF). This puts tough requirements on the linearity of the adder.

- The 90° stage adds significant noise to the receiver. Moreover, this stage is limiting the bandwidth of the Hartley architecture to narrow bands only.

Weaver Architecture   The weaver architecture as illustrated in Fig. 1.13 is very similar to Hartley architecture. The only difference is the replacement of the 90° stage with another stage of IQ down-conversion. The advantage of this architecture in comparison with Hartley architecture is that the IQ down-conversion can be implemented for wider bandwidth. It does not suffer from the gain imbalance as mentioned in Hartley architecture. Nevertheless if the second down-conversion is to a non-zero IF, then the second image problem may appear.

There are several examples of employing IR architectures in multi-standard applications. Some of these examples are [25], [23], [26] and [27].
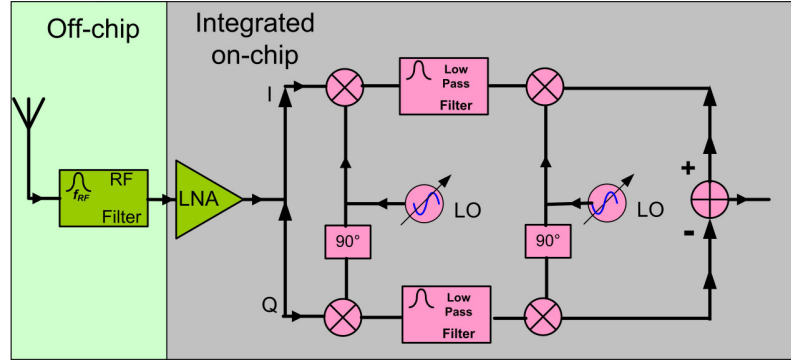
Figure 1.13: Weaver IR receiver architecture.

Homodyne receiver

The receiver which translates the RF directly to BB is called the Homodyne architecture. It is also called "'Zero-IF"' or "'direct-conversion"' architecture. A simple homodyne receiver is shown in Fig. 1.14. It should be noted that the output signal from down-conversion must be quadrature. Otherwise a part of data is missed since the lower and upper side of data containing different piece of information are overlapping after down-conversion. One of the advantages of
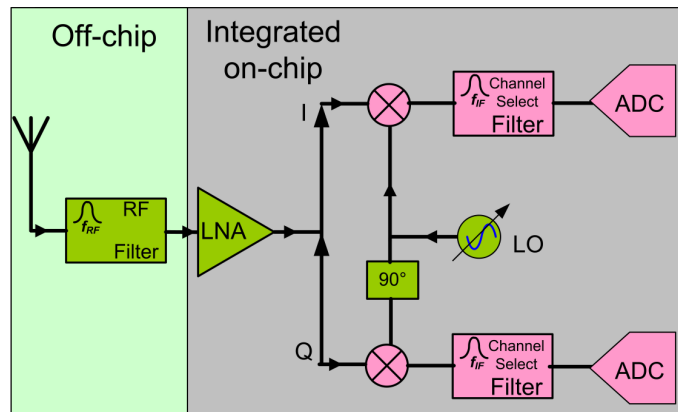
Figure 1.14: Homodyne receiver architecture.

this receiver is that the problem of image is totally alleviated since the signal plays the role of image for itself. This is performed through setting the frequency of local oscillator to the same frequency as the desired signal. Thus there is no more need to bulky external IR filter. This will result to the high integrability level and lower cost. The other advantage is the substitution of all the IF signal processing blocks with subsequent BB blocks. This is highly acquiescent with the monolithic integration resulting in much less power consumption. The pros of this architecture are:

- The problem of image signal is completely evaded by selecting IF=0. Consequently there is no need to IR filter. This circumvents the requirements on extra 50 Ω buffering. Totally, this means less power consumption, complexity and lower cost.

- The subsequent IF signal processing blocks in heterodyne is substituted by BB blocks which highly acquiescent with the monolithic integration. This results in higher degree of integration.

- The frequency plan is simple since the IF signal is already determined to be zero. This makes the receiver profitable for multi-standard applications. The local oscillator (LO) frequency and subsequent LPF can be implemented programmable which is desirable for receiving and down-converting several signals.

There are several disadvantages with this receiver as listed below:

- The signal is down-converted to zero frequency. Thus all the low frequency offsets and BB noise effect the desired signal. In general the problems are: DC offset, flicker noise, self-mixing, even-order distortion and LO leakage. With the superimposition of these effects on the desired signal, the SNR degrades significantly. These problems are alleviated by methods such as analog feedback loop or adaptive signal cancellation [14].

- IQ mismatch is another drawback of this receiver. This problem arises from the fact that the RF signal is down-converted to quadrature output signals. The errors caused by deviations from 90° or amplitude mismatch increases the BER.

Due to the indispensable advantages of this architecture for multi-standard application, numerous examples exist. It has good flexibility, high level of integration, low cost and power dissipation and feasible frequency plan for several signals. A number of examples of using this architecture for multi-standard applications are: [28], [29], [30], [31], [32], [33], [34] and [35].

Low-IF receiver

To combine the advantages of homodyne and heterodyne architectures, the low-IF receiver was proposed. It has the integrability of the homodyne receiver, but with less sensitivity to BB noise receiver. The RF signal is down-converted to very low frequency close to the BB. However, this causes the architecture to still suffer from the image problem. In other words in this architecture, the signal is not the image for itself anymore. An image signal in the serious form exists due to the small IF. Different possible architectures may be used to realize the low-IF receiver, depending on the chosen variation. Two generic building blocks of this architecture are shown in Fig. 1.15. As illustrated in Fig. 1.15(a), the IF to BB down-conversion could be performed digitally to evade the second image in the architecture. The LPFs can be replaced with complex filters such as polyphase filters as shown in Fig. 1.15(b). This selection will relax the IQ as well. The other options could be moving the ADC and the amplifier so that another IF to BB down-conversion is done prior to digitization. This will relax the speed requirements of ADC.

This architecture is vastly used in multi-standard applications. Some examples are [36], [37], [38], [25].
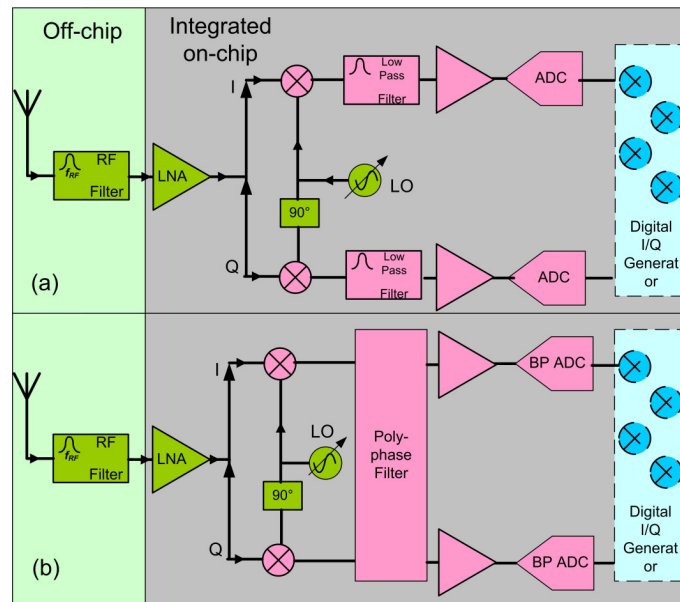
Figure 1.15: Low-IF receiver architecture.

1.3.2 Alternative approaches to the SDR

The lack of appropriate ADCs for direct digitization of RF signals especially in hand held devices encourage the designers and researchers to search for alternative approaches to the SDR. The big question is where is the most appropriate place for the ADC in the receiver chain to reach to the best possible flexibility and hardware reuse. Two examples of such architectures are presented in this section. The main specifications of the receivers and the placing of the ADC in each architecture are outlined in Table. 1.7.

Digital IF receiver

In a dual-stage heterodyne receiver, the second lower frequency down-conversion and filtering is feasibly achievable in digital domain. In this architecture which is called the "'Digital IF architecture"' the first IF signal is digitized as illustrated in Fig. 1.16. Subsequently in digital domain, the signal is down-converted via mixing with digital quadrature phases of a digitized sinusoidal. The signal is then digitally filtered and capitulated to the BB processing blocks. This architecture is one of the promising architectures for SDR. It is an alternative solution which shifts the digitization procedure to lower frequencies to realize the feasibility of finding an appropriate ADC to digitize the signal.

An issue with this architecture is that still there is high requirement on the selection of the appropriate ADC. The ADC is digitizing the IF signal which is only filtered with band-select filters. Thus, the ADC must have a large dynamic range to accommodate both the high power blockers and low power signal. The filtering subsequently is done in digital domain later. The other issue is that due to the image problem, the IF should have large values. This will place the image signal in further distance. On the other hand, this will set high requirement on the ADC

to be able to work in high frequencies. A high resolution and high quality ADC is required to digitize the data at high IF frequencies. Consequently, such a high speed ADC is power hungry which is contradicting the battery-powered devices.
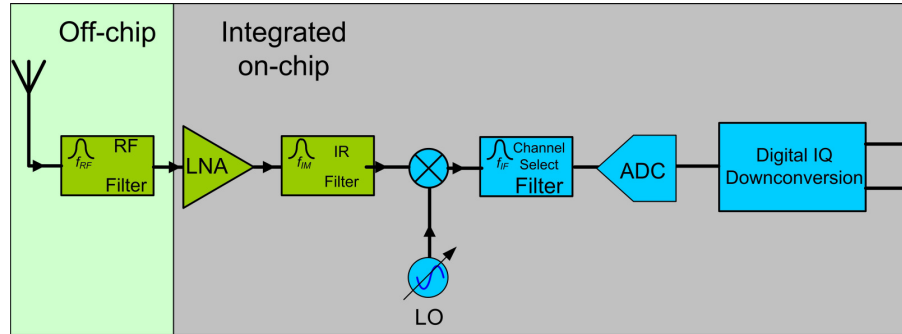
Figure 1.16: Digital IF receiver architecture.

Sub-sampling receiver

As mentioned before, it is difficult (if not impossible!) to find very high frequency ADCs to realize SDR. One of the other alternative approaches is to shift the digitization procedure to lower frequency through sampling.

The RF sub-sampling is a receiver technique in which the desired RF signals are sampled, and aliased down intentionally without using conventional mixers, to lower frequencies. Since the receiver samples the data at a rate greater than twice the cumulated information bandwidth around carrier frequencies, instead of twice the total bandwidth, the requirement on the sampler is much more relaxed [2,3]. Thus, by transferring the data to discrete-type IF , the requirements of sampling rate and dynamic range of the ADC is relaxed. It provides very high level of integration, since it is feasible to process several signals with one receiver chain. However, it has several disadvantages. One of the major drawbacks of this architecture is its large noise figure. Along with the desired signal, noise is replicated in multiples of sampling frequency. So, it is crucial to provide sufficient noise pre-filtering in sub-sampling receiver architecture, to avoid this effect. The generic block diagram of the receiver is illustrated in Fig. 1.17. Since this architecture
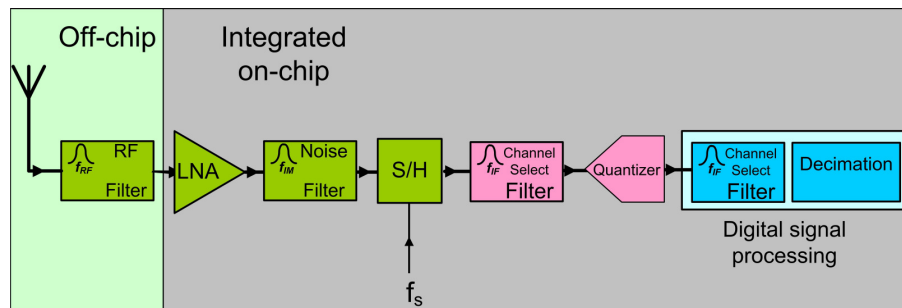
Figure 1.17: Sampling receiver architecture.

is the selected architecture of this thesis, a detailed discussion will be presented in the following

chapters. This architecture is explored as one of the appropriate approaches for designing multi-standard RF front-ends by introducing high level of integration. There are several examples of employing this architecture for multi-frequency applications such as [2], [3], [39] and [40].

1.3.3 SDR and SR

The SDR and SR have been the ambitious architectures since many years. However the short-coming in technologies such as high speed ADCs, digital signal processing (DSP)s and field-programmable gate array (FPGA)s prevent the complete realization of this architecture. The
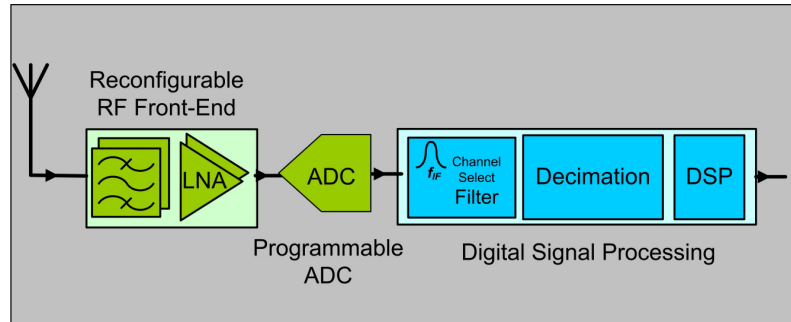
Figure 1.18: SDR architecture.

idea of the SDR architecture is to move the ADC close to the antenna and digitize the data soon in the receiver chain. In other words, the purpose is to reduce the analog hardware circuitry and define a generic digital hardware under a flexible software architecture. The architecture is illustrated in Fig. 1.18.

Finally, the SR architecture is the ultimate goal in the evolution of radio architectures. It is based on placing an ultra wide-band ADC after the antenna which digitize all the received RF signals. All the rest is performed under software. There are a lot of advantages along with using the SDR and SR architectures:

- It introduces a flexible architecture with high level of integration in a single UE. In the digital domain, the unique functionalities of each standard can be set in the digital signal processing (DSP) part by employing SDR. Consequently, it is more feasible to have several parallel communication links integrated in a device.

- It is a reconfigurable architecture. It gives an ultimate chance to the user to choose and reconfigure the desired receiver on demand. It is easy to connect to internet and download a software to receive a new standard with the same UE.

- It is very robust to have most functionalities in digital domain and in software instead of analog hardwares.

However, the major disadvantages of these architectures are the lack of enabling high-speed components such as ADCs, FPGAs and DACs. These architectures are ambitious architectures for research centers and companies. However, a number of examples exist claiming the employment of SDR such as [41], [42], [43] and [44].

Due to the key role of ADCs as the enabling components of these architecture, a state-of the art survey has been performed. several suitable or partly suitable ADCs for RF applications are listed in the following.

State-of-the art ADC

ADCs are the core enabling components of the SDR/SR. However as mentioned, it can be labeled as one of the important bottle-necks of realizing the SDR/SR. The existing ADCs are far from the required speed power consumption, linearity and resolutions to be embedded in the SDR transceiver chain at GHz applications. To further investigate the issue, a state-of-the art investigation has been performed on the existing ADCs with impressive performances. The summary of the investigation is outlined in Table 1.6.

Table 1.6: State-of-the art ADCs for SR/SDR applications.

Manufacturer	Part number	ADC Architecture	Bits	BW[MHz]	f_s [MSPS]	Power
Maxim [45]	Max 109	Flash ADC	8	2800	2200	6.8 W
	Max 108	Flash ADC	8	2200	1500	5.25 W
	Max 106	Flash ADC	8	2200	600	5.25 W
	Max 104	Flash ADC	8	2200	1000	5.25 W
National [46]	ADC081000	Folding/interpolation	8	1700	1000	1.45 W
	ADC081500	Folding/interpolation	8	1700	1500	1.2 W
	ADC083000	Folding/interpolation	8	3000	3000	1.9 W
Texas instrument [47]	ADS5463	Pipeline	12	2300	500	2.2 W
	ADS5463	Pipeline	14	1400	400	2.5 W

It is concluded from Table 1.6 that the power consumption of the available ADCs is too high for the battery operated device of the current dissertation.

1.3.4 Summary

The pros and cons of different architectures are outlined in Table 1.7. As mentioned, the place of ADC has important role in the overall performance of the receiver. It effects the complexity, power consumption, configurability, integration level and cost of the receiver [20]. Thus, it is covered in Table 1.7. Besides that, the type of information which enters to the ADC is mentioned as one of the determining factors for the selection of architecture.

1.4 Specific problem and scientific challenges

The challenge in transceiver design is to define a universal platform capable of processing several technologies at the same time as discussed in this section thoroughly. To avoid expensive and power hungry parallel transceivers it is vital to find more efficient and flexible solutions. The ultimate goal is the SDR and SR with majority of processing being done in digital domain. The bottle neck of realizing them is the shortcoming of the existing technologies in developing very high speed ADCs, DSPs and FPGAs to serve the purpose.

The overall goal of the project was to develop techniques to efficient, robust, and flexible multi-band receiver architecture and conquer the shortcoming of the technologies with scientific methods. The main motivation of the project was to design a receiver with:

- Multi standard- multi mode capability

- Maximum hardware Reuse

- Maximum mitigation of the receiver's impairment errors

- Feasible Frequency plan for multi-band application- Maximum Interference cancellation

- Reasonable Power consumption

A survey in the existing architectures reveals the sub-sampling architecture as a viable choice for RF multi-band applications with the accessible developed technologies.

The requirement on very high speed ADC and subsequent digital processing blocks is moderated in this architecture. The reason is that the desired RF signals are sampled and aliased down intentionally to the IF prior to the ADC. Moreover in the sub-sampling based receivers, the data is sampled at a rate greater than twice the cumulated information bandwidth around carrier frequencies instead of twice the total bandwidth which is desirable for high frequency applications. By transferring the data to discrete time and employing RF sub-sampling, the requirements of sampling rate and dynamic range is relaxed.

The RF sub-sampling architecture has several advantages with respect to the main motivations of this project. It introduces high level of integration by the capability of processing several signals in one receiving chain. This can be performed by appropriate choice of sampling frequency so that several RF signals can be aliased down to the non-overlapping portions of Nyquist band. The substitution of conventional analog multipliers with samplers presents more flexibility in the frequency plan of the receiver for multi-band application as illustrated in Fig. 1.19. Depending on the bandwidth of the sampler, several signals can be transferred in frequency domain.

However there are also some challenges and problems with the architecture; (i) the architecture is noisy in nature due to noise folding in the sampling process [48], (ii) also direct distortion by image mixing may be a problem [49], [39], and (iii) The frequency plan of the receiver for several signals is complex. The sampling frequency must be chosen to transfer several signals to non-overlapping portions of Nyquist band. The issues related to this architecture are covered in the current thesis.
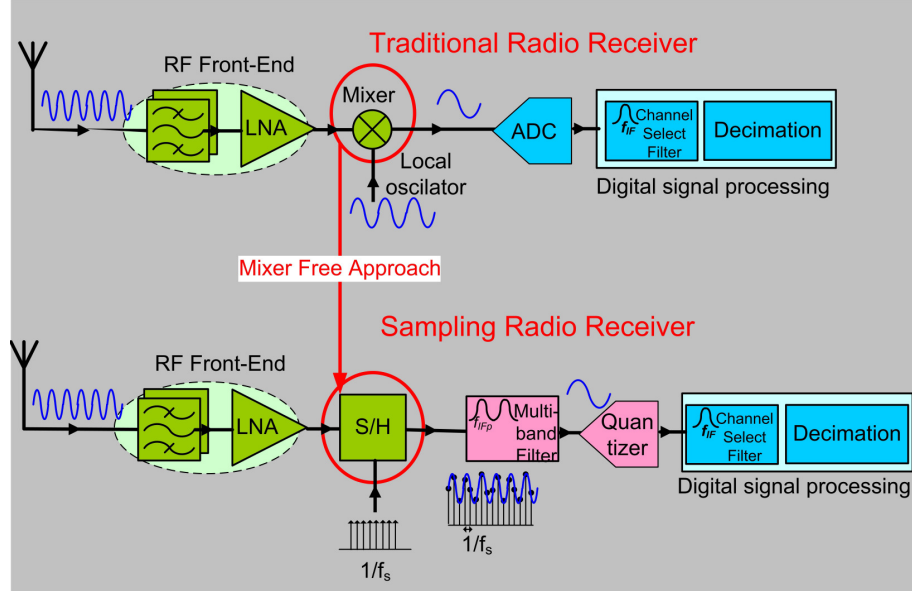
Figure 1.19: The comparison of mixer based architecture with sub-sampling architecture.

1.5   Research methodology

To simulate the RF sub-sampling receiver and the corresponding issues, a time domain system level simulator was established in Matlab [50]. The simulator operating with the UMTS and WLAN signals is depicted in Fig. 1.20. The generation of UMTS and WLAN signals are
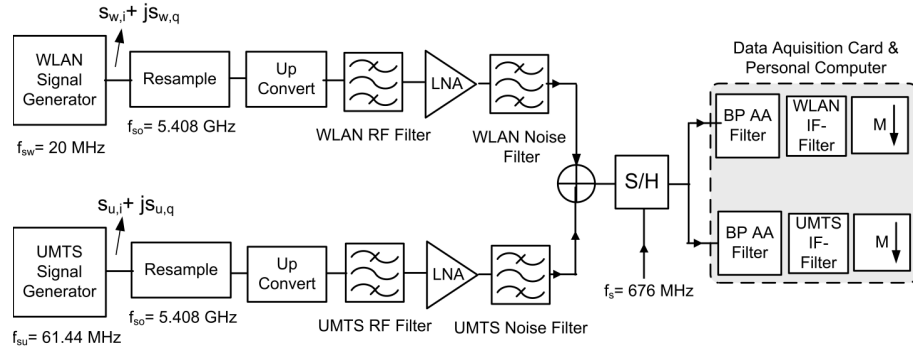
Figure 1.20: The time domain Matlab Simulator for WLAN and UMTS RF sub-sampling receiver.

explained in sub-sections 1.5.1 and 1.5.2. The generated signals are resampled to the new rate (f_{so}) of 5.408 GHz. The reason behind the selection of this sampling rate is that there are two distinct signals with the maximum frequency component of 2.483 GHz in the multi-standard scenario of this dissertation. Thus, the resampling to a new higher rate is done for the system to accommodate twice of the highest frequency of the scenario. This is required for the sampling rate of the system to fulfill the Nyquist criteria. The resampling is done by the Matlab function *resample* from *signal processing toolbox* [50]. This command utilizes a FIR low-pass filter. This filter is designed by using *firls* with a Kaiser window. The resampling here is done with the

intention of upsampling with a non-integer ratio. On the other hand, the downsampling in the lower frequency is performed by the *downsample* command from the same toolbox. The rate is decreased by keeping one sample from every n^{th} sample starting from the first sample. The signals are then up-converted to the carrier frequency of each channel. Filters are designed with the *Matlab Filter Design and Analysis Tool (FDAtool)*.

The signals are added together and entered the sample and hold (S/H) block. The signals are sampled with the sampling frequency (f_s) of 676 MHz or sampling time (t_s) of 1.48 nS (nano seconds). The reason of selecting this sampling frequency is discussed extensively in the following chapters. The S/H block is modeled according to its required functionality to sample the signal in a portion of sampling period and then hold it in the rest. So in the first period of the t_s the signal is sampled and in the second period the value of the previous time period is hold. In the simulation of this thesis, the sampling time (t_s) is divided into two periods: (i) sample time ($\tau \cdot t_s$), and (ii) Hold time (($\tau - 1) \cdot t_s$). The τ was chosen to be 0.25 which is a realistic choice according to the commercially available components.

The LNA is modeled by the gain value. Thus the output product from LNA block is obtained by multiplying the input signals with the gain of LNA. The power spectral density is estimated via Welch method. The root mean square (RMS) values of the error vector magnitude (EVM)s are calculated according to the methods presented in the standards [5] and [7].

1.5.1   Generator for UMTS

The QPSK modulated UMTS signal is one of the desired signals of this thesis represented in Fig. 1.20 as $s_{u,i}(t)$ and $s_{u,q}(t)$. The $s_{u,i}$ is the in-phase component or the real part of signal and $s_{u,q}$ is the quadrature component or the imaginary part. The signal generation procedure is illustrated in Fig. 1.21.

Several data and control channels are added together to form the IQ of the UMTS signal. The IQ of UMTS signal is spread and scrambled to form a complex chip sequence number (s_u) as illustrated in Fig. 1.21. The real and imaginary parts of s_u are filtered by a pre-defined root raised cosine filter ($\alpha = 0.22$) [5]. The chip rate is 3.84 Mcps. More detailed information about generation of the UMTS signal is out of the scope of this dissertation and can be found in [5].
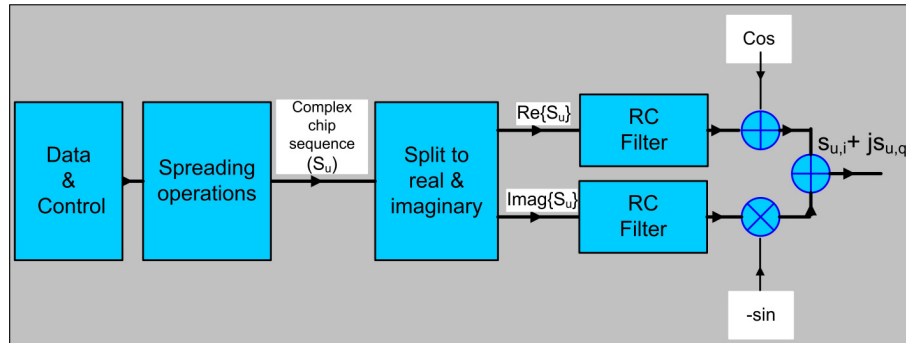
Figure 1.21: The UMTS signal generator.

The signals $s_{u,i}(t)$ and $s_{u,q}(t)$ before resampling are shown in Fig. 1.22. Since it is eas-
ier to visualize the signal in the frequency domain, the power spectral density (PSD) of the
corresponding baseband UMTS is depicted in Fig. 1.23(a). The PSD of the upsampled and
up-converted UMTS signal to the desired carrier and (f_{so}) is shown in Fig. 1.23(b) (The power
level in these figurers is not normalized). The oversampling ratio used inside the generator is
16 which results in the rate of 61.44 MHz ($16 \times 3.84MHz$) at the output of generator. The
data type used for this simulation is *slot* type (Each slot contains 2560 chips). The total data
generated contains two slots with the length of 2560 chips and oversampled with the rate of
16. Therefore the overall data length used during the simulation is 81282 bits to ensure metric
convergence.
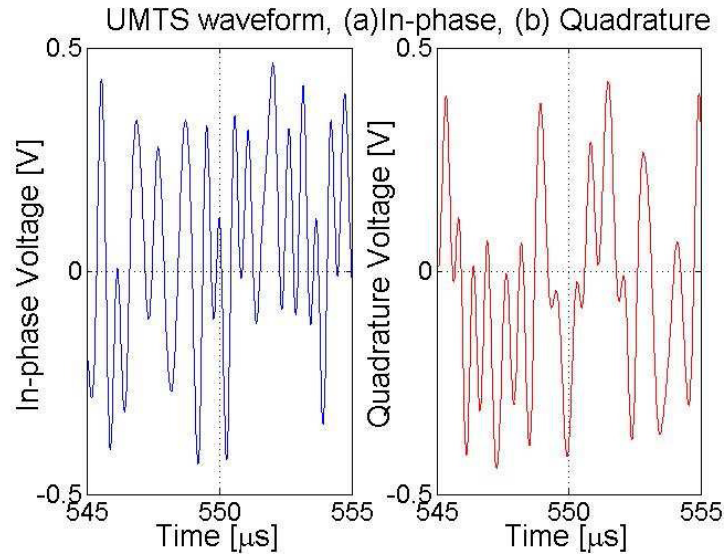
Figure 1.22: The real and imaginary parts of the UMTS time domain signal.

1.5.2 Generator for WLAN

The IQ OFDM WLAN is the other desired signal of this dissertation. The signal generation
is done according to OFDM signal modulation as depicted in Fig. 1.24. The IQ signals are
mapped and zero padded consequently. The process is continued by applying the inverse fast
fourier transformation (IFFT) function. The guard interval and cyclic pre/post fixed are added
to the signal and finally it is filtered by root raised cosine filter ($\alpha = 0.15$) [7]. Further detailed
information about generation of WLAN signal is out of the scope of this dissertation and can
be found in [7].

The generated time domain WLAN signals $s_{w,i}(t)$ and $s_{w,q}(t)$ are depicted in Fig. 1.25. The
PSD of the baseband WLAN signal with the sampling rate of 20 MHz is plotted in Fig. 1.26(a).
Its upsampled and up-converted version to the desired carrier frequency and (f_{so}) is shown in
Fig. 1.26(b).

For WLAN data, the processing is done on frames. Each frame contains 3500 information
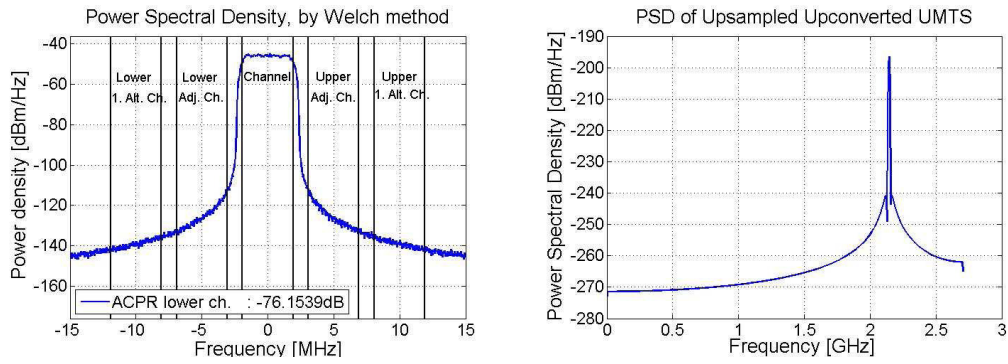
Figure 1.23: (a) PSD of the UMTS baseband signal sampled at 61.44 MHz and (b) PSD of the upsampled up-converted UMTS signal with the rate 5.408 GHz (The power level of the signals is not normalized).
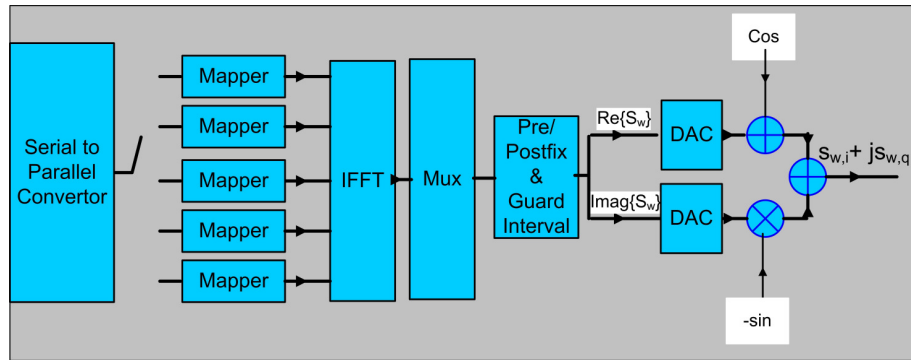
Figure 1.24: The WLAN signal generator.

bits [7]. Totally 20 frames are chosen to ensure metric convergence. The convergence is checked in each simulation frequently.
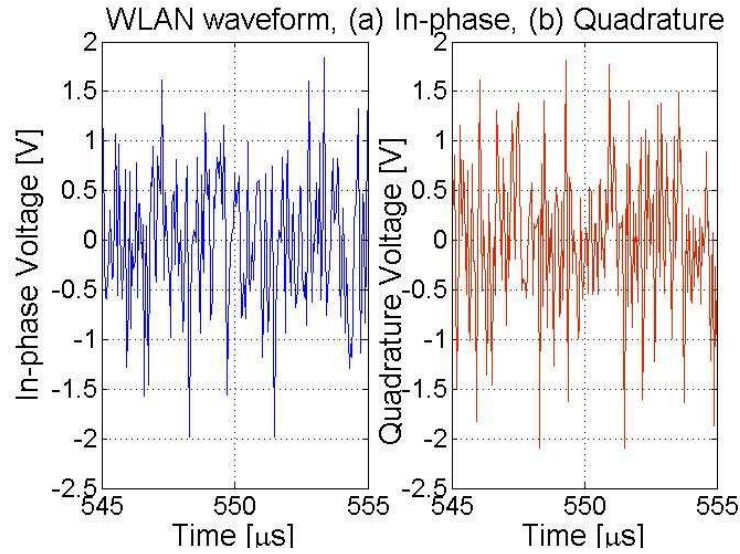
Figure 1.25: The time domain real and imaginary parts of WLAN signal.
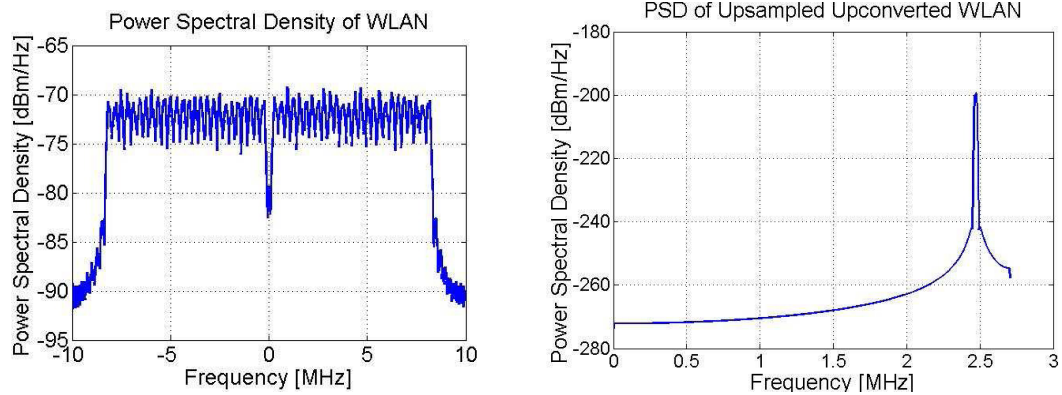
Figure 1.26: (a) PSD of the WLAN baseband signal sampled at 20 MHz.; (b) PSD of the upsampled up-converted WLAN signal with the rate 5.408 GHz (The power level of the signals is not normalized).

Table 1.7: Outline of multi-standard capabilities of different receiver architectures.

Receiver architecture	Pros	Cons	AD partitioning	ADC input
Heterodyne	Reliable Performance No DC offset Good IQ matching No flicker noise	Expensive Large and bulky Power consuming Low-integration level	BB or IF	IQ
IR	High integration level Cheap No flicker noise No DC offset	RF/IF QDC Bad IQ matching Gain and phase imbalance Narrow band(Hartley) Second Image (Weaver)	BBorIF	IQ
Homodyne	Feasible frequency plan High integration level Cheap No image	RF/IF QDC DC offset Flicker noise LO leakage Self mixing	BB	IQ
Digital IF	Feasible frequency plan High integration level Hardware reuse Good IQ matching Good flexibility	High ADC Req.	IF	
Low-IF	High integrability cheap Hardware reuse No flicker noise	Image RF/IF QDC	BB or IF	IQ
Sampling	High integrability High flexibility Hardware reuse Feasible frequency plan	Image Noise Jitter	IF	
SDR	Excelent integrability Excelent flexibility Excelent Hardware reuse Feasible frequency plan	High ADC and FPGA and DSP requirements	RF or high-IF	

Chapter 2

RF Sub-sampling Receivers

The selected architecture of the current dissertation is described in this chapter. The sub-sampling receiver architecture is a promising architecture for multi-standard applications with potential of high level of integration. However, there are also problems with the architecture; it is noisy in nature due to noise folding in the sampling process and the sampling errors such as jitter can distort the signals severely. Moreover, direct distortion by image mixing may be a problem. These problems are identified and the potential solutions are proposed.

This chapter is arranged as follows. A system level investigation of the sub-sampling architecture is provided in Section 2.1. The basic sub-sampling principles are presented. Section 2.2 investigates the major noise sources in this architecture. Focus is given to the thermal noise and jitter because of their importance in the RF high frequency applications. Section 2.3 presents the important blocks in RF sub-sampling front-end and their role to combat the major noise sources. Great emphasis is given to the RF bandpass filters, low noise amplifier (LNA)s and Analog to digital converter (ADC) as the main focal blocks of the front-end. The image distortion and its effects in sub-sampling receiver is discussed in Section 2.4. Finally, Section 2.5 provides a summary and conclusion of the presented discussion in this chapter.

2.1   RF sub-sampling front-end

2.1.1   Sampling theory

The *sampling* operation is a critical signal processing operation in the sub-sampling systems. Thus, it is shortly reviewed in this sub-section.

Prior to mentioning the theory of the sampling, it should be noted that seen from sampling interval viewpoint, the sampling operation can be divided into two main categories: Uniform Sampling (US) and Non Uniform Sampling (NUS) [51], [52] and [53]. In many applications, it is a fair assumption to consider the samples are uniformly taken from the original waveform. However in practical communications systems, there are a lot of applications with the irregular and non-uniformly distributed sampling periods. For example in communication systems, the obtained samples are generally non-uniformly distributed when data from uniformly distributed

samples are lost. However, it is assumed that the requirement for uniform sampling is held in this dissertation.

Consider a continuous signal $s(t)$ is sampled at a uniform rate of t_s. This converts the continuous signal to a discrete-time signal $s(mt_s)$ consisting of infinitive terms at integer values of "'m"'. The discrete-time signal has values only in specific discrete time instances and is not defined in all the other time domain. The sampled signal can be written mathematically [54]:

$$\tilde{s}(t) \; = \; \sum_{m=-\infty}^{\infty} s(mt_s)\delta(t - mt_s) \tag{2.1}$$

The Fourier transformation of the sampled signal $\tilde{s}(t)$ is [55]:

$$\tilde{S}(f) \; = \; f_s \sum_{m=-\infty}^{\infty} S(f - m\,f_s) \tag{2.2}$$

Thus $S(f)$ is a periodic function with the period of f_s. In other words, the signal is replicated in the frequency domain by sampling. The original waveform is extractable from each of these replicas as long as they do not overlap. This is confirmed by following the Nyquist criterion of Shannons sampling theorem for low-pass sampling [56]. According to this theorem, a band-limited signal is completely extractable from its uniformly sampled version if the sampling rate is at least higher than twice the maximum frequency[1].

When the sampling frequency is not higher than twice the maximum frequency (under-sampling), the frequency components above the maximum frequency is aliased back into the Nyquist band $[\frac{-f_s}{2}, \frac{f_s}{2}]$. The spectral overlapping of these replicas is called aliasing. This phenomena is illustrated in Fig. 2.1. The black spectrum of the Fig. 2.1 is sampled at a correct
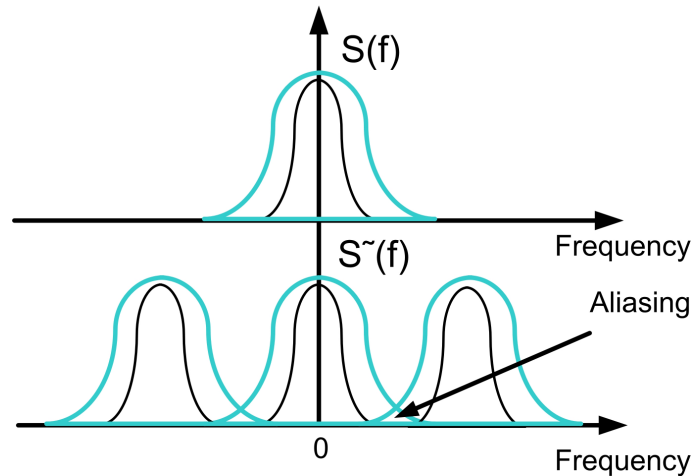
Figure 2.1: Illustration of the spectrum of a continues signal (up) and the sampled version (down).

rate according to the Nyquist criteria and the signal is extractable from each replica. However

---

[1]Theorem 1: If a function $f(t)$ contains no frequencies higher than W cps (in cycles per second), it is completely determined by giving its ordinates at a series of points spaced $\frac{1}{2W}$ seconds apart [56].
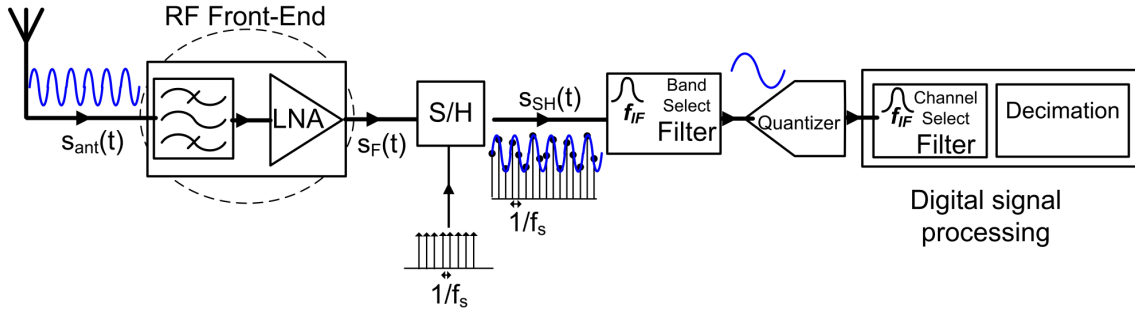
Figure 2.2: Block diagram of the RF sub-sampling receiver.

the blue spectrum is sampled at a rate which does not fulfill the Nyquist criteria. A part of the signal is missed due to aliasing. The sampling frequency needs to be tactically selected to make use of a harmless signal spectrum aliasing. More discussion about selection of the sampling frequency will be presented in Chapter 3.

2.1.2 Basic sub-sampling Receiver principle

The block-diagram of the sub-sampling receiver is illustrated in Fig. 2.2. For a single frequency scenario, the front-end consists of a filter-LNA section where the output signal is denoted $s_F(t)$. For a multi-band application, several filter-LNA sections may be employed for different signals. In this case, a multiplexer exists just at the down stream of the separate front-ends to add all the signals together[2]. The variable gain LNA modules adjust the signal of the given frequency band to comply with the needed signal range for the sampler. The RF filters have the important role of suppressing the out-of-band interference signals. The received signal at the antenna terminals is given by:

$$s_{ant}(t) = \sum_{n=0}^{N} s_{ant,n}(t) \tag{2.3}$$

$$= \sum_{n=0}^{N} a_n(t) \cos(2\pi f_n t + \theta_n(t)) \tag{2.4}$$

where $a_n(t)$ and $\theta_n(t)$ are the envelope and phase signals related to the carrier frequency f_n. Each input signal occupies the frequency band $f_n - \Delta f_n/2 \leq f \leq f_n + \Delta f_n/2$. The signals are organized such that $s_{ant,0}(t)$ is the desired signal and $s_{ant,1}(t), \ldots, s_{ant,N}(t)$ are undesired blocking signals with carrier frequencies $f_1 < \cdots < f_N$ for single frequency scenario. In the dual-band application, $s_{ant,0}(t)$ and $s_{ant,1}(t)$ are the desired signals and the rest are blocking signals. This is stated for each application throughout the thesis individually. Additive noise is ignored as only the main principles are considered. The signal after the front-end module is

---

[2]For some applications, one front-end can be reused by several signals. It can be realized by employing the multi-band LNAs [32], tunable LNAs [57], multi-band or tunable filters [58], [59] and multi-mode synthesizers [60], [61].

then given by:

$$s_F(t) = \sum_{n=0}^{N} k_n \, a_n(t) \, \cos(2\pi f_n t + \theta_n(t)) \tag{2.5}$$

where k_n is the signal gain seen from the antenna terminal to the output of the front-end module at the carrier frequency f_n. The front-end module is assumed to have phase linearity and constant gain within the signal band. This seems to be a realistic assumption for practical designs. In the frequency domain $s_F(t)$ translates to:

$$S_F(f) = \sum_{n=0}^{N} S_{F,n}(f - f_n) + \sum_{n=0}^{N} S_{F,n}^*(f + f_n) \tag{2.6}$$

where $S_{F,n}(f), S_{F,n}^*(f) \to 0$ for $f \notin [f_n - \Delta f_n/2; f_n + \Delta f_n/2]$ contains the frequency domain information of the envelope and phase of the carrier frequency f_n. $S_{F,n}^*(f)$ is the complex conjugate of $S_{F,n}(f)$. The sampling process is modeled as multiplying the input signal to the S/H device by a pulse train. The receiver must sample the data at a rate greater than $2\Delta f_0$. The multiplication by a pulse train in time domain implies convolution in frequency domain which results in replicas of the signals at multiples of the sampling frequency [40] at the output as depicted in Fig. 2.3:

$$
\begin{aligned}
S_{SH}(f) &= f_s \sum_{m=-\infty}^{\infty} S_F(f - m \, f_s) \tag{2.7}\\
&= f_s \sum_{m=-\infty}^{\infty} \sum_{n=0}^{N} S_{F,n}(f - (f_n + m \, f_s)) \\
&\quad + f_s \sum_{m=-\infty}^{\infty} \sum_{n=0}^{N} S_{F,n}^*(f + (f_n + m \, f_s)) \tag{2.8}
\end{aligned}
$$

Thus, the signals $S_{F,0}, S_{F,1}, \ldots S_{F,N}$ are down-converted to lower (and higher) frequencies by sub-sampling. It is also worth noting from Eq. (2.8) that the envelope and phase signals of signal n is only found directly at DC in the special case where f_n/f_s is an integer. In all other cases, the information is found at an intermediate frequency $(0 \le |f_{IF}| < f_s/2)$:

$$S_{F,0}: \quad f_{IF} = f_0 - \text{round}(\frac{f_0}{f_s}) \cdot f_s \tag{2.9}$$

$$S_{F,0}^*: \quad f_{IF} = -f_0 + \text{round}(\frac{f_0}{f_s}) \cdot f_s \tag{2.10}$$

The resulting intermediate frequencies accept any positive or negative value in the Nyquist band. This concept is in analogy to high/low side mixing in traditional analog multipliers. This is an important observation which leads to the image concept in the multi-band sub-sampling architectures. The sub-sampling techniques do not only stand by the theoretical analysis but has also been implemented and measured in various communication systems, e.g. [62], [49], [63], [64], [65], [66], [67], [68] and [69].
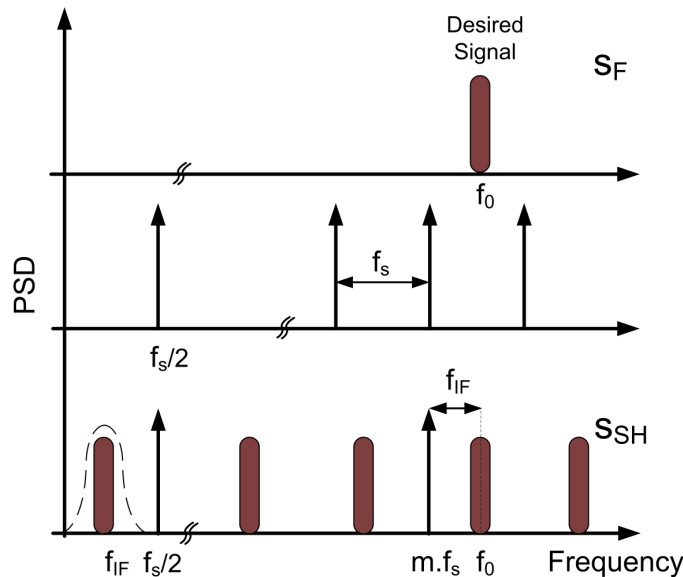
Figure 2.3: Illustration of the sampling operation in frequency domain.

2.2 Nonideal behavior of RF Sub-sampling architecture

The noise is one of the main limitations in the sampling circuitry with the sampler as the focal component. It may be produced by two major sources— the switch internal or the external sources. From the internal noise sources the flicker noise and thermal noise are two crucial ones [70] and [71]. Since, the frequencies in the current dissertation is much higher than baseband, only the thermal noise is considered.

From the non-idealities produced by the external sources in the sampling switches, sensitivity to the clock jitter is considered in the current dissertation. That is due to the fact that in high speed systems such as the system under investigation, the jitter could cause severe problems. The reason is that in the sub-sampling circuitry, the jitter from the clock is highlighted by a factor of sub-sampling ratio squared. This is discussed more in this section.

2.2.1 Thermal noise

To understand the noise behavior of this architecture, it is crucial to investigate the noise performance of the sample and hold (S/H) block as the focal component. [3]

The general block diagram of the S/H block is depicted in Fig. 2.4(a). The switch is opening and closing according to the state of the clock. This imposes two different noise powers to the architecture: (i) The sampling noise power $(P_{n,s})$ when the clock is "'on"' and (ii) the holding noise power $(P_{n,h})$ when the clock is "'off"'. The combination of these two forms the total noise power of the S/H block (P_n) with power spectral density of $S_N(f)$ [71]. To derive the noise power in each state, the two mentioned timing partitions are investigated as depicted in

---

[3]It should be noted that Besides the switching thermal noise (kT/C noise) of S/H block, there are less dominant noise sources in practical SC circuits such as opamp wide-band noise and opamp 1/f noise [72].
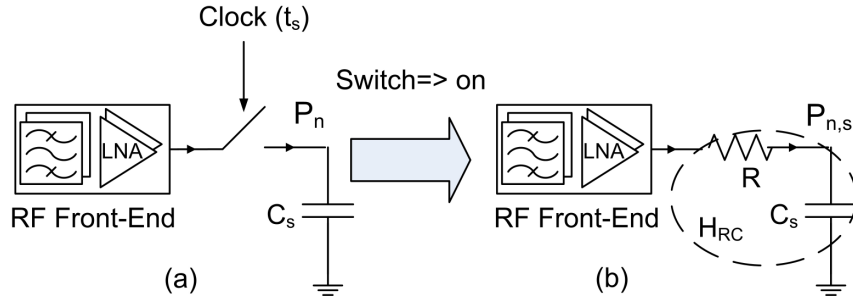
Figure 2.4: (a) Block diagram of the S/H and (b) the equivalent circuit of S/H in "'on"' situation.
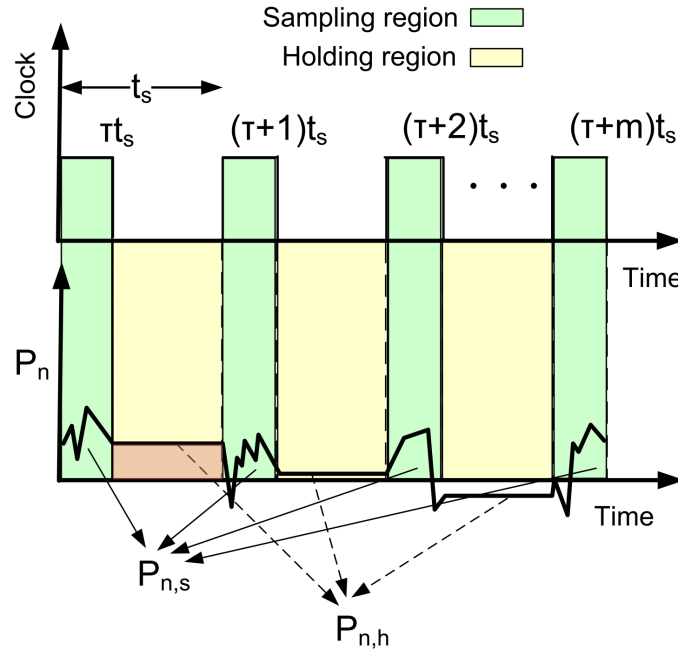
Figure 2.5: Illustration of the clock signal and the corresponding noise in the S/H block.

Fig. 2.5.

1. In the first time period of each sampling interval (t_s) or τt_s ($\tau \leq 1$), the signal is sampled and the switch is in its "'on"' state. The equivalent figure of the S/H block in this time duration is shown in Fig. 2.4(b). The capacitor and the "'on resistor"' of the sampler form an RC filter. The frequency response of the RC filter ($H_{RC}(jw)$) is derived from the fundamental equations of the RC circuits. It is done by taking laplace transform of the $e^{-t/RC_s}/RC_s$ and then replacing "'s"' with "'jw"' [73]:

$$H_{RC}(jw) \; = \; \frac{1}{RC_s} \int_0^{\tau t_s} e^{-t(jw+1/RC_s)} = \frac{1 - e^{(jw+1/RC_s)\tau}}{1 + (jwRC_s)} \tag{2.11}$$

The RC_s is the time constant of the system. The "'on"' resistance of the switch introduces the thermal noise at the output equal to $4kTR$ [16]. The noise is stored on the capacitor along with the instantaneous value of the input voltage when the switch turns off. The
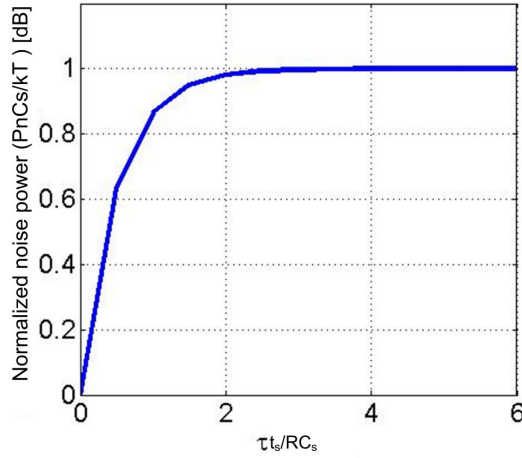
Figure 2.6: Normalized thermal noise power versus $\frac{\tau t_s}{RC_s}$.

power spectral density (PSD) of noise in the sampling state is calculated:

$$S_{N,s}(f) \;=\; \frac{P_{n,s}}{\Delta f} \;=\; (4kTR)\,|H_{RC}(f)| \tag{2.12}$$

where k is the Boltzmann constant and T is the absolute temperature. R is the on resistor of the MOS switch and C_s is the sampling capacitor. Eq. (2.12) is simply obtained by passing the thermal noise through the filter transfer function (H_{RC}) shown in Fig. 2.4(b). The $P_{n,s}$ is evaluated by considering the bandwidth effect in the PSD [74]:

$$P_{n,s} \;=\; \int_0^\infty S_{N,s}(f)df = \int_0^\infty (4kTR) \left| \frac{1 - e^{(jw + 1/RC_s)\tau}}{1 + (jwRC_s)} \right| df = \frac{kT}{C_s}\left(1 - \frac{1}{e^{-2(\frac{\tau t_s}{RC_s})}}\right) \tag{2.13}$$

The noise power $P_{n,s}$ is normalized by $\frac{kT}{C_s}$ and is plotted versus $\frac{\tau t_s}{RC_s}$ in Fig 2.6 [74].

Fig 2.6 reveals that practically for the sampling periods which are bigger then 3 times of the time constant, the thermal noise power of the S/H block in the switch-on duration is estimated as kT/C_s. This assumption is held throughout the current thesis as well.

kT/C_s noise is valid for the S/H device if the switch stays "'on"' for ever. Eventually, the "'on"' duration of the switch longs for the period τt_s ($\tau \leq 1$). Therefore to consider this fact in modeling the block, the noise power in this period is multiplied by τ and stated as $\tau kT/C_s$.

This indicates that the thermal noise power in this time period is proportional to the reverse of the sampling capacitor and sampling frequency. The bigger the capacitor is chosen, the less noise is imposed to the architecture. However this is contradicting with the obtained result of this paragraph that the time constant of the system should be desirably low. So although practically the noise power will set the size of the capacitor,

care must be taken to select the best trade-off according to the targeted application. Noting that, bigger capacitors are equivalent to more power dissipation in the analogue circuitry as well. The same discussion is applicable for the sampling frequency. Bigger sampling frequency mitigates the thermal noise of the sampler. On the other hand, it imposes more power consumption and tougher requirement on the subsequent circuitry especially the ADC. So the selection of different parameters to decrease the thermal noise should be done according to the best trade-off. They should be tactically chosen according to the cost, complexity and performance analysis of the system.

2. The second period is the "'switch-off"' duration. In the holding state, the transfer function of the $H_{RC}(jw)$ is zero and the value of the previous state is being held. In other words, the value obtained in the time instant τt_s will be held till the launch of the next sampling period as depicted in Fig. 2.5. Thus, the PSD of the noise in the hold period is dependent to the PSD of the noise in sampling period in time instants $((\tau \pm m)t_s$ for $m = 0, 1, \cdots)$. Where "'m"' indicates the index of the clock period. For the first order S/H device, the data exhibits a spectrum with roll-off of $(sinc)^2$ [75]. Consequently the holding noise $(P_{n,h})$ in Fig. 2.5 is manipulated according to mentioned parameters [71]:

$$S_{N,h} = \frac{P_{h,s}}{\Delta f} = [(1-\tau)sinc(\pi(1-\tau)f)]^2 \sum_{m=0}^{\infty} S_{N,s}(f \pm m f_s) \qquad (2.14)$$

Eq. (2.14) indicates that the noise from all the replicas in multiples of the sampling frequency is adding up together. The aliasing of noise due to sampling causes the noise power of several replicas to be down-converted to the Nyquist band. Hence, the noise power spectral density for the holding period can be calculated from [71]:

$$S_{N,h} = \frac{P_{h,s}}{\Delta f} = \left[(1-\tau)sinc(\frac{\pi(1-\tau)f}{f_s})\right]^2 \frac{kT}{f_s C_s} \qquad (2.15)$$

The thermal noise mentioned in this section is applied to the simulator set up illustrated in Fig. 1.20. The Parameters used in the simulation obey the specifications mentioned in Section 1.5. The plotted signal to thermal noise ratio versus different variables (sampling frequency and sampling capacitor) is shown in Fig 2.7. Several S/H bandwidth are tried to achieve a complete view of how different parameters effect the signal to thermal noise ratio. In the simulation, the following parameters are defined:

• The noise of the front-end except the thermal noise of the switch is ignored in the simulation. In other words, the other noise generators of the system are deactivated. This is done to provide a clear magnified view of the role of these parameters in setting the signal to thermal noise ratio of the receiver. Activating the other noise generators of the system will decrease the signal to noise ratio (SNR) by injecting more noise to the simulation.

• The signal gain of the receiver is assumed to be 20 dB. It is enough for verifying the role of the parameters since the other front-end noise generators are ignored. Thus the signal
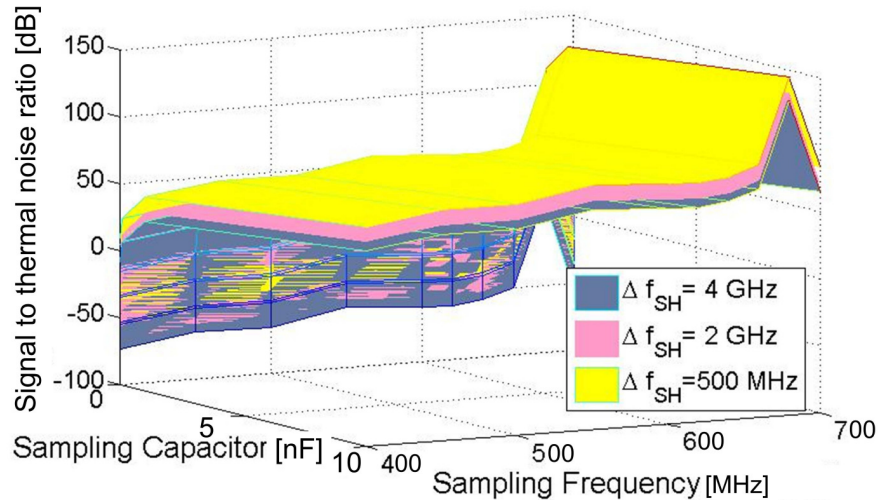
Figure 2.7: Simulated signal to thermal noise ratio versus sampling frequency, f_s, Sampling capacitor, C_s, and the bandwidth of the sampler, Δf_{SH}.

power in the input of the sampler (the combination of the universal mobile telecommunications system (UMTS) and wireless local area network (WLAN) signals) is measure to be -87 dBm. The signals are spectrally located at 2142.5 MHz and 2472 MHz for the UMTS and WLAN respectively. The sampling frequency is swept between 400 and 700 MHz.

- The thermal noise is added to the simulator according to the formulas derived in this section. In the sampling time duration, kT/C_s noise is imposed on the information. In the holding period, the thermal noise injected to the simulator follows Eq. (2.15). The simulated signal to noise ratio versus sampling capacitor and sampling frequency is depicted in Fig 2.7.

From Fig 2.7, it is concluded that the sampling capacitor and sampling frequency have the reverse effect in the thermal noise of the sampler. In other words to decrease the thermal noise in the sub-sampling architecture, the sampling frequency or sampling capacitor must be increased. Thus the size of the capacitor and the sampling frequency are chosen according to a trade-off between the acceptable thermal noise and the bandwidth of the sampler. It should be noted that a big capacitor or very large sampling frequency are contradicting with the goals of the battery-powered devices by increasing the size and power consumption.

2.2.2 Jitter noise

In practical sampling systems, the samples are not captured at exact desired time instants due to the errors in clock and controlling voltage. This uncertainty in capturing exact samples is
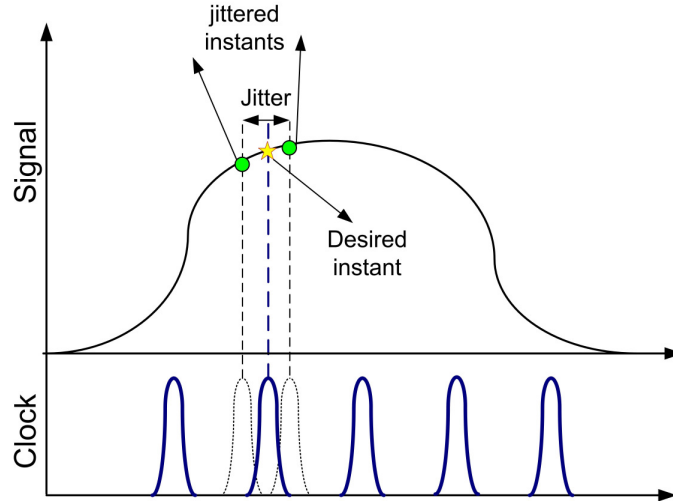
Figure 2.8: Jitter-induced Signal and the corresponding error.

called the jitter. Especially in high speed systems, jitter could be assumed as one of the limiting factors for the speed and accuracy of the system. The intention of this sub-section is to find the voltage error caused by the jitter in the high speed sampling system of the current thesis. To transfer the jitter to the voltage and see its effects, the root mean square (RMS) value of the slope of voltage is used as the transfer factor. In other words, the variance of the error in the jittered signal is given by the multiplication of the variations of the signal and the variance of the jitter. It is assumed that the jitter has normal distribution with variance of δ_ς^2. Thus for a given signal $s_F(t)$ at the input of the sampler, the variance of the jitter-induced signal can be written as [76]:

$$\delta_{SH}^2 \ = \ (\frac{1}{T} \int_0^T (\frac{ds_F(t)}{dt})^2 dt) \times \delta_\varsigma^2 \tag{2.16}$$

The substitution of an input sine wave such as Eq. (2.5) into Eq. (2.16) results in jitter-induced noise power of the signal [76]:

$$\delta_{SH}^2 \ = \ 2(\pi f_n k_n \, a_n(t)\delta_\varsigma)^2 \tag{2.17}$$

However, the local oscillator specification is normally expressed as the phase noise power (δ_{PN}^2) instead of the jitter. The variance of the jitter has a direct relationship with the phase noise of the oscillator:

$$\delta_{PN}^2 \ \approx \ (2\pi f_s)^2 \delta_\varsigma^2 \tag{2.18}$$

By substituting the Eq. (2.18) into the Eq. (2.17), it is concluded that the ratio of the power of the jitter-induced error on the sampled signal to the phase noise power of the local oscillator is $(\frac{f_n}{f_s})^2$. Thus, the jitter on the sampling clock results in the phase noise that will be highlighted with the factor of $(\frac{f_n}{f_s})^2$ while being transfered to the radio frequency (RF) sampled signal.
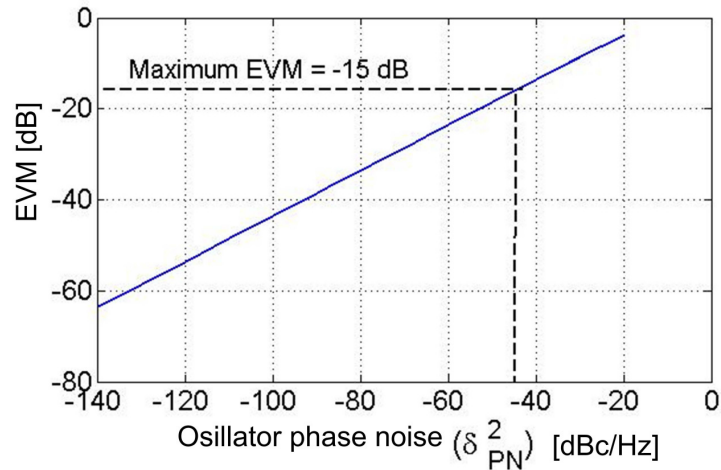
Figure 2.9: Simulated EVM in dB versus phase noise variance for UMTS signal,δ_{PN}^2.

To clarify the role of the jitter in the target dual-band receiver of the current research, the theoretical jitter concept is applied in simulation and the result is reported. The Parameters used in the simulation obey the specifications mentioned in Section 1.5 and the set up illustrated in Fig. 1.20. Besides, the following considerations are made for the simulation:

- Random data is generated based on a pseudo random number generator (PRNG) in Matlab with the command *randn* [50].

- It is weighted with the desired average power density of the oscillator phase noise (δ_{PN}^2).

- The ratio $(\frac{f_n}{f_s})^2$ is multiplied with the phase noise and then low-pass filtered to narrow the bandwidth of the noise signal. The considered desired bands are spectrally located at 2142.5 MHz and 2472 MHz for the UMTS and WLAN signals respectively. The sampling frequency is 676 MHz.

- This random error is imposed to the phase of the desired signal which is the addition of UMTS and WLAN signal. Each signal is filtered separately and it is compared with the original non-jittered signal. The resulting error vector magnitude (EVM) in dB versus phase noise variance (δ_{PN}^2) is depicted in Fig. 2.9.

As it is illustrated, the oscillators with phase noise of less than -42 dBc/Hz have acceptable performance in such an application. They can provide EVMs less than the maximum boundary EVM of UMTS which indicates the acceptable performance for the sampler. However, generally the oscillators with highly pure spectrum such as crystal oscillators are employed in such applications [77]. So the jitter is not a problematic issue here.

The same simulation is done for the WLAN signal. It reveals that the jitter has even looser requirement for the WLAN application. Thus, the result is not included in the dissertation. The effect of jitter for the general input signal case is discussed in [78] and [79].

2.3 RF front-end components

As mentioned in Section 2.1, the signal down-conversion in the sub-sampling receivers are done by intentionally aliasing the desired signals to the Nyquist band. This provides high integrability and flexibility in the frequency plan of the receiver due to the elimination of the mixer. However, the noise of the front-end becomes a critical issue because of the noise folding along with signals to the desired band. Moreover the noise of the S/H is typically high due to the thermal noise effects as discussed in Section 2.2. Thus, there are special expectations from the RF front-end components in the sub-sampling architecture to mitigate the mentioned noises as much as possible. These expectations and trade-offs are addressed in the following section.

2.3.1 RF noise filter and LNA

An abstracted model of a dual-standard sub-sampling front-end is depicted in Fig. 2.10. It consists of several filter and LNA sections. The LNAs are suppose to increase the magnitude of the weak signals received to the antenna to the desirable level for the receiver. The filters have the important role of keeping the desired signal untouched while attenuating all the undesired signals and noise contributers.
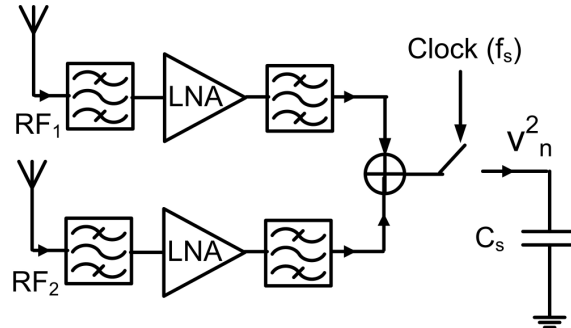
Figure 2.10: Illustration of an abstracted model of the dual-standard sub-sampling front-end.

In order to quantify the functionality of the front-end components especially to mitigate the noise of the sub-sampling architectures, a comprehensive noise analysis is performed. The role of the RF noise filters and LNA sections are investigated.

An equivalent block diagram of Fig. 2.10 for noise analysis is depicted in Fig. 2.11. The $S_{N,RFn}$ and $S_{N,LNAn}$ are the input referred noise power densities of the RF sources and the LNAs. The $S_{N,mux}$ is the input referred noise power spectral density of the multiplexer and k_n is the total signal gain seen from the antenna terminal to the output of the front-end module at the nth carrier frequency. The equivalent noise bandwidth of each signal is Δf_n. The Δf_{SH} is the equivalent noise bandwidth of the S/H block in order to accommodate the cumulative noise bandwidth of all the desired signals. To simplify the following analysis, the switching noise of the capacitor is considered as the only noise source in the S/H block, and the RC-filtered white noise is replaced by the band-limited white noise with the same power within an effective bandwidth Δf_{SH}. By employing bandpass sampling, the wide-band kT/C noise is folded due
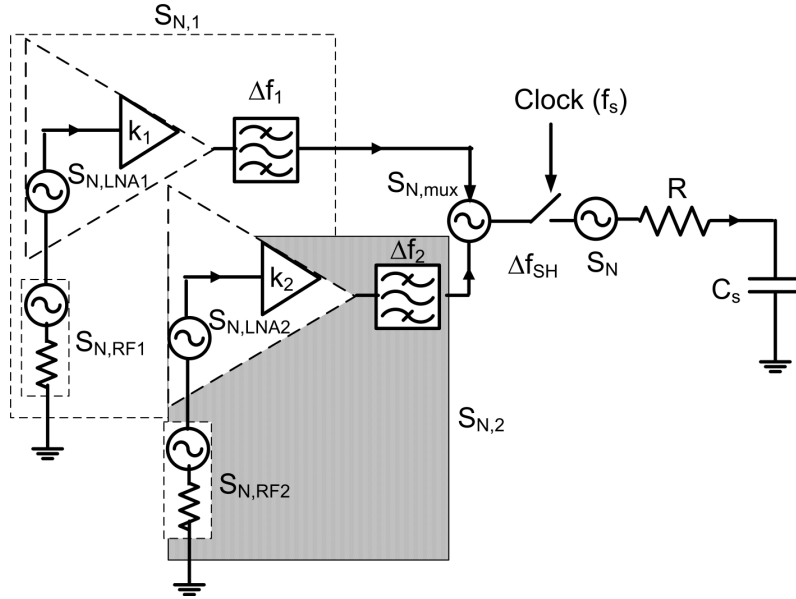
Figure 2.11: Illustration of an equivalent noise model of a dual-standard front-end.

to the effect of the sampling. Thus the resulting SNR by the band-limited signal is lower than the equivalent low-pass system in the presence of the same noise source due to noise folding. The degradation of the SNR is given as [80]:

$$SNR_{red} = \frac{2\Delta f_{SH}}{f_s} \tag{2.19}$$

Thus all the other effective noise bandwidths of the system will be affected by the same concept mentioned in Eq. (2.19). The noise power spectral density referred to the first receiving path for the bandpass sampling system is written [81] and [82]:

$$S_{NT1} = [S_{N,RF1} + S_{N,LNA1}] \times \frac{2\Delta f_1}{f_s} + \left[\frac{S_{N,mux} + S_{N,2}}{(k_1)^2}\right] \times \frac{2\Delta f_{SH}}{f_s} + \left[\frac{S_N}{(k_1)^2 \cdot f_s}\right] \tag{2.20}$$

where S_N is the power density of the S/H block and $S_{N,2}$ is the equivalent noise power spectral density of the second receiving chain refer to the first chain input. For simplicity, the gain contribution of the multiplexer is ignored.

The same calculation is applicable to derive the noise power spectral density referred to the input of the second chain:

$$S_{NT2} = [S_{N,RF2} + S_{N,LNA2}] \times \frac{2\Delta f_2}{f_s} + \left[\frac{S_{N,mux} + S_{N,1}}{(k_2)^2}\right] \times \frac{2\Delta f_{SH}}{f_s} + \left[\frac{S_N}{(k_2)^2 \cdot f_s}\right] \tag{2.21}$$

Eqs. (2.20) and (2.21) reveal several important properties of the sub-sampling architecture and the corresponding front-end components:

- The noise figure (NF) of the S/H block is generally high resulting in a high noise figure for

the receiver. This effect is controllable by increasing the gain of the front-end. According to Eq. (1.3), the noise of the subsequent blocks can be mitigated by increasing the gain of the former blocks. This effect is also visible in Eq. (2.20).

- On the other hand, increasing the gain has undesirable effects on the noise performance of the receiver. By increasing the in-band gain of the front-end, along with the desired signals the in-band noise is amplified. In other words, the noise contribution in-band is higher due to the injection of more noise to the receiver.

- From Eqs. (2.20) and (2.21) it can be seen that the other determining factor in the noise performance of the receiver is the noise bandwidth of the filters, S/H block and the sampling frequency. The first terms of Eqs. (2.20) and (2.21) indicate that the noise power of the front-end is multiplied by the ratio of the front-end noise bandwidth to the sampling frequency. Increasing the sampling frequency decreases the noise power of the total chain. Alternatively, decreasing the noise bandwidth improves the noise performance. Consequently, it can be stated that it is desirable to increase the ratio of the sampling frequency to noise bandwidth of the receiver. The same discussion is valid for the second terms of Eqs. (2.20) and (2.21). The improvement in the ratio of the sampling frequency to the bandwidth of the sampler has direct effect on mitigation the noise power of the receiver.

2.3.2 ADC and dynamic range

The most important parameters for the ADCs employed in the RF sampling architectures are dynamic range, power dissipation, sampling frequency and the size. In the current research since the implementation is intended to prove the concepts (not the real production), the power dissipation and size of the ADC are not emphasized. The requirement of the sampling frequency of this architecture is discussed extensively in Chapter. 3. The required dynamic range of the ADC to accommodate the signals of the current research is investigated here. The ADC dynamic range for a bandpass sampling receiver for the UMTS standard may be calculated by using the different tests specified in the 3GPP standard [5] such as:

- Reference sensitivity test

- Maximum signal level

- In-band blocking test

To find the most stringent requirements for the ADC's dynamic range, the in-band blocking test case is investigated. The main reason is that it is possible to handle the first two cases by using gain adjustment. However for the last case, the receiver must work properly in the existence of an interferer with strength of P_{Blk} dBm when the power level of the wanted signal in the blocking test scenario is -114 dBm ($P_{R,DPCH}$). Thus the minimum dynamic range of

the ADC must be equal to or greater than [83]:

$$DR_{ADC} = P_{Blk} + PAR - (P_{R,DPCH} - \Delta G \qquad\qquad (2.22)$$
$$- (E_b/N_t)_{eff} + 10log(PG) - N_I)$$

where the effective bit energy to noise density (E_b/N_t) including an implementation margin for various baseband imperfections is 7 dB to meet the BER requirement [84], ΔG is the tolerance due to non-perfect gain control, PG is processing gain equal to 25 dB [85] and PAR is the peak to average ratio. The N_I in the formula is the noise and interference contribution which is 3 dB according to the assumed noise budget (50 percent) specified in Chapter 4 [86]. As it is mentioned, the in-band blocking test is used to derive the dynamic range. According to the 3GPP standard, the receiver must tolerate an in-band blocker of -44 dBm at the offset of 15 MHz. The PAR is chosen equal to 9 dB from an ADS simulation. Thus, the dynamic range of the ADC is equal to 65 dB. The requirements for the ADC can be derived according to the achieved DR. For example, the required number of bits for a N-bit analog-to-digital converter can be calculated from [83]:

$$SNR_{dB} = 6.02 \cdot N + 1.76 + 10 \cdot log(\frac{f_s}{2\Delta f_n}) \qquad\qquad (2.23)$$

where Δf_n is the information bandwidth. Thus, an ADC with at least 10.5 bits is required for the calculated dynamic range without oversampling. It may be required to have 12 or 13 bits to reach to an effective dynamic range of 65 dB. Employing oversampling provides the possibility to increase the dynamic range with the same N-bit ADC.

The same calculation is applicable for the WLAN signal. The maximum receiver input power is -20 dBm according to [7] providing the packet error rate (PER) less than 10% for any supported modulation signal or data rate. The standard specifies the receiver sensitivity of -82 to -65 dBm depends on data rates. The minimum required SNR (SNR_{Req}) depends on modulation type and data rate. It changes between the 6.02 dB for 6 Mb/s to 24.56 dB for 54 Mb/s. To provide the required signal to noise ratio, the acceptable noise and distortion level for WLAN (P_N) is -88.06 to -89.56 dBm respectively. The selected data rate is 54 Mb/s which corresponds to the P_N of -89.56 dBm. The Peak to average ratio (PAR) in theory is 17 dB for this standard similar to IEEE 802.11a standard. Thus the DR_{ADC} is calculated 53 dBm which corresponds to 9 bits. The ADC requirement is tabulated in Table 2.1.

Table 2.1: ADC Specifications for UMTS and WLAN UE [5], [7].

	UMTS	IEEE 802.11g
DR_{ADC} (dBm)	65	53
ENOB	10.5	9
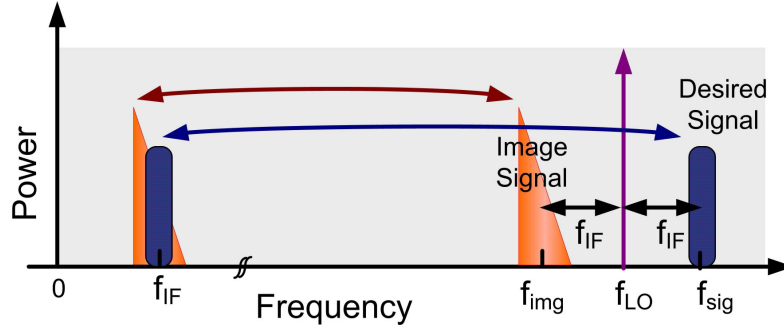
Figure 2.12: Illustration of the image problem in conventional receivers.

2.4   Image distortion

The concept of image signals is well known in traditional receivers where mixers are used for down-conversion. Consider the situation where a pure cosine at frequency f_{LO} is applied as the local oscillator signal, and the output is observed at the intermediate frequency f_{IF}. In this case an input signal at $f_{sig} = f_{LO} + f_{IF}$ as well as an image at $f_{img} = f_{LO} - f_{IF} = f_{sig} - 2f_{IF}$ both result in an output contribution at the intermediate frequency f_{IF} as illustrated in Fig. 2.12. This leads to distortion of the desired signal.

From the above discussion, it is worth nothing from Eq. (2.6) that the image signal related to each carrier frequency f_n in conventional receivers is given by:

$$s_{img}(f) = \sum_{n=1}^{N} s_{img,n}(f - f_{img,n}) + \sum_{n=1}^{N} s^*_{img,n}(f + f_{img,n})$$

$$= \sum_{n=1}^{N} s_{img,n}(f - (f_n - 2f_{IF,n})) + \sum_{n=1}^{N} s^*_{img,n}(f + (f_n - 2f_{IF,n})) \tag{2.24}$$

Where $s_{img,n}$ is the impending image signal of $s_{F,n}$ at the output of the front-end. One could hope that this type of problem is alleviated in sub-sampling receivers since the mixer is absent. However, the problem of image signal still exists due to the sampler — even in a more severe form due to folding of the signals and noise in multiples of sampling frequency as seen from Eq. (2.8).[4]

To formulate the image in sub-sampling receivers, the signals are replicated in multiples of the sampling frequency as seen from Eq. (2.8). Thus along with the desired signals at f_n, any impending disturbance at $f_{img,n}$ are also folding in the multiples of sampling frequency. It can be seen from the Eq. (2.8) and (2.24) that the image signals at the output of the S/H block are

---

[4]In principle this phenomenon also exist in traditional multiplying mixers. However, the mixers are generally designed to have a
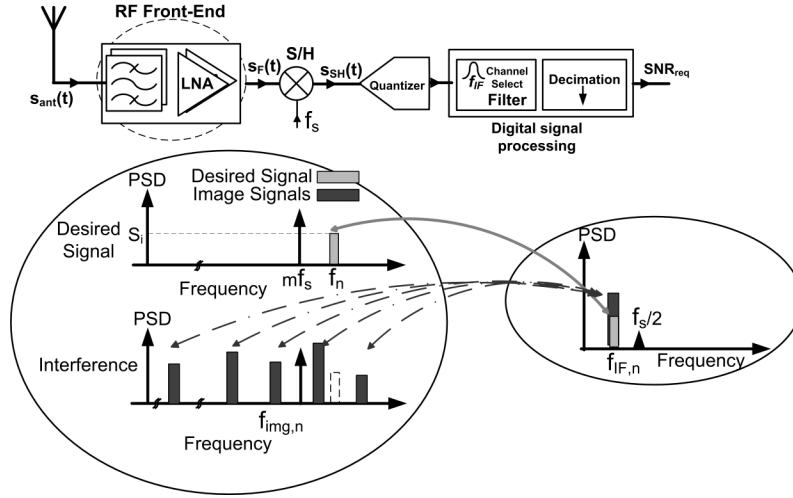
Figure 2.13: Block diagram of the RF sub-sampling receiver and the corresponding image problem scenario.

located at:

$$
s_{imgSH}(f) = f_s \sum_{m=-\infty}^{\infty} \sum_{n=1}^{N} s_{img,n}(f - (f_{img,n} + m\,f_s)) + f_s \sum_{m=-\infty}^{\infty} \sum_{n=1}^{N} s_{img,n}^{*}(f + (f_{img,n} + m\,f_s))
$$

$$
= f_s \sum_{m=-\infty}^{\infty} \sum_{n=1}^{N} s_{img,n}(f - ((m\,f_s \pm f_{IF,n})) + f_s \sum_{m=-\infty}^{\infty} \sum_{n=1}^{N} s_{img,n}^{*}(f + (m\,f_s \pm f_{IF,n}))
$$

$$(2.25)$$

From Eq. (2.25) it is concluded that since the signals are replicated in the infinite values of
"'m"', numerous signals play the role of the image disturbance for the desired signals in the
sub-sampling architecture. Conclusively in sub-sampling receivers, all the signals at the $\pm f_{IF,n}$
spacing from the multiples of sampling frequency due to the sampling are considered as image
distortions for the desired band. For the desired signal $S_{F,0}$ or its complex conjugate $S_{F,0}^{*}$, the
corresponding image distortions can be written:

$$
S_{F,0}: \qquad f_{img,0} = m\,f_s \pm f_{IF,0} \quad \text{for} \ \ m = 0, \pm 1, \ldots \tag{2.26}
$$

$$
S_{F,0}^{*}: \qquad f_{img,0} = -m\,f_s \mp f_{IF,0} \quad \text{for} \ \ m = 0, \pm 1, \ldots \tag{2.27}
$$

where $f_{img,0}$ is the image distortions for the desired signal $S_{F,0}$. The block-diagram of the
receiver and the corresponding image scenario is shown in Fig.2.13. Since there are numerous
images for each desired signal, the most challenging part of the image problem arises from the
closest images to the desired band ($m = \pm \text{round}(\text{fc}/\text{fs})$). The closest images to the desired band
provide the most stringent requirement for the receiver's selectivity since they are more difficult
to suppress them with the image-rejection (IR) filters. This sets a very though requirement
in selection of sampling frequency and frequency plan of the receiver to cope with the image
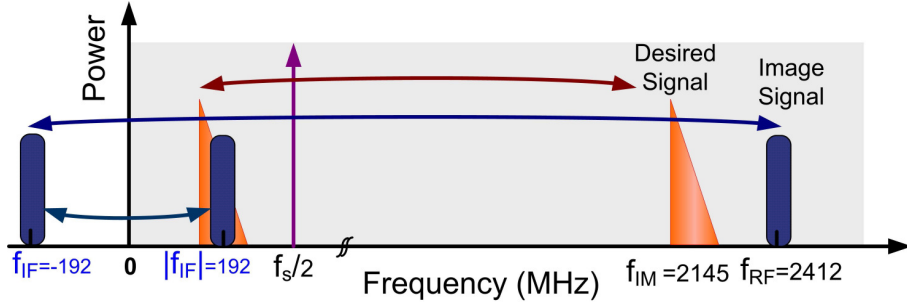
Figure 2.14: Illustration of Image problem in the current illustrative Example.

problem since the image signals are tightly dependent to the sampling frequency as seen in Eq. (2.25).

In the multi-band sub-sampling receivers, the signals from several different sources may act as the images for desired signals: (i) it could be originated from an out-of-band signal located at the image signal spacing from the desired signal band or (ii) one of the other desired signals may play the role of image for the desired signal.

To cover and eliminate all the potential sources of image signals in the multi-band scenarios, the image problem must be verified for each of the desired signals individually with the impending image signals out of the reception band. Moreover, the image requirement must be confirmed for each pair of desired signals separately. The solutions to the image problem in sub-sampling architecture are proposed in the next sections.

2.4.1 An illustrative example

One example illustrating the image problem is in the reception of a UMTS FDD call while the receiver is located fairly close to a WLAN access point — a very realistic situation. To simplify things, first assume that there is no selectivity in the front-end wrt. the WLAN downlink signal. In this example, the UMTS call is located at $f_0 = 2145$ MHz, and the WLAN data is transferred in the $f_1 = 2412$ MHz band. Using the standard procedure for finding allowed sampling rates [2], [3] implies that a sampling frequency of $f_s = 651$ MHz should be an acceptable choice. However, with this choice of sampling frequency, the WLAN signal acts as an image signal for the UMTS signal as illustrated in Fig. 2.14.

From Eqs. (2.9) and (2.10) we get that for UMTS, $S_{F,0}$ at the intermediate frequency $f_{IF} = f_0 - 3f_s = 192$ MHz and the complex conjugate $S_{F,0}^*$ at $-f_{IF} = -f_0 + 3f_s = -192$ MHz. For WLAN the similar situation is the signal $S_{F,1}$ at the intermediate frequency $f_{IF} = f_1 - 4f_s = -192$ MHz and $S_{F,1}^*$ at $-f_{IF} = -f_1 + 4f_s = 192$ MHz. This means that the $S_{F,1}$ falls directly on top of $S_{F,0}$ — i.e. the WLAN down-link signal acts as an image signal for the UMTS reception.

In the description above the selectivity provided by the front-end has been completely ignored. In a practical case there must obviously be some selectivity. But the needed and costly (form factor, price, power) selectivity can be reduced by a more careful and proper selection of the sampling rate and intermediate frequency than what is shown in the example above.

2.5 Discussion and summary

The selected receiver architecture of the current research is the "'RF sub-sampling architecture"'. This architecture is investigated and discussed throughly in this section. The important issues of the receiver are highlighted and presented. The major non-idealities of the receiver by considering the sampler as the focal component are "'Thermal noise"' and "'Jitter"'. The latter problem is not a critical issue in the case-study of this thesis. The thermal noise of the sampler depends on the sampling capacitor/frequency and the bandwidth of the S/H block. The effect of each factor on the total signal to thermal noise ratio of the receiver is presented. Beside the S/H as the focal block, the role of the LNA, RF filters and ADC is investigated. The image problem in sub-sampling architecture is described.

Chapter 3

Frequency planning of the Receiver

The main task of the radio frequency (RF) receiver in communication systems is to translate and process the received radio frequency signal to its corresponding digital bit stream, while adding minimum noise to it. The receiver technique employed in the current dissertation is the sampling technique. The frequency down-conversion is done by intentionally aliasing the signals from RF to the Nyquist band. This method is desirable for multi-band applications by introducing higher level of integration. On the other hand, the frequency plan corresponding to the multi-frequency scenarios of such a receiver is very complicated.

In general, the frequency plan for a multi-standard system is substantially more complex than the combination of several single-frequency systems. Specifically for sampling receiver, the case is more severe since several signals, their replicas in multiples of the sampling frequency and the images of all signals are involved in the frequency plan of the receiver. In addition to the desired signals of the scenario, numerous noise and blockers may be folding along with desired signal.

The aim of this chapter is to provide a complete understanding of the frequency planning for the multi-band sub-sampling receivers. The chapter is organized as follows: A brief introduction is provided to give an overview of the problem of frequency planning associated with this type of receivers. Special issues should be handled which is discussed thoroughly in Section 3.1. The selection of sampling frequency has an important role in down-converting several signals to non-overlapping portions of the Nyquist band. This is investigated intensively from different viewpoints in Section 3.2. A complete algorithm is proposed consequently for the selection of the sampling frequency by obeying all the required constraint. A new sub-sampling based architecture is proposed in Section 3.3. The main intention of introducing this architecture is to reduce the problem of image in sub-sampling receivers by sensing the environment and adapting the sampling rate of the receiver to the best possible selection. The proposed concepts are supported by simulations on a sub-sampling receiver provided in Section 3.4. Finally, Section 3.5 provides a summary and conclusion of the presented discussion in this chapter.

3.1   Introduction

The trend toward multi-feature homogeneous piece of hardware makes the design of the transceivers more and more complex. The single hand-held device is supposed to work as the mobile phone, personal digital assistants (PDA), global positioning system (GPS), video camera and so on. The receiver must be able to receive all the signals in high frequencies and translate them to their corresponding digital bit streams. In order to perform this operation, finding the appropriate architecture and the requirements of the analogue circuitry is the first complex task. The requirements on each analogue block are vary enormously depending on the selected standards of the application and selected architecture. Totally, it forms a complicated procedure to organize all the decisive factors to receive several standards with high performance, low complexity and acceptable power consumption. Moving most of the process to digital circuitry has the advantages of reducing this risk immensely.

Consequently, making good system level investigation and decision have crucial role in the performance of the multi-band receivers. According to the time of production, time to market and available technologies, the best architecture should be selected. The frequency plan of the receiver should be done according to the selected architecture, corresponding blocks and the partitioning between the analogue and digital circuitry. With the available technologies, most of the receivers still contain notable analogue and mix signal parts beside digital signal processing parts [87], [88] and [89]. This reduces the flexibility and put more constraint on the design of the front-end. The more digital circuitry involved in the design, the more flexibility will be obtained.

It is mentioned that sub-sampling is a technique based on undersampling the modulated signal to perform the frequency translation by harmless aliasing. It provides higher level of integration by the ability of processing several signals with one receiver chain. By employing the sub-sampling technique the signals are replicated in the frequency spectrum and the corresponding low frequency signals can be filtered and further processed. An example of a multi-signal sampling scenario is depicted in Fig. 3.1. The RF signals are down-converted to lower frequencies by sampling. The replicas of the signals are folded in the segments of the Nyquist band at multiples of the sampling frequency. A harmless translation of signals in one-to-one order through sampling is shown in Fig. 3.1(a). The signals in each segment have the same frequency order as their RF signals. Fig. 3.1(b) illustrates the case that the signals and their images are interfering with each other. Consequently, the useful information is lost and the signals are not extractable to their corresponding bit streams. Fig. 3.1(c) depicts an acceptable aliasing of several signals to non-overlapping portions of the Nyquist band through sampling. Depending on the existence of the original signal or its image in the Nyquist band (according to the Eq. 2.6), the equivalent translated intermediate frequency (IF) signal is selected. In this case, the signals at IF may not have the same order as the original RF signals. The selection of the signal or its complex conjugate is depicted in Fig. 3.2. By focusing on the positive spectrum in the figure, the selected signal in the Nyquist band could be the original signal (up) or its complex conjugate (down). It depends on which signal exists in the band of interest $[0{:}f_s/2]$.
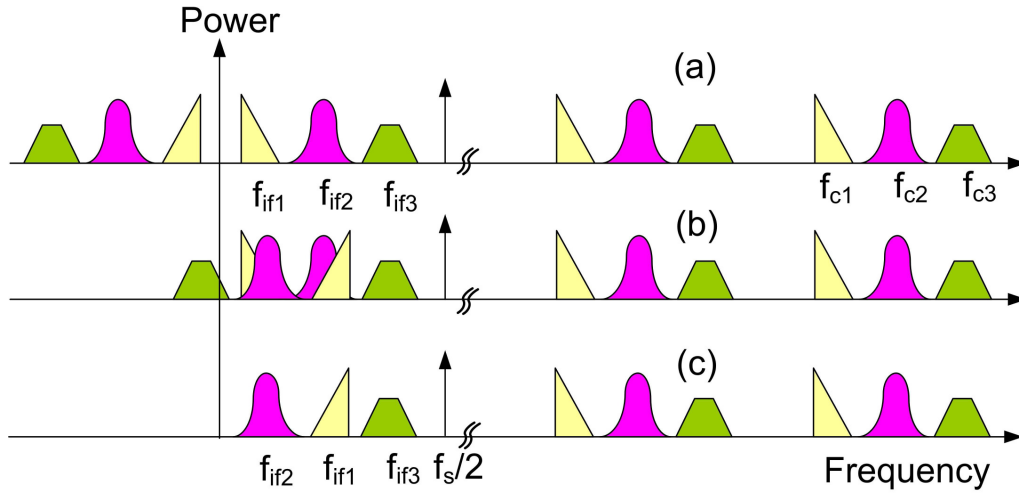
Figure 3.1: Illustration of the spectrum of multi-signal sampling (a) harmless one-to-one translation, (b) unacceptable down-conversion due to aliasing, (c) folding the RF signals to non-overlapped portion of the Nyquist band at IF.
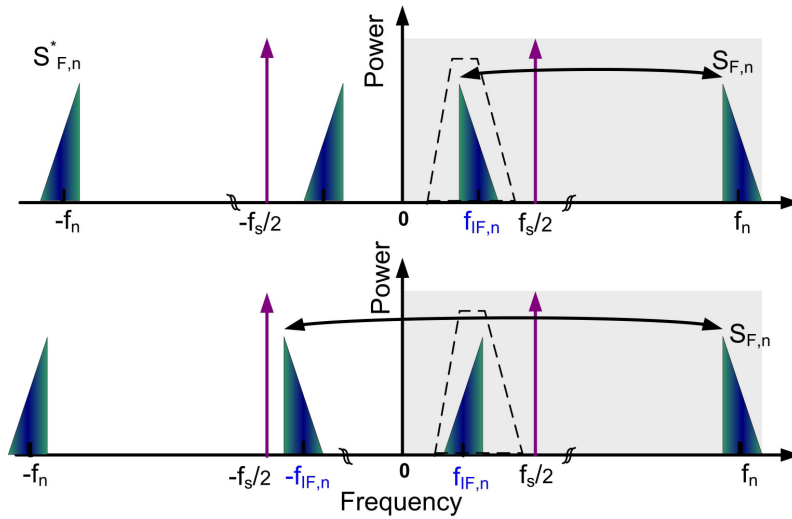
Figure 3.2: Illustration of a band-pass signal with carrier frequency f_n and bandwidth Δf_n and the equivalent signal at IF in the Nyquist zone. The focus is on the positive part of the frequency spectrum.

The filtered IF signal could be the same as the RF signal or the mirrored version of the original signal. This should be considered while doing the further signal processing.

Governing the signals and their images in non-overlapping portions of the Nyquist band has crucial role in the frequency plan and the reception quality of the receiver. In other words, harmless aliasing which is the intended goal of the sub-sampling technique could be realized through proper selection of the sampling frequency and the correspondent frequency plan. This is discussed extensively in this section.

3.2   Calculation of sampling frequency

The choice of the acceptable sampling frequencies to avoid the disparaging aliasing plays an imperative role in the sub-sampling receivers, especially when simultaneous reception is intended. The disparaging aliasing occurs when the associated IF signals violate the Nyquist criteria or any interference arises in the Nyquist band. The acceptable selection of the sampling frequency to avoid the disparaging aliasing is governed by several parameters such as the carrier frequency of the signals, their associated bandwidths and desired intermediate frequencies.

Given that there are several expected and unexpected bands in the frequency spectrum with the high probability of causing interference in the desired band, first an interference profile is developed in this section. This profile checks the minimum frequency distance from any disturbing contribution to the desired intermediate frequency versus the chosen sampling rate in the Nyquist zone. It provides an overview of how the frequency distances from other signals of the scenario are varying versus the sampling frequency. This profile is applicable to all the desired and unwanted signals at the antenna.

Since this distance is dependent to the sampling rate, it can be interpreted that the sampling frequency is employed as a control tool to place the interfering signals (other desired or unwanted signals) in appropriate frequency distances from the desired signal: (i) appropriate spacing means that the undesired signals are at a distance from the desired signal which is suppressible by the provided selectivity of the front-end at that frequency. This approach is further used in Chapter 4 to find a technique for determining the required selectivity of the receiver in each disturbance frequency offset. (ii) From the other desired signals, it means that it should be no interference in the Nyquist zone between them. By this profile, the relative situation of each signal to all the other existing signals will be detected.

The interfering profile employed in several steps to check all the requirements for an acceptable sampling frequency. The total steps form a generic algorithm for calculation of the proper sampling rate in the sub-sampling receivers.

The algorithm starts with developing the interfering profile to check the Nyquist criterion for each signal individually. Furthermore, the case is considered that several desired in-band signals should be translated to the portions of the Nyquist band and do not overlap with each other. Thus constraint is derived to prohibit the overlap of the desired information bands in the IF after down-conversion. This constraint is added to the derived constraint from the previous step to extend the single frequency f_s requirements to a scenario containing multiple signals.

The sampling frequency requirements are pursued by introducing a technique on how to select the sampling frequency based on sensing the environment and adapting the sampling rate of the receiver to the best possible selection. This technique is extremely useful in mitigating the image noise problem of the receiver and improving the signal to noise ratio (SNR) of the receiver significantly.

The last part of the sampling frequency selection is based on mitigating the noise in the front-end. It is discussed in Section 2.2 that the major noise sources of the sample and hold (S/H) block are dependent to sampling frequency [81] and [82]. Thus one of the considerations while

selecting the sampling frequency is to achieve to an acceptable noise power level of the front-end.

The combination of the mentioned profile (constraint in Sections 3.2.1, 3.2.2, 3.2.3 and 3.2.4) with the selectivity requirements of the front-end gives the best possible sampling rate set for the sub-sampling receivers. The constraint are summarized in the proposed algorithm for selection of sampling rate at the end in Section 3.2.5. The selectivity requirements is discussed in Chapter 4.

The following constraints are explained throughout this section:

- Each signal individually should be spaced properly within the Nyquist band. This is discussed in the Section 3.2.1.

- All the desired signals of the scenario must be down-converted to non-overlapping portions of the Nyquist band. The requirement on the sampling frequency to fulfill this requirement is described in the Section 3.2.2. The case for handling the undesired signals is described in Chapter 4.

- A novel technique is introduced in the current dissertation to select the sampling frequency based on adapting the receiver with environment. The idea is to enhance the reception quality of the receiver and the correspondent frequency plan by considering the neighbouring milieu as a decisive factor. It provides the chance of down-converting the weakest interferes along with the desired signal to the band of interest while all the other interferes could be properly filtered in the front-end. The requirement related to the milieu adapting techniques are discussed in the Section 3.2.3.

- In sub-sampling receivers, a part of the noise contribution from the receiver is governed by the sampling frequency. Thus the noise contribution from the selected f_s must be checked to be below the required level specified in the noise budget of the receiver. This is explained in Section 3.2.4.

- Combining all the mentioned requirements together forms an algorithm summarized in in Section 3.2.5. constraints are organized according to their priority and outlined in three steps to select the best sampling frequency for each application.

The mentioned steps are performed by using a novel interfering indicator which is introduced in this chapter. This indicator is employed in a recurrence manner by considering all the existing signals in the scenario for all the above mentioned steps. The total steps form the interfering profile. The interfering profile is an elegant way of monitoring the distance from each desired signal and all the other existing disturbing contributions in the Nyquist zone for each sampling frequency. This can be used to allocate the signals properly in the Nyquist zone by the correct selection of the sampling rate. The sampling frequencies providing proper allocation of the signals in the Nyquist zone could be selected. Proper allocation of signals is interpreted as adequate separation from the boarders of the Nyquist zone and all the other signals of the scenario.

Interfering indicator and interfering profile

In the multi-standard scenario, several signals $S_{F,0}, S_{F,1}, \ldots S_{F,N}$ are down-converted to lower (and higher) frequencies by sub-sampling. A double-frequency scenario is assumed in this dissertation which makes the $S_{F,0}, S_{F,1}$ the desired signals and all the rest $S_{F,n}$ for $2 \leq n < N$ as the undesired blockers. It should be noted that since the interference with the boarders of the Nyquist zone is prohibited, these boarder's frequencies at 0 and $f_s/2$ are treated as two of the interfering signals, $f_{IF,n}$. The desired signal under investigation is still assumed to be $S_{F,0}$ (all the required steps is the same for $S_{F,1}$ consequently and it is not repeated).

In sub-sampling technique, the signals are down-converted to the IF through intentional aliasing. It is also worth noting from Eq. (2.8) that the envelope and phase signals of the signal n is only found directly at DC in the special case where f_n/f_s is an integer. In all other cases, the information is found at an intermediate frequency ($0 \leq |f_{IF}| < f_s/2$):

$$S_{F,n}: \quad f_{IF,n} = f_n - round(\frac{f_n}{f_s})f_s \tag{3.1}$$

$$S_{F,n}^*: \quad f_{IF,n} = -f_n + round(\frac{f_n}{f_s})f_s \tag{3.2}$$

The resulting intermediate frequencies accept any positive or negative value in the Nyquist band. This concept is in analogy to high/low side mixing in the traditional analog multipliers.

It can be seen that the intermediate frequency is chosen according to Eq. (3.1) for reception of $S_{F,0}(f)$ or Eq. (3.2) for $S_{F,0}^*(f)$. This means that f_{IF} follows from a selection of f_s. In other words, the intermediate frequency f_{IF} is not a degree of freedom — but f_s is. Thus, the proper frequency plan of the receiver could be done through the appropriate selection of the sampling frequency.

To make a good selection of the sampling rate f_s it is thus needed to take each disturbing signal one by one and see if the required frequency distance between $f_{IF,0}$ and the closest distortion products is provided at each specific f_s. The $f_{IF,0}$ is assumed to be the intermediate frequency of the desired signal occupying the bandwidth Δf_0. There exist two distortion products to consider for each signal similar to Eqs. (3.1) and (3.2). For the $S_{F,n}(f)$ signal the smallest frequency distance to the desired intermediate frequency $S_{F,0}(f)$ which is called the "'Interfering Indicator"' is:

$$\Delta F_{n,0} = ||f_{IF,n}| - |f_{IF,0}|| - \frac{\Delta f_n + \Delta f_0}{2} \tag{3.3}$$

and for $S_{F,n}^*(f)$ the similar smallest distance is:

$$\Delta F_{n,0}^* = -||f_{IF,n}| - |f_{IF,0}|| + \frac{\Delta f_n + \Delta f_0}{2} \tag{3.4}$$

The illustration of interfering indicator is shown in Fig. 3.3.

It shows the distance from each disturbing contributors at each sampling frequency. It

includes the distance from boarders of the Nyquist band (which treated as disturbing contributions in the current dissertation to reach to a unique methodology). By repeating the calculation done in Eqs. (3.3) and 3.4 for all the interfering contributors (other desired or undesired signals of the scenario), a complete overview of the location of the IF signals in the Nyquist zone is apprehended. The sampling frequency that provides the best allocation of the signal in intermediate frequency would be selected as the most appropriate sampling rate of the scenario.

To repeat the interfering indicators for all the disturbing contributors, an interfering profile is developed. The profile can thereby be written as:

For each sampling frequency from all valid f_s

  Initialize $\Delta F_{min} = 0$

- For disturbing signal p=1:N
  - Calculate $\Delta F_{p,0}$ from Eq. (3.3)
  - If $|\Delta F_{p,0}| > \Delta F_{min}$ then $\Delta F_{min,abs} = |\Delta F_{p,0}|$
  - else go to the next f_s
  - Calculate $\Delta F_{p,0}^*$ from Eq. (3.4)
  - If $\left|\Delta F_{p,0}^*\right| > \Delta F_{min}$ then $\Delta F_{min,abs} = \left|\Delta F_{p,0}^*\right|$
- end

  $\Delta F_{min,abs}[p] = \Delta F_{min,abs}$

  $f_s[p] = f_s$

end

---

where $\Delta F_{min,abs}$ gives the information about the closest signal to the desired band at each sampling frequency with no interference. Once this algorithm is used it is possible to check the minimum frequency distance from any disturbing contribution to the desired intermediate frequency versus the chosen sampling rate. The acceptable sampling frequency set is the assembly of the rates providing adequate separation of all the distortions from the desired signal. The adequate separation has two different meaning for the other desired or undesired contributors:

- For the other desired signals, adequate separation means the cumulative half of the bandwidth of two signals plus a margin for filtering. The reason is that when both signals are desired, any interference between them causes a part of the useful information to be missed. So they should be allocated far a part from each other, to avoid any interference which can be done by employing the mentioned interfering profile.
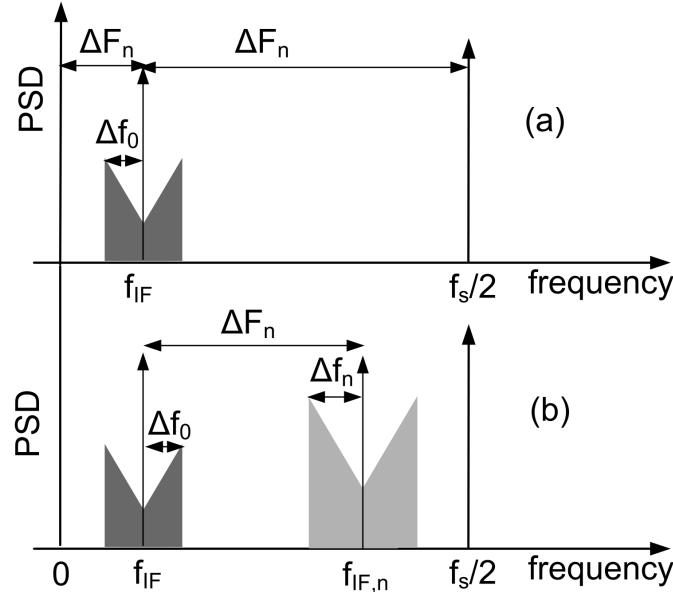
Figure 3.3: Illustration of the interfering indicator in intermediate frequency (a) to the boarders of the Nyquist zone and (b) to the other desired signal.

- The other undesired disturbing contributions should be located in a distance that is suppressible by the provided front-end selectivity. This is discussed more in Chapter 4.

3.2.1   Based on single-frequency requirement— Nyquist criterion

According to the classic band-pass sampling theorem, the sampled signal is re-constructible if the sampling rate is at least [90]:

$$f_s^{min} = 2f_u / (\left\lfloor \frac{2f_u}{\Delta f_n} \right\rfloor) \tag{3.5}$$

where f_u is the upper boundary of bandpass signal $(f_n + \Delta f_n/2)$ and f_n is the carrier frequency of the nth signal. The $\lfloor x \rfloor$ denotes the largest integer less than or equal to x. In several previous research [91], [92], [93] and [94], it is seen that the minimum band-pass sampling rate is applied only for integer band positions in uniform sampling, i.e., $\left\lfloor \frac{f_u}{\Delta f_n/2} \right\rfloor$ is an integer [90]. The preliminary requirement depends on the position of the band-pass signal and its bandwidth.

To formulate the basic requirement for the sampling frequency, a band-pass signal with carrier frequency of f_n is assumed which occupies the frequency band $f_n - \Delta f_n/2 \leq f \leq f_n + \Delta f_n/2$ as depicted in Fig. 3.4. The position of the band is fractional. In other words, it is not necessarily an integer and it could be located any where in frequency spectrum. By sampling the mentioned band-pass signal with sampling frequency f_s replicas of signal is created represented by dashed-line signals in Fig. 3.4. From the figure, it could be graphically shown
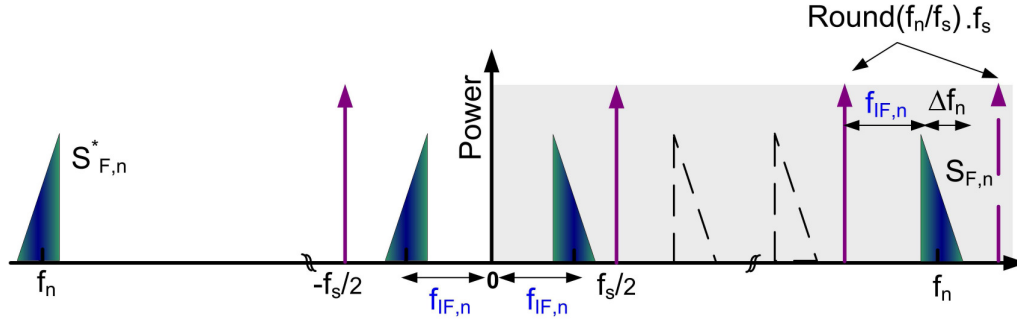
Figure 3.4: Illustration of the spectrum of an example band-pass signal with a fractional band position located at f_n and $-f_n$.

that the following expression is hold:

$$f_n - f_{IF,n} = round(\frac{f_n}{f_s}) \cdot f_s \tag{3.6}$$

and for the complex conjugate signal the similar equation is:

$$-f_n - f_{IF,n} = -round(\frac{f_n}{f_s}) \cdot f_s \tag{3.7}$$

Eqs. (3.6) and (3.7) indicate that by varying the carrier frequency versus sampling frequency, the signals may be down-converted to positive or negative portions of the Nyquist band. This is illustrated in Fig. 3.5. The carrier frequency and sampling frequency are swept in Eqs. (3.6) and (3.7) and the resulted IFs are plotted. It illustrates the concept of f_s dependency of the intermediate frequency in sub-sampling based receivers.

To take the advantages of harmless aliasing and translate the complete band to non-overlapping portions in lower frequency, the first constraint comes from the fact that the down-converted signals in the Nyquist zone should not interfere with the boarders of the Nyquist band $[-f_s/2; f_s/2]$. The complete two-sided signal containing the real and complex parts in frequency domain is modeled according to the Eq. (2.6). To avoid the interference with boarders of the Nyquist zone, the following constraint must be met:

$$-f_s/2 + \Delta f_n/2 < f_{IF,n} < f_s/2 - \Delta f_n/2 \tag{3.8}$$

However, it is not required to check this constraint recurrently for both sides of the two-sided signal. That is due to the fact that the translation to the negative IF is analogy to high-side mixing. Thus, checking for either positive or negative part of the Nyquist zone is sufficient. In the current dissertation, the positive part of the frequency spectrum is considered. The following constraint should be ensured in the positive part of the Nyquist zone [2]:

$$|f_{IF,n}| > \Delta f_n/2 \tag{3.9}$$
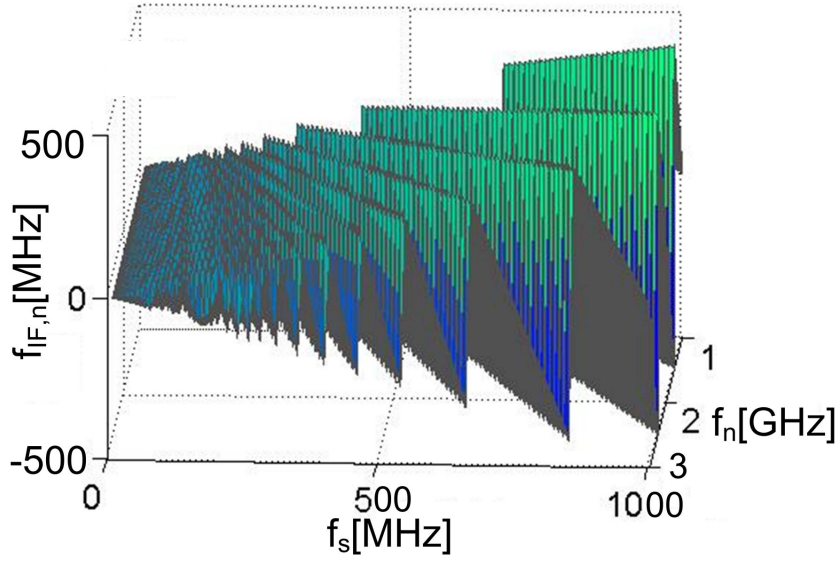
Figure 3.5: Simulated intermediate frequency, f_{IF}, versus the sampling frequency and carrier frequency.

$$|f_{IF,n}| < f_s/2 - \Delta f_n/2 \tag{3.10}$$

In other words to be immune from harmful aliasing in the positive spectrum, the replicas in each Nyquist segment should not overlap with the boundaries of that segment which may cause the interference of the signals in different segments with each other. This can be ensured in lower frequencies $[0 : f_s/2]$ by satisfying the constraint mentioned in Eqs. (3.9) and (3.10).

The mentioned technique guaranties harmless aliasing for each signal individually. In other words if only one signal comes at the antenna, fulfilling constraint in Eqs. (3.9) and (3.10) indicates that the signal could be extracted and translated to its correspondent digital stream. However it is not the case for many practical applications. If several distinct signals are to be processed in the receiver, the procedure of selecting the proper sampling frequency is much more sophisticated than satisfying only constraint presented in Eqs. (3.9) and (3.10). The complexity of selecting the sampling frequency increases dramatically for the real life applications when in addition to the desired signals, numerous strong blockers, interferes and image signals are involved in the scenario of signal processing. This is discussed in the next sub-section extensively.

To achieve to a common methodology in the current thesis, the interfering indicator is used as the common indicator to check all the sampling frequency requirements. Thus to map constraints in Eqs. (3.9) and 3.10) to the interfering profile mentioned in Section 3.2, it is required to define the interfering indicator specified to this step. To perform this, the boarders of the Nyquist band should be considered as disturbing signal (f_n). This means that although there is no real signal in the boarders of the Nyquist zone, virtual signals are assumed to be allocated at 0 and $f_s/2$. The bandwidth of the virtual signal at f_n is zero. This simplifies the development of a general algorithm to count for all the possible disturbing contributors. This
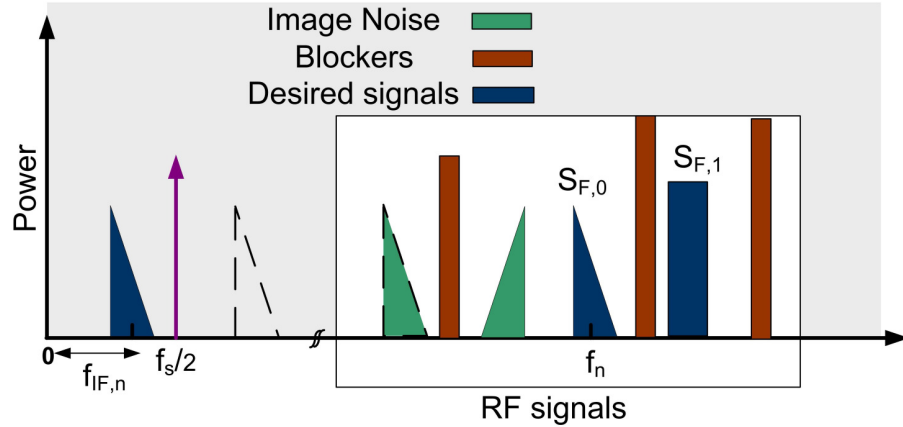
Figure 3.6: Illustration of the spectrum of the signals at RF when the desired signals, blockers and image noise exist at the antenna.

is shown in Fig. 3.3(a).

3.2.2 Based on multi-standard requirements

The receiver in the multi-standard scenario should be able to process several desired signals while attenuating the undesired signals significantly. The reason is that in a practical noisy environment, several signals may be received by the antenna of the receiver. Since for a multi-standard application, the receiver is naturally tuned to receive several signals in wider bandwidth, the possibility of receiving undesired signals is higher. Fig. 3.6 is the snapshot of RF interferes and in-band power levels at the antenna of a receiver. The receiver must be capable of recognizing and distinguishing the desired signals from all the other contributors.

In receivers based on sub-sampling techniques, the selection of an appropriate sampling frequency has important role to organize and down-convert the desired signal bands to non-overlapping portions of the Nyquist zone while keeping the undesired signals as far as possible. That is due to the fact that the resulted IFs in the sub-sampling receivers follow the selection of f_s according to the Eqs. (3.6) and (3.7) as shown in Fig. 3.5 (It can be seen that the resulted IF signals are varying versus sampling frequency and carrier frequency). The requirements for the successful selection of the sampling frequency for each single frequency individually are already discussed in the Section 3.2.1. However to design the multiple-signal scenario, several more requirements are imposed on the selection of the sampling rate. In a multi-standard scenario, there exist several desired signals and disturbing contributors. For each desired signal, there are two types of interfering contributions— the other desired signals of the scenario and the undesired blockers. Different policies are required to cope with these two signal types: (i) the other desired signals of the scenario are what we are interested in for the further processing. It is required to keep them unchanged by allocating them in the adequate separations from the desired signal and (ii) the undesired blockers or image distortions should be filtered out properly. They should be allocated in the proper spacing from the desired band which could be suppressible by the provided selectivity of the front-end. This is discussed thoroughly in

Chapter 4 since it is more related to the selectivity requirements of the receiver.

The case for two desired signals is investigated in this section. The only governing factor for proper down-conversion of the two desired signals is the adequate separation of the signals in the Nyquist band. This separation is controllable by the selection of the sampling frequency. The filtering is not of any interest when both signals are wanted signals of the scenario since none of them can be filtered out.

Thus to sample several desired signals with the minimum acceptable sampling rate and translate them to non-overlapped portions of the Nyquist band, it is required to choose the sampling frequency carefully to provide a minimum required spacing between the desired bands. The sampling rate should be selected in a way that the resulted IF signals do not overlap in the frequency spectrum of the Nyquist zone [2] and [3]. The overlap of signals after down-conversion results in missing the useful information.
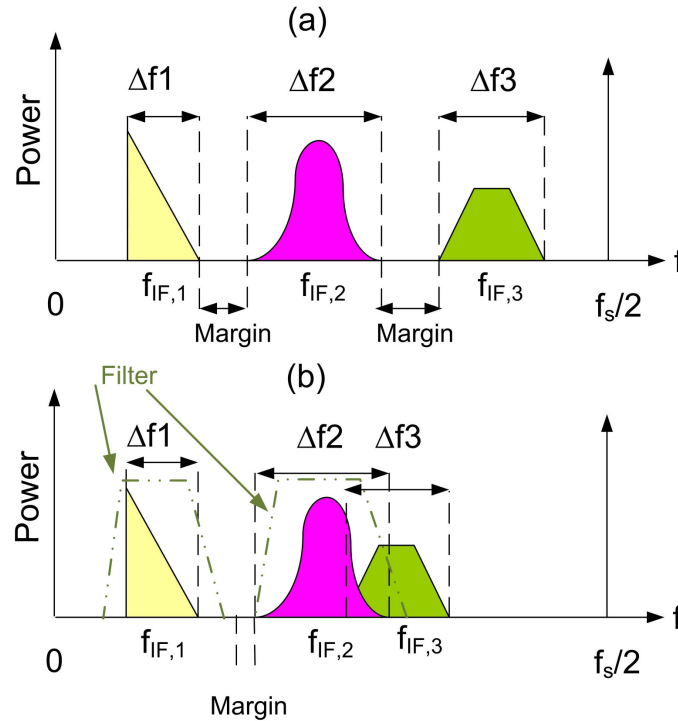
Figure 3.7: Illustration of the multi-standard scenario when the signals are down-converted to (a) non-overlapping portions of the Nyquist band or (b) overlapping portions of the Nyquist band (the depicted margins in the figure is to take the filter characteristics into account).

An example of the snapshot of the translated IF signals in a multi-standard receiver is depicted in Fig. 3.7. In Fig. 3.7(a), the case is shown when the selected sampling frequency is down-converting several signals to non-overlapping portions of the Nyquist band. Fig. 3.7(b) depicts the case when two signals of the scenario are interfering with each other. It can be seen from the figure that a part of the information is missing due to interference. This can be prohibited by controlling and selecting the proper sampling frequency. The minimum required spacing between two desired signals should be half of the cumulative information bandwidths

of them. The required separation of the aliased signals to prohibit their interference with each other can be written:

$$||f_{IF,n+1}| - |f_{IF,n}|| - \frac{\Delta f_{n+1} + \Delta f_n}{2} > 0 \tag{3.11}$$

Eq. (3.11) represents the minimum spacing requirement to avoid the interference of each pair of signals with each other. This constraint is a derivation from the interference profile by entering two desired signals into the system and limiting the smallest frequency separation of the signals to the half of their cumulative bandwidth. This provides a useful controlling tool to organize the desired signals in the non-overlapping portions of the Nyquist band by ensuring the adequate separation between them.

Nevertheless this constraint is valid if the ideal filter shape is assumed to filter the signals at IF. Care must be taken in defining the required spacing for the real case to take the non-ideal filter characteristics into account. In other words, the margin between the signals are necessary as depicted in Fig. 3.7 to count for the non-ideality of the filters. The Eq. (3.11) should be rewritten as:

$$||f_{IF,n+1}| - |f_{IF,n}|| - (\frac{\Delta f_{n+1} + \Delta f_n}{2} + margin) > 0 \tag{3.12}$$

This is a recurrence constraint, repeating for each pair of the desired signals. Thus, the set of the acceptable sampling frequencies for this part is the assembly of all the frequencies fulfilling constraint mentioned in Eq. (3.12) for all the desired signals of the multi-band scenario in pairs. Nevertheless in the notation of this thesis, the margin is assumed to be included in the summation of the bandwidth similar to the Eq. (3.11). Therefore, the Eq. (3.12) is referred to as Eq. (3.11) for simplicity.

Similar constraint was developed in several proposed procedure such as [2] and [3]. However, the nobility of constraint presented in Eq. (3.12) is that it prohibit the image problem as well. The worst type of the image problem is raised when the two desired signals of the scenario are image of each other. This constraint is written in a way to consider and prohibit the two desired signals play the role of image for each other as explained in Section 2.4. Using the former proposed procedures such as [2] and [3] do not prohibit the two desired spot frequencies of the scenario to be image for each other. Reference [2] allows the choice of sampling frequency that results in image problem for two spot carrier frequencies and [3] gives the "'undefined numerical result"' in that case.

3.2.3   Based on pursuing the environment and mitigating the image

The intention of this section is to provide a technique on sensing the environment and adapting the sampling rate of the receiver to the best possible selection to mitigate the image problem significantly. A receiver architecture based on this technique is developed in this dissertation in Section 3.3. The working principals of this receiver is discussed here.

The method is based on sensing the nearby spectrum and modeling the in-band interferes

when the receiver is not receiving any data. The functionality of the receiver in this state is similar to the spectrum analyzer. The power of interferes are calculated over the captured time and the weakest signals are selected as the perspective closest images to the desired band of the scenario. After receiving the original signal, the sampling frequency is governed by the existing carrier frequency and the perspective images. The further selection is done according to constraints mentioned in Sections 3.2.1, 3.2.2 and 3.2.4 to perform the best selection. The method is explained more thoroughly in Section 3.3.

To derive the required procedure of the receiver to determine the sampling frequency from the image distortion, the signals are modeled in this section. The receiver is receiving several signals at each time slot with carrier frequencies f_n— consisting of the desired signal and the blockers. The signals are organized such that the signal at f_0 occupying the frequency band Δf_0 is the desired signal and $f_1, \ldots, f_N$ are undesired blocking signals or other desired bands with the bandwidths of Δf_n. This is the assumption which is kept in this dissertation.

It is known that along with the desired signal, another undesired signal (called the image) results in an output contribution at the same intermediate frequency f_{IF}. Traditionally, this image is defined as a signal located at $2f_{IF}$ from the desired signal [17]. However in sub-sampling receivers, this concept is extended to all the signals at the $f_{IF,n}$ spacing from the multiples of the sampling frequency due to the sampling operation. For the desired signal or its image, it can be written:

$$s_{F,0} : f_{img,0} = m f_s \pm f_{IF,0} \quad for \;\; m = 0, \pm 1, \ldots \tag{3.13}$$

$$s_{F,0}^* : f_{img,0} = -m f_s \mp f_{IF,0} \quad for \;\; m = 0, \pm 1, \ldots \tag{3.14}$$

where $f_{img,0}$ is the image for the desired signal f_0. The illustration of the concept of image signal is depicted in Fig. 3.8.
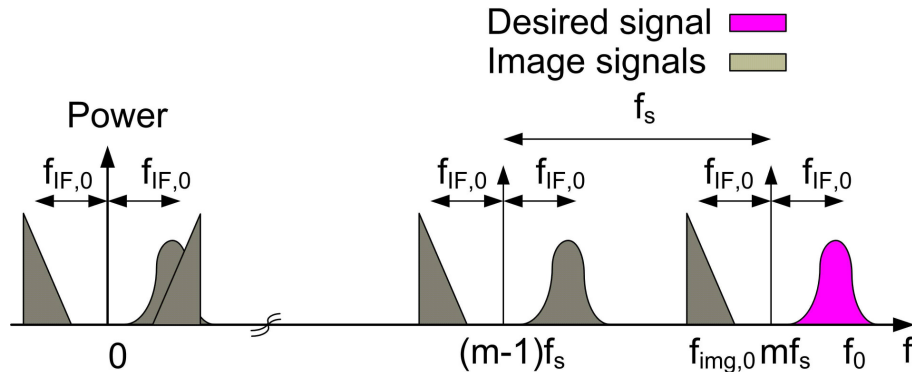
Figure 3.8: Illustration of the desired signal and its image distortions folded in multiples of the sampling frequency.

The replication of the image signals is problematic if they are not properly mitigated. The idea behind this method is to recognize the weakest signals in the environment and set the

weakest one as the closest image distortion to the desired band. It assists to reduce the re-
quirement for very costly and bulky filters in the front-end by applying weaker blockers to the
receiver.

The time slot when no signal is receiving (idle state), the receiver is employed as a spectrum
analyzer. The model of the neighboring blockers and undesired signals is captured in the
receiver. This is depicted in Fig. 3.9(a). After modeling the environment, the receiver starts
to process the captured information over the idle time. The average power of the blockers is
estimated in baseband processors over the captured time. The frequency of the weakest average
signal powers are selected and recognized as the perspective image distortions of the scenario.
This ensures a weak image signals delivery on top of the desired signal in IF while the real
signal is received and processed.
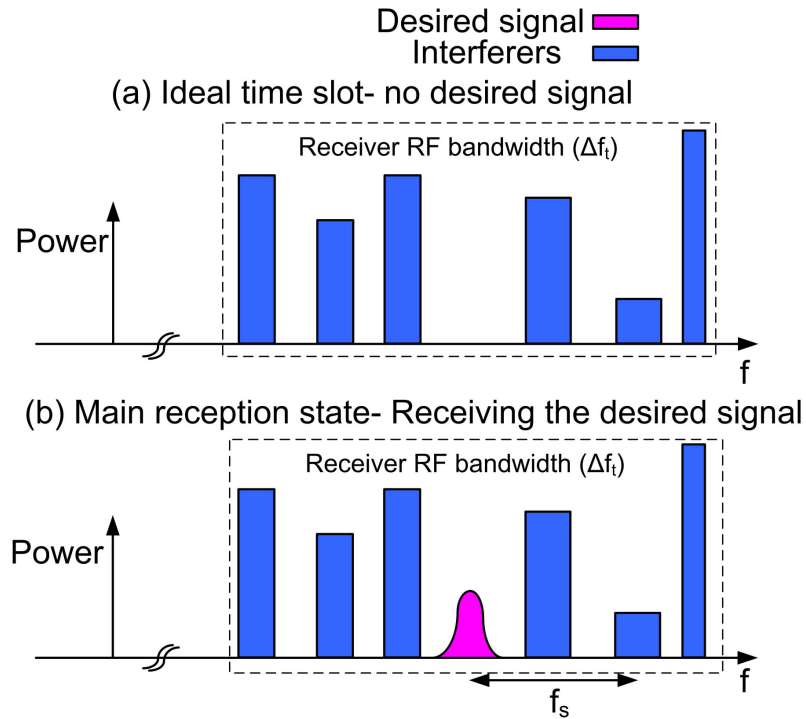
Figure 3.9: Illustration of the frequency response for the desired signal and the blockers in different time slots.

After receiving the original signal, the processors are able to determine the sampling fre-
quency from the desired carrier frequency and image distortions. The best sampling frequency
is selected to be the rate fulfilling the requirements mentioned in Sections 3.2.1, 3.2.2 and 3.2.4
properly. From Eqs. (3.1), (3.2), (3.13) and (3.14), we get the required formula for calculating
the sampling frequency given the image signal ($f_{img,0}$) and the desired received signal (f_0).

$$f_{img,0} = m f_s \pm (f_0 - round(\frac{f_0}{f_s})f_s) \qquad (3.15)$$

$$f_{img,0} = -m f_s \mp (-f_0 + round(\frac{f_0}{f_s})f_s) \qquad (3.16)$$

The receiver's base-band processors are programmed to calculate the sampling frequency from Eqs. (3.15) and (3.16) for the closest image to the desired band ($m = \pm$round(fc/fs)). The reason is that there are numerous images for each desired signal replicated at multiples of sampling frequency due to the sampling. Among all the image frequencies, the closest image to the desired band provides the most stringent requirement for the receiver's selectivity since it is more difficult to suppress it with the IR filters. Consequently, the m variable in Eqs. (3.15) and (3.16) is set equal to $\pm$round(fc/fs) to calculate the closest image frequency to the desired band.

In addition to the closest image band, calculating the further image frequencies from Eqs. (3.15) and (3.16) for the other values of m is useful. It is used to tune the suppression of the tunable IR filter to reject the frequencies located at the other farther image spacing. The further the images are spectrally located, the easier it is to suppress them with the stop-band attenuation of the IR filter.

This method can provide great improvement in rejection of images in sub-sampling receivers. It provides a complete reliable approach to control and suppress all the images in this architecture. To prove the method in practice, the proposed concepts of this letter are supported by simulations and measurements on a sub-sampling receiver.

3.2.4 Based on mitigating the noise

In order to obtain the expected performance of the receiver, the noise of the receiver needs to be controlled and kept below the certain level determined from the receiver's noise budget. This level is derived based on the specifications mentioned in each individual standard and the requirements set by each special application. This is explained more in Chapter 4.

With respect to the cost, complexity and performance analysis done for the receiver depends on the application, a target noise budget is selected. The various blocks of the architecture must be designed in a way to keep the total noise of the receiver below the allowed power according to the noise budget.

One of the determining factors in the noise of the sub-sampling receiver is the sampling frequency as discussed in Chapter 2. Several noise contributions of the sub-sampling architecture such as the thermal noise and jitter noise are governed by the sampling frequency as shown in Section 2.2. Care must be taken during the selection of the sampling frequency to keep the SNR above a certain level by controlling the f_s governed noise contributions. After the selection of the most appropriate sampling frequency from previous steps, the corresponding noise contribution must be estimated. It is important to assure that the f_s controlled noise contribution is below the levels determined in the noise budget of the receiver. Otherwise, the sampling frequency is not acceptable and the next sampling frequency must be tried.

3.2.5 Algorithm for selection of the sampling rate

The procedure of selecting the best sampling frequency satisfying all the mentioned requirements is summarized in this Section. The basic idea is to narrow down the selection of sampling

frequencies based on their compliance with the requirements stated in Sections 3.2.1, 3.2.2, 3.2.3 and 3.2.4. All these steps are summarized and organized in 3 steps in this Section. The summarized flow-chart of the algorithm is shown in Fig. 3.10.
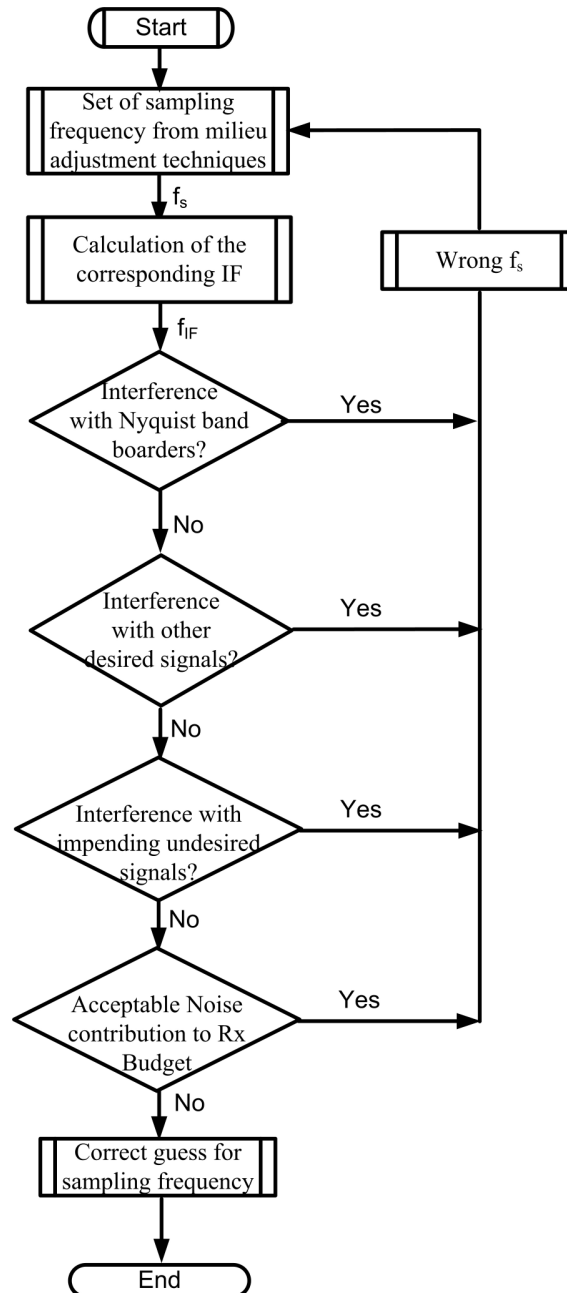
Figure 3.10: Illustration of the flowchart for selecting the best sampling rates.

1. In the first step, the set of the sampling frequencies providing maximum SNR at the output of the receiver are recognized from the milieu adapting method described in Section 3.2.3. The receiver senses and models the neighboring interferes while it is in its idle mood—

the front-end is not receiving any desired signal. The receiver is performing similar to a spectrum analyzer with limited bandwidth. The signals apprehended in the receiver are being processed in the base-band processors.

The corresponding frequencies of the weakest average power signals are set as the perspective closest images to the desired signal. After receiving the original signal, several sampling frequencies are governed by the carrier frequency of the desired signal and the selected images from Eqs. (3.15), (3.16). A set of the acceptable sampling frequencies which results in maximum SNR are obtained. The best possible sampling frequency is selected among these frequencies by perusing the algorithm mentioned in this section.

Finally the selected sampling frequency is reported through a feedback loop to the programmable clock generator (PCG) and applied to the received signal. The PCG is one of the clocking solutions that provides the necessary clock signals to high speed systems such as the developed programmable clocks by Cypress Semiconductor Corporation [95] and Rambus Inc [96]. This ensures a high probability of receiving the pure signal since the image is weak and suppressible by the front-end selectivity. Therefore, a union of all the sampling frequencies resulting high values of the SNR at the output of the receiver are determined from this step.

2. The set of sampling frequencies selected from the milieu adapting techniques are not necessarily in comply with the other fundamental requirements mentioned in sections 3.2.1, 3.2.2,and 3.2.4. Thus the compliance with the Nyquist criterion and prohibition of the interference should be checked for all the down-converted signals for the set of all the acceptable sampling frequencies from the previous step. This helps the receiver's processors to pick up the best sampling frequency among all the frequencies in compliance with the milieu adapting method and return it to the PCG.

The requirement for fulfilling the Nyquist criteria in addition to locating in non-overlapped portions of the Nyquist band for all the signals is summaries in this step. It is an iterative procedure which is repeated for all the desired signals of the scenario one by one. The interference is checked for each desired signal with the other desired and the disturbing signals of the scenario. The technique is based on the interference profile presented in Section 3.2. The minimum spacing between each pair of the signals is checked and the required separation is assured.

The first part of the mentioned procedure narrow down the selection to the union of the frequencies that comply with the Nyquist criteria through adequate spacing from zero and $f_s/2$. The largest frequency component of each signal $(F_n + \Delta F_n/2)$ is compared with the upper boarder of the Nyquist band. If there is any intersection, the algorithm decides to discard the sampling frequency and goes to the next sampling frequency of the set. Otherwise, the minimum frequency component of the signal $(F_n - \Delta F_n/2)$ is compared with the lower boarder of the Nyquist band for the probable violation of the Nyquist criterion. If the signal provides the required spacing from zero frequency, the signal is picked for

further investigation. Otherwise, next sampling frequency is entered to the algorithm and the current one is completely discarded.

Passing successfully through the first part ensures that the signal is individually in comply with the Nyquist criteria. Next part is to check whether the signal is interfering with any other signal (desired or undesired) in the Nyquist zone. This is performed in the second part of the procedure for the intersections with the other desired signals. Each disturbing desired signal at the antenna is taken one by one and the distance between the most approximate frequency components of the disturbing signal and desired signal at IF is checked. Unless all the disturbing signals are not spaced in the enough spacing from the desired signal, the corresponding sampling frequency is not pursued by the algorithm. In other words, the set of all the acceptable sampling frequencies are formed from the ones placing the signals in non-overlapped portions of the Nyquist band.

To ensure the acceptability of the sampling frequency for each desired signal, the spacing from all the other desired signals of the scenario must be checked one by one. Furthermore, all the impending undesired signals at the antenna must be checked. The undesired signals cover a wider range of all interferes, blockers and image noise at the antenna. The way to how handle the undesired signals is explained in Chapter 4. Special care is taken regarding the impending images at the antenna. In spite of the idea presented in the milieu adapting technique to suppress the image signals, there is still the risk of delivering the image noise on top of the desired signal. Thus the sampling frequencies that make a strong blocker at the antenna to be the image frequency of the desired signal calculated from Eq. (2.25) should be prohibited.

3. The third and last step determines the noise contribution corresponds to the selected sampling frequency. According to the noise budget of the receiver, the S/H block should have a specified noise contribution. As discussed in section 2.2, the noise contributions from the sampling block is reversely proportional to the sampling frequency. Thus the determined sampling frequency must be checked to keep the noise contribution from the sampling block below the allowed noise of the noise budget. This ensures that the noise figure of the receiver is not violated because of the selection of sampling frequency.

To yield the full set of acceptable sampling frequencies, the combined requirement in three mentioned steps must be checked for each sampling frequency in the range. The same concept in the form of a flowchart is depicted in Fig. 3.10.

For all valid f_s

Part I

Initialize $\Delta F_{min,abs}$ & $\Delta F_{min} = 0$

Initialize $|f_{IF,n}| = f_s/2$ & $\Delta f_n = 0$

Calculate ΔF_n & ΔF_n^* from Eqs. (3.3), (3.4)

- if $|\Delta F_n \mid$ & $|\Delta F_n^*| > \Delta F_{min,abs}$
  - then continue with the same f_s
  - else Go to next f_s
- end

$\Delta F_{min} = min[\Delta F_n, \Delta F_n^*]$

Initialize $|f_{IF,n}| = 0$ & $\Delta f_n = 0$

Calculate ΔF_n & ΔF_n^* from Eqs. (3.3), (3.4)

- if $|\Delta F_n \mid$ & $|\Delta F_n^*| > \Delta F_{min,abs}$
  - then continue with the same f_s
  - else go to next f_s
- end

$\Delta F_{min} = min[\Delta F_n, \Delta F_n^*, \Delta F_{min}]$

Part II

For disturbing signal n=1:N

- Calculate ΔF_n & ΔF_n^* from Eqs. (3.3), (3.4)
- if $|\Delta F_n| \& |\Delta F_n^*| > \Delta F_{min,abs}$
  - then continue with the same f_s
  - else go to the next f_s
- end

$\Delta F_{min} = min[\Delta F_n, \Delta F_n^*, \Delta F_{min}]$

end

$\Delta F_{min}[n] = \Delta F_{min}$

$f_s[n] = f_s$

3.3   RF sub-sampling receiver architecture based on the milieu adapting techniques

A novel RF sub-sampling receiver architecture is developed based on the milieu adapting techniques introduced in section 3.2.3. It is known that in the multi-standard sub-sampling receivers, the appropriate sampling frequencies are selected based on their abilities to down-convert several desired signal of the scenario to non-overlapping portions of the Nyquist Band. In spite of all the attempts to select the best sampling frequency based on this approach [2], [3], there can be a lot of unwanted signals at the antenna other than the desired which at least partly gets down-converted to the desired band. These impending signals at the antenna are called image bands. The image bands are unavoidable regardless of the applications. A sub-sampling receiver architecture is introduced in this letter which works based on environmental tracking and adjusting techniques. The idea is to allocate the weakest signal power in the environment as the closest image by proper selection of the sampling rate and suppress the other images by a tunable IR filter. This leads to improvements in the SNR of the receiver.

The proposed RF sub-sampling receiver is illustrated in Fig. 3.11. The main idea is to sense the environment and select the sampling frequency in such a way that it leads to be best possible SNR. In other words what is striven for is to select the sampling frequency such that the weakest image signal is the one being delivered on top of the desired signal as described in section 3.2.3. Image signals can never be avoided — but it is possible to select the sampling such that the one image causing the least problems is the one chosen. This technique may result in great improvement in the SNR as discussed further in the current thesis.
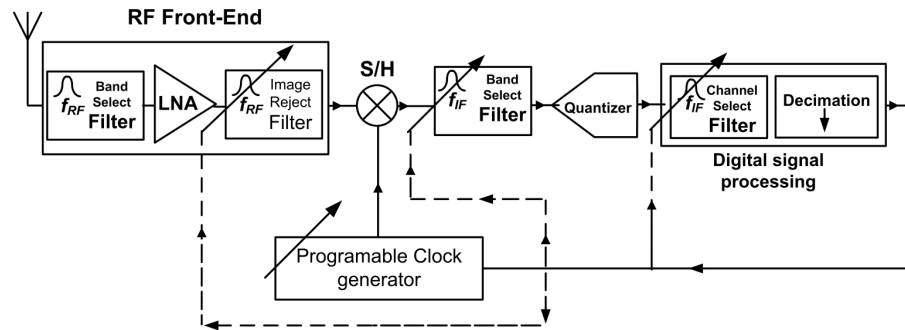
Figure 3.11: Proposed RF sub-sampling receiver architecture based on milieu adapting technique.

As it can be seen from the Fig. 3.11, to serve the purpose the receiver employs a PCG, tunable image reject (IRF) and intermediate frequency (IFF) filters. A feedback loop is implemented from the base-band processors to the PCG. The enabling steps for the receiver to sense and adjust to the neighboring milieu are outlined below:

1. **The idle state**: In this time period when the receiver is not receiving any real data, it starts to detect the existing signals. It means that the receiver front-end is not in its reception mode. A simple model of the nearby frequency spectrum and neighboring blocker levels is made in the receiver. All the signals in the RF bandwidth of the receiver

are captured by the front-end. This procedure is done by sensing the adjacent milieu and the receiver acts as a spectrum analyzer with a limited bandwidth in this state.

2. **Pre-processing state**: In this time period, the receiver is processing the neighboring blockers that have been sensed during the receiver's idle state. The average powers of the blockers are estimated in the base-band processors over the captured time. This is done by sweeping the sampling frequency step by step in the entire receiver's RF bandwidth and down-convert all the in-band disturbing contributions. The weakest blocker is recognized and set as the perspective closest image signal.

3. **Main Reception phase**: The desired signal is received to the antenna. The sampling frequencies are determined from the desired channel and allocated images by employing the method mentioned in section 2.4. The most appropriate sampling frequency is determined based on the compliance with the algorithm introduced in section 3.2.5. The processed information of the allocated sampling frequency is returned back to the PCG via the feedback loop. The PCG block produces the calculated sampling frequency and applies it to the desired signal. This guarantees that the image signal is one of the weakest possibilities when the desired signal is being processed. Subsequently, the IRF and IFF are tuned to the desired band. The IRF is tuned to reject the signals in the image frequencies to ensure the best rejection of images.

3.4   Simulation results

According to the defined scenario of this paper, the UE enables both wireless local area network (WLAN) and universal mobile telecommunications system (UMTS) to operate concurrently. Since UMTS is frequency Division Duplex (FDD) operating standard, both the UMTS uplink (UL) and UMTS downlink (DL) signals may exist at the same time with the separation in frequency domain. The duplexer is responsible of isolating these two signals in the 3G transceiver. However, the WLAN UL and WLAN DL are operating in different time periods due to the time division duplex (TDD) capability of the IEEE 802.11 standard. Therefore, in each moment, only one of the WLAN UL or DL may exist in the user equipment. Thus the desired signals considered are the received the UMTS and WLAN signal from the base station and the interference sources are defined as the internal blocking signals leaking from the UMTS transmitter at the same transceiver as shown in Fig. 3.12. This snapshot of interferer and in-band power levels will be referenced throughout this chapter.

The simulations in this chapter show the effect of several mentioned parameters of Sections 3.2.1, 3.2.2, 3.2.3 and 3.2.4 in the selection of the best possible sampling frequency. Since the frequency spacing of the signals are of more interest in this part, more focus is given to the placement of the signals in frequency spectrum. The signals are generated based on the specifications outlined in Table 1.1. The Parameters used in the simulation obey the specifications mentioned in section 1.5 and the set up illustrated in Fig. 1.20. Besides, the following considerations are made for the simulation:
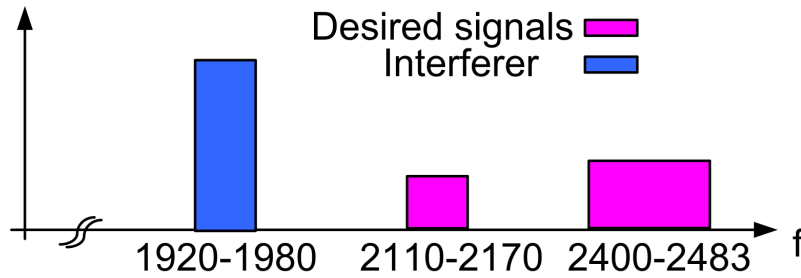
Figure 3.12: Illustration of frequency spectrum of UMTS UL, UMTS DL, and WLAN DL.

- The receiver is suppose to process the UMTS DL and WLAN DL concurrently. Thus they are both considered as the desired signals of the scenario. At the same time, the UMTS UL exists at the antenna as the interference to the desired bands. This scenario is held for all the simulations presented in this section except the part related to the Section. 3.3. In this simulation more interferes is involved in the scenario to prove the concept.

- The UMTS signal has 12 non-overlapping channels in the total band of $2110 - 2160$ MHz. The channels start from 2112.5 MHz and the channel spacing is 5 MHz. The last channel exists at 2167.5 MHz [5].

- The WLAN signal consists of 3 non-overlapping channels located at 2412, 2442 and 2472 MHz respectively [7].

- The minimum possible sampling frequency is $2(\Delta f_0 + \Delta f_1 + \cdots + \Delta f_N)$; where N is the number of desired signals. In other word, the sampling frequency must be at least twice the cumulative information bandwidth of the desired signals.

The simulations are done for each constraint mentioned in Section 3.2 separately. It is presented in the separate Sections 3.4.1, 3.4.2 and 3.4.3. The overall algorithm for calculation of the sampling frequency is approved by simulations presented in Section 3.4.4.

3.4.1 Simulations of single-frequency requirements— Nyquist criterion

The first step of selecting the sampling frequency is to recognize each down-converted signal follows the Nyquist criterion individually. This is performed by finding the frequencies that satisfy constraint presented in Eqs. (3.9) and (3.10). An iterative procedure is employed to narrow done the frequencies greater than the minimum f_s to the sampling frequencies satisfying the Nyquist criterion. Each sampling frequency within the range is tried one by one and the down-converted IF signal in the Nyquist band is monitored.

Eqs. (3.1) and (3.2) are used for plotting the resulted IF signals by varying the sampling frequency. Figs. 3.13(a) and 3.14(a) illustrate the resulting IF for the information bands UMTS and WLAN signals for all 12 and 3 channels respectively. The zoom of the same figures are depicted in Figs. 3.13(b) and 3.14(b). The sampling rates from zero to 1 GHz are tested (although only the frequencies greater than 54 MHz which is twice the cumulative bandwidth

Figure 3.13: (a) Illustration of the resulting UMTS IF DL versus the sampling frequency, f_s and (b) Zoomed view of (a).
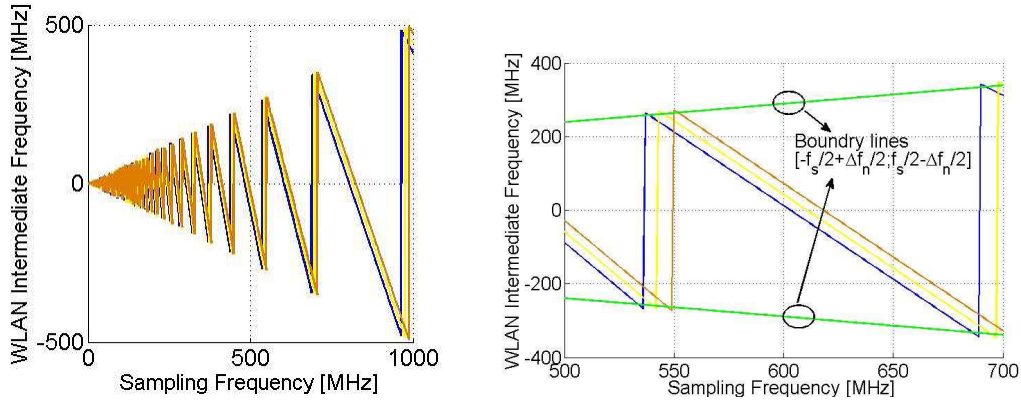
Figure 3.14: (a) Illustration of the resulting WLAN IF DL versus the sampling frequency, f_s; (b) zoomed view.

of the signals are acceptable). It is obvious that the frequencies below the 54 MHz are not acceptable because it is less than twice the cumulative information bandwidth.

The boundary lines in Figs. 3.13(b) and 3.14(b) indicate the two Nyquist band boarders explained in Eq. (3.8) for the general two-sided signal located between $[-f_s/2 + \Delta f_n/2; f_s/2 - \Delta f_n/2]$. The acceptable sampling frequencies in the first step are the ones providing the adequate spacing from the boundaries of the Nyquist band. Checking the requirements for both the positive and negative spectrum is analogy to high-side and low-side mixing. To avoid the duplication in checking the requirements, only the positive frequency spectrum is considered in this dissertation.

The positive version of f_{IF} is $|f_{IF}|$. The $|f_{IF}|$ is plotted in Figs. 3.15(a) and 3.16(a) by sweeping the sampling frequency in the Eqs. (3.1) and (3.2) and considering the positive part. The zoom of the same curves for f_s swept between 500 and 700 MHz is illustrated in Figs. 3.15(b) and 3.16(b). The reason of sweeping sampling frequency between 500 and 700 MHz is later described in multi-frequency requirements. When only the positive part of the spectrum is considered, the boundary limits of the Nyquist criteria is changed to 0 and $f_s/2$ instead. More
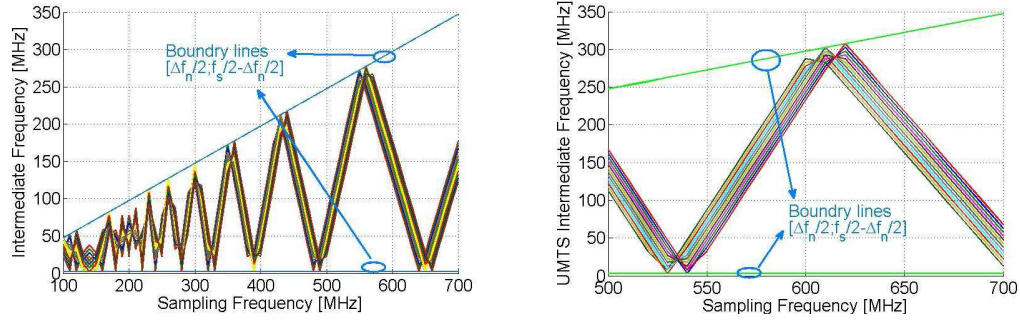
Figure 3.15: (a) Illustration of the resulting UMTS IF DL versus the sampling frequency, f_s— considering only positive spectrum and (b) Zoomed view of (a).
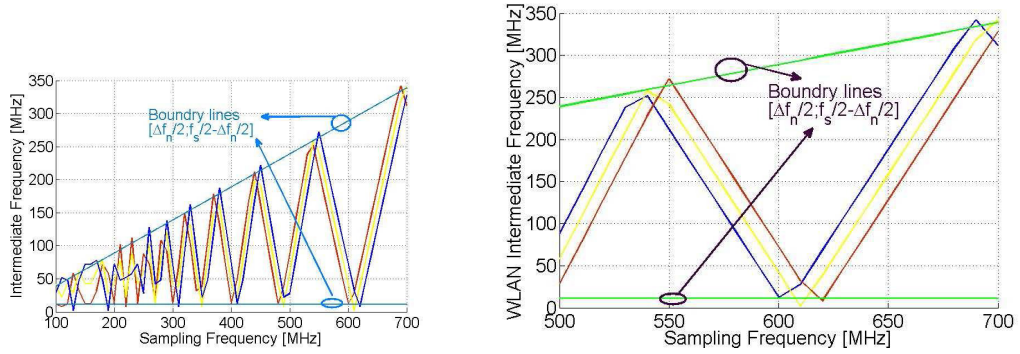
Figure 3.16: (a) Illustration of the resulting WLAN IF DL versus the sampling frequency, f_s— considering only positive spectrum and (b) zoomed view.

precisely, the boundary is written as $[\Delta f_n/2; f_s/2 - \Delta f_n/2]$ including the information bandwidth effects.

As depicted in Figs. 3.15 and 3.16 and mentioned in Section 3.2.1, all the sampling frequencies result in the IF signals lying between two boundaries of the Nyquist band are acceptable selections to the Nyquist criterion. It is important to note that the first f_s selection step assembles the set of the sampling frequencies satisfying the Nyquist criterion for each individual standard separately. Excluding the frequencies which violate the boundaries of the Nyquist band, all the other sampling frequencies are acceptable selections. The minimum acceptable sampling frequency for both the WLAN and UMTS is about 60 MHz. As seen from Figs. 3.15 and 3.16, numerous signals fulfill this requirement afterward. The sampling frequencies fulfilling the Nyquist criteria are further narrowed down by checking other steps mentioned in sections 3.2.2, 3.2.3 and 3.2.4.

3.4.2   Simulations of f_s related multiple-frequency requirements

The set of the acceptable sampling frequency from the previous step is the union of all the frequencies which assures the compliance with the Nyquist criteria for each standard separately. The second step is to limit the sampling frequencies to the set which fulfills the multi-standard
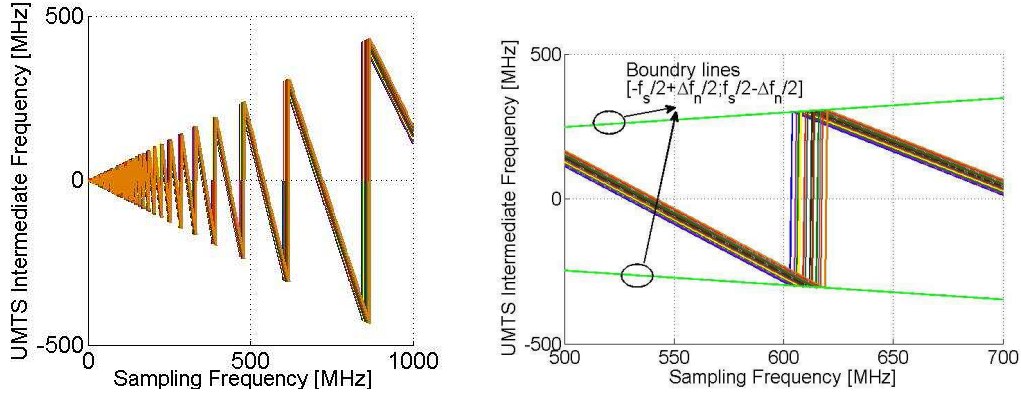
Figure 3.17: (a) Illustration of the resulting UMTS IF DL and WLAN IF DL versus the sampling frequency, f_s and (b) zoomed view.

Figure 3.18: (a) Illustration of Resulting UMTS IF DL and WLAN IF DL versus the sampling frequency, f_s; (b) Zoomed view of (a) (considering only positive spectrum).

attitude of the application. As mentioned before, it is required to translate several RF signals of the multi-standard scenario to non-overlapping portions of the Nyquist band. The aliased intermediate equivalents of the UMTS DL and WLAN DL signals versus the sampling rate are depicted in Fig. 3.17(a) with the zoomed view of the same plot between $f_s = 500$ to 700 MHz in Fig. 3.17(b). The positive intermediate frequencies of the same plot by sweeping the sampling frequencies are plotted in Fig. 3.18(a) and the zoomed plot in Fig. 3.18(b). Eq. (3.12) is verified for the set of all the sampling frequencies satisfying the Nyquist criteria from the previous step. In other words, Eq. (3.12) is coupled with the Eqs. (3.9) and (3.10) to narrow down the selected sampling frequencies to the set which provides non-overlapping aliasing of several signals in the Nyquist band. The minimum frequency spacing between each pair of desired signals must be at least half of the cumulative information bandwidth of the signals including required margin for filter as mentioned before. It can be interpreted from Fig. 3.18 as well. For the UMTS DL and WLAN DL, this spacing (half of the cumulative information bandwidth) is 27 MHz excluding the margin. So the sampling frequencies for which the distance between all the different channels of UMTS DL and WLAN DL at intermediate frequencies are more than 27 MHz in Fig. 3.18 are acceptable selections.
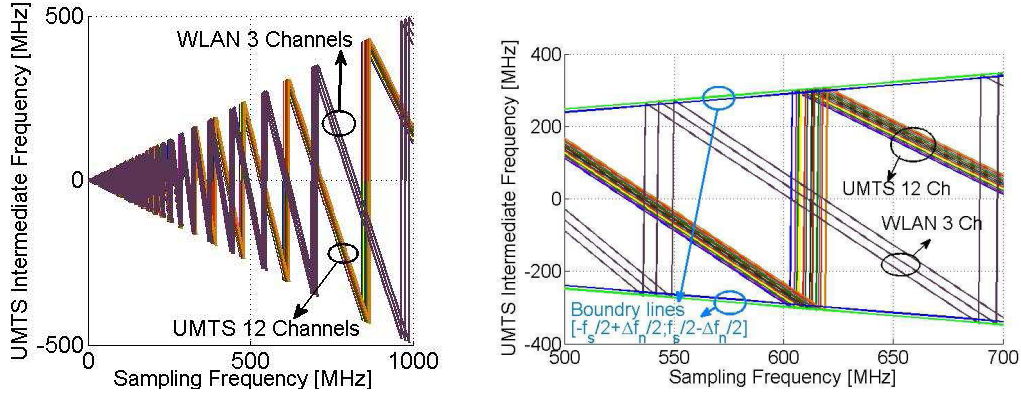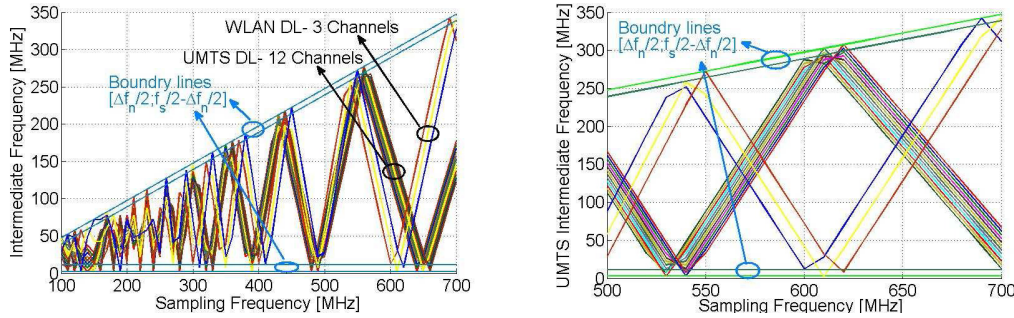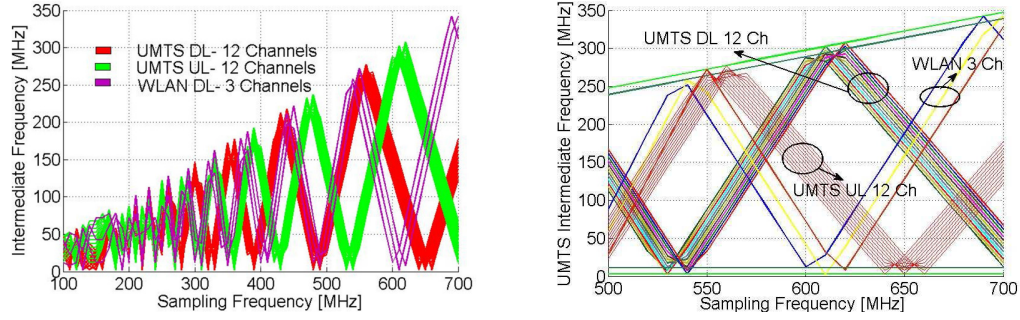
Figure 3.19: (a) Illustration of the resulting UMTS IF DL, UL and WLAN IF DL versus the sampling frequency, f_s; (b) Zoomed view (considering only positive spectrum).

The minimum sampling frequency that satisfies Eqs. (3.9), (3.10) and (3.12) is 186.6 MHz if only the UMTS DL and WLAN DL are considered. The set of all the sampling frequency larger than 186.6 MHz which are not violating the Nyquist criteria and providing enough separation of IFs are acceptable sampling frequencies for the scenario containing the UMTS DL and WLAN DL only.

However as shown in Fig. 3.12, the UMTS UL exists in the frequency spectrum due to the FDD operation of the UMTS signal. Thus it should be considered as one of the contributors to the frequency plan and consequently to the selection of sampling frequency. In other words, practically the frequency planning of the receiver must be done for the three mentioned signals. The variation of the three down-converted signals of the scenario in IF versus sampling frequency is shown in Fig. 3.19(a). The zoom of the same plot to the sampling frequencies between 500 and 700 MHz is illustrated in Fig. 3.19(b).

As it can be seen from Fig. 3.19 that for each f_s, three groups of translated IFs exist. Thus in addition to the Nyquist criteria for each individual signal, the adequate spacing between each pair of signals must be fulfilled. In other words, the acceptable down-conversion is performed when each signal of the scenario has sufficient separation from the borders of the Nyquist band and the two other signals.

The reason of sweeping the sampling frequency between the 500 and 700 MHz comes from the scenario consisting of 3 different signals. The 3 signals (UMTS DL, UL and WLAN DL) are interfering with each other in most of the spectrum depicted in Fig. 3.19(a) before 500 MHz. The first acceptable region which provides adequate spacing of all the channels of the 3 signal from each other is between 389 to 393 MHz. However, this is a very narrow band and in this band the signals are very close to the borders of the Nyquist band or each other (even though, they fulfill the requirements). Thus, the considered region of selecting the sampling frequency in this research is shifted to the band between 500 and 700 MHz. In this spectrum band, several sampling frequencies fulfill the requirements in addition to providing more relaxed situation in down-converted bands. The organization of the down-converted signals is more desirable since the signals have adequate spacing from the other signals and the borders of the Nyquist band.
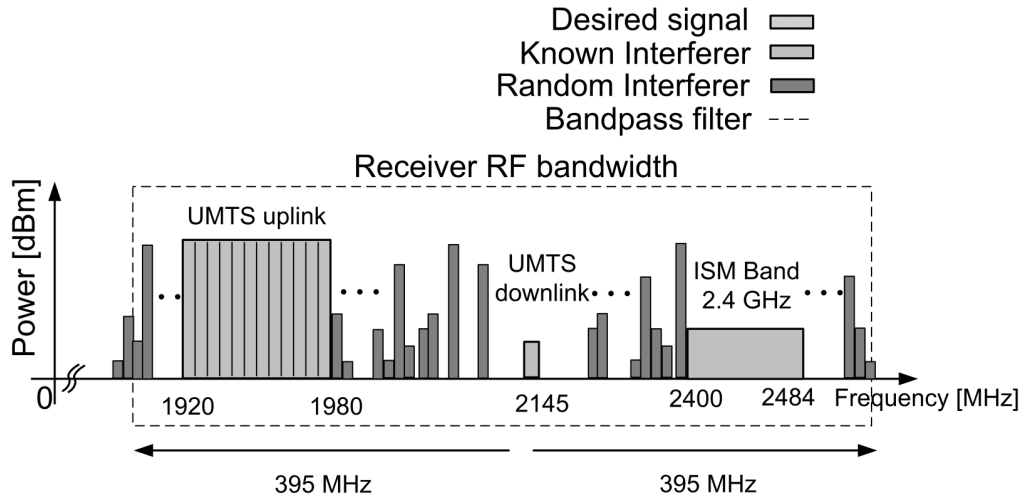
Figure 3.20: Illustration of the spectrum of desired signal, in-band power levels and interferes at RF.

3.4.3 Simulations of pursuing the environment and mitigating the image distortions

To show the milieu adapting technique, the scenario of the case study of the thesis is assumed to be in a user congested (noisy) environment. In other words, numerous undesired signals exist in the spectrum in addition to the desired RF bands. A spot view of the desired signal and the blockers inRF is depicted in Fig. 3.20. The scenario is inspired from a very realistic situation: the reception of the UMTS FDD call while the receiver is located in a noisy environment. Interferes are modeled in Matlab [50] according to the realistic situation. Since UMTS FDD is considered in this research, both the UMTS uplink and downlink signals exist at the same time with the separation in frequency domain. Thus different channels of UMTS uplink exist in frequency spectrum in addition to the UMTS downlink signal. Different channels of WLAN downlink are present in the spectrum due to the fact that the receiver is assumed to be located fairly close to a WLAN access point. The rest of interferes are created randomly with uniform distribution between the maximum input level and minimum sensitivity levels of the UMTS receiver [5]— -114 dBm and -25 dBm. Each interferer has equal chance of settling in one of the frequency spectrum positions. To match the desired frequency band, the signals are assumed to be segmented in bands of 5 MHz. The total bandwidth of the receiver is assumed to be 790 MHz (395 MHz from each side of the carrier frequency). The UMTS downlink signal is transmitted in 2145 MHz. The Bandpass filter depicted in Fig. 3.20 is assumed to have constant stop-band suppression of 20 dB relative to the pass-band.

The receiver is simulated in Matlab similar to the set up illustrated in Fig. 1.20. It is programmed to follow the technique mentioned in Section 3.3. In the idle state prior to the reception of the desired signal, the receiver apprehend a model of the neighboring blockers and interferes by sensing the nearby milieu. The signals are processed over the captured time duration in the receiver and the weakest signals at 2055, 1785 and 1911 MHz are selected as

the image signals. The desired signal is received to the receiver consequently. The sampling frequency of 420 MHz is decided from Eqs. (3.15), (3.16) given the f_0 at 2145 MHz and the image $f_{img,0}$ at 2055 MHz. The same discussion is valid for the image frequencies at 1785 and 1911 MHz. The corresponding sampling frequencies are 655 MHz and 676 MHz providing the maximum SNR at the output of the receiver. This forms the set of sampling frequencies which are providing the maximum SNR at the output of the receiver. The processors check the other mentioned parameters in Section 3.2.5 such as the Nyquist criteria and decide which f_s is the best possible selection fulfilling all the requirements.

The PCG receives the information about the desired sampling frequency from the baseband processors through the feedback loop and generates the sampling frequency accordingly. The signals are sampled with the desired rate. The SNR of the receiver with and without enabling the milieu adapting technique is depicted in Fig. 3.21. The selection of the smallest images at 2055, 1785 and 1911 MHz and sampling frequency of 420, 655 and 676 MHz accordingly are shown with a round circle. The solid line in the figure is when the milieu adapting feature is disabled and the selection of sampling frequency is done randomly. Using the standard procedure for finding allowed sampling rates [2] and [3] implies that most of the sampling frequencies depicted in Fig. 3.21 are acceptable. For example, the $f_s = 460$ MHz which results in the worst SNR of the scenario has acceptable performance according to the conventional techniques [2] and [3]. However with the selection of such $f_s = 460$ MHz, a great requirement will be set on the selectivity of the front-end to suppress the powerful image noise. But the needed and costly (form factor, price, power) selectivity can be reduced significantly by a more careful and proper selection of the sampling rate and intermediate frequency. By controlling the image noise of the receiver through the mentioned technique, the requirement on the selectivity of the receiver is very relaxed. In the presented scenario, the difference from maximum ($34.03dB$) and minimum ($-51.87dB$) SNR was 85.9 dB (including and excluding the milieu adapting techniques). The potential extensive improvement in SNR signifies the usability of the mentioned technique for the receiver to achieve to higher level of performance.

3.4.4   Simulations of the algorithm for selection of sampling frequency

The mentioned algorithm in Section 3.2.5 is employed to design the suitable sampling frequencies for a multi-standard receiver operating with WLAN and UMTS signals. The sampling frequency (f_s) is swept within the set of all the frequencies that are not lower than $2(\Delta f_0 + \Delta f_1)$ or 54 MHz. The UMTS is assumed to be spectrally located at f_0 and WLAN at f_1.

1. To make a good selection of the sampling frequency, one does not need to sweep all the values between 54 MHz and infinity. The milieu adapting technique introduced in Section 3.2.3 is applied to the multi-standard receiver. The sampling rates providing the maximum SNR at the output of the modulator is recognized. For multi-standard scenario, care must be taken that the selected sampling frequency provides acceptable SNR for all the desired signals of the scenario.
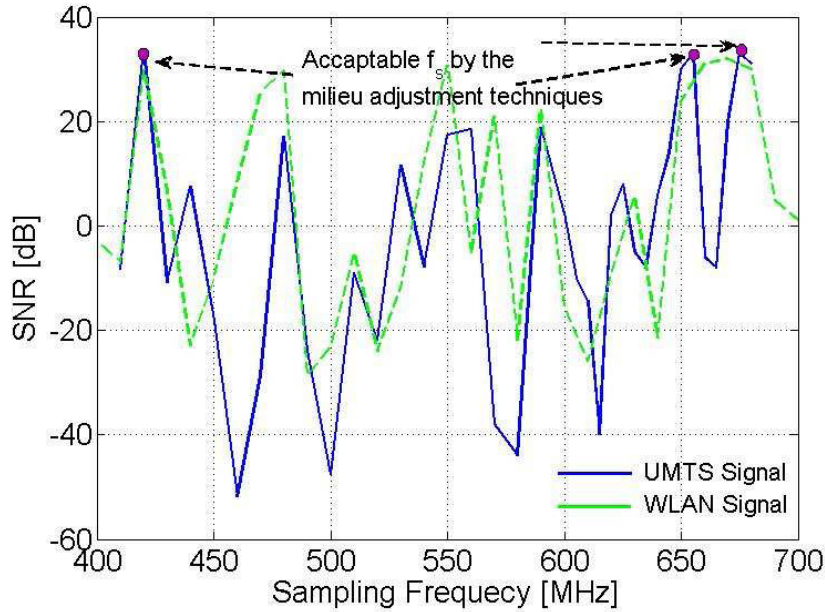
Figure 3.21: Simulated SNR [dB], versus sampling frequency, f_s [MHz] with and without enabling milieu adapting technique for the UMTS signal (solid-line) and WLAN signal (dash-line).

The sampling frequencies which provide the maximum SNR for the UMTS signal are detected in the baseband processors. The set of frequencies in this step consists of 420, 655 and 676 MHz as seen from Fig. 3.21. These sampling frequencies are checked and assured to provide acceptable SNR for the WLAN signal as shown in Fig. 3.21 with dash-line. Although they are not necessarily providing the maximum SNR for the WLAN signal, they have acceptable SNR. That is due to the fact that the focus is on the UMTS signal as mentioned before.

The next steps of selection of the sampling frequency will be performed according to the steps explained in the Section 3.2.5 to find out the best sampling rate. If none of these sampling frequencies can pass the rest of the algorithm successfully, the sampling frequency which provides the lower values than the maximum value will be selected and examined.

2. The interfering profile presented in Section 3.2 makes it possible to plot the minimum frequency distance from any disturbing contribution to the desired intermediate frequency versus the chosen $f_s/2$ set from the first step. This idea is used to find a general method of verifying and recognizing the most appropriate sampling frequency for each application.

The first step of the sampling frequency algorithm narrows down the sampling frequencies from the previous step to the set of frequencies that comply with the Nyquist criteria through adequate spacing from zero and $f_s/2$. This is done based on the idea presented in the interfering profile. The resulted intermediate frequencies versus sampling frequency for both the UMTS DL, UL and WLAN DL are plotted in Fig. 3.19. The set of the
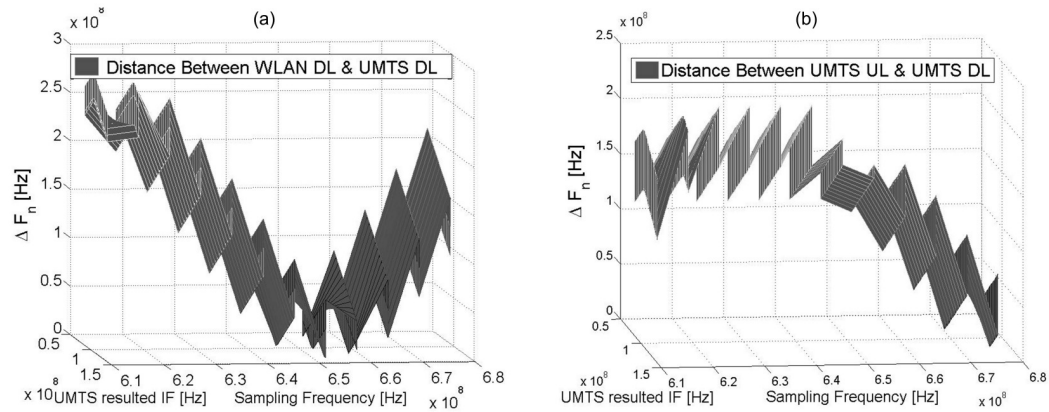
Figure 3.22: Simulated distance between the UMTS DL and (a) WLAN DL (b) UMTS UL versus sampling frequency (All the 12 channels of the UMTS signal are taken into account).

acceptable sampling frequencies in this step consists of the frequencies with adequate distance from the lower and higher limit of the Nyquist zone shown with dash-lines (0 and $f_s/2$ including bandwidth effects).

Based on the interfering profile, the second part of the algorithm checks and ensures the required frequency distance between each two signals of the scenario. This part should be applied to each desired signal of the scenario individually and the frequency distance to all the other desired or distorting signals must be checked one by one. The desired signals are WLAN DL and the UMTSDL for the specific case-study of this dissertation. The UMTS UL is considered as the disturbing undesired signal that exists in a proximate distance to the desired signals of the scenario in the frequency spectrum. As mentioned before, the focus is on the UMTS DL as the main desired signal.

The result of the ΔF_n between the UMTS DL and WLAN DL (as the other desired signal) without their bandwidth effects is plotted in Fig. 3.22(a). The frequency distance between the UMTS UL and UMTS DL is plotted in Fig. 3.22(b). The minimum required distance between each two signals is half of their cumulative bandwidth of the signals including the margin for non-idealities of the filter. That is due to the fact that the bandwidth effects are not included in Fig. 3.22.

Among all the signals from milieu adapting technique, the sampling frequency of 676 MHz fulfills all the steps successfully. It is described later.

3. The f_s governed noise contribution must be below the allowed noise specified in the noise budget for the selected sampling frequency. This is discussed thoroughly in Chapter 4 and Chapter 5 when noise budget of the receiver is determined. The sampling frequency of 676 MHz provides acceptable noise contribution according to the noise budget of the receiver.

Simulations of the algorithm

To summarize the sampling frequency selection steps, the set of acceptable f_s providing the maximum SNR at the output of the receiver for both the UMTS and WLAN signals is determined from the milieu adapting techniques explained in Sections 3.2.3, 3.3. This set of frequencies is examined through the algorithm mentioned in Section 3.2.5 to further narrow down the sampling frequencies. The acceptable f_s is determined from the rates which provide adequate distance from zero and $f_s/2$. This can be determined from Fig. 3.19 or the first part of the algorithm (second part) in Section 3.2.5. Moreover, the desired signals must be located in non-overlapping portions of the Nyquist band. The separation of all the distortions from the desired signal should be suppressible by the provided front-end selectivity. This can be determined from the distance of the distortion from the desired band which is plotted in Fig. 3.22 and the available selectivity of the front-end at that distance. This is discussed more in Chapter 4.

Among all the acceptable sampling rates determined from milieu adapting method, the frequency of 676 MHz is chosen. It fulfills the Nyquist criteria in addition to settling all the signals of the scenario in non-overlapping portions of the Nyquist band for both signals. The reason of this selection is mentioned in more details:

All the steps of the algorithm of Section 3.2.5 are checked for the set of promising f_s from the milieu adapting techniques; for both the UMTS DL and WLAN DL. It is summarized in Tables. 3.1 and 3.2. The f_s that fulfills the $|\Delta F_n|$ & $|\Delta F_n^*| > \Delta F_{min,abs}$ in each step of the algorithm is marked "'ok"' in the tables. The "'not ok"' mark interprets the violation of one of the required steps of the algorithm of Section 3.2.5. An intersection is happened in the Nyquist band between the desired signal under consideration and any other desired or undesired signal in the "'not ok"' case. Thus the algorithm will discard the sampling frequency after the first "'not ok"' situation during the total procedure. Since this indicates that one of the required steps are not fulfilled for that specific sampling frequency.

Table 3.1: Summary of the required steps for selection of f_s correspond to the UMTSDL.

Sampling Frequency [MHz]	Nyquist criteria	Spacing from WLAN DL	Spacing from the UMTSUL
420	ok	not ok	ok
655	ok	ok	ok
676	ok	ok	ok

The compliance with the Nyquist criteria is checked for both signals. The required spacing between each pair of signals are investigated from Fig. 3.22. It can be seen from Tables. 3.1 and 3.2 that the 420 and 655 MHz are not acceptable sampling rates due to having one "'not ok"' mark. The algorithm discards these two sampling frequencies and selects the 676 MHz as the best possible sampling frequency.

Table 3.2: Summary of the required step for selection of f_s correspond to WLAN DL.

Sampling Frequency [MHz]	Nyquist criteria	Spacing from UMTSDL	Spacing from UMTS UL
420	ok	ok	ok
655	ok	ok	not ok
676	ok	ok	ok

This selection is also confirmed by plotting the ΔF_{min}. As mentioned in the previous parts, the ΔF_n and ΔF_n^* are the frequency separations between the desired signal and any disturbing signal or the borders of the Nyquist band (including half of the cumulative bandwidth of the signals). In each step, the separation between the desired signal and any other desired or undesired signal is checked and ensures to provide a value greater than zero. Consequently if the ΔF_n stays greater than zero during the procedure of Section 3.2.5, it indicates the acceptable selection of the sampling frequency.

ΔF_{min} which is the minimum of $|\Delta F_n|/|\Delta F_n^*|$ is plotted for the scenario of the UMTSDL signal as the main desired signal and WLAN DL as the other desired signal in Fig. 3.23(a). The zoom of the same plot is illustrated in Fig. 3.23(b). The plot can interprets as the closest disturbance to the desired signal at each sampling rate. The set of the acceptable sampling frequencies can be determined from the ones corresponds to $\Delta F_{min} > 0$ in Fig. 3.23. Depending on the scenario in each time slot at the antenna of the receiver, different sampling frequencies may provide maximum SNR. Each of these sampling frequencies must be checked to provide $\Delta F_{min} > 0$ in Fig. 3.23. For the selected sampling frequency of this research 676 MHz, this is checked and confirmed. The green plate in Fig. 3.23 represents $\Delta F_{min} = 0$ boundary.

In Fig. 3.24, ΔF_{min} is plotted for the scenario with the UMTS DL signal as the main desired signal and the UMTSUL as the disturbing signal. The same discussion is applicable for this figure as well. The 676 MHz sampling frequency is checked and confirmed for this scenario separately. The two other sampling frequencies of 420 and 655 MHz are mapped to $\Delta F_{min} < 0$ and the algorithm discards them. That is due to the fact that they can not fulfill one of the steps of the algorithm of Section 3.2.5.

The last step is to determine whether the noise contribution of the sampling frequency is in compliance with the total noise budget of the receiver. The receiver noise budget is discussed in detail in Chapter 4. An example of varying the thermal noise power of the receiver versus the sampling frequency for different values of C_s is shown in Fig. 3.25. Depending on the noise budget of the receiver, the sampling frequency must be checked to keep the f_s dependent noise below the required values.
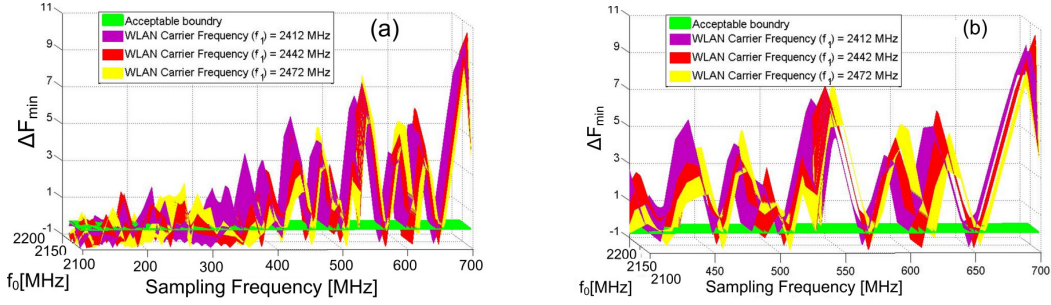
Figure 3.23: (a) Illustration of ΔF_{min} for UMTS IF DL and WLAN IF DL versus the sampling frequency, f_s; (b) Zoomed view (considering only positive spectrum).
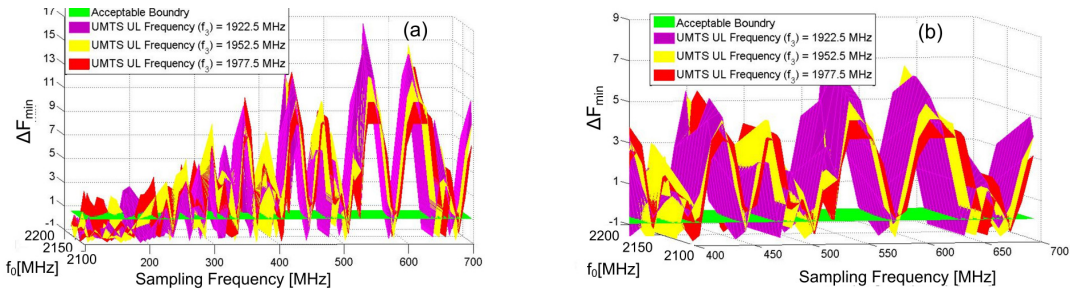
Figure 3.24: (a) Illustration of ΔF_{min} for UMTS IF uplink and downlink versus the sampling frequency, f_s and (b) zoomed view (considering only positive spectrum).

3.5   Discussion and summary

One of the bottlenecks of employing the sub-sampling architecture in multi-standard applications is its complicated frequency plan. The reason is in addition to in-band desired signals and blockers, the replicas of signals are involved in the frequency plan.

Several signals must be down-converted to non-overlapping portions of the Nyquist band in order to benefit from harmless aliasing of this architecture. One of the determining factors in this perspective is the sampling frequency. The equivalent intermediate signals follow from the selection of sampling frequency. Thus, the sampling frequency could be used as a tool to organize the signals in the best possible order in lower frequency.

According to the requirements on the organization of signals in IF, several different constraints should be applied during the selection of sampling frequency. This requirement and constraints are discussed in this section. They are combined with each other and formed an algorithm for selection of sampling frequency. The best possible sampling rate set can be recognized by employing the mentioned algorithm.

To enrich the sampling frequency selection according to the real life environment, a new sub-sampling receiver architecture is proposed in this section. The architecture employs the milieu adapting techniques to sense the neighboring environment and make the appropriate frequency plan accordingly. It benefits from higher level of image rejection capabilities and the requirements on the image rejection bulky filters are relaxed.
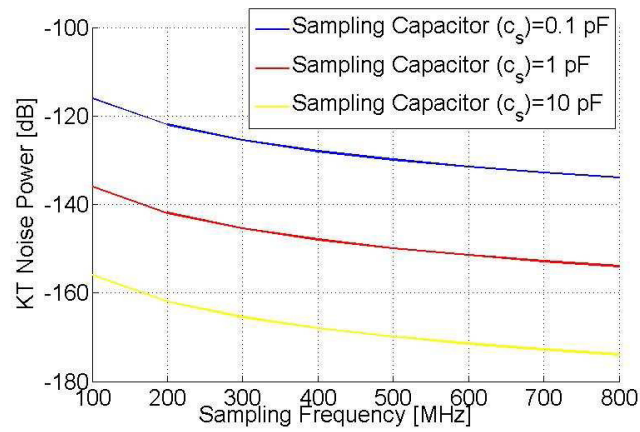
Figure 3.25: Simulated thermal noise power of the receiver, versus sampling frequency, f_s [MHz] for different values of the sampling capacitor. The gain of the receiver is set to 50 dB.

The milieu adapting technique is combined with the algorithm of selecting sampling frequency to give a complete frequency plan procedure of the receiver in the real life application. The last consideration that must be made before selecting the sampling frequency is the noise contribution corresponds to that should be in compliance with the noise budget of the receiver.

Chapter 4

RF requirements of the sub-sampling receiver

To design a multi-standard receiver, different architectures may be selected according to the target application. Regardless of the selected architecture, the receiver must have satisfying performance for each individual standard. Even though several signals have to been processed, the receiver must be able to maintain the adequate performance of each signal by preserving the bit error rate (BER) below a certain value stated in the specifications of each standard.

The RF requirements of a multi-standard receiver in the presence of the noise and nonlinear distortions are investigated in this chapter. The necessary design constraints are also derived. The receiver design must be in accordance with the derived requirements in order to obtain an acceptable compromise among the noise, linearity and the selectivity. The derived constrains for selectivity and linearity are not dependent on any specific receiver architecture and are applicable for all types of receivers. The special selectivity requirements in accordance with the RF sub-sampling receivers are derived consequently.

The chapter is organized as follows. Section 4.1 presents an overall view to the chapter. Section 4.2 presents the sensitivity requirement for the receiver. The required formulation and constraints are derived to estimate the sensitivity and the noise figure of the receiver. Since special focus is on the multi-standard reception, the methodology proposed in this chapter covers the multi-standard transceiver requirements. The linearity issues with respect to the multi-standard functionality is presented in Section 4.3. The selectivity related issues are covered in Section 4.4. The requirements for optimized filters in multi-standard sub-sampling receivers are derived. Great emphasis is given to the selectivity requirement associated with the image rejection and suppression of the intermodulation products. The proposed concepts in the chapter are supported by simulations and calculation in Section 4.5. Finally, Section 4.6 provides a summary and conclusion of the presented discussions.

4.1   Introduction

To characterize and quantify the wireless receivers, the key parameters are the sensitivity, linearity and the selectivity. The sensitivity of the receiver is quantified by the overall noise figure. The channel selection, blocking and the image rejection of the receiver are governed by the selectivity of the receiver. The intermodulation distortion is determined from the linearity of the receiver. These parameters should be controlled according to the limitations in the standards to reach to an acceptable reception performance.

These issues are key performance parameters regardless of the selected architecture and the target application. However, implementing the multi-standard front-end intensifies some of the previous design challenges in conventional receivers [1]. One of the main challenges is the coexistence of several standards in one user equipment (UE). The key parameters of the receiver should be designed carefully to serve the multi-standard requirements. The noise budget must be able to accommodate all the noise contributors from other desired signals or undesired blockers of the scenario. The interference in multi-standard receivers is a major problem because each desired signal may act as an interferer for the other received signals in addition to the blockers and interferes. Since it becomes desirable to use simultaneous operation in a multi-standard receiver, it is important to meet the requirements specified in the standard for each application by controlling the interfering power of the other signals in the same user equipment. The calculations are provided according to the defined case-study of the thesis.

4.1.1   Coexistence between UMTS and WLAN

According to the defined scenario of the thesis, the UE enables both the WLAN and the UMTS to operate concurrently. The UMTS is known as a full-duplex system. Thus both the uplink (UL) and downlink (DL) may exist at the same time with the separation in frequency domain in the same transceiver. The duplexer is responsible of isolating these two signals in the 3G transceiver. However, the WLAN UL and DL are operating in different time periods due to the time division duplex (TDD) capability of the IEEE 802.11 standard. For deriving the worst case requirements of the receiver, the desired signal considered is the received UMTS signal from the base station and the interference sources are defined as the internal blocking signals leaking from the WLAN and UMTS transmitters at the same transceiver as shown in Fig. 1.2 with solid-line arrows.

The second probable case for this scenario is when the WLAN DL is active instead of WLAN UL while the UMTS transceiver operating at the same time shown in Fig. 1.2 with dashed-line arrows. In this case the received signal is in the range between -82 to -65 dBm (the sensitivity of the WLAN signal that depends on the data rates) which is well below the first case in comparison with the WLAN transmitted signal. Thus, to derive the most stringent requirements, the first case is investigated here. The spectrum of the UMTS DL and the UMTS UL and WLAN UL signals at the antenna ports is illustrated in Fig. 4.1. The receiver specifications according to the standards is outlined in Table 4.1.

A high isolation duplexer from Murata [97] with part number of "'DFYHA1G95HFHAA"' is
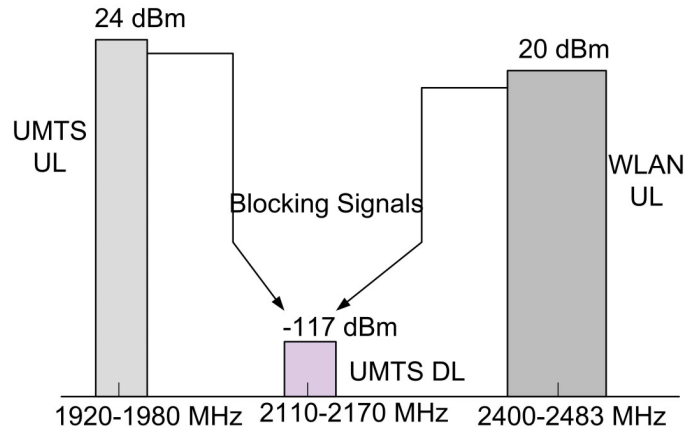
Figure 4.1: Illustration of frequency spectrum of UMTS UL, UMTS DL, and WLAN UL.

Table 4.1: Required receiver specifications for WLAN and UMTS standards [5], [7].

Parameter	UMTS	WLAN
Sensitivity [dBm]	-117 / -114 in blocking tests	-65 to -82 / depend on data rates
Maximum input level [dBm]	-25	-20
Maximum BER	0.001	10^{-5}
Intermodulation characteristics	iIP_{INT}= -46 dBm / at offsets $\pm 10/\pm 20$	not specified
SNR_{Req}	-18	6 to 25

employed to separate the UMTS received and transmitted signals with the parameters depicted in Table 4.2.

Table 4.2: Duplexer parameters [97].

	Bandwidth	Insertion Loss	Attenuation
Transmitter	60 MHz	2.5 dB	55 dB (2110 to 2170 MHz)
Receiver	60 MHz	2.0 dB	70 dB (1920 to 1980 MHz)

4.2 Sensitivity

The reference sensitivity level is the minimum input power at the antenna port of the receiver at which the BER does not exceed a certain level specified in each communication standard. The maximum tolerable noise figure (NF) of the front-end is determined from the sensitivity test. All the noise and distortions of the receiver must be suppressed to keep the total noise below the acceptable noise and distortion level (P_N) to comply with the receiver's out-of-band requirement and maintain the minimum required signal to noise ratio (SNR_{Req}) at the input of the base-band modulator. The maximum acceptable noise and distortion level of the receiver (P_N) is determined from:

$$P_N = S_i - SNR_{Req} \quad \text{[dBm]} \tag{4.1}$$

where S_i is the power level of the wanted signal in the out-of-band blocking test scenario seen from the antenna terminal. The SNR_{Req} is calculated from:

$$SNR_{Req} = (E_b/N_t)_{eff} - 10log(PG) \quad \text{[dBm]} \tag{4.2}$$

where (E_b/N_t) is the effective bit energy to noise density including an implementation margin for various baseband imperfections to meet the BER requirement stated in the standard and PG is the processing gain (PG). When there is not any noise in the environment and the only noise contributor is the receiver itself, the target receiver noise power for the desired signal including antenna noise is given by:

$$P_{N0} = k \cdot T_o \cdot \Delta f_0 \cdot NF \quad \text{[W]} \tag{4.3}$$

Where k is Boltzmann's constant, T_o is the standard noise temperature [16] and Δf_0 is the corresponding bandwidth of the desired signal $S_{F,0}$. It is assumed that the antenna noise temperature is equal to T_o.

However in a practical situation, several other signals have contributions in the desired signals band. For the practical case when the other noise contributors are turned on, the actual noise power is:

$$P_{N0} > k \cdot T_o \cdot \Delta f_0 \cdot NF + \sum_{n=1}^{N} P_{Nn} \quad \text{[W]} \tag{4.4}$$

where P_{Nn} is the noise leakage power from other sources in the Rx band at the receiver input signal, $S_{F,0}$. This equation is illustrated in Fig. 4.2. The maximum NF of the receiver is obtainable from the specification in each standard. This is the level of the noise below which the receiver has acceptable performance. The noise contribution from other sources must be controlled in the desired received band to keep the overall NF of the receiver below the maximum allowed level.
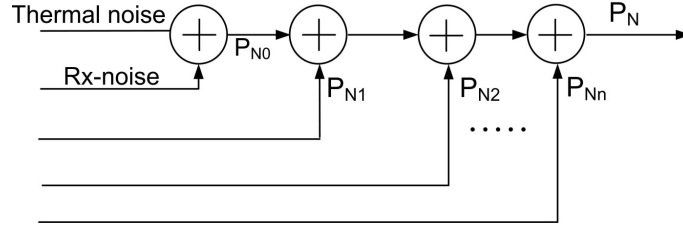
Figure 4.2: Illustration of the noise power budget for any generic receiver.

4.3   Linearity

The calculation of the intermodulation products is important in order to find the necessary constrains that guaranty the linearity of the receiver. The two tone test is a common measure of the intermodulation characteristics of the system in most of the wireless standards. The receiver linearity is determined by the amount of noise imposed to the fundamental product from the superimposition of the two tones. The corruption of signal by intermodulation products usually happen with odd order products specially third-order non-linearity except the zero-IF receivers. In zero-IF receivers, the even-order products corrupts the signals at baseband [98]. Since this is not the case for the current dissertation, the third-order product is considered as the major intermodulation source.

Two different intermodulation tests are examined for the proposed multi-standard receiver and the linearity constrains have been defined. The first test is performed with the classical two-tone test and the amount of the intermodulation distortion imposed on top of the desired signal is derived. The second test devotes to the case when a CW blocker in combination with either of the other signals of the scenario is providing intermodulation distortion in the desired band:

- Minimum in-band third order intercept point (iIP_3)

- Minimum out-of-band receiver's iIP_3

The minimum required k^{th} order intercept point can be calculated from Eq. (4.5) [98] where k is the non-linearity order, iIP_{INT} and iIP_{dis} are the interference power and the acceptable level of distortion power (referred to the input) respectively [98] and [83]:

$$iIP_k \geq \frac{k}{k-1} \cdot iIP_{INT} - \frac{1}{k-1} \cdot iIP_{dis} \ \ [\text{dBm}] \tag{4.5}$$

Eq. (4.5) is graphically illustrated in Fig. 4.3. The oIP_{INT} and oIP_{dis} are the interference power and the acceptable level of distortion power referred to the output respectively

1. As mentioned, the in-band third-order intercept point is determined from the two-tone test. Two equal-power tones are assumed to be located in the determined frequency offsets from the desired signal. These interfering signals are a CW blocker and a modulated signal. The level of the signals and their frequency offsets are specified in the standard.
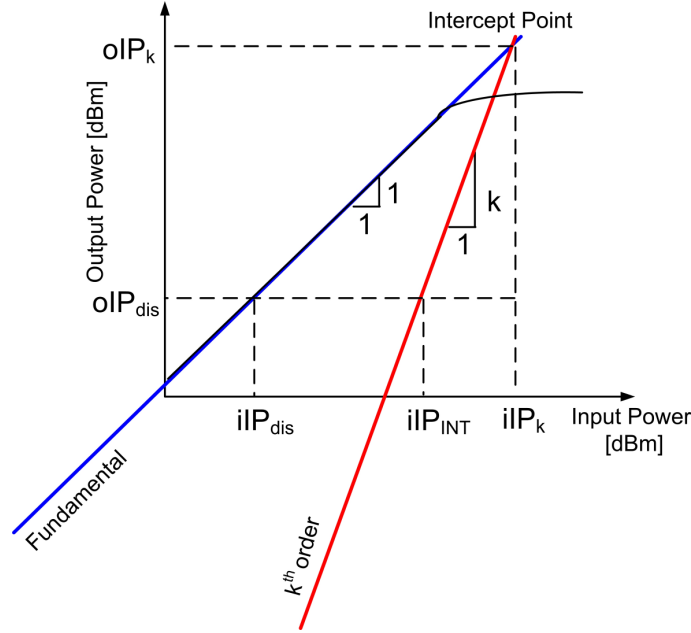
Figure 4.3: Illustration of the fundamental and k^{th} order intermodulation.

The frequency offsets are governed so that the combination of the two tones imposes intermodulation distortion on top of the desired band. The required intercept point is calculated from Eq. (4.5) which is governed by the allowed distortion power and the power of the interferes.

2. The other third-order intercept point considered in the research is the out-of-band receiver's iIP_3. It happens when a CW blocker in combination with either of the signals of the scenario creates an intermodulation product on top of the desired signal. Consequently, it sets an additional iIP_3 requirement on the receiver. The CW blocker power (P_{Blk}) can be determined from the out-of-band blocking test defined in the standard. Eq. (4.5) is employed to calculate the third-order intercept point for the signals of the scenario one-by-one. The calculation of the third-order intermodulation for a three-signal scenario is depicted in Fig. 4.4.

P_{INT2} is the power of the other signals of the scenario located at f_{INT2}. The CW blocker exists at f_{INT1} with the power level of P_{INT1}. The offsets from desired signals are calculated from the fact that these two signals have third-order intermodulation products in band. Thus the signals have third order harmonics at $|2f_{INT1} - f_{INT2}|$ and $|2f_{INT2} - f_{INT1}|$ which is the same as the desired band frequency. Since the offset from the P_{INT2} is already known, the P_{INT1} can be calculated as depicted in Fig. 4.4. The out-of-band intermodulation requirement for both leakages of the case study of the current research is calculated in Section 4.5.
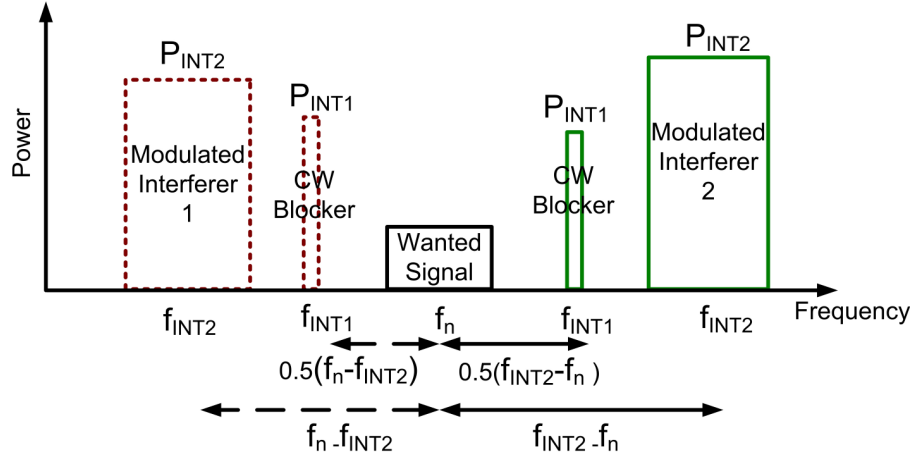
Figure 4.4: Illustration of the out-of-band third-order intermodulation test.

4.4 Selectivity

The selectivity is one of the key parameters specially for the sub-sampling receivers. In particular, this architecture is very sensitive to the signals located at the spectral replicas of the desires band since they are folding in the multiples of f_s to the desired band and distorting the signal significantly. Thus the receiver should be able to maintain the adequate performance by preserving the BER below a certain value (which is specified in each wireless standard) even in the existence of the numerous undesired signals at the antenna. This is done by providing adequate selectivity in the front-end to suppress all the undesired contributions below the required noise and distortion level. To calculate the maximum allowed noise level in the receiver, the required information is provided in each standard. The generic method is explained below.

The required level of the in/out-of-band emissions at different frequency offsets are specified in each wireless standard. According to the transmission mask of each signal, the signal is transmitted in three different emission areas as depicted in Fig. 4.5(a)— the in-channel, out-of-channel and out-of-band areas [20]. For each area, the required level of the desired or undesired signal is extractable from the correspondent wireless standard. The receiver must maintain the adequate performance by keeping the emissions from other signals in different frequency offsets below the required limit. This is shown in Fig. 4.5(b). The signal and its transmission mask are illustrated besides the out-of-band emission requirements. Each wireless system standard specify a minimum required signal to noise ratio (SNR_{Req}) at the input of the base-band modulator. The distortion must be suppressed to the appropriate level (P_{N+I}) to comply with the receiver's out-of-band requirement and maintain the SNR_{Req} at the input of the base-band modulator. This level which is the maximum acceptable noise and distortion level of the receiver (P_{N+I}) is determined from:

$$P_{N+I} = S_{id} - IL - SNR_{Req} \ \ [\text{dBm}] \tag{4.6}$$

The insertion loss (IL) is determined from the duplexer loss [97]. The S_{id} is the power level
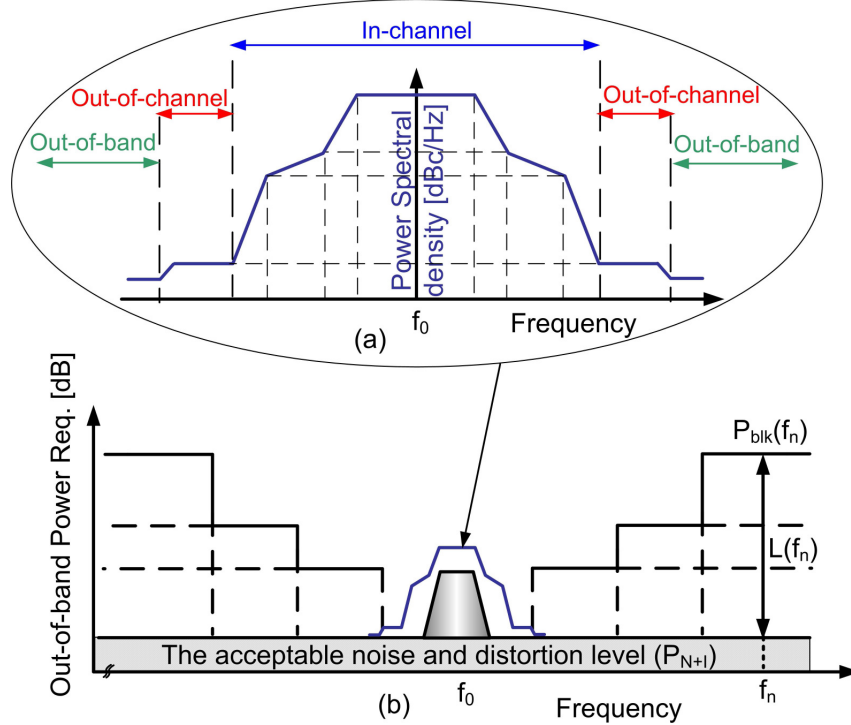
Figure 4.5: Illustration of the front-end requirement (a) transmission mask; (b) the desired signal and required out-of-band blocking powers.

of the wanted signal in the out-of-band blocking test scenario seen from the antenna terminal which is usually assigned to be 3 dB above the receiver sensitivity level in wireless standards. This is defined as the level of wanted signal in blocking test.

The required level of blocking is identified in wireless standards as well for different test such as blocking, two tone or out-of-band blocking tests. To maintain the required BER and the SNR_{Req} of the receiver within the acceptable limits, all the in/out-of-band blockers must be suppressed to the level below the required level P_{N+I}. To suppress the blocking signal power (P_{blk}) located at f_n below the P_{N+I}, the required front-end selectivity at each specific frequency should be:

$$L(f_n) \geq P_{blk}(f_n) - P_{N+I} \quad [\text{dB}] \tag{4.7}$$

where $L(f_n)$ is the required front-end suppression seen from the antenna terminal at the frequency f_n and $P_{blk}(f_n)$ is the required out-of-band blocking power specified in each RF standard. This general formula is investigated for two specific cases of intermodulation and image rejection selectivity.

4.4.1 Intermodulation

The selectivity requirements related to the intermodulation distortion is investigated.

Selectivity requirements for in-band third order intercept point (iIP_3)

The common measure of the intermodulation performance of the receiver is the two-tone test. In this test, two tones in pre-defined frequency separation and equal powers are used to formulate the intermodulation products which are imposed in-band of the desired signal. The BER shall not exceed a certain value in the presence of the two signals defined as a CW signal and a modulated signal with equal powers with intermodulation contribution in the desired band. The test is illustrated in Fig. 4.6. The P_{blk} is the power of the blockers located at offset frequencies of f_{of1}/f_{of2} from the desired signal.
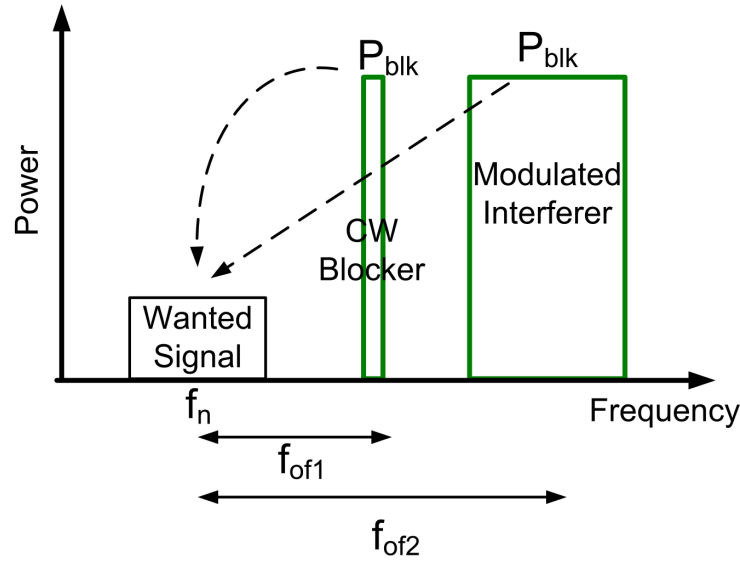
Figure 4.6: Illustration of the two-tone test.

According to the disturbance budget distribution of the receiver, the allowed intermodulation products in-band is specified to be IM_{dB}. Thus the acceptable power level of each blocking signal or intermodulation product after the duplexer is:

$$iIP_{dis} = P_{N+I} - IM_{dB} - IL \quad [\text{dB}] \tag{4.8}$$

where iIP_{dis} is the acceptable level of distortion power referred to the input and IL is the insertion loss. Consequently, the receiver iIP_3 can be calculated from Eq. (4.5) by substituting the iIP_{INT} with the P_{blk} specified in the wireless standard and iIP_{dis} calculated from Eq. (4.8). The required selectivity to suppress the intermodulation products at the frequency offsets of f_{of1}/f_{of2} can be calculated accordingly.

This required selectivity at offset frequencies of f_{of1}/f_{of2} to suppress the intermodulation products below the required level is calculated from Eq. (4.6) by considering the effect of IM_{dB} in the acceptable noise and distortion level:

$$L(f_{of1}/f_{of2}) \geq iIP_{INT} - (P_{N+I} - IM_{dB} - IL) \quad [\text{dB}] \tag{4.9}$$

It should be noted that by using Eq. (4.9), the same selectivity value of $L(f_{of1}/f_{of2})$ is obtained for both signals at different frequency offsets of f_{of1}/f_{of2}. However in a practical situation, different suppression may be applied to these two tones in the filtering procedure depending on their allocation in the spectrum of the filter [83]. An example is shown in Fig. 4.7 where two tones will experience different suppressions of $L(f_{of1})$ and $L(f_{of2})$.
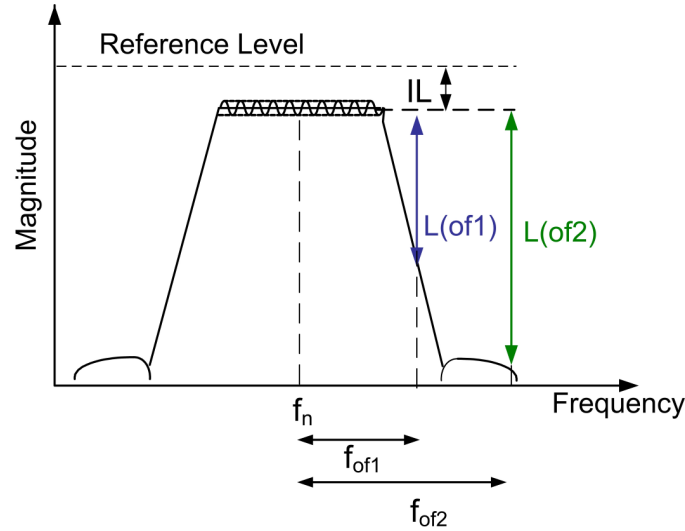
Figure 4.7: Illustration of the spctrum of the RF bandpass filter and allocation of the two tones accordingly.

In this case, the total suppression is the average value of the two suppressions [83]:

$$L(f_{of}) = \frac{k-1}{k} \cdot L(f_{of1}) + \frac{1}{k} \cdot L(f_{of2}) \ \ [\text{dB}] \tag{4.10}$$

where k is the order of the non-linearity product which is three for this test.

Selectivity requirements for out-of-band receiver's iIP_3

There is a possibility that a CW blocker in combination with either of the other signals of the scenario creates an intermodulation product on top of the desired signal. Therefore, it sets an additional iIP_3 requirement on the receiver.

According to the out-of-band blocking test defined in the standard, the required CW blocker (P_{Blk}) is specified in different frequency offsets as shown in Fig 4.5. Dissimilar to the in-band two-tone test (that the tones have equal powers), the power of the two tones after RF filtering for this test are not necessarily equal. They have different power levels experiencing different suppressions from the RF filter. That is due to the fact that one of the two tones is another desired signal of the scenario received at the antenna which is not necessarily at the same level as the CW blocker. We assume that the signals are spectrally located at the frequency offsets of f_{of1}/f_{of2} as shown in Fig. 4.7 similar to the case for the in-band two-tone test. Two signals with different power levels will experience different suppressions by RF filtering. So there is a big possibility that they do not have equal power levels. However to use the two-tone test

concept, the signals must be averaged and replaced with two equal-power signals.

The signals after attenuation are called iP_{INT1} and iP_{INT2} as depicted in Fig. 4.4. To calculate the iIP_k product, the two signals are replaced by an equal value calculated from the following formulation [85]:

$$iIP_{INT} = \frac{k-1}{k} \cdot (iP_{INT1}) + \frac{1}{k} \cdot (iP_{INT2}) \quad [\text{dBm}] \tag{4.11}$$

where k is the order of the intermodulation product which is 3 for the third order nonlinearity calculations. According to the allowed amount of noise from other signals in the desired band and the receiver's noise budget, the iIP_{dis} can be estimated. Consequently, the minimum requirement for the out-of-band iIP_k is calculated from Eq. (4.5). To calculated the selectivity for out-of-the band intermodulation, similar discussion to the in-band intermodulation is valid. Eq. (4.9) could be used to calculate the required selectivity.

4.4.2   Image rejection

The suppression of the out-of-band impending image signals is governed by the total selectivity of the RF front-end. The RF filtering prior to the sample & hold block plays a vital role since it prohibits folding of the image noise along with the desired signal to the band of interest. In other words, one of the major tasks of the radio frequency (RF) filter is to reduce the power of the unnecessary spectral replicas centered at $|mf_s \pm f_{IF}|$. The signals located in these frequencies (called image signals) are at least partially down-converted to the desired band.

To design the multi-standard RF sub-sampling receiver, the technique mentioned in Chapter 3 is used to select the best sampling rate. However, this technique is only useful to down-convert the expected signals at the antenna to non-overlapping portions of the Nyquist band.

In spite of all the attempts to develop sampling frequency techniques to alias signals to non-overlapping portions of the Nyquist band, the sub-sampling architecture is still very sensitive to the impending signals located at the image frequencies. This is the task of the RF filters to govern the required selectivity of the front-end to prohibit the problem of image. Especially since in sub-sampling receivers, we face with the replication of the sampling frequency which makes the case even more complex.

One of the effective control tools to solve this problem is the sampling frequency of the front-end. Since the location of the image frequencies in RF sub-sampling receivers depend on the selected f_s, it can be used as a proper tool in combination with the provided selectivity of the front-end to achieve to the appropriate image rejection in the receiver. The allocation of the image distortions will be controlled with the f_s to be located in the part of the spectrum, with sufficient suppression provided by the front-end's selectivity. This is done by employing the following procedure:

1. The required selectivity of the receiver is calculated at image rejection frequencies (for each f_s) to reach to a required SNR at the input of the base-band modulator.

2. To govern the adequate separation of the image distortion from the desired signal, the interfering profile proposed in Section 3 is employed. The profile works based on controlling each acceptable f_s achieved from the algorithms such as $[2, 3]$ and see if all the corresponding in-band image distortions for that f_s at RF are suppressible by the provided front-end selectivity.

The selectivity of the front-end is decided from the blocking tests of the relevant communication standard. Thus it is required to combine the image properties of the sampling architectures with the blocking tests of the relevant communication standard to figure out the best frequency plan of the front-end. An efficient way on how to calculate the needed front-end selectivity in the presence of the image distortion to obtain a specified SNR at the output of the sampler is presented in this chapter. The method contains all the required consideration to place the image in a distance from the desired band which is completely suppressible by the selectivity of the front-end.
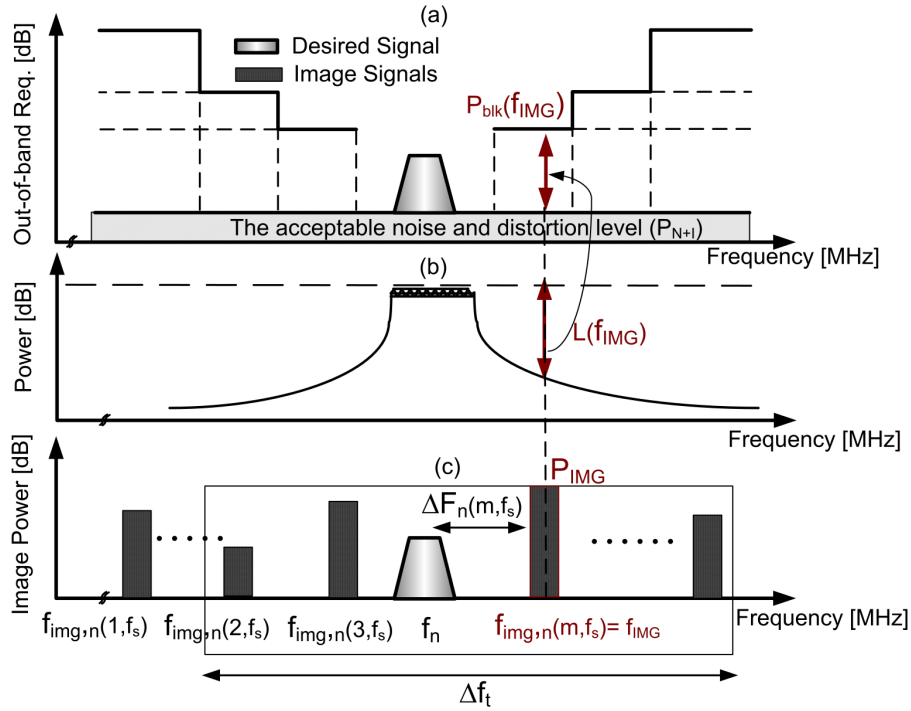
Figure 4.8: Illustration of the front-end Selectivity Requirements: (a) the desired signal and required out-of-band blocking, (b) front-end selectivity frequency response and (c) the image signals allocation (the δf_t is the receiver's total bandwidth).

The idea is to use the interference profile presented in Section 3.2 and combine it with the selectivity requirements of the receiver and f_s dependency of the image frequencies. The disturbing signals in this scenario for the interference profile are the impending image signals at the antenna. From subsequent chapters, it is known that the f_s dependent image distortions

of sub-sampling architecture are spectrally located at:

$$S_{F,n} : f_{IMG} = f_{img,n}(m, fs) = m\, f_s \pm f_{IF,n} \quad \text{for} \quad \text{m} = 0, \pm 1, \ldots \tag{4.12}$$

$$S_{F,n}^* : f_{IMG} = f_{img,n}(m, fs) = -m\, f_s \mp f_{IF,n} \quad \text{for} \quad \text{m} = 0, \pm 1, \ldots \tag{4.13}$$

The intermediate frequencies $f_{IF,n}$ are calculated from Eqs. (3.1) and (3.2). To render an undisruptive signal on top of the desired signal in the Nyquist band and maintain the SNR_{Req}, the required front-end selectivity at the image frequency must be sufficient:

$$L(f_{IMG}) \geq P_{blk}(f_{IMG}) - P_{N+I} \quad [\text{dB}] \tag{4.14}$$

where $L(f_{IMG})$ is the required front-end suppression seen from the antenna terminal at the image frequency, f_{IMG}, and $P_{blk}(f_{IMG})$ is the required out-of-band blocker specified in each RF standard at the image frequencies as illustrated in Fig. 4.8(a). The front-end selectivity must be able to provide the suppression of at least $L(f_{IMG})$ at the frequency of f_{IMG} as depicted in Fig. 4.8(b). The mentioned procedure provides the set of the required attenuations by the filter in the image frequencies at each sampling frequency. The RF band-pass image rejection filter could be effectively designed to remove the impending images.

However, this approach is helpful only in suppressing the image signals which are located far enough from the desired signal to be attenuated by the RF filter. In other words, the undisruptive down-conversion of the image noise on top of the desired signal is feasible if:

$$P_{IMG} \leq P_{N+I} + L(f_{IMG}) \quad [\text{dB}] \tag{4.15}$$

where P_{IMG} is the power level of the image signal at f_{IMG} as shown in Fig. 4.8(c). If Eq. (4.15) is not met, the front-end selectivity is not able to prevent the folding of the corresponding image noise with the desired signal at that specific sampling frequency. Obviously, the signal is totally distorted in this case and the sampling frequency corresponding to this image distortion should be discarded from set of the acceptable sampling rates of the target application. This procedure is written in the form of an algorithm which must be tried for all the sampling frequencies selected from Chapter 3. The sampling rates which can not fulfill the selectivity requirements of the front-end are discarded by this method.

Governing selectivity based on Sampling Rate Considerations

The algorithm proposed here can be treated as an extension to the sampling rate procedure in Chapter 3. After selecting the best possible sampling rate based on the mentioned constraints, they should be checked and assured to have the image distortion in the suppressible distances from the desired band.

To make a good compromise between receiver's selectivity and f_s it is thus needed to take each probable disturbing signal at image frequencies one by one and see if the required selectivity

could be provided by the front-end at that frequency or not. This procedure must be repeated for all the valid f_s selected from the presented algorithm in Section 3. If the receiver's selectivity is not sufficient for all the image distortions (of any f_s) in the total band of the receiver (even for one of them), the sampling rate must be discarded and the next one must be tried.

The mentioned technique is necessary to be examined in addition to the sampling selection techniques presented in Section 3.2 because of two important reasons:

1. The first reason is that even the down-conversion of the weakest image distortion to the desired band could be problematic in the absence of the required selectivity.

2. Moreover, the technique mentioned in Section 3.2 sets the weakest blocker in the environment as the closest image distortion to the desired band. However, the sub-sampling architecture suffers from numerous image distortions in the multiples of sampling frequency and one of the other images could cause problems.

Thus providing sufficient selectivity at all the image frequencies (of each f_s) guarantees the reception of the signal with less noise and acceptable quality. This can be done by combining the technique mentioned in Section 3.2 with the selectivity requirements.

First of all the intermediate frequency at each sampling frequency is chosen according to Eqs. (3.1) for reception of $S_{F,0}(f)$ or Eq. (3.2) for $S_{F,0}^*(f)$. Consequently, the image frequencies are calculated from Eqs. (4.12) and (4.13). This means that f_{IF} and f_{IMG} follow from a selection of f_s. In other words, the intermediate frequency f_{IF} and the image frequency f_{IMG} are not a degree of freedom — but f_s is. To make a good selection of the sampling rate f_s it is thus needed to take each disturbing signal at image distortion frequencies one by one and see if the corresponding f_s gives adequate frequency distance between the carrier frequency and the image distortion products at RF. Adequate frequency distance means a distance at which the image distortion is suppressible by the selectivity of the front-end and Eq. (4.15) is valid. This should be performed for all the in-band images individually at each sampling frequency.

By ignoring the effect of image distortion in sub-sampling receivers, several image signals may be delivered on top of desired signal and make it completely distorted. To check the required selectivity at each sampling frequency, the frequency distance from each correspondent image distortion to the desired carrier frequency at RF is calculated from:

$$\Delta F_n(m, f_s) \;=\; |f_n - (m.f_s \pm f_{IF,n})| \quad \text{for} \quad m = 0, \pm 1, \dots \qquad (4.16)$$

where $f_{IF,n}$ is the intermediate frequency calculated from Eqs. (3.1) and (3.2). It can be seen from Eq. 4.16 that the image distortions can be spectrally located in infinite frequencies. To limit it to the practical case, only the images in the total frequency band of the receiver (Δf_t) are considered as shown in Fig. 4.8(c). The in-band images are the distortions that are really folding down along with the desired signals to the desired band. The images out-of-the band of receiver will be filtered out by the stop-band attenuation of the front-end.

The algorithm for determining the adequacy of the selectivity in each image frequency can be written:

For all valid f_s

  Initialize $m=0$

  For disturbing signal $p=1:N$

- For m=m+1
- Calculate $f_{IMG} = f_{img,p}(m, fs)$ from Eqs. (4.12) and (4.13)
- Calculate $\Delta F_p(m, f_s)$ from Eq. (4.16)
- if $\Delta F_p(m, f_s) \leq \Delta f_t$
    - Estimate P_{IMG} at f_{IMG}
    - Estimate $L(f_{IMG})$
    - if Eq. (4.15) is valid
    -   then continue with the same f_s
    -   else go to the next f_s; end
- end

  acceptable f_s

end

This algorithm is based on calculating the distance from the desired signal to all the in-band images one by one for all the valid f_s(calculated from Section 3.2). If this distance is within the desired band of the receiver, it means that the corresponding image distortion could be problematic for the desired signal. This is graphically depicted in Fig. 4.8(c). In the next step, the power of the image signal at that point is estimated from the model which already apprehended in the receiver based on the technique presented in Section 3.3. Accordingly, the suppression of the front-end filter at the image frequencies could be estimated from the transfer function of the filter.

As mentioned before, the required selectivity of the front end could be calculated from the blocking tests of the relevant communication standard. Thus to estimate the required selectivity, the required blocking power in each frequency offset is derived from the wireless standard as depicted in Fig. 4.5. Consequently, the required blocking power in the image frequency offsets could be determined as shown in Fig. 4.8(a).

This makes it possible to see if the image distortion at that frequency offset is suppressible with the existing front-end selectivity according to Eq. (4.15). This is shown in Fig. 4.8(b), (c). If the suppression is enough, the sampling frequency and provided front-end's selectivity are sufficient. Otherwise, the sampling frequency must be discarded and the algorithm starts to try the next sampling frequency for checking the selectivity requirements of all the in-band image distortions. For each signal sampled at each valid sampling frequency, all the image distortion replicas in-band must pass Eq. (4.15) in order to provide an acceptable compromise between

the selectivity and sampling rate. Even if one of the images denies following Eq. (4.15), it indicates that a harmful delivery of a strong blocker will happen on top of the desired signal.

4.5   Calculations and simulation results

4.5.1   Calculations for receiver sensitivity

UMTS DL path

The reference sensitivity level for the UMTS is the minimum input power at the antenna port of the receiver at which the bit error rate (BER) does not exceed 0.001 [5]. The maximum tolerable NF of the front-end is determined from the sensitivity test. The effective bit energy to noise density (E_b/N_t) including an implementation margin for various baseband imperfections is 7 dB to meet the BER requirement [84]. The minimum UMTS DL power level before de-spreading in the front end (S_i) is -117 dBm/3.84 MHz [5]. The duplexer IL is 2 dB [97], and the PG is 25 dB [85]. To meet the requirements specified in the standard, the acceptable noise and distortion level (P_N) after the duplexer is equal to -101 dBm/3.84 MHz calculated from Eqs. (4.2) and (4.1) by including the IL:

$$P_N = S_i - IL - (E_b/N_t)_{eff} + 10 \cdot \log(PG) \quad [\text{dBm}] \tag{4.17}$$

When the transmitters are turned off, the receiver noise power including antenna noise (P_{N0}) is calculated from Eq. (4.3). It is assumed that the antenna noise temperature is equal to T_o. When the transmitters are turned on, the actual noise power is calculated from Eq. (4.4) with two other noise contributors:

$$P_{N0} > k \cdot T_o \cdot \Delta f_0 \cdot NF + P_{N1} + P_{N2} \quad [\text{W}] \tag{4.18}$$

Where k is Boltzmann's constant, T_o is the standard noise temperature and Δf_0 is the signal bandwidth [16]. P_{Nn} is the transmitter noise leakage power in the Rx band at the receiver input according to the scenario defined in Section 4.1. This equation is illustrated in Fig. 4.9.

If the transmitters are turned off, the only contributor to noise is the receiver noise power including the antenna noise. Thus, the acceptable noise and distortion level (P_N) is equal to receiver plus thermal noise (P_{N0}) resulting to a receiver noise figure of 7 dB by using Eq. (4.3). To make a room for the noise leakages from WLAN and UMTS transmitters in the receiver noise budget, the receiver noise figure must be reduced consequently. The disturbance budget that has been chosen allows 1 dB noise figure reduction in the receiver. After all filtering, amplification and suppression, the coming disturbances from the UMTS UL (P_{N1}) and WLAN UL (P_{N2}) in UMTS DL are sharing the remaining noise and disturbances equally that leads to the noise power budget defined in Fig. 4.9 [98]. Other choices of NF reduction and allowed transmitter noise leakages may be made according to a cost analysis for the transceiver.

The acceptable UMTS UL and WLAN UL noise power in UMTS DL (at the antenna port)
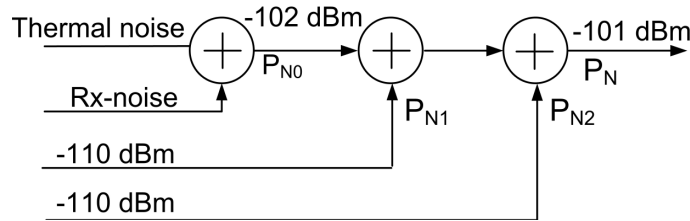
Figure 4.9: Illustration of the noise power budget for the multi-standard receiver supporting WLAN and UMTS.

must not exceed -110 dBm with respect to the noise budget. The allowed out-of-band power of WLAN is 40 dB below the Power Spectral density (PSD) of the transmitted signal [7]. The power level of the WLAN transmitter is 20 dBm (the PSD is -52 dBm/Hz). Therefore, the WLAN PSD in the UMTS receive-band is -92 dBm/Hz or $-26 dBm/3.84$ MHz at the WLAN antenna. To obtain a level of -110 dBm, it is required to provide an isolation of 84 dB. This does not seem realistic to be achievable only by the separation of antennas and filtering in the receiver path. Thus, a reduction of the noise in the WLAN transmitter is required.

WLAN DL path

To provide a complete overview of the sensitivity requirements, it is calculated for the case when the WLAN transceiver is downloading information or the WLAN DL is active instead of uplink. This provides extra information required for the design of the front-end in addition to the scenario defined in the current analysis. Similar calculation performed for the UMTS standard is applicable for the WLAN signal.

Table 4.3: Performance requirements of WLAN for UE [7].

Rates (Mbps)	Sensitivity without ACI (dBm)	Sensitivity with ACI (dBm)	SNR (dB)	EVM (dB)	P_N (dBm)	P_{N+I} (dBm)
6	-82	-79	6.02	-5	-88.06	-85.06
9	-81	-78	7.78	-8	-88.78	-85.78
12	-79	-76	9.03	-10	-88.03	-85.03
18	-77	-74	10.79	-13	-87.79	-84.79
24	-74	-71	17.04	-16	-93.04	-90.04
36	-70	-67	18.80	-19	-88.08	-85.08
48	-66	-63	24.05	-22	-90.05	-87.05
54	-65	-62	24.56	-25	-89.56	-86.56

The packet error rate (PER) shall be less than 10% at a PSDU length of 1000 bytes for rate-dependent input levels specified in Table 4.3 [7]. The minimum required SNR (SNR_{Req})

depends on the modulation type and data rate [7]. It changes between the 6.02 dB for 6 Mb/s to 24.56 dB for 54 Mb/s. To provide the required SNR for 54 Mb/s (the data rate considered in this analysis), the acceptable noise and distortion level for WLAN (P_N) is calculated equal to -89.56 dBm respectively calculated from Eq. 4.1. To include the IL from duplexer, the -2 dB loss must be added to these numbers. The performance requirement of the WLAN signal for different data rates is outlined in Table 4.3.

4.5.2   Calculations of the Intermodulation products and selectivity requirements

Three different intermodulation tests are examined for the proposed multi-standard receiver and the linearity constrains have been defined:

- Minimum in-band third order intercept point (iIP_3)

- Minimum out-of-band receiver's iIP_3 (UMTS UL)

- Minimum out-of-band receiver's iIP_3 (WLAN UL)

In-band Test

The two-tone test has been defined to set the requirements for the in-band iIP_3 of the receiver. The BER shall not exceed 0.001 in the presence of the two signals defined as a CW signal (I_{ouw1}) and a modulated signal (I_{ouw2}) with equal power of -46 dBm [5]. Interferes are located at the offset frequencies of 10 and 20 MHz, respectively. The third order distortion caused by these two signals in the desired channel is added on top of the wanted signal. By proper choice of the filters in the receiver, the signal leakages from the WLAN and UMTS UL signals can be sufficiently suppressed. Therefore, the direct blocking effect is avoided. A budget distribution is assumed for the intermodulation test that covers all the different noise and distortions as presented in Table 4.4.

Table 4.4: Budget distribution for disturbance [85].

Disturbance	Percentage	Level
Noise (antenna, receiver, WLAN and UMTS UL)	50%	-3 dB
Intermodulation products	15%	-8 dB
Modulated interferer blocking	15 %	-8 dB
CW interferer blocking	15%	-8 dB
Oscillator noise	5%	-13 dB

The acceptable power level of each blocking signal or intermodulation product after the duplexer is $(P_{N+I}) - 8$ dB $= -106$ dBm. The receiver $iIP_3 \geq -19dBm$ is calculated from

Eq. (4.5). The receiver selectivity must limit the blocking effect of the two interfering signals. The required selectivity at 10 and 20 MHz frequency offsets is calculated equal to 60 dB using:

$$Selectivity(10/20 \text{ MHz}) \geq \text{iIP}_{\text{INT}} - (\text{P}_{\text{N+I}} - 8\text{dB}) \tag{4.19}$$

Out-of-band CW blocker

There is a possibility that a CW blocker in combination with either of the WLAN or UMTS UL signals creates an intermodulation product on top of the desired signal (UMTS DL). Therefore, it sets an additional iIP_3 requirement on the receiver. According to the out-of-band blocking test defined in the 3GPP standard [5], the CW blocker (P_{Blk}) with the power level of -44, -30, and -15 dBm may exist at the frequency offset of 15, 60 and 85 MHz, respectively as shown in Fig. 4.11. The out-of-band intermodulation requirement for both leakages is calculated in the following section.

UMTS UL leakage   The test case is illustrated with brown color in Fig. 4.10.

The CW interferer and the UMTS transmitter leakage are located at the offsets of 65 and 130 MHz from the desired signal. The signal powers are -30 and 24 dBm respectively. They suppressed to -60 dBm and -46 dBm, respectively after passing through the duplex filter (providing 30 and 70 dB attenuation, respectively as shown in Table 4.2) and duplexer specifications [97].
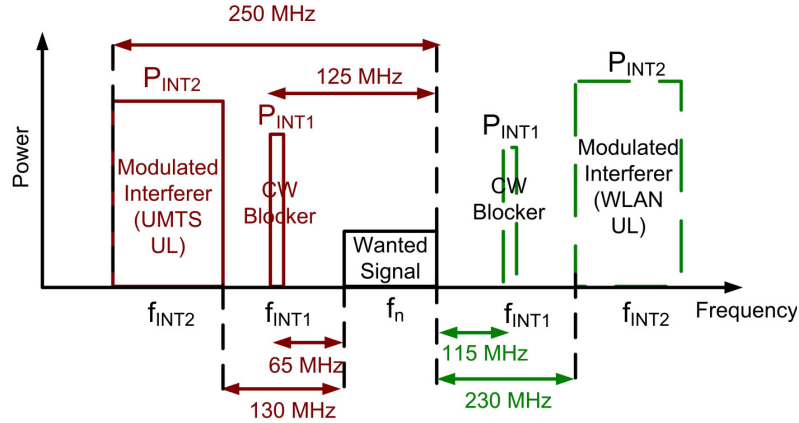
Figure 4.10: Illustration of Out-of-band intermodulation test (WLAN UL green color, UMTS UL brown color).

To calculate the iIP_3 product, the two signals are replaced by an equal value from Eq. (4.11) [85]:

$$iIP_{INT} = \frac{1}{3} \cdot (-46) + \frac{2}{3} \cdot (-60) = -55.3 \ \ [\text{dBm}]$$

Because of the large frequency offset, the blocking effects are negligible and the allowable interference level is $P_{N+I} - 3$ dB (noise contributes 50 percent of the power). The duplexer IL is assumed to be 2 dB. Therefore, the minimum requirement for the third order intermodulation

is calculated from Eq. (4.5):

$$iIP_3\,(65/130MHz) \geq -32.5\ \ \text{[dBm]}$$

WLAN UL leakage Since the minimum distance between UMTS DL and WLAN is 230 MHz, the CW blocker is always located at the frequencies with more than 85 MHz offset from the desired signal. The calculations are done for the case that two closet channels from UMTS DL and WLAN are considered.

The CW blocker is located at 115 MHz offset and the modulated interferer (the UMTS UL signal) is placed at the 230 MHz offset from the UMTS DL as illustrated in Fig. (4.10) with green color. The 20 dBm leakage from the WLAN UL signal is attenuated 57 dB by the duplex filter [97]. The CW blocker is suppressed 52 dB by duplex filter and reaches -67 dBm (out-of-band blocker at distances more than 85 MHz is -15 dB [5]). The two signals are replaced by an equal value from Eq. (4.11) [85] which is:

$$iIP_{INT} = \frac{1}{3} \cdot (-37) + \frac{2}{3} \cdot (-67) = -57\ \ \text{[dBm]}$$

With similar discussion to the UMTS UL, the iIP_3 is derived from Eq. (4.5) to:

$$iIP_3\,(115/230MHz) \geq -35\ \ \text{[dBm]}$$

From the intermodulation test calculations, it comes out that the requirement for in-band iIP_3 is more stringent than the requirement for out-of-band third order intermodulation. Moreover, it should be mentioned that the duplexer specifications have great impact on the out-of-band iIP_3 requirement calculations as it is mentioned in the previous section.

4.5.3 Calculations & Simulations

UMTS DL

The RF filtering prior to sample and hold (S/H) block has the important role of suppressing the powers of undesired replicated images. As mentioned in Section 4.4.2, the image distortions are spectrally located at $|mf_s \pm f_{IF}|$. The f_{IF} follows the selection of f_s according to Eqs. (3.1) and (3.2). Consequently, the image is varying versus the sampling frequency. The f_s dependency of the the image frequencies is also mentioned in Eqs. (4.12) and (4.13).

To calculate the selectivity requirements for the UMTS DL for the image rejection or intermodulation suppression, the UMTS out-of-band emission profile depicted in Fig. 4.11 is considered. It is due to the fact that the image-rejection capability of the receiver can be determined from the out-of-band blocker test.

Depending on the selection of the sampling rate, the image distortions are spectrally located at predictable offsets from the desired band. These offsets are formulated in Eq. (4.16). The combination of the image locations and the out-of-band requirements of the standard determines the required image rejection of the front-end.
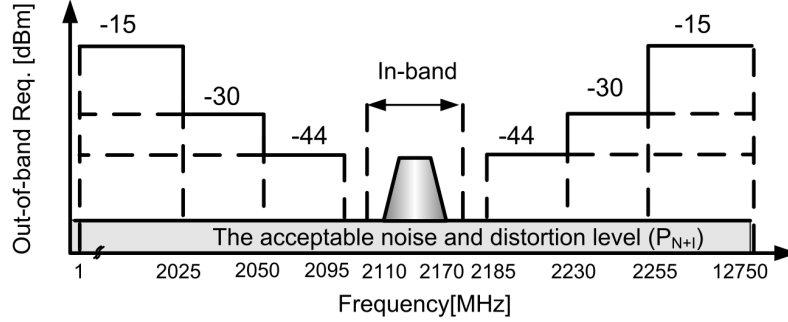
Figure 4.11: Illustration of the out-of-band intermodulation characteristics of the UMTS signal.

It can be seen from Fig. 4.11 that the out-of-band requirements for the UMTS signal is divided into three main regions. According to the out-of-band blocking test defined in the standard, the CW blocker (P_{Blk}) with the power level of -44, -30, and -15 dBm may exist at the frequency offset of 15, 60 and 85 MHz, respectively. To derive the overall image rejection requirements, the image rejection in each region is calculated based on the method mentioned in Section 4.4.2.

1. If the blockers located at more than 85 MHz offset, The required selectivity is calculated equal to 86 dB from Eq. (4.14) noting that the noise has the 50 percent contribution:

$$L(> 85MHz) \geq P_{Blk} - (P_{N+I} - 3dB) \tag{4.20}$$

2. The same calculation is done for the blockers located at the interval of [60 MHz;85 MHz]. The required selectivity is calculated L($[60MHz; 85MHz]$) $\geq$ 71 dB.

3. The last out-of-band region is [15 MHz;60 MHz]. The required selectivity of L([15 MHz;60 MHz])$\geq$ 57 dB is calculated for this region.

Based on the allocation of the image distortion related to the desired band, one of the calculated selectivities should be applied to the image distortion frequencies.

From several images for each desired signal, the closest images are considered to derive the filtering requirements as the most severe image distortions. That is due to the fact that the closest images to the desired signal are more difficult to suppress with the front-end filters. There is a high risk that they are down-converted to the desired Nyquist band along with the signal. The further the images are spectrally located, it is easier to suppress them with the stop-band attenuation of the front-end filter.

The closest images are spectrally located at $|-2f_{IF}|$ and $|f_s - 2f_{IF}|$ offsets from the desired signal based on Eq. (4.16). This is graphically depicted in Fig. 4.12. The image offset of $|-2f_{IF}|$ is called "'closest image toward zero"' since it should be valid for the signal as well as its complex conjugate. The reason is that this variable provides the information about the image signal which is in the side of the desired band which is toward the zero frequency. On

contemporary, the $|f_s - 2f_{IF}|$ offset variable is called "'closest image toward $\pm\infty$"'. This is marked in Fig. 4.12.
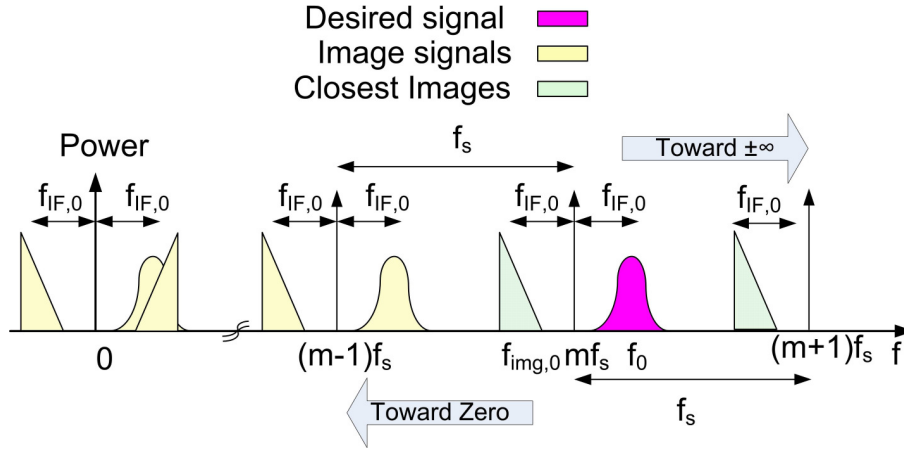
Figure 4.12: Illustration of the spectral allocation of the closest images to the desired band.

The frequency offsets from the closest images versus the sampling frequency is depicted in Figs. 4.13 and 4.14 for different channels of the UMTS DL band. Fig. 4.13 depicts the $|-2f_{IF}|$ variations and 4.14 shows the variations of $|f_s - 2f_{IF}|$ offsets from the desired band. Totally, the y axis of these figures presents the closet image frequency offset from the desired signal.
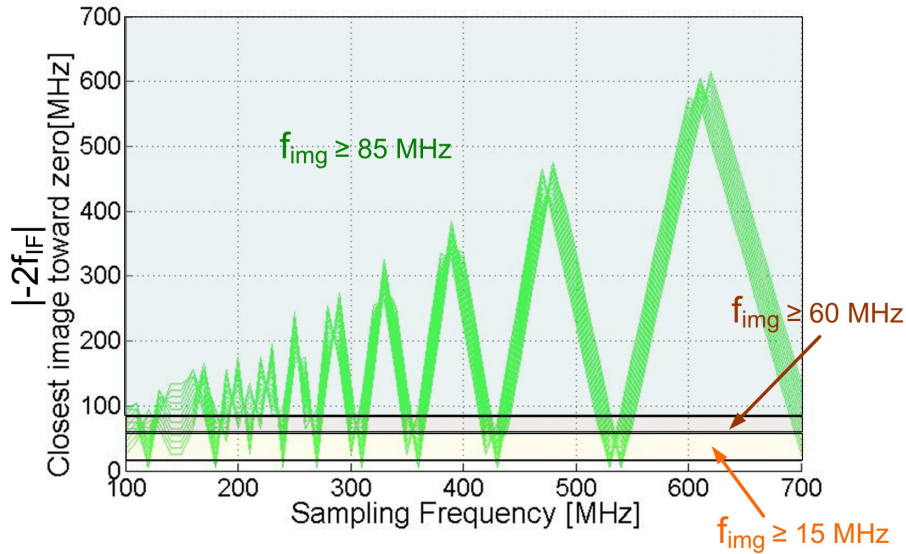
Figure 4.13: Illustration of the closest image frequencies toward zero and their allocation in the out-of-band requirement regions of UMTS signal. The zero offset (zero of the y axes) represents the allocation of the UMTS desired band.

To match the image spacing with out-of-band requirements, the three different regions of Fig. 4.11 is mapped to Figs. 4.13 and 4.14. In the region marked with $f_{img} \geq 85$ MHz, the image distortions are categorized in the frequency offset of more than 85 MHz. In this region
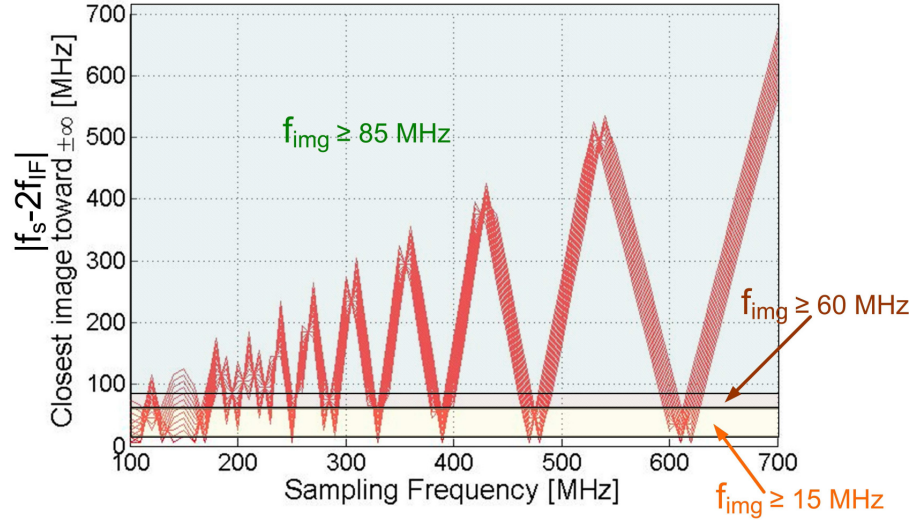
Figure 4.14: Illustration of the closest image frequencies toward infinity and their allocation in the out-of-band requirement regions of the UMTS signal. The zero offset (zero of the y axes) represents the allocation of the UMTS desired band.

the required image rejection is calculated from item 1 stated in the paragraph above this page and is equal to 86 MHz. All the sampling rates result in image distortions in this frequency range must follow the out-of-band requirements of more than 85 MHz.

The region marked with $f_{img} \geq 60\,\mathrm{MHz}$ in Figs. 4.13 and 4.14 is correspondent to the offsets of [60 MHz;85 MHz] in out-of-band requirements. The images spaced in this region from the desired band must be suppressed with the selectivity formulated in item 2. The image rejection capability of the receiver should be more than 71 dB according to the calculations.

The last area marked with $f_{img} \geq 15\,\mathrm{MHz}$ in Figs. 4.13 and 4.14 correspond to the offsets of [15 MHz;60 MHz] in out-of-band requirements. In this region, the required image rejection provided by the front-end should be more than 57 dB.

The same concept is depicted in the 3D plot of Fig. 4.15. Instead of the frequency offsets of Figs. 4.13 and 4.14, the total band is presented in the Z axis of Fig. 4.15. The UMTS in-band area and the out-of-band requirements are shown and marked in the figure. The in-band information lies between two parallel yellow plates of the figure marked "'in-band"'. The three out-of-band requirement regions from both sides of the in-band signal similar to Fig. 4.11, is depicted with parallel green and red plates marked out-of-band Req. in Fig. 4.15.

Moreover, the two close image bands are varied versus sampling frequencies and the carrier frequencies. Dependent on the allocation of the image in each of the out-of-band regions, the required image rejection should be calculated. This is outlined in Table 4.6. The specific requirements for the design of the case-study of this dissertation is provided in Chapter 5.
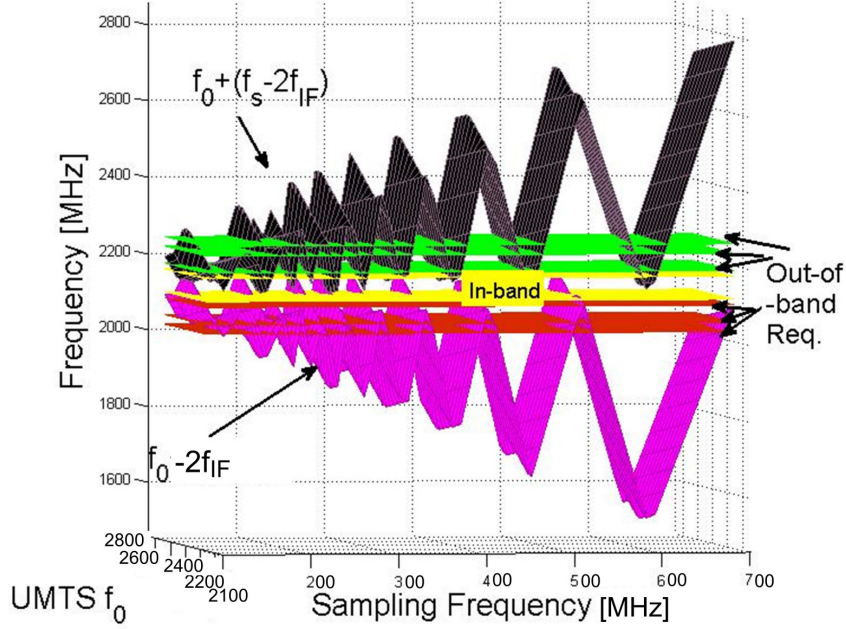
Figure 4.15: Illustration of the closest image frequencies in different out-of-band requirement regions of the UMTS signal.

WLAN DL

The image rejection for the WLAN standard is calculated from Eq. (4.14) noting the P_{N+I} is outlined in Table 4.3 for all the different data rates. As mentioned in Table 4.1, the out-of-band blocking requirements are not specified in the WLAN standard [7]. Thus the out-of-band requirement in this analysis is inspired from the transmission mask of the WLAN signal. It is specified in the standard that the transmitted spectrum shall have -40 dBr (dB relative to the maximum spectral density of the signal) degradation at 30 MHz frequency offset and above. In a WLAN transceiver where the transmitted signal has the maximum power level of 20 dBm, the P_{Blk} is defined as 40 dB below the maximum level:

$$L(> 30MHz) \geq P_{Blk} - (P_{N+I} - 3dB) \tag{4.21}$$

The image rejection requirements for all the different data rates is outlined in Table 4.5.

Table 4.5: WLAN image rejection requirements for UE [7].

Rates [Mbps]	6	9	12	18	24	36	48	54
Image rejection [dB]	68.06	68.78	68.03	67.79	73.04	68.08	70.05	69.56

4.6   Discussion and summary

The UE receiver requirements have been derived for a multi-standard front-end supporting the UMTS and IEEE 802.11g standards simultaneously. The results are valid for any chosen architecture and are outlined in Table 4.6. The frequency Division Duplex (FDD) operation of the UMTS signal allows both the transmitter and receiver to operate at the same time. In addition to the UMTS signal, one of the uplink or downlink signals of the WLAN exists. Thus, due to the coexistence of all these signals, a more stringent requirement is applied to the receiver linearity requirement specially in-band iIP_3. Beside the linearity requirements, the noise level plan of the receiver must be adjusted for the multi-standard operation. Thus, to achieve to an acceptable performance according to the specified requirements in the 3GPP standard, the noise figure of the conventional UMTS receivers must be reduced to a lower amount by the proper design of the transceiver as it is mentioned in this chapter.

Table 4.6: Summary of receiver requirements for UMTS.

Rx parameter	UMTS Requirements
Noise figure [dB]	≤ 7
Selectivity [dB]	
In-band selectivity (10 / 20 MHz)	≥ 60
Image rejection (≥ 85MHz)	≥ 86
Image rejection (≥ 60MHz)	≥ 71
Image rejection (≥ 15MHz)	≥ 57
Intermodulation [dBm]	
iIP_3 (10/20 MHz)	≥ -19
iIP_3 ($UMTS\ UL\ leakage$)	≥ -32.5
iIP_3 ($WLAN\ UL\ leakage$)	≥ -35

The image rejection performance is investigated in this chapter and the image rejection selectivity requirements for the scenario of the current research is derived. An algorithm is proposed to combine the required selectivity with the sampling rate dependency at the image frequencies. This helps extensively to prohibit the big blockers at the image frequencies to fold down along with the desired signal to the band-of.interest.

Chapter 5

UMTS & WLAN Multi-standard sub-sampling receiver

In the current chapter, a novel RF sub-sampling receiver front-end based on milieu adapting techniques supporting WLAN and UMTS simultaneously is designed. To conquer the high noise contribution of sampler and relax the ADC requirements, a two-stage sub-sampling architecture is chosen. The design related issues of the multi-standard multi-mode sub-sampling receivers are investigated. The RF requirements of the receiver for the specific multi-frequency application supporting WLAN and UMTS concurrently are derived and outlined. The receiver frequency plan is performed to fulfill the multi-signal attitude of the current analysis. Following to the theoretical investigations to model the sub-sampling receiver, a behavioral model of the receiver is implemented in Matlab. It works in time domain and follows the discussed functionality of the blocks such as filtering, amplification and sampling step by step.

The chapter is organized as follows. Section 5.1 presents the proposed two-stage RF sub-sampling receiver supporting the UMTS and WLAN signals simultaneously. The RF requirements and the design objectives of the receiver are outlined in this section. The best sampling frequency is derived based on the method presented in Section 3. The frequency plan with respect to the two-stage receiver architecture is presented. Section 5.2 discusses the system modeling of the receiver for the special case-study of this thesis. The time domain simulations are oriented step by step in accordance with the design to minimize missing effects. Finally, the results are discussed and concluded in Section 5.3.

5.1   Proposed RF-sampling receiver front-end

5.1.1   Two-stage sub-sampling receiver

It is mentioned in the subsequent chapters that the sub-sampling technique is an efficient way to partly alleviate the limitations on the ADC Power consumption and performance with the existing technologies. The requirement for very high sampling rate is relaxed by sampling at twice the cumulative bandwidth instead of the total bandwidth [3].

However as mentioned in Chapters 3 and 4, there are a lot of limitations and considerations in the selection of the sampling frequency. Consequently in a practical design, the sampling frequency which fulfills all the mentioned requirements is much larger than twice the information bandwidth. Thus to handle the high sampling frequencies, the key enabling component of this architecture which is the high speed Analog to digital converter (ADC) is still considered as a bottle-neck. There are limitations on the developed high speed ADC in terms of the power consumption, size and performance for the high-speed applications especially hand-held devices. Moderate solution is required to link the existing components with the ambitious idea of sampling the data directly at the radio frequency (RF) with high sampling rates.

One solution is to employ several stages of down-conversion instead of one stage. This idea is to distribute the sampling frequency and selectivity requirements of the receiver among several stages of filtering and down-conversion. This makes the requirement frames more realistic according to the existing developed technology. Each successive stage consists of filter followed by the downsampler. The filter prevents the aliasing effects caused by downsampler. It provides an additional bandpass function to further suppress the out-of-band signals.

This approach also helps in selection of the feasible sampling rates. There are several disadvantages with selecting a low sampling rate such as high noise level due to aliasing of the thermal noise, jitter and tougher requirement on the RF filtering (since the image noise is closer to the desired band). A high sampling frequency reduces the noise aliasing as it is mentioned in Section 2. On the other hand, there are some limitations on the implementation of the receiver with very high sampling rate due to shortcomings in the existing technologies. It imposes a tough requirement for the choice of analog to digital converter. Thus, employing several-down-conversion approach assist with the selection of more reasonable sampling frequencies.

Nevertheless, employing several stages of filtering and down-conversion offers improved performance at the expense of more hardware. This is acceptable for the current research since the intention is to prove the proposed concepts. To take the advantages of several-down-conversion approach, a two-stage RF sub-sampling receiver is proposed in this analysis as shown in Fig. 5.1.
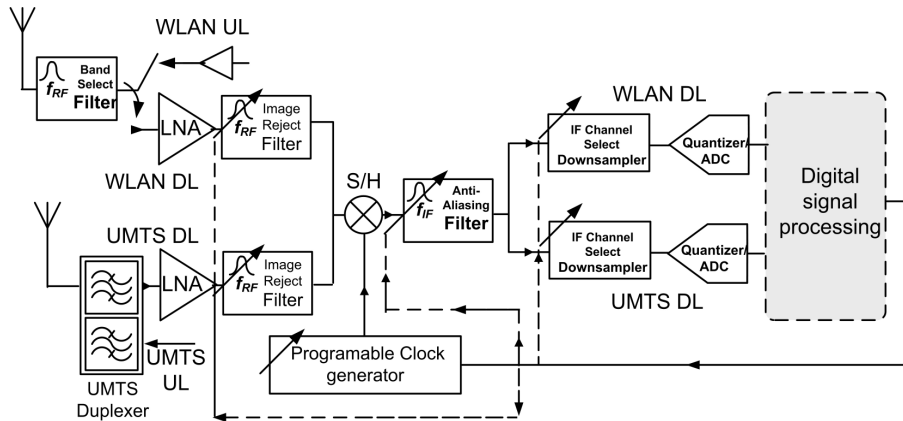

Figure 5.1: Block diagram of the proposed RF sub-sampling receiver architecture supporting the UMTS and WLAN signals.

As illustrated in Fig. 5.1, the receiver contains two different front-ends (filters and amplifiers) for receiving the WLAN and UMTS signals. The reason is that the UMTS signal is an frequency Division Duplex (FDD) and the WLAN is a time division duplex (TDD) system. Employing one front-end to receive both signals simultaneously will cause big power losses in the front-end. In the transmit periods when the WLAN transmitter is working and its receiver is not active, half of the transmit power will be directed to the WLAN receiver. Each RF signal is filtered via two filtering stages. The first stage to filter out the desired RF band while the second stage rejects the image signals.

The amplified and filtered WLAN and UMTS signals from the two different paths are added together via the duplexer. The combined WLAN and UMTS signal enters the sample and hold (S/H) block. The RF signal is down-converted to intermediate frequency (IF) through sampling. Thus the discrete-time signal after sampler is converted to lower frequencies via aliasing. In this stage the requirement is much more relaxed since the second down-conversion is applied to a lower frequency signal.

To perform the down-conversion in second stage, the decimation by an integer factor is used. If in the second stage the sampling rate of the first stage is decimated by a factor of M, then the resulting sampling rate could be calculated from:

$$f_M \;=\; \frac{f_s}{M} \quad \text{for} \;\; M = 1,\, 2,\, 3, \cdots \tag{5.1}$$

Where f_s is the sampling rate applied to the RF signal in the first stage. The down-sampling with the new sampling rate of f_M down-converts the signals at the first f_{IF} to the second intermediate frequency f_{IF2}. This frequency can be calculated from Eqs. 2.9 and 2.10:

$$S_{IF}: \quad f_{IF2} \;=\; f_{IF} - round(\frac{f_{IF}}{f_M}) \cdot f_M \tag{5.2}$$

$$S_{IF}^*: \quad f_{IF2} \;=\; -f_{IF} + round(\frac{f_{IF}}{f_M}) \cdot f_M \tag{5.3}$$

One more stage of downsampling is along with the aliasing of image distortions around f_{IF} to the band of interest. The image signals are located at:

$$S_{IF}: \quad f_{img2} \;=\; m\, f_M \pm f_{IF2} \tag{5.4}$$

$$S_{IF}^*: \quad f_{img2} \;=\; -m\, f_M \mp f_{IF2} \tag{5.5}$$

Therefore, the anti-aliasing filtering prior to the second downsampler must be designed to suppress the images located at frequencies calculated from Eqs. 5.4 and 5.5. It should be noted that since the sampling rate of the second stage and the corresponding IF are much smaller than the first stage, the complete image rejection is not possible. The images are spectrally located very close to the desired band which toughen the complete required image rejection. Further suppression of these images must be performed in the baseband filters.

5.1.2   RF-sampling radio receiver planning

The frequency plan associated with the simultaneous reception of the UMTS and WLAN signals is presented in this section. As mentioned, a two-stage down-conversion receiver is employed to relax the requirements on the sampling frequency and consequently selection of the IF signal. The sampling frequency of the first stage is decided to be 676 MHz with respect to several important factors such as minimizing the interference and image rejection as discussed in Chapter 3. The first down-conversion of the receiver is shown in the frequency plan depicted in Fig. 5.2. The 12 channels of the UMTS band and 3 channels of the WLAN band are down-converted to non-overlapping portions of the Nyquist zone as shown in the figure. The replication of the signals in multiples of the sampling frequency is illustrated. The desired IF signals spectrally located at $[82MHz; 303MHz]$ are filtered to suppress all the unwanted aliases.

The desired IF signals are sampled and further down-converted to lower frequencies in the second stage. The selection of the sampling frequency for this stage is discussed in detail in the following sections. The downsampling factors of 9 and 4 are selected for the UMTS and WLAN signals respectively. The frequency plan of the signals after second down-conversion stage is shown in Fig. 5.3. Separate frequency planning for the UMTS and WLAN signals are further discussed.
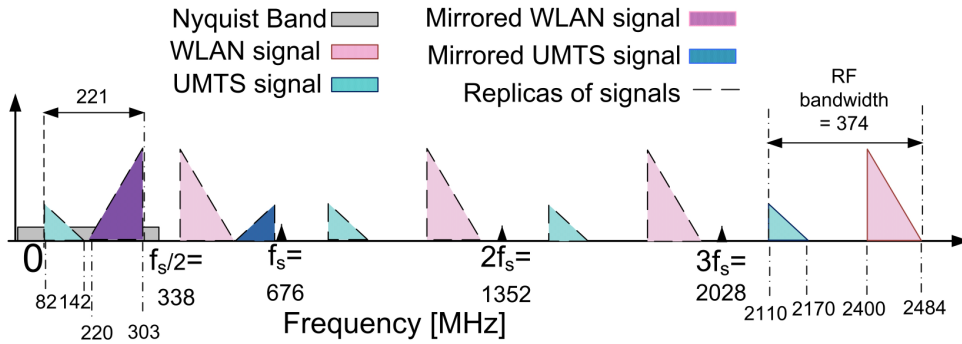

Figure 5.2: Illustration of the combined frequency spectrum of the UMTS UL, UMTS DL and their first down-conversion by sampling at the rate $f_s = 676$ MHz.
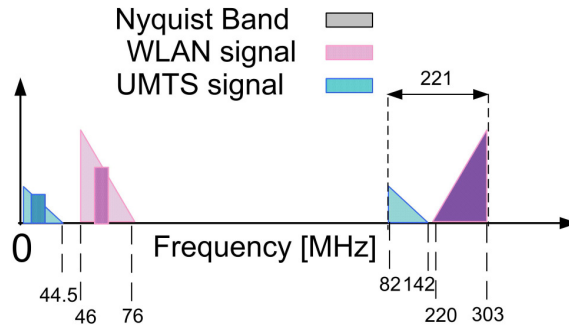

Figure 5.3: Illustration of the combined frequency spectrum of UMTS UL, UMTS DL and their second down-conversion by sampling at the rate f_s/M for M= 9 for the UMTS and M= 4 for WLAN signal.

UMTS DL receiver planning

The assigned frequency band for the UMTS signal is from 2110 to 2170 MHz [5]. The signal bandwidth is 3.84 MHz with the channel separation of 5 MHz. The sampling frequency of 676 MHz is calculated from the algorithm presented in Section 3. Sampling the UMTS signal with this rate translates the RF information to the IF with frequencies at the range between 84.5 to 139.5 MHz (with 5 MHz spacing from each other).

For this sampling frequency, the closet images to the edges of the UMTS band (2112.5 to 2167.5 MHz) are located at 169 and 397 MHz offset as discussed in Section 4.5.3. Thus, both of the closest images are placed more than 85 MHz away from the UMTS band. According to the calculation done in the same section, the images at more than 85 MHz offset must be suppressed by 86 dB.

In the UMTS DL path, the required selectivity of the front-end is provided with the combination of the duplexer and RF filter as depicted in Fig. 5.1. A commercially available off-chip RF filter has the attenuation of 48 dB at 169 MHz offset and 38 dB at 397 MHz offset [99]. The commercially available duplexer such as [97] is able to provide 70 dB attenuation at 169 MHz and 50 dB at 397 dB offsets. Thus, it is feasible to attenuate the images of the chosen sampling rate with commercially available filters and duplexer [97] and [99].

For the selected sampling rate, the UMTS IF channels are located at 84.5 to 139.5 MHz (with the steps of 5 MHz) calculated from Eqs. (2.9) and (2.10). The signals at these frequencies will be further down-converted through the second stage of down-conversion.

The new sampling frequency of the second stage must be able to down-convert all the channels of the UMTS to non-overlapping portions of the new Nyquist band. The new second-stage sampling rate is derived by decimating the first-stage f_s with an integer number. The result of trying different integers or downsampling factors (M) for the UMTS band calculated from Eq. (5.1) are outlined in Table 5.1.

The down-conversion factor of $M = 9$ is selected after trying different integers. This factor is selected since it is capable of down-converting the IF signals from the first stage to non-overlapping portions of the Nyquist band associated with the second sampling rate. It prohibits the interference with the WLAN channels.

The chosen downsampling factor is depicted with bold font in Table 5.1. By employing the Eqs. (5.2) and (5.3), the second-stage IF signals are calculated which in the range of 9.4 to 35.7 MHz. It is illustrated in Fig. 5.3.

WLAN DL receiver planning

The WLAN signal is spectrally located at the frequency range of 2400 to 2483.5 MHz [7]. In this 83.5 MHz band, 3 non-overlapped channels with the occupied bandwidth of 16.6 MHz exist at 2412, 2442 and 2472 MHz [7]. The WLAN signal is sampled with the sampling frequency of 676 MHz calculated from the algorithm presented in Chapter 3. The signals are intentionally aliased down to the intermediate frequencies of 292 , 262 and 232 MHz respectively.

---

[1]There is no interference with the WLAN channels only when the UMTS downsampling factor is 9.

Table 5.1: UMTS second downsampling factor selection.

downsampling factor (M)	f_s/M [MHz]	interference with UMTS	interference with Nyquist band boarders
2	338	yes	no
3	225.3	yes	yes
4	**169**	**no** [1]	**no**
5	135.2	yes	yes
6	112.6	yes	yes
7	96.57	yes	yes
8	84.5	yes	yes
9	75.11	yes	yes
10	67.6	yes	yes

The calculation of the corresponding intermediate frequencies makes it possible to calculate the closet image signals to the RF desired bands as discussed in Section 4.5.3. The closest images to WLAN band edges (2112 to 2472 MHz) are spectrally located at 548 and 92 MHz offset. Consequently, the total attenuation of 69.5 MHz is required to suppress the undesired signals below the harmless noise level.

At the frequency offset of 548 MHz this level is simply achievable with the combination of the commercially available RF filter and image rejection filter [100]. However, the other image signal at 92 MHz offset is very close and difficult to suppress with the commercially available filters. This image may partially down-converted along with the signal to the band-of-interest.

The WLAN IF channels located from the first-stage are further down-converted to the second-stage IF. To find the decimation factor capable of down-converting all the WLAN IF channels to non-overlapping portions of the new Nyquist zone, different downsampling factors have been tried and outlined in Table 5.2. The selected downsampling factor for WLAN signal is 4 as shown with bold font in Table 5.2. By using this factor, the WLAN first-stage IF channels are translated to non-overlapping portions of the Nyquist band. The second-stage IF signals for the new sampling rate 75.11 MHz is calculated from Eqs. (5.2) and (5.3). The new IF signals are spectrally located at 63 , 76 and 46 MHz as shown in Fig. 5.3.

---

[2]There is no interference with the UMTS channels only when the WLAN downsampling factor is 4.

Table 5.2: WLAN second downsampling factor selection.

downsampling factor (M)	f_s/M [MHz]	interference with UMTS	interference with Nyquist band
2	338	yes	no
3	225.3	no	yes
4	169	yes	yes
5	135.2	yes	yes
6	112.6	yes	yes
7	96.57	yes	yes
8	84.5	yes	yes
9	**75.11**	**no** [2]	**no**
10	67.6	yes	yes

5.1.3   Summary of the receiver requirements and Frequency Plan

The required specification of the receiver is derived and outlined in Table 5.3. The detailed calculations are provided in Section 4.

Table 5.3: Summary of Frequency Plan for the proposed receiver.

Parameter [MHz]	UMTS Spec	WLAN Spec
Carrier Frequency	$2112.5+ 5n_{ch}$	$2400+ 30p_{ch}$
	$n_{ch}=0\cdots11$	$p_{ch}=0,\ 1,\ 2$
Signal Bandwidth	3.84	16.6
Sampling Frequency	676	676
Intermediate Frequency	$84.5+ 5n_{ch}$	$292- 30p_{ch}$
Closest image at $2f_{IF}$	$169+ 10n_{ch}$	$584- 60p_{ch}$
Closest image at $f_s - 2f_{IF}$	$507- 10n_{ch}$	$92+ 60p_{ch}$
Second sampling rate(f_M)[MS/s]	75.11	169
Second Intermediate Frequency	9.4, 14.4, 19.4, 24.4	63, 76, 46
	29.4, 34.4, 10.7, 15.7, 25.7	
	20.7, 25.7, 30.7, 35,7	
Selectivity [dB]		
Selectivity [dB]		
In-band (10 / 20 MHz)	≥ 60	—
Image rejection	≥ 86 [3]	≤ 69.5
Intermodulation [dBm]		
iIP_3 (10/20 MHz)	≥ -19	—
iIP_3 (UMTS UL leakage)	≥ -32.5	—
iIP_3 (WLAN UL leakage)	≥ -35	—

5.2   System modeling and simulation

5.2.1   High-level modeling and simulation

To support and verify the RF sub-sampling receiver design, a mathematical model of the receiver is developed in Matlab [50]. The model works in time domain and follows the procedure shown

---

[3]Since all the images are further then 85 MHz from UMTS desired band (Table 4.6), the out-of-band blocking for more than 85 MHz is considered.

in Fig. 1.20.

A number of noise sources are embedded in the model such as thermal noise an jitter induced noise. The model is very useful to prove the ideas presented in this dissertation. For example, the algorithm for selection of the sampling frequency, the RF requirement and specially selectivity and image rejection criterion are tried and proved with the developed model.

The Parameters used in the simulation obey the specifications mentioned in Section 1.5. The UMTS and WLAN signals are generated according to the method mentioned in the same section. The simulated spectrum of all the channels of the UMTS and WLAN bands are depicted in Fig. 5.4. The front-end for receiving the UMTS and WLAN bands are and modeled in Matlab.

As shown in Fig. 5.1, two RF bandpass filters are proposed for each standard in the multi-standard RF sub-sampling receiver front-end. The first RF filters are responsible of selecting the whole RF band of the desired signal (UMTS or WLAN). The second proposed filters are mainly responsible of protecting the receiver against the harmful aliasing. They are placed after the low noise amplifier (LNA) and designed to attenuate the image distortions to guarantee the proper functionality of the receiver.

The signals are added together through a multiplexer and entered to a wide-band S/H block. This block down-converts the signals to non-overlapping portions of the Nyquist band. This is feasible by sampling the signal at the calculated rate of 676 MHz. It should be noted that all 12 channels of UMTS and 3 non-overlapping channels of WLAN may be received to the antenna. Thus, the receiver is designed and simulated to be able to process all the 36 different combination of the received signal.

The RF signal is translated to IF by sampling. The resulting information in IF is discrete-time information. An anti-aliasing filter is proposed and modeled in Matlab after the S/H block to remove the harmful aliasing.

To relax the requirements such as sampling rate, power consumption and bandwidth on the ADC, a second stage of down-conversion is proposed. The IF channels are selected, filtered and down-sampled to lower frequencies by using a tunable IF channel-select downsampler. This is a combination of IF channel select filter and a downsampler. The explanation of each component and its realization in Matlab is explained in the following Sections.

5.2.2 Design of first RF filters

The first RF filter has the role of suppressing the out-of-band blockers and interferes. Thus the information in the reception band will be passed through the filter untouched while all the out-of-band unwanted signals are being attenuated.

For the UMTS signal, the duplexer shown in the Fig. 5.1 is playing the role of the first RF filter. The filter transfer function is depicted in Fig. 5.5. The proposed RF filter for the WLAN signal is shown in Fig. 5.6.

To design the first RF filters, the well-known Chebyshev Type I filters are used. The transition from passband to stop band is sharper in this type of filters in comparison to the
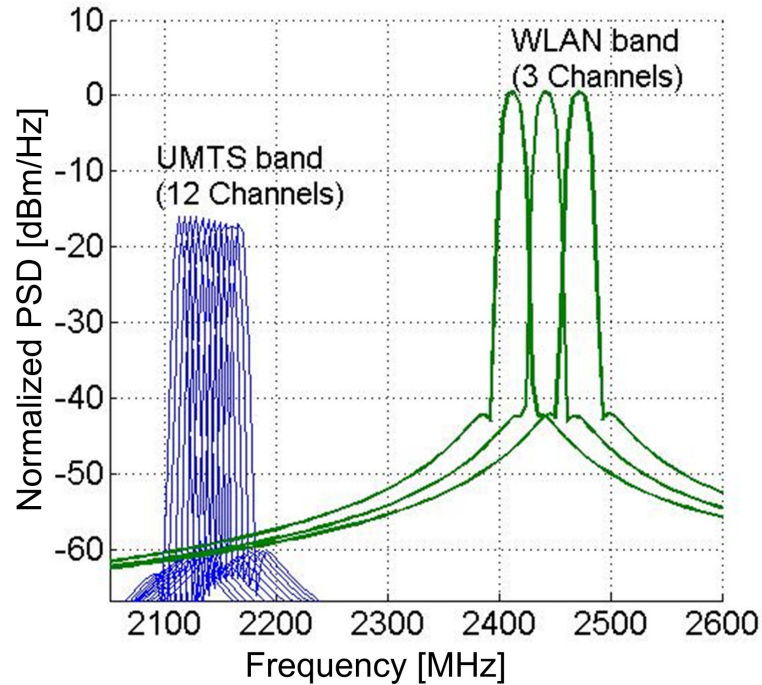
Figure 5.4: Simulated 12 UMTS channels forming the 60 MHz total UMTS band and the 3 non-overlapping channels of WLAN signal.
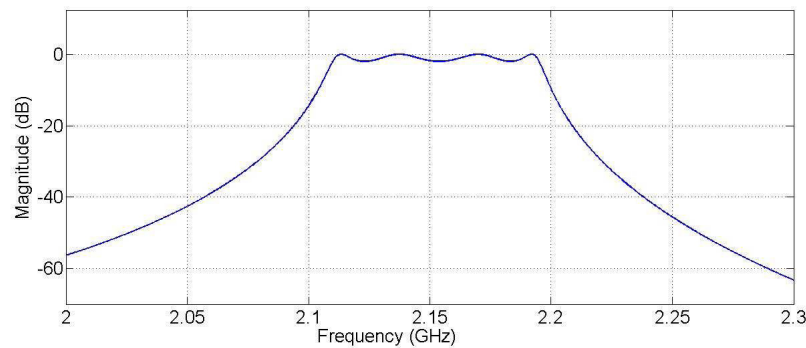

Figure 5.5: Simulated first UMTS filter (duplexer) frequency response.

Butterworth filters. To design the filters for RF sub-sampling architecture, this is useful since it has a sharper edge to cut the unwanted bands. This will reduce the harmless aliasing to the desired band.

This type of filter is designed based on minimizing the absolute difference between the actual and ideal frequency response all over the passband. This is done by including an equal ripple in the passband. The stop-band is designed to be maximally flat [50]. This filter suits well with the desired application of the first RF filter to select the band of interest and attenuate the out-of-band blockers. The "fdatool" from signal processing toolbox of Matlab is used to design the filters [50].
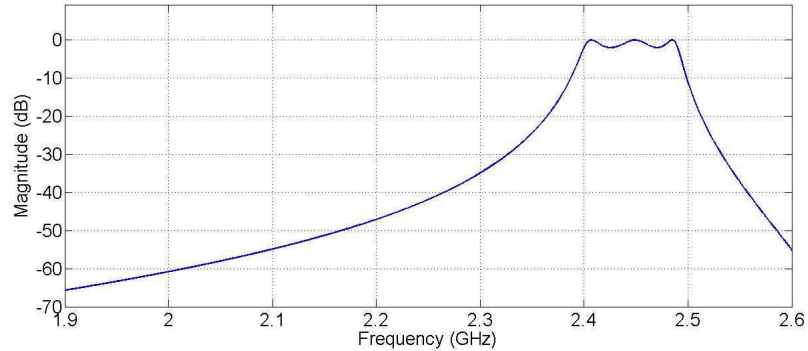
Figure 5.6: Simulated first WLAN filter frequency response.

5.2.3   Design of second RF Filters

To prohibit the harmful aliasing specially aliasing from closer images to the desired band, the second RF filter is embedded in the front-end chain. The image rejection requirements of the receiver is discussed throughly in Section 4.4.2. Based on the presented discussion, the summary of the parameters for the image rejection filters are outlined in Table 5.4.

Table 5.4: Second RF filters requirements.

Standard	Filter cut-off frequency [MHz]	First IR frequency [MHz]	Required attenuation [dB]
UMTS	2110 - 2170	1943.5 - 2546.5	86
IEEE 802.11	2400 - 2483.5	1828 - 2564	69.5

   The filters are designed according to the parameters presented in Table 5.4. The "fdatool" from signal processing toolbox of Matlab is used to design the filters [50]. The well-known Chebychev Type II filter is employed to design the image rejection (second RF) filters. The minimization of absolute difference between the actual and ideal frequency response is done in the stop-band for this filter. In other words, an equal ripple is incorporated in the stop-band while the passband is kept maximally flat.

   This is useful in designing the image rejection filters. The design is done in a way that the image rejection frequencies are allocated in the lowest values of the ripples of the stop-band of the filters. Thus, the image suppression is done more extensively than the suppression of the rest of the stop-band. Since the images are at least partly down-converting to the desired band, it is important to suppress them below the harmless level. The designed and simulated filters for the UMTS and WLAN signals respectively are shown in Figs. 5.7 and 5.8.

   As shown in the Figs. 5.7 and 5.8, the calculated image rejection frequencies are designed to be located in the lowest peaks of the stop-band of the filters.

   The design is performed in a way that the summation of the attenuations from the two RF
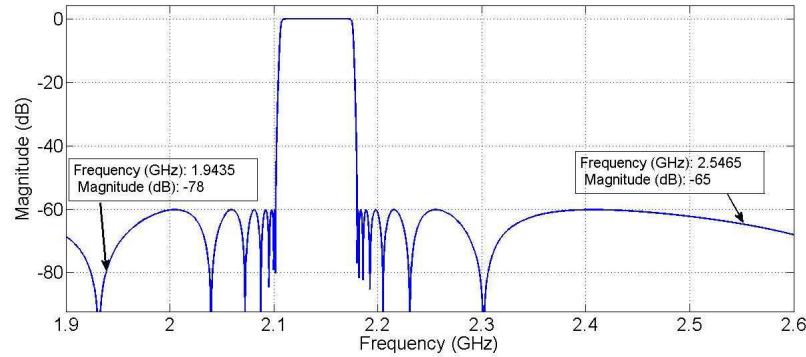
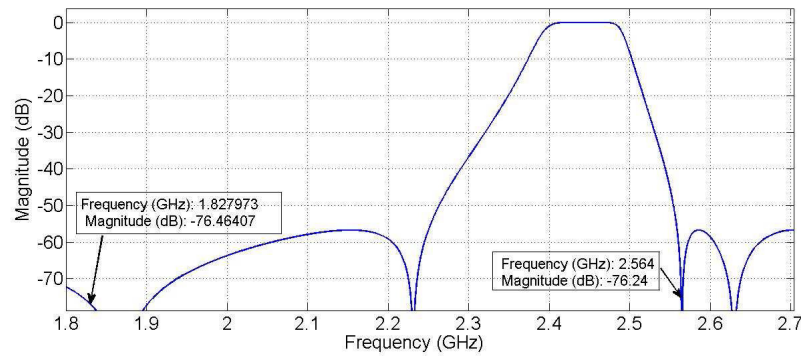**Figure 5.7:** Simulated second UMTS filter frequency response.

Figure 5.8: Simulated second WLAN filter frequency response.

filters for each standard at image rejection frequencies can provide the total required attenuation outlined in Table 5.4. In case the required attenuation can not be provided by the designed RF filters at the image rejection frequencies, the desired signal is distorted significantly. To illustrate the distorting effect of the image noise on the signal to noise ratio (SNR) of the signal, this effect is investigated when only one image distortion exists for each of the desired signals. The SNR is measured while the image power is varying. From the two RF filters, only one of the filters is active and the other one is ignored. This is performed to make the effect of the image distortion on the desired signal visible. Increasing the image power level is associated with decreasing the SNR of the signal.

This simulation is performed to emphasis on the importance of the image rejection in the sub-sampling receivers. Nevertheless, employing the two RF filters for each standard to reject the images lessen the problem of image noise significantly.

5.2.4   Design of the S/H block

The S/H block is realized in Matlab [50]. It is a time domain model providing the required S/H functionality explained in Sections 1 and 2.

- The S/H block is modeled in order be able to sample the input signal at the simulation

time-step instant. In this model, the signal is sampled during the sampling period and subsequently held until the next initialization of the next sampling instant. The input signals to this block is the summation of the RF input signals and an RF clock signal to govern the sampling functionality. The input is sampled at the falling instant when the clock signal crosses a threshold of its lower value. In the hold state of the S/H block, the output voltage stays at a constant rate determined by the last value of the sampling state.

- The Sampler model samples the entire spectrum and the output signal contains the signal itself and the replicas of the signal at multiples of the sampling frequency.

The input and output time domain signals of the S/H block sampled at the clock rate of 676 MHz are shown in Fig. 5.9. The input signal is the summation of the frequency modulated RF UMTS and WLAN signals sampled at 5.408 GHz.
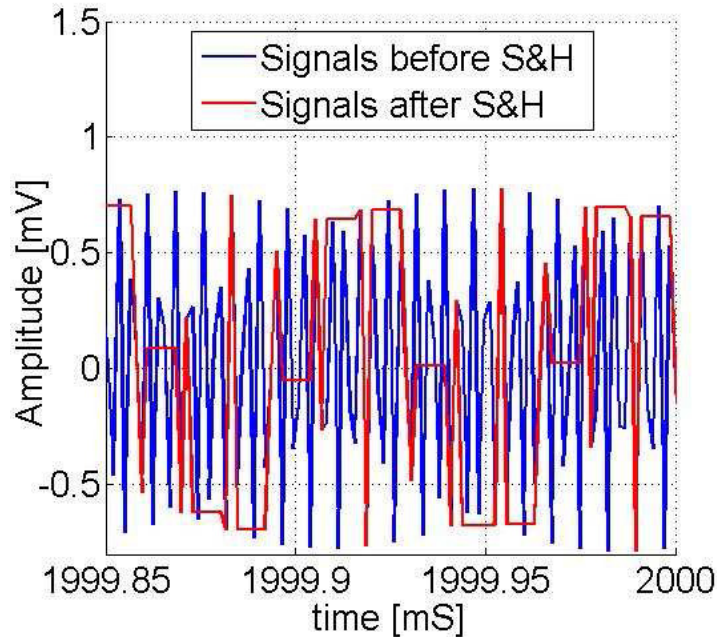
Figure 5.9: Simulated WLAN and UMTS signals before and after S/H in time domain.

It can be seen from Fig. 5.9 that the frequency of the signal after S/H block is decreased through sampling. This is the sample and hold operation interpretation in time-domain. Since it is easier to visualize the frequency down-conversion in frequency domain, the spectrum representation is depicted in the following parts as well.

In frequency domain, the signals at RF in addition to their replication in multiples of the sampling frequency are shown in Figs. 5.10 and 5.11. Fig. 5.10 shows the two signals at RF with focus on replication of the UMTS signal. The filtered UMTS signal at IF is illustrated with a dash-line box.

The two RF signals with focus on replication of the WLAN signal sampled at 676 MHz is depicted in Fig. 5.11. In the Nyquist band, the image of the WLAN signal located at $f_s/2 - f_{IF}$
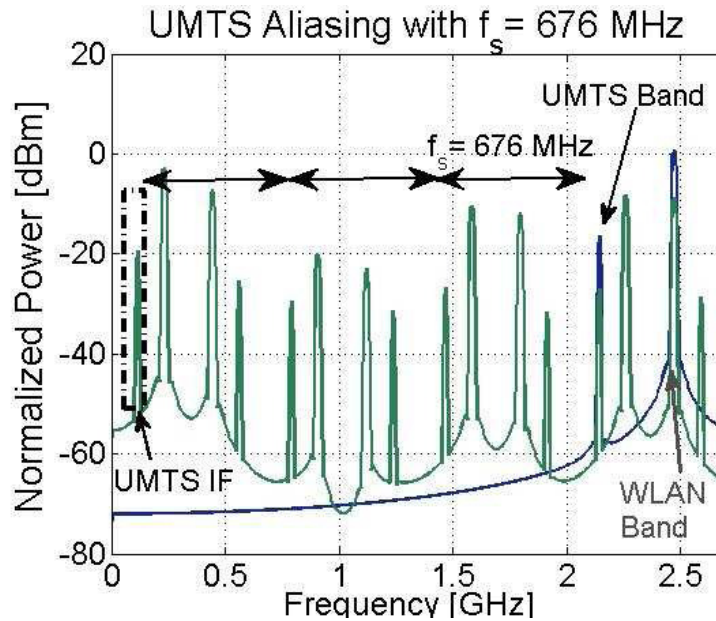
Figure 5.10: Simulated spectrum of the UMTS signal before and after the S/H in frequency domain. The signal is sampled with the calculated rate of 676 MHz. The frequency plan and the filtered signal at IF is shown.

is selected instead of the signal located at f_{IF}.
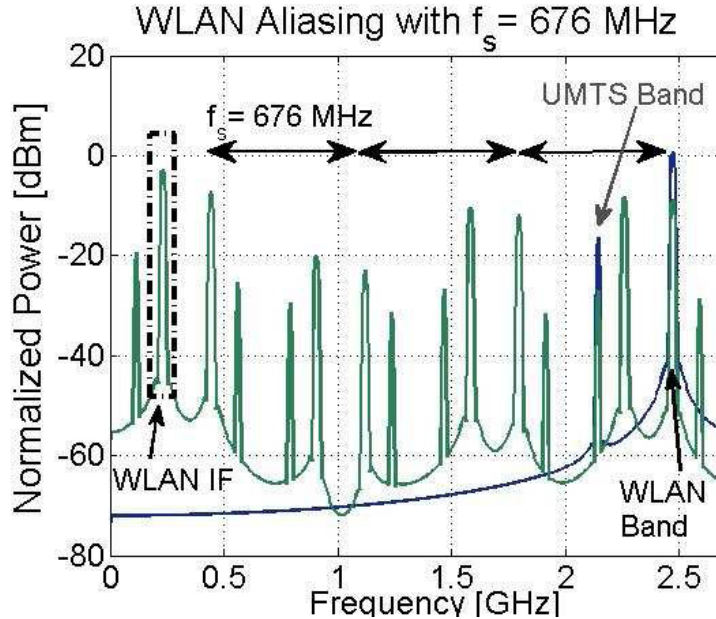
Figure 5.11: Simulated spectrum of the WLAN signal before and after S/H in frequency domain. The signal is sampled with the calculated rate of 676 MHz. The frequency plan and the filtered signal in IF is shown.

The results from simulations fully agree with the concept of the sub-sampling receiver. To eliminate the effects of the harmful aliasing after sampling, one stage of anti-aliasing filtering is required. A dual pass-band Finite Input Response (FIR) filter based on hilbert window is designed using the *firl* function in Matlab [50]. The filter frequency response is depicted in Fig.

5.12.

Figure 5.12: Simulated anti-aliasing filter for filtering the combined UMTS and WLAN signal after the S/H block.

The *firls* command realizes the least square linear-phase FIR filter. The weighted, integrated squared error between an ideal piecewise linear function and the magnitude response of the filter is minimized over a set of desired frequency bands. The combined sampled WLAN and UMTS signal is passed through this filter. The desired IF signals is remained unchanged while the power of the all unnecessary replicas are attenuated. The sign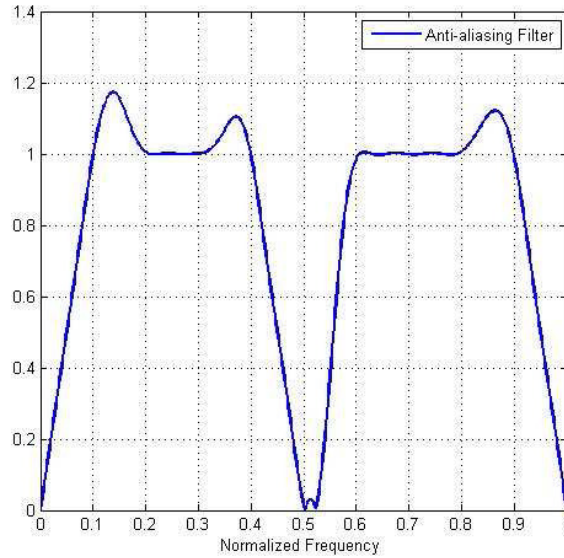al after this filter enters to the IF channel-select downsampler. The simulated signals after these filtering is illustrated in Chapter 6 where the results from simulation are compared with measurement results. It is not repeated here to avoid duplication.

5.2.5   Design of the IF channel-select downsampler

The IF Channel-Select filter is shown in Fig. 5.1. The channel-selection and downsampling operations are done by employing these filters. It is exploited separately for the individual channels of each standard. The FIR filter is employed to realize the band-pass filtering operation. The frequency spectrum of the bandpass sampling combined with FIR filtering can be written in general form:

$$\tilde{S}_F(f) \; = \; f_s \sum_{m=-\infty}^{\infty} H(m\,f_s)S(f - m\,f_s) \tag{5.6}$$

where $H(m\,f_s)$ is the FIR filter transfer function. In the discrete-time, the filter transfer function

can be written:

$$H(Z) \; = \; \sum_{i=0}^{N-1} \beta_i(Z_0\,Z))^{-i}|_{Z=e^{j2\pi m\,f_s}} \tag{5.7}$$

where β_i is the ith filter coefficient and N is the number of the filter taps. The factor $(Z_0))^{-i}$ is selected such that in combination with the frequency of Z element the folded band is shifted to the left of the spectrum by the required downsampling frequency. This provides the expected functionality of this block which is "'IF channel-selection downsampling"'.

The tunable filters are designed for the WLAN and UMTS channels separately. Special care is taken to suppress the image frequency located at image frequencies calculated from Eqs. (5.4) and (5.5).

5.3   Results and discussion

The case-study of a WLAN/UMTS multi-standard double-stage receiver followed in the current dissertation is simulated and presented. The signals with the sampling frequency of 5.408 GHz are received at the antenna. They are added together after the required filtering and amplification in the front-end. The resulting signal enters the S/H block and is sampled with the sampling frequency of 676 MHz. The translated signals to IF are spectrally located at $82-142$ MHz. The signal processing is followed by one stage of anti-aliasing filter. The second stage of downsampling is done to move the signals to lower frequency after channel selection.

The SNR of the first down-conversion stage vs. sampling frequency for different front-end gains is shown in Fig. 5.13. The curves indicate that the SNR is increasing with the increasing of the sampling frequency. However, depending on the selected technology and sampling capacitor, it starts to settle around a constant value. It is crucial to note that the signal to noise ratio for this simulation is the ratio of the desired signal to sampled noise from front-end plus the thermal noise from S/H block and the noise aliased down to the band from the out-of-band contributors. After starting to settle down, the variations seen in the Fig. 5.13 comes from the fact that the noise may be caused from different sources as mentioned above. Depending on which noise contributers play the predominant role in noise level, we may experience some variation in the SNR. However in general, it can be seen that choosing a larger sampling frequency leads us to a larger SNR as expected. The selected sampling frequency of the current dissertation provides an acceptably large SNR. This further approves the selection of the sampling frequency. Fig. 5.13 indicates that the SNR of the front-end is increasing by increasing the total gain of the chain seen from antenna port. Nevertheless, the employment of the sub-sampling technique limits the maximum reachable SNR [81]. Fig. 5.14 depicts the variation of the noise figure (NF) of the first down-conversion stage versus the sampling frequency for different front-end gains. It indicates that the proper selection of the gain for the front-end has a key role as discussed in Chapter 2. The gain of 30 dB shown in Fig. 5.14 is an example of wrong selection of gain for the front-end. It results in a high front-end NF and degrade the receiver's performance.

In general, the simulations do fully agree with the presented concepts in the previous chap-

Figure 5.13: Simulated signal to noise ratio, SNR, versus the sampling frequency, f_s. The SNR is varying with the corresponding gain and sampling frequencies.
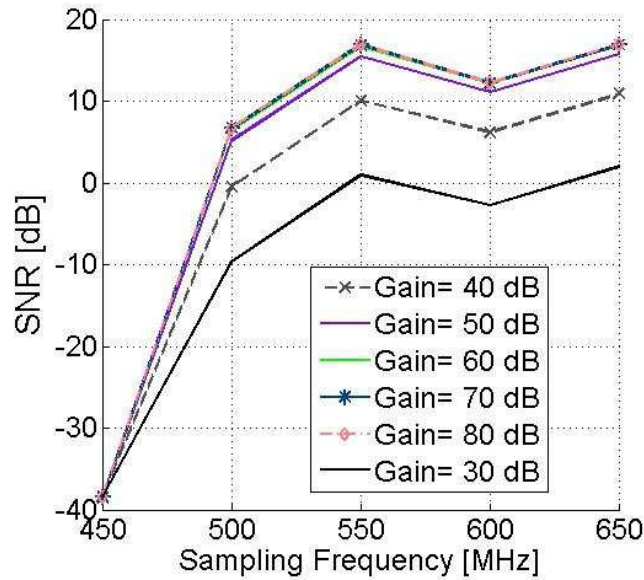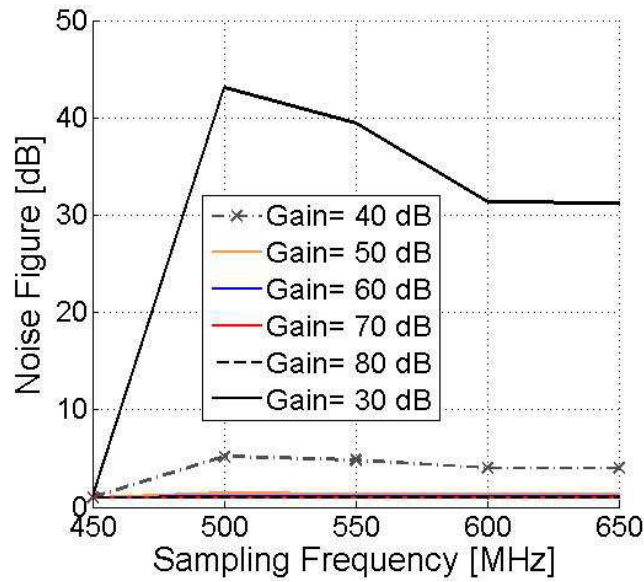

Figure 5.14: Simulated noise figure, NF, versus the sampling frequency, f_s. The NF is varying with the corresponding gain and sampling frequencies.

ters. Using the provided methods in Sections. 2 to 4 result in the acceptable frequency plan and RF requirements for the receiver. This is further approved by analyzing the results of the simulations.

Chapter 6

Experimental sub-sampling receiver

This chapter presents several experiments to verify the theoretical and simulation results pre-sented in subsequent chapters. An experimental sub-sampling receiver with the commercially available components is developed. The proposed concepts of the thesis are supported by mea-surements on the sub-sampling receiver.

The chapter is organized as follows. Section 6.1 gives a brief introduction to the chapter. The important practical issues are discussed and the practical set-up is presented. The measurements on the implemented receiver is presented in 6.2. In Section 6.3 an experiment is presented to verify the sampling rate algorithm presented in Section 3. Section 6.4 describes the experimental data to prove the milieu adapting technique explained in Section 3.3. The image rejection and selectivity requirements of the receiver is proved in Section 6.5. Finally, conclusions are drawn in Section 6.6.

6.1   Introduction

This chapter presents four sets of experiments to proof the concepts and results presented in Chapters 3, 4 and 5.

1. The first experiment is done to investigate the feasibility of designing a flexible receiver capable of receiving several standards with a single user equipment by employing the sub-sampling techniques. The intention is to show the feasibility of implementing the receiver by the existing off-the-shelf components and conquering the presented limitations in technologies. It is done by using two consequent stages of filtering and down-conversion.

2. The second experiment is organized to investigate the precision of the presented sam-pling frequency flow chart and the corresponding calculated sampling frequencies. The algorithm presented in Chapter 3 is verified via the experiment.

3. The third experiment is done to prove the milieu adapting techniques presented in Chapter 3.

4. The last experiment is done with the intention of proving the image rejection and selectivity requirements of the receiver.

The theoretical and experimental results do fully agree.

6.1.1   Experimental sub-sampling receiver

The RF sub-sampling front-end prototype is designed and implemented using of-the-shelf components aiming to receive the UMTS and WLAN signals simultaneously. The input UMTS and WLAN signals are down-scaled to one sampling frequency lower in spectrum to be in the functional bandwidth of the analogue to digital converter. Since the signals are replicated in the multiples of sampling frequency, the spectrum allocation of the total scenario is sustained. Thus, it can be used for proving the concept. The UMTS and WLAN main specifications are presented in Table. 6.1.

Table 6.1: UMTS and WLAN Specifications for UE [5], [7].

	UMTS	IEEE 802.11g
Duplexing	FDD	TDD
Frequency	1920 - 1980 MHz: UL 2110 - 2170 MHz: DL	2.4 - 2.4835 GHz
Receiver Sensitivity	-117 dBm	-82 to -65 dBm
Channel Bandwidth	3.84 MHz	16.6 MHz
Transmitter Power Level	24 dBm (Class 3)	20 dBm (Europe)

The block diagram of the experimental set-up is depicted in Fig. 6.1. The MITEQ low noise amplifier AM-3A-0520 is used to adjust the signal level to the required level at the input of the analog to digital converter. The filters assembly is the tunable filter provided by Trilithic and its pass-band is tuned to the desired band of interest. The signals are added together
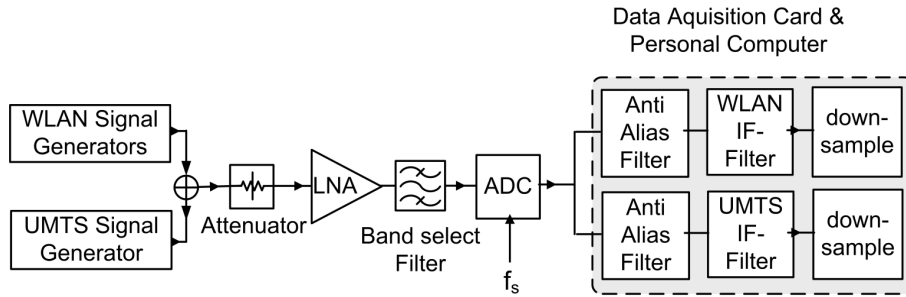

Figure 6.1: Illustration of the block diagram of designed and built RF sub-sampling front-end. The desired signals are the UMTS and WLAN signals.

through the splitter model ZFSC-2-2500 made by Mini-Circuits. The Maxim Max108 Analog

to digital converter (ADC) is used just at the down-stream of the RF front-end. It is an 8-bit resolution ADC that can go up to 1.5 GHz of sampling frequency for the input signals within the bandwidth of 2.2 GHz. The full scale input range of the device is $500\,\mathrm{m}V_{p-p}$. The 8 output bits of the ADC are entered to the data acquisition card followed by the personal computer. The data is further processed by a software based receiver executed in Matlab. The process consists of FIR filtering and IIR channel select filtering followed by digital decimation and down conversion of the signals.

6.1.2   RF signals and clock generation

The RF sub-sampling front-end is implemented according to the block-diagram shown in Figs. 6.2 and 6.3 in addition to the description provided in Section 6.1.1.
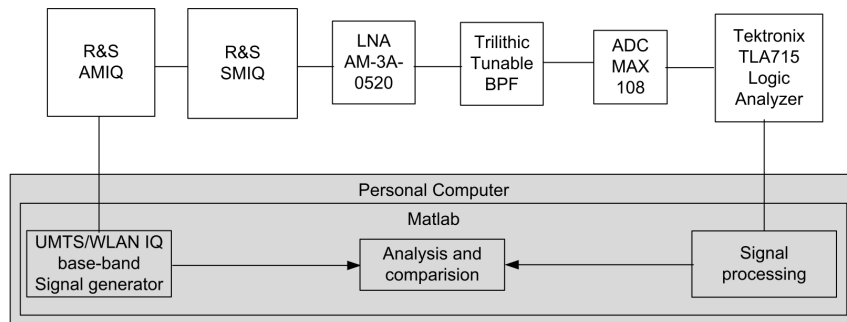
Figure 6.2: Illustration of the block diagram of the experimental setup for the single-frequency reception.
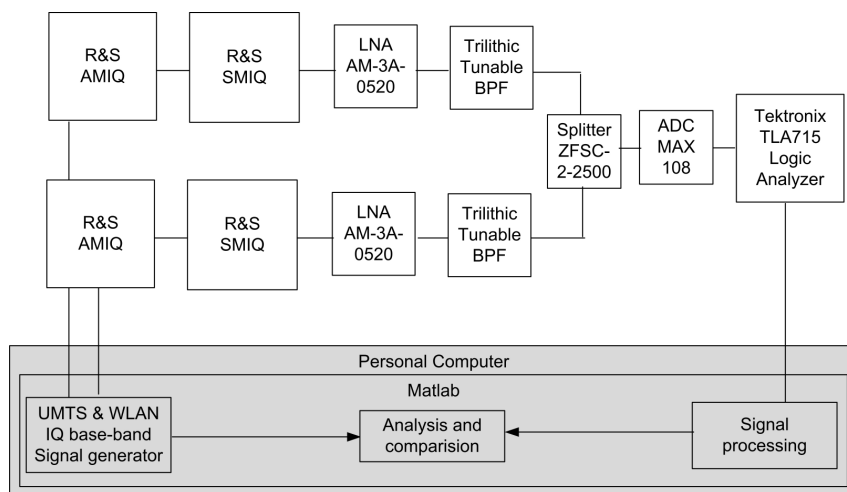
Figure 6.3: Illustration of the block diagram of the experimental setup for the multi-frequency reception.

The sampling clock generation is done with the Rohde & Schwarz SMIQ 03B (Vector Signal Generator) [101]. The clock input of the system is differential consisting of clk^+ and clk^- inputs. The generated signal from signal generator is connected to clk^+ while the clk^- is terminated to ground via a $50\,\Omega$ resistor. According to the specification of the ADC board, the amplitude

of the generated clock is 4 dBm. The frequency is modified in each experiment according to the required sampling rate.

To generate the UMTS and WLAN signals, the signals have been provided by Matlab through the method mentioned in Section 1.5. This is done to create the same signals for simulations and the measurements. Having the same signals creates a common ground for analysis and makes it possible to compare the results from the simulations with the measurements. The generation of the RF signals from the Matlab custom provided baseband signals is performed by a combination of the I/Q Modulation Generator R&S AMIQ [102] and R& S Vector Signal Generator SMIQ [101] as illustrated in Figs. 6.2 and 6.3.

The custom provided I/Q signals are generated by the R&S AMIQ I/Q modulation generator and the WinIQSIM simulation software [103]. The R&S AMIQ is a dual-channel modulation generator to be employed as an I/Q source. The programming software provided to control this source called WinIQSIM [103] which is worked in combination with AMIQ to download the signal to the instrument. The AMIQ is able to generate base-band and low-IF signals (up to 100 MHz). To up-convert the the I/Q baseband signal to radio frequency (RF), the R&S SMIQ vector signal generator is employed [101]. This approach is employed in the current dissertation as well to generate the pre-specified RF signals.

6.1.3   Practical issues

It is important to take several practical issues during the experiments. Some of them are outlined below:

- All the powers connected to the biasing circuits of the experiment is checked to verify they are precisely correct. It is assured that these sources are capable to supply the proper current requirements. The supply currents should meet the data-sheet specifications especially the required values for the ADC [?]. That is due to the fact that providing enough current especially for the digital biasing path of the ADC has very important role in proper functionality of the receiver chain. In case insufficient current enters to the system, a drop of voltage in the digital biases will happen and the system will not work properly. Thus, it is assured that the provided current for the system is sufficient according to the ADC data-sheet.

- Separate supplies for analogue, digital and output drivers must be employed. The Sources used as supplies are Hewlett Packard E3631A.

- It is critical to verify the supply currents and check whether they are "running away" or are elevated.

- There could be a slight voltage drop across the wires connecting the sources to the ADC board, depending on what type of wires are used and how many power pads are connected to each supply.

- The probes between the power supplies and the ADC board should not fulfill any special requirements. But it's important that the system is configured properly for the outputs. For instance, if a single-ended logic analyzer is employed, either the true or the complementary output of the differential outputs should be used and not both.

- To run the ADC board, first the supply voltages are switched on and then the input voltages and the clock. It is the good approach to always establish power supply connections first before applying input signals to ensure not running into unwanted latch-up behavior. Although it is claimed that the selected converter of this thesis (Maxim Max108) show a high level of resilience regarding latch-up, there could be a condition that potentially causes problems.

6.2 Proof of multi-signal reception capability of the RF sub-sampling receiver

The idea in this experiment is to investigate the feasibility of implementing the multi-standard RF sub-sampling receiver by off-the-shelf components. First the operation of the receiver for the single-frequency application is examined. Then the functionality of the receiver in the multi-frequency applications is verified via experiment.

6.2.1 Single-frequency reception

To prove the functionality of the receiver in single-frequency application, a single signal is applied to the input of the receiver. This is to verify the principle operations of the receiver such as correct frequency down-conversion. The UMTS and WLAN signal generated by the method mentioned in Sections 1.5 and 6.1.2 are applied to the receiver separately.

The output intermediate frequency (IF) signal of the receiver was measured by clocking each RF input signal(the UMTS or WLAN) one-by-one at 676 MHz. The summary of the specifications used for this experiment is outlined in Table 6.2. As mentioned before, the input UMTS and WLAN signals are down-scaled to one sampling frequency lower in spectrum to be in the functional bandwidth of the analogue to digital converter (this new frequency is called applied frequency in Table 6.2). Furthermore, the expected intermediate frequencies which are calculated from Eqs. 2.9 and 2.10 are outlined in Table 6.2).

The frequency plans of the signals are illustrated in Fig. 6.4. The signals are down-converted to IF through sampling by $f_s = 676$ MHz.

The spectrum of the measured UMTS IF signal at the output of the ADC is depicted in Fig. 6.5. As mentioned in Table 6.2, the UMTS signal at 2142.5 MHz which is sampled at the rate $f_s = 676$ MHz results the output IF signal at 114.5 MHz. This can be seen from Fig. 6.5 as well. From the two signals illustrated in Fig. 6.5, one is the expected IF signal at 114.5 MHz and the other one is its image at $f_s/2 - 114.5$ or 223.5 MHz.

To further process the signal and compare it with the similar signal from simulation, the

Table 6.2: The UMTS and WLAN signal Specifications used for single-frequency experiment [5], [7].

	f_0 [MHz]	Applied Freq. [MHz]	BB clock rate [MHz]	Amplitude [mV]	f_s [MHz]	f_{IF} [MHz]
UMTS	2142.5	1466.5 $f_0 - f_s$	61.44	225	676	114.5
IEEE 802.11g	2442	1766 $f_0 - f_s$	20	225	676	262 or $f_s/2 - f_{IF}$
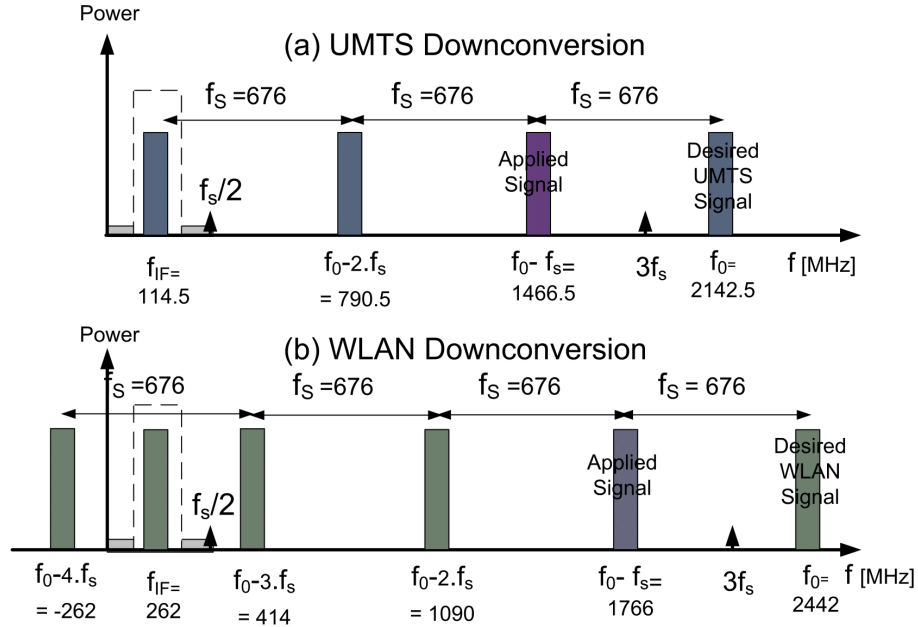
Figure 6.4: Illustration of the UMTS and WLAN frequency plans and the expected IF signals.

down-converted signal at 114.5 MHz is filtered with a Finite Input Response (FIR) filter. The filtered signal is depicted in Fig. 6.6

The measured and simulated spectrum of the UMTS signal sampled at 676 MHz at 114.5 MHz is depicted in Fig. 6.7(a). To make the signal frequency contents visible, the zoomed view of the same plot is depicted in Fig. 6.7(b).

It can be seen that the signal is down-converted to the correct frequency and occupies the correct bandwidth. Further investigation of the performance of the receiver and the resulted error vector magnitude (EVM) is presented in the Section 6.2.2.

The same test is applied to the WLAN signal. A WLAN signal, generated by the method mentioned in Sections 1.5 and 6.1.2 is applied to the input of the receiver. The specifications of the applied signal are outlined in Table 6.2. The measured spectrum at the output of the receiver is depicted in Fig. 6.8. Accordingly, the filtered signal is shown in Fig. 6.9. Due to the
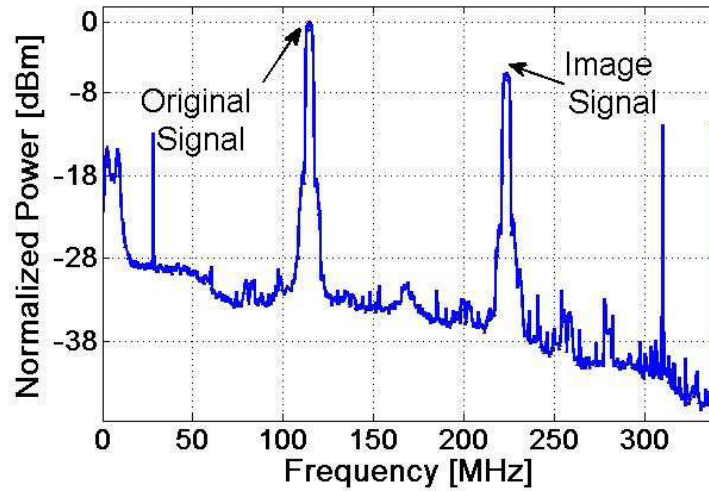
Figure 6.5: Measured frequency response of the UMTS signal and its correspondence image in the Nyquist zone.
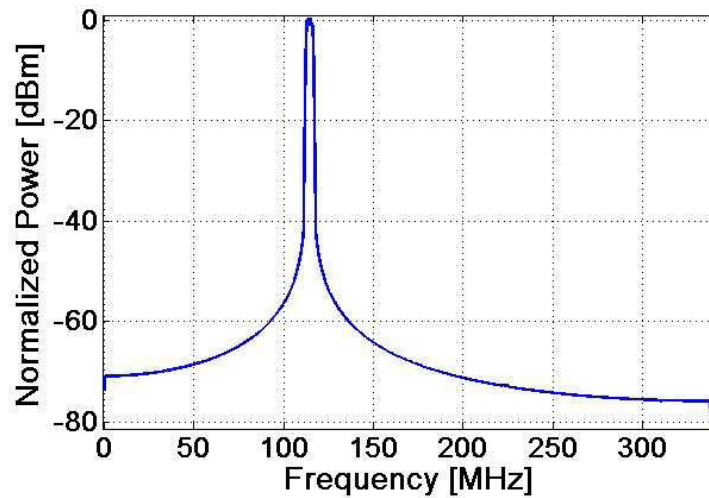

Figure 6.6: Measured frequency response of the UMTS signal after FIR filtering in the Nyquist zone.

better quality of the image, the image signal at $f_s/2 - 262$ MHz or 76 MHz is selected and filtered out for the further analysis.

The measured and simulated spectrum of the WLAN signal sampled at 676 MHz at 76 MHz is depicted in Fig. 6.10(a). The zoomed view of the in-band information is shown in Fig. 6.10(b).

The measured WLAN signal is spectrally placed in the correct frequency position and its bandwidth is in comply with the IEEE 802.11g specifications. Although the measurements reported in this section are only focused on one of the UMTS or WLAN channels, the other channels of these signals were tried one by one and the correct frequency down-conversion functionality of the front-end is approved. This assures the appropriate functionality of the
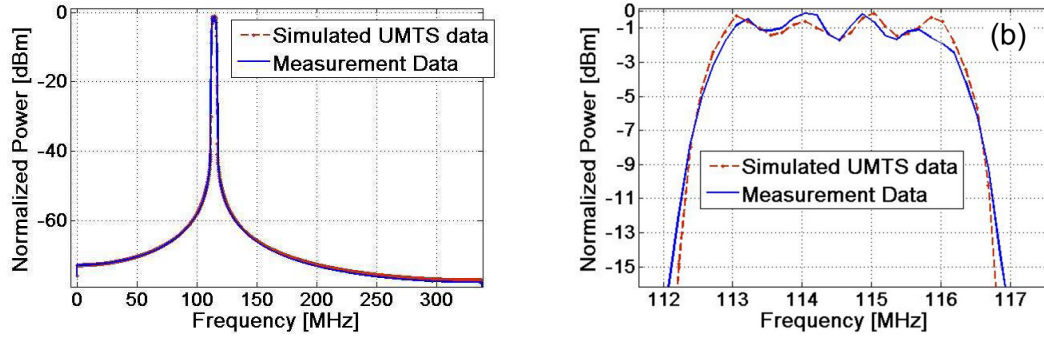
Figure 6.7: Simulated and measured Normalized output Powers relative versus frequency (a) Measured simulated UMTS spectrum at intermediate frequencies; (b) The zoom of the in-band data.
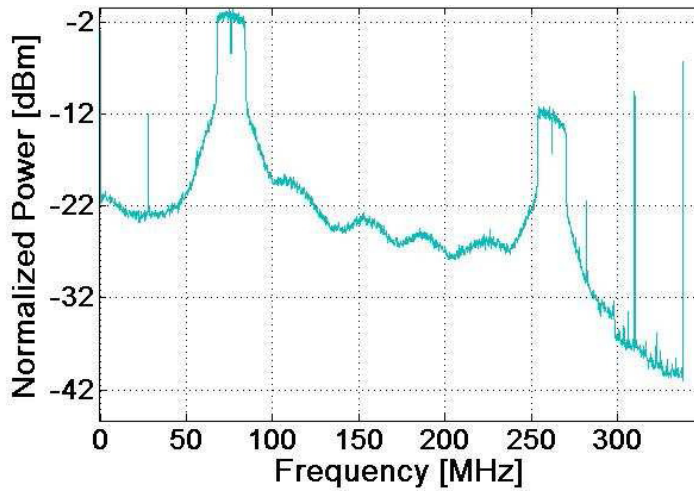

Figure 6.8: Measured frequency response of the WLAN signal and its image in the Nyquist zone.

receiver in down-converting the signals to the expected frequencies at IF for all the bands of the scenario with correct bandwidth.

6.2.2 Multiple-frequency reception

The performance of the experimental dual-frequency receiver has been evaluated by applying both of the UMTS and WLAN signals simultaneously to its input. The signals are generated and added together via a multiplexer as illustrated in Fig. 6.1. The signal coming out of multiplexer is sampled at 676 MHz. The set-up specification is outlined in Table 6.3. Two different channels from the single-frequency reception were chosen to show the satisfactory performance of the front-end for more number of channels.

The frequency plan scenario used for the measurement of the two signals is depicted in Fig. 6.11. As mentioned in Chapter 3, the spacing between the RF signals is not specifically kept the same for the equivalent down-converted signals at IF.

The spectrum of the measured IF signal is shown in Fig. 6.12. These are the combined
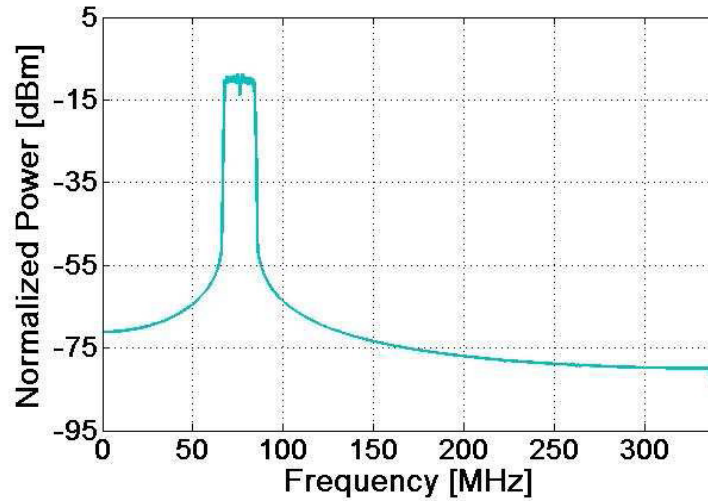
Figure 6.9: Measured frequency response of the WLAN signal after FIR filtering in the Nyquist zone.
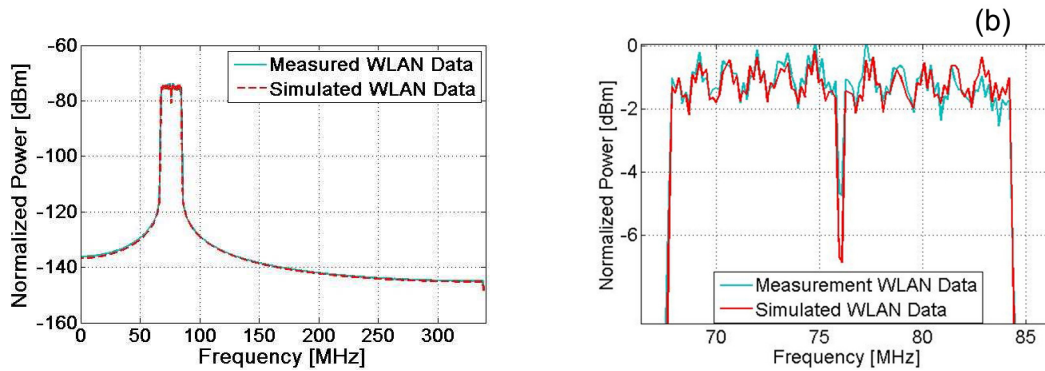
Figure 6.10: Simulated and measured Normalized output Powers relative versus frequency. (a) Measured simulated WLAN spectrum at intermediate frequencies; (b) The zoom of in-band data.

RF frequency bands which are folded into the IF. The signals are filtered with the UMTS and WLAN corespondent IF filters as shown in Fig. 6.1. The filtered IF signals are depicted in Figs. 6.13(a) and 6.14(a) for the UMTS and WLAN signals respectively. The next step is to down convert the signals to base-band. Consequently, the second down-conversion is applied to the signals. The signals at base-band are shown in Figs. 6.13(b) and 6.14(b). The sampling frequency of the signals in this stage is still 676 MHz.

According to Fig. 6.1, the signals must be down-sampled to the required base-band rates outlined in Table 6.3. Thus the UMTS signal is down-sampled to 61.44 MHz and WLAN signal to 20 MHz respectively.

Receiver EVM Performance

These down-converted and down-sampled signals must be compared with the corresponding base-band values from simulations to evaluate the performance of the implemented receiver.

Table 6.3: The UMTS and WLAN signal Specifications used for multiple-frequency experiment [5], [7].

	Desired band [MHz]	Applied Freq. [MHz]	BB clock rate [MHz]	Amplitude [dBm]	f_s [MHz]	f_{IF} [MHz]
UMTS	2167.5	1491.5 $(f_0 - f_s)$	61.44	-10	676	139.5
IEEE 802.11g	2472	1796 $(f_1 - f_s)$	20	0	676	232 or $f_s/2 - f_{IF}$
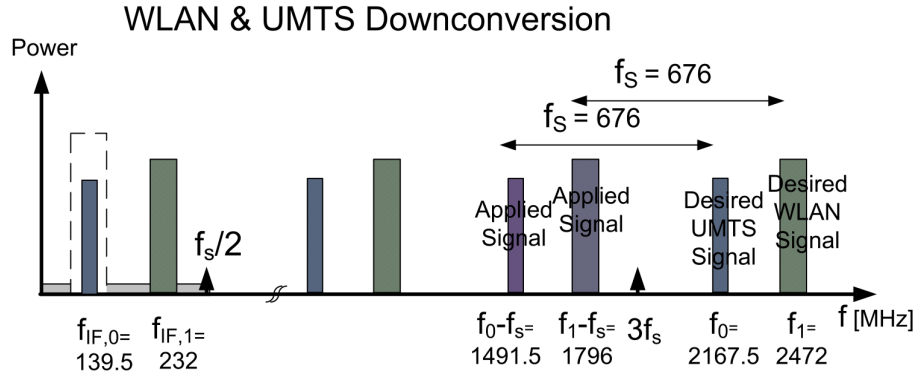
Figure 6.11: Illustration of the simultaneous UMTS and WLAN frequency plan and the expected IF signals.

However, to make the processed signal comparable with its original simulated equivalent signal, two processing steps are required:

1. The first step to make the signal comparable is to reconstruct the signal after sampling. As mentioned in Section 2.1, a band-limited signal can be precisely reconstructed from its uniform samples if it is sampled according to the Shannons sampling theorem [104]. The reconstruction formula is represented by Whittaker [105]:

$$s(t) \;\; = \;\; \sum_{m=-\infty}^{\infty} s(mt_s) \cdot sinc(2\Delta f_n \cdot (t - mt_s)) \tag{6.1}$$

where $s(mt_s)$ represents equally spaced samples and t_s is the reverse of $2\Delta f_n$. Thus the reconstruction of the input signal is equivalent to an ideal low-pass filtering.

2. To do the correct comparison of the measured and simulated data, the two signals should launch from the same time instant since no synchronization has been performed. In other words, it is required to compensate for the time lag between two signals [106] and make them time-aligned. The required lag to have comparable time aligned signals, was recognized as the maximum value of the cross-correlation function between the input simulated baseband (BB) signal to the AMIQ and the output signal from the ADC.

Figure 6.12: Measured frequency response of the combined WLAN and UMTS signal and their images in the Nyquist zone.
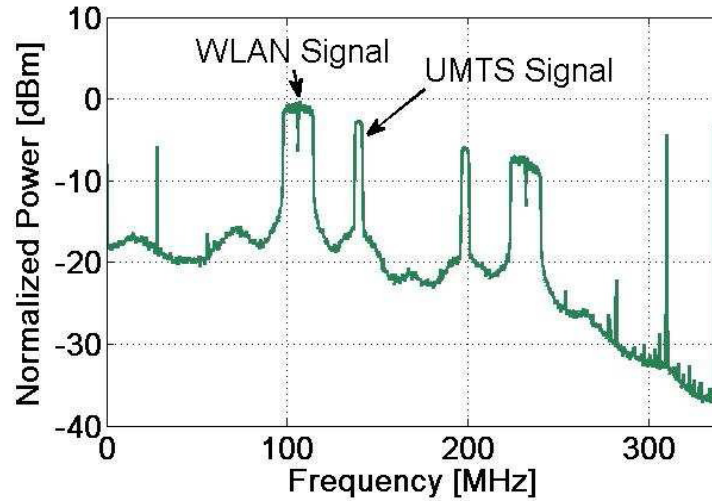
Misalignments of these signals will create major distortion. Consequently, the measured signal after reception process is cross-correlated with the original generated signal from method presented in Sections 1.5 and 6.1.2. For two signals x and y the cross-correlation is expressed as [106]:

$$R_{yx}(m) \quad = \quad \frac{1}{N} \sum_{n=0}^{N-1-k} y_{n+k} x_n \tag{6.2}$$

By moving one of the signals on top of the other, it can be figured out where the signals are most resemble to each other. This can be done with cross-correlating the signals with each other. In other words, cross-correlation measures how well parts of one signal resemble parts of another. It indicates how much is the time lag between these two most resemble parts. Then the measured signal will be shifted time-wise according to the lag calculated from the cross-correlation to make the signals time-aligned.

Thus to compare the output from sub-sampling receiver front end with its correspondent signal from simulation, the measured processed signal is first low-pass filtered to compensate for the non-idealities of the sample and hold operation. Then, it is cross-correlated with the original simulated signal to do the time alignment. To perform the cross-correlation, the required steps are:

- The time lag between the two signals is estimated and compensated to make them time aligned.

- Each signal is normalized so that their autocorrelations at zero lag are identically 1.

Then the signals are compared and the EVM of the signals are calculated consequently.

Figure 6.13: Measured Normalized output Powers relative versus frequency (a) measured UMTS spectrum at intermediate frequencies after FIR filtering; (b) measured UMTS filtering after filtering, down-conversion to base-band and down-sampling.

To verify the functionality of the receiver, the UMTS and WLAN RF signals are applied to the receiver at the same time. The calculated RF requirements and frequency plan of the receiver is followed according to the provided discussions in the current thesis. The signals are processed in the receiver. They are amplified, filtered, Added together and sampled at the rate of 676 MHz. After the IF channel selection and down-conversion to base-band, the EVM of each signal is measured separately. These EVMs are depicted in Fig. 6.15.

It can be seen that the EVM of WLAN signal was measured to be between -36 to $-29\,$dB which indicates a good performance of the receiver for this signal. The maximum acceptable EVM for the WLAN signal is -25 dB [7]. The measured EVM of the UMTS signal varying between -25.6 to $-17.5\,$dB indicates an acceptable performance of the receiver for this standard (req. < -15.4 dB) [5].
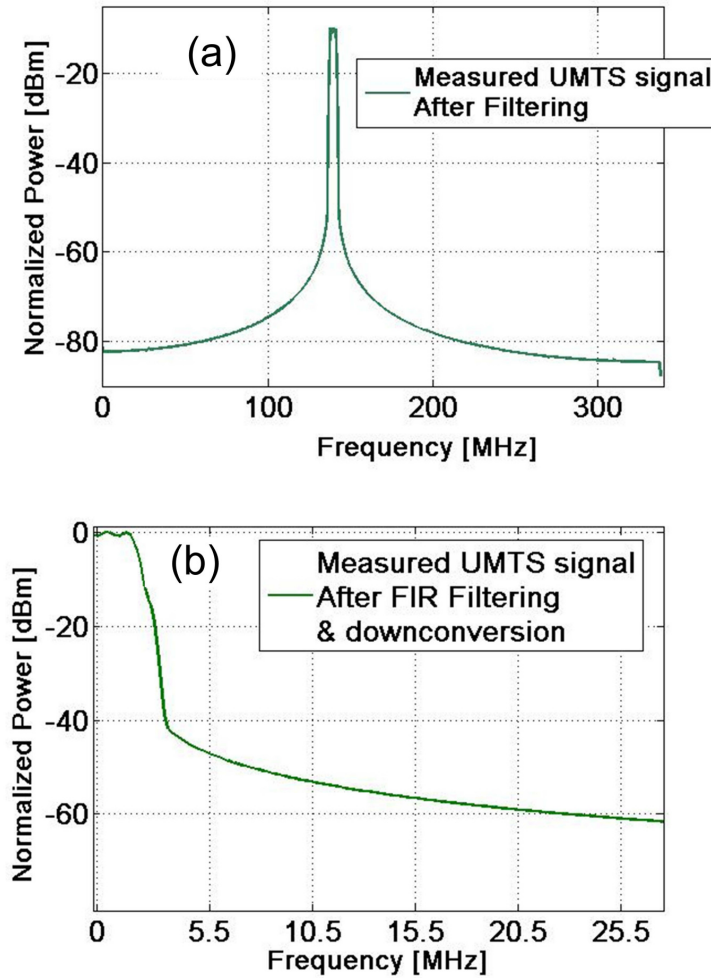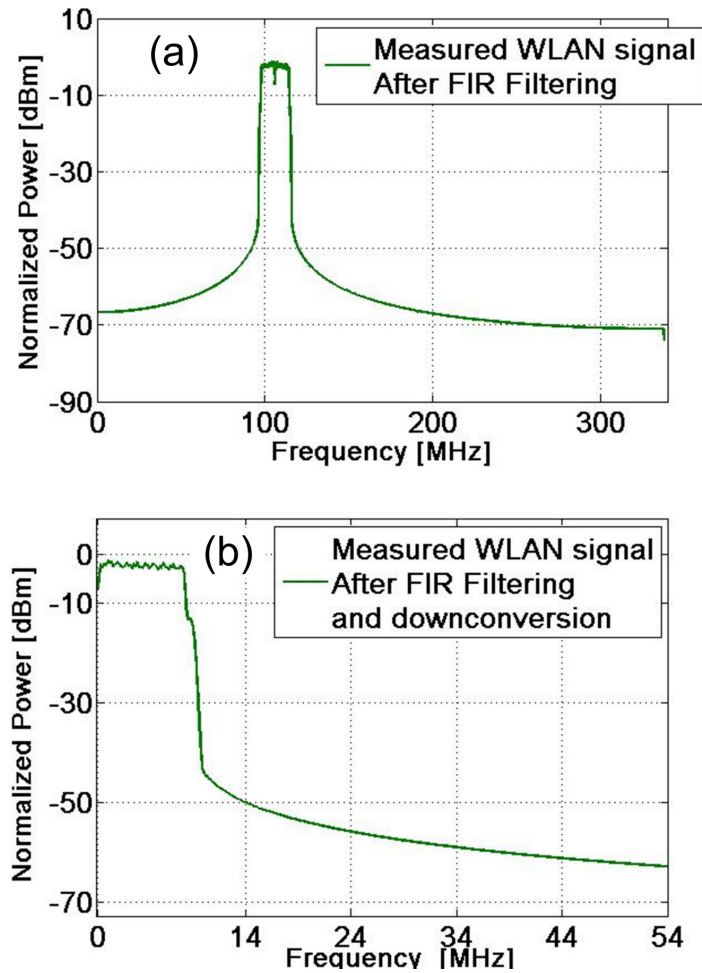
Figure 6.14: Measured Normalized output Powers relative versus frequency (a) measured WLAN spectrum at intermediate frequencies after FIR filtering; (b) measured WLAN signal after filtering, down-conversion to base-band and down-sampling.

6.3 Proof of sampling rate algorithm

The idea in this experiment is to verify the theory presented in Chapter 3. To do the experiment, several channels of the UMTS and WLAN band are generated and applied to the input of the receiver as illustrated in Fig.6.1 in pairs. The channels which were chosen for this experiment are outlined in Table 6.4. The selected channels for both the WLAN and UMTS standards are two upper and lower edges channels in addition to one channel in the middle of the band. This provides a complete overview since all the other channel will be accommodated between the upper and lower edge channels. The setting of the power and base-band clock rates are the same as the values outlined in Table 6.3.

The combination of the two signals are applied to the input of the receiver. The signals are sampled via the sample and hold (S/H) block. The sampling frequency is swept and the frequency of the output IF signals are monitored and measured. The measured data is depicted

Figure 6.15: Measured receiver EVM performance for the UMTS and WLAN signals versus input power, s_i.

Table 6.4: UMTS and WLAN channels selected for Proof of the Sampling Rate Algorithm.

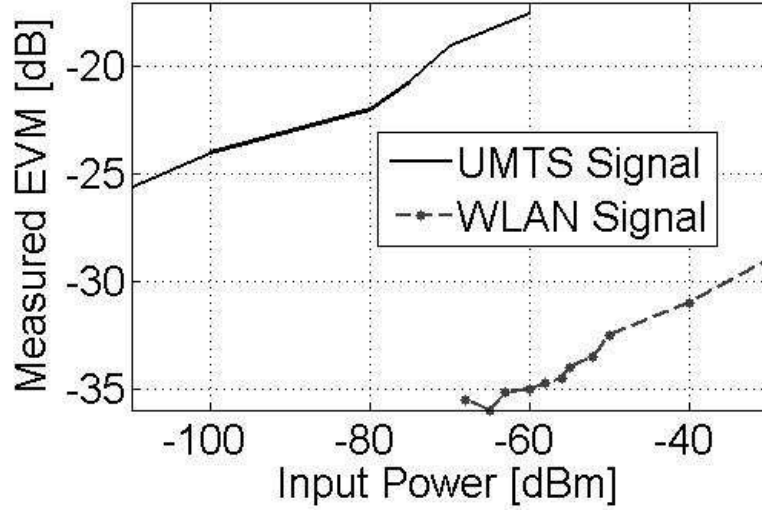| Frequency of the channels [MHz]	Lower edge	middle	upper edge
UMTS	2112.5	2142.5	2167.5
IEEE 802.11g	2412	2442	2472

in Fig. 6.16. It can be seen that the measurement results obtained from the set-up shows high agreement with the results from the theory and simulations presented in Section 3. The selected sampling frequency of the current thesis is highlighted with a red line in Fig. 6.16. The UMTS and WLAN channels are completely separated from each other at this frequency and there is no interference. The boarders of the Nyquist band $[0; f_s/2]$ for $f_s = 676$ MHz are marked in the Fig. 6.16 with green crosses. The measured points from both the WLAN and UMTS channels are located in enough distance from the Nyquist boarders and fulfill the Nyquist criterion. The measurements confirm the algorithm of selecting the sampling frequency. The acceptability of this sampling frequency is further confirmed in the image rejection and selectivity requirements of the receiver.

6.4   Proof of the Milieu Adapting Techniques

The schematic of the UMTS experimental receiver for single frequency application is shown in Fig. 6.17. It is exactly the same as the set-up shown in in Fig. 6.1 except two differences: (i) it is only required to process the single-frequency application since the focus is on the reception of UMTS signal only and (ii) the first generator is used to generate the desired RF UMTS signal and the other generators are employed to generate the disturbing signal in neighboring
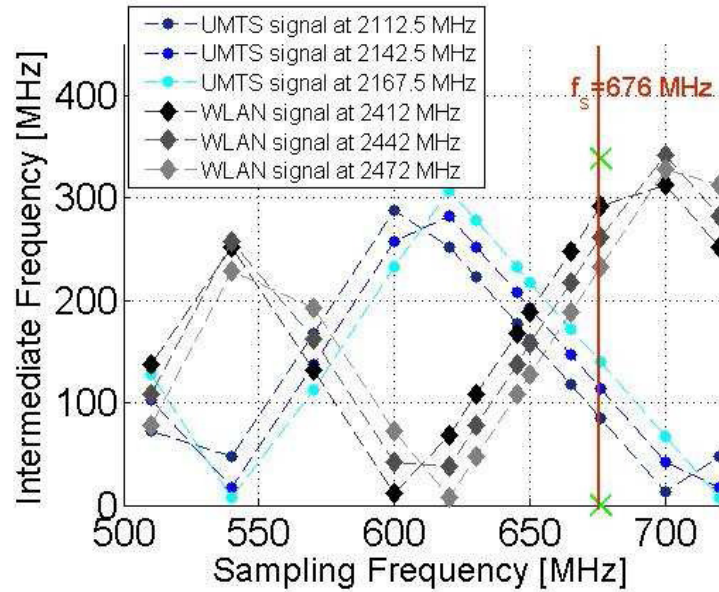
Figure 6.16: Measured receiver EVM performance for UMTS signal.

environment. They are called "'Image Noise Generators"' in the figure.

All the set-up configurations are similar to what explained in previous experiments. The feedback loop and programmable clock generator are replaced by manual adapting of the clock to the calculated sampling frequencies. Since the intention of the measurements is to prove the concept, this serves the purpose. However, the number of available high speed PCGs is rapidly growing and finding an appropriate PCG for further complete implementation is possible such as the productions of Cypress Semiconductor Corporation [95] and Rambus Inc [96].
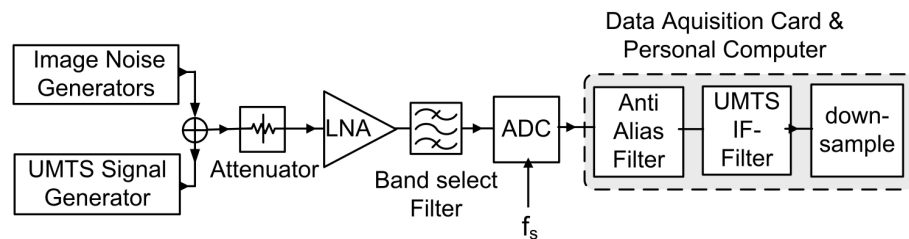
Figure 6.17: Schematic of the designed and built RF sub-sampling UMTS front-end. The noise generators are generating the image distortions. The selectivity provided by the IRF has been deliberately ignored to prove the ability of the milieu adapting technique in relaxing the IRF requirement.

To do the measurements, a number of interferes are generated according to the simulation model in Fig. 3.20. To model the interferes, the UMTS signal with the bandwidth of 3.84 MHz and channel separation of 5 MHz is used.

Interferes are individually down-converted to the base-band and averaged over the captured time. The weakest signals at 2055, 1785 and 1911 MHz are selected as the closest image distortions of the scenario. The desired signal is received to the receiver consequently. The sampling frequencies of 420 ,655 and 676 MHz are determined from Eqs. (3.15), (3.16) given

the f_0 at 2145.

The proper f_s of 676 MHz is selected among all the appropriate frequencies by employing the algorithm mentioned in Section 3.2.5. The sampling rate of 676 MHz is in comply with the requirements described in the Algorithm.

Consequently, the received signal and the generated image distortions are added together through multiplexer and sampled with the calculated f_s. To show the functionality of the method in improving the SNR, the signals are sampled with several other randomly selected f_s. The measured SNR for different f_s is depicted in Fig. 6.18.
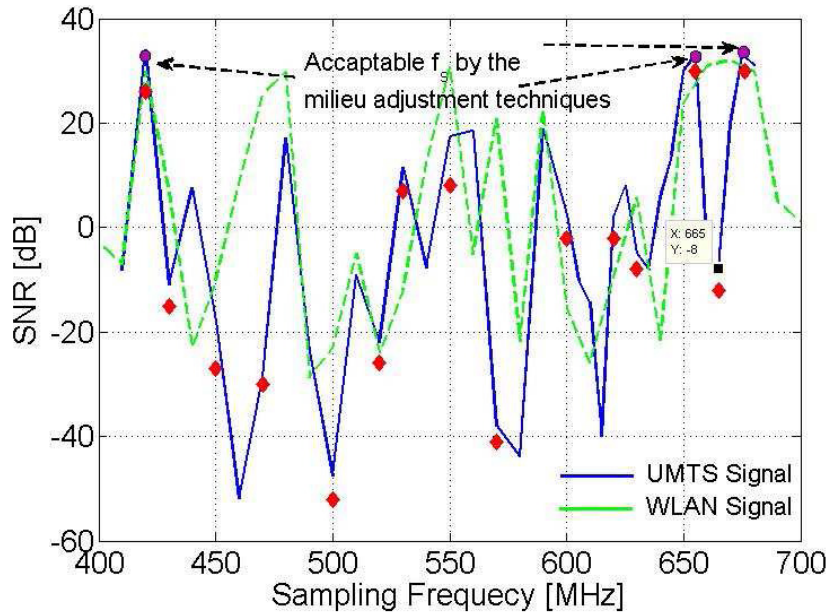
Figure 6.18: Simulated and measured SNR [dB], versus sampling frequency, f_s [MHz] with and without enabling Milieu adapting technique. The measurement data is shown with red quadripartite in the figure.

The measurements fully agree with the simulations and the presented concept is validated. Selecting the sampling frequency of the receiver according to the method mentioned in Secs. 3.2.3 and 3.3 shows a promising improvement in the result. The greatest SNR of the scenario is obtained for the sampling frequency approved by milieu adapting techniques.

6.5   Proof of the Image Rejection and Selectivity Requirements

To clarify the problem of image in sub-sampling receivers and the required selectivity, the illustrative example of Section 2.4.1 is verified. The block diagram of the experimental set-up used for this experiment is the same as the set-up depicted in Fig. 6.17. The image noise generators are replaced by a WLAN signal generator.

The image noise effect is studied by applying the input UMTS signal with power of -114 dBm at 2145 MHz and sweeping the image noise power at 2412 MHz within the power level range of WLAN signal (-69 to -86 dBm in 16.6 MHz bandwidth) [7]. Alternatively, it can be

interpreted as varying the selectivity of the front-end at the closest image frequency 2412 MHz. It includes the attenuation provided by the front-end. The total bandwidth of the receiver band-select filter in the simulation is 690 MHz which is the same as the bandwidth of the real filter used for the experimental receiver. The scenario of this example is shown in Fig. 6.19. The only in-band image is located at 2412 MHz and the rest are out-of-the band. The output power spectral density is observed at the output of the receiver at intermediate frequencies.
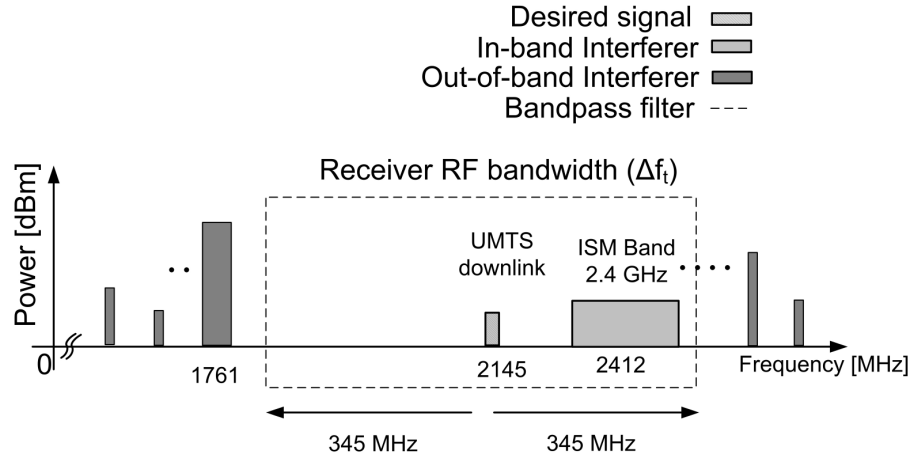

Figure 6.19: Illustration of the spectrum of the desired signal, in-band power levels and interferes at RF.

The measured spectrum after filtering and level adjustment is depicted in Fig. 6.20. It illustrates the UMTS reception without any interference and its comparison with the UMTS signal affected by two different image noise powers— a weaker and a stronger image noise. To show the image distortion which affects the UMTS signal, the down-converted image signal is illustrated in the figure. It should be noted that in reality the image distortion is located at 2412 MHz and it is depicted at IF frequency only for illustration purposes. It can be seen that the spectrum is visibly affected in the existence of the strong interference (-70 dBm) at its image spacing.

To see the distorting effect of the image noise, the degradation of the signal is quantified by measuring the cross-correlation of the distorted and undistorted signals.

Fig. 6.21 shows the simulated and measured normalized cross-correlation of the undistorted signal with the distorted ones versus image varying power. As expected, the results indicate that there is a direct relationship between the amount of image power delivered to the desired band and the signal distortion. Increasing the power of the image distorts the signal more and makes it more dissimilar to the undistorted version.

On the whole the measurement indicates that the two mentioned issues related to the image problem are important to predict and avoid the image signals distortion in the desired band: (i) the sampling frequencies which result in image signals that do not fulfill Eq. (4.15) are poor choices of sampling rates and must be prohibited such as the example presented in this article. The illustrated image noise was not suppressible to the required level by the provided front-end selectivity in the example and distorts the signal significantly due to the absence of required
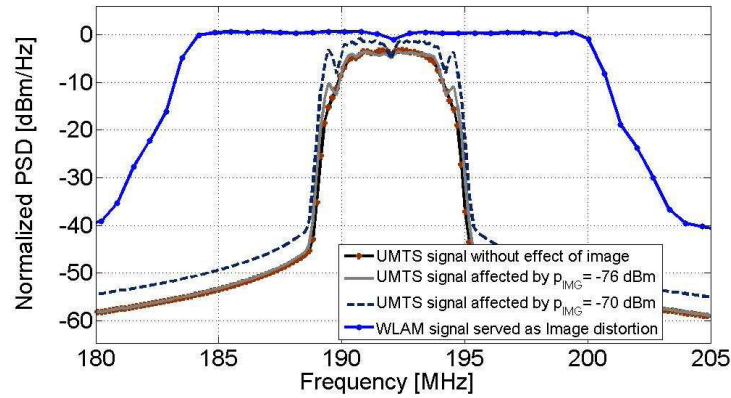
Figure 6.20: Measured Power Spectral Density at the intermediate frequencies. The signal without any distortion is compared with the two distorted signals with the image power of -70 and -76 dBm. It includes the image distortion which is down-converted to IF for illustration purposes. The signals are normalized.
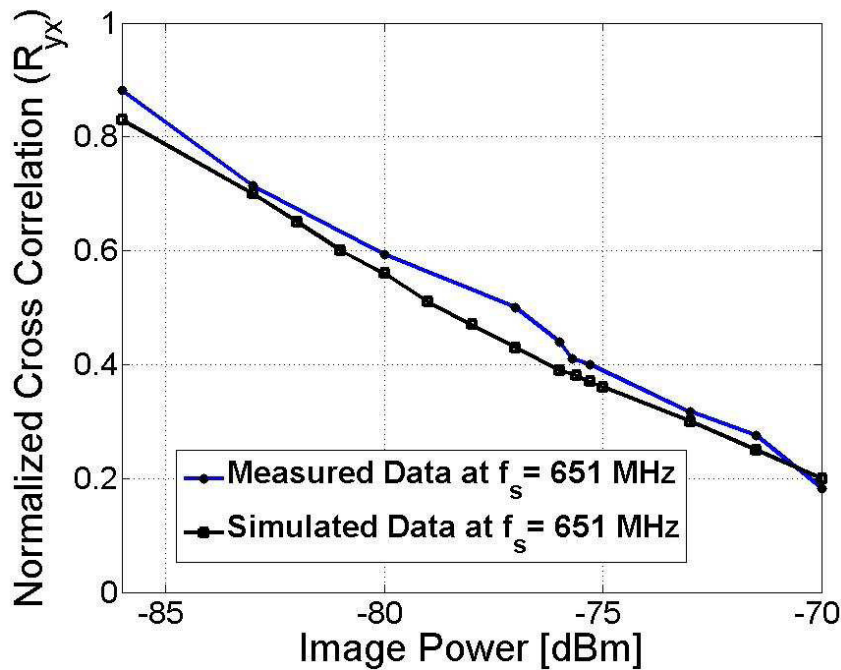
Figure 6.21: Simulated and Measured cross correlation between the signals before and after image distortion.

selectivity of the front-end. According to the out-of-band blocking test defined in the 3GPP standard [5], the CW blocker (P_{Blk}) with the power level of -44, -30, and -15 dBm may exist at the frequency offset of 15, 60 and 85 MHz, respectively. The required selectivity to suppress the blocker to a level less than the acceptable noise and distortion level is 54, 68 and 83 dB [86] which does not fully provided in the presented example. The image signal exists at 2412 MHz which is more than 85 MHz far from signal. The front-end selectivity is required to provide at least 86 dB suppression at this spacing which is only partly provided here. (ii) Thus, only the sampling frequencies providing enough image spacing from the desired signal according to the

available selectivity of the front-end are the best possible sampling rates. The results correspond very well with the interference profile described in Section 4.4.2. The Eq. (4.15) is not fulfilled for $f_s = 651$ MHz which indicates a poor choice of sampling frequency. The interfering profile will discard this sampling rate and consequently solve the mentioned problem.

6.6   Results and discussion

To prove the concepts presented in the current dissertation, four set of experiments are presented. The first experiment presents the proper reception functionality of the implemented RF sub-sampling receiver for single-frequency and multiple-frequency applications. The second experiment compares theoretical and experimental results to proof the proposed algorithm for selection of the sampling frequency. The third experiment compares theoretical and experimental results for the milieu adapting technique. Finally to clarify the problem of image in sub-sampling receivers and the required image rejection selectivity, the forth experiment compared the simulated and the measured data. Good agreement between theoretical and experimental results are obtained for all the experiments.

Chapter 7

Conclusions and Future Work

software defined radio (SDR) architectures for omni-purpose wireless communications has been desirable choice due to their enormous potentials since many years. However, they are not vastly employed due to the limitations on the currently developed technologies including CMOS, analogue-to-digital and digital to analogue conversion, application specific integrated circuits (ASIC)s and field-programmable gate array (FPGA)s. As an alternative solution to SDR, the RF sub-sampling architecture is considered a viable choice to realize multi-feature front-ends. This is one step toward the digital transceivers with the majority of processing being done in digital domain.

The first part of the current thesis provides an introduction over the whole work. The specific focus is on the multi-standard hand-held user equipments. Different radio receiver architectures are reviewed and compared with respect to multi-standard inherent of the receiver. The main motivation of the dissertation is to define a novel receiver architecture which could be used as an alternative architecture for the SDR as previously mentioned. To fulfill this, the RF sub-sampling receiver architecture is considered as a viable choice. The aim of this investigation is set to study the advantages and disadvantages of this architecture for a multi-standard mobile application. To focus on a realistic example, a case-study is defined in which a multi-standard transceiver is operating simultaneously with WLAN and UMTS signals. The research methodology is defined

By selecting the RF sub-sampling architecture as the main architecture, more detailed focus is set to this architecture . The principles of sampling theory is explained. The down-conversion in sub-sampling technique is performed based on intentionally aliasing down the signals. It is proved that this architecture is noisy in-nature due to folding of noise. Some of the important non-ideal effects of sampling architecture such as thermal noise and jitter is discussed. It is shown that the thermal noise effects is governed with the sampling frequency and capacitance as well as the associated bandwidth of the sample and hold (S/H) block. Depending on the design goals , the best compromise should be hold among these parameters. The important components of this architecture containing the low noise amplifier (LNA), RF filters and Analog to digital converter (ADC)s are investigated. Special care is taken to study the role of this components for sub-sampling architectures. The ways to deal with the performance degradation due to

149

noise aliasing in sub-sampling receivers is proposed by governing some of the design constrains of these components. The LNA should be selected carefully since it is shown that the noise level of this architecture is controllable by proper assignment of sampling frequency and gain of the front-end. The noise bandwidth of the RF filters plays an important role in limiting the harmless aliasing of undesired signals to the desired band. The other important component which is the key enabling component of the SDR is the ADC. The dynamic range requirement of this component for the case study of this dissertation is investigated. The required number of bits for a N-bit analog-to-digital converter is calculated to be 10.5 and 9 bits for UMTS and WLAN respectively. The image distortion in sub-sampling receivers is investigated. Due to replication of signals in this architecture, the impending image may be seriously decrease the performance of the receiver.

To use the great potentials of RF sub-sampling receivers for multi-standard applications, it is required to overcome some of the limitations provided by the architecture. In the current thesis, techniques are proposed to conquer the major problems and shortcomings of this type of receiver. Two major issues are investigated throughly with respect to the multi-frequency hand-held application— the optimum frequency plan and RF requirements of the receiver. Special care is taken to mitigate the image distortions. The reason is that the appropriate performance of this architecture can be achieved with providing adequate amount of image rejection. Therefore based on the investigations, a novel RF sub-sampling architecture is proposed that solve the problem of image distortion wisely. The architecture is worked based on sensing the neighboring environment and allocating the smallest blocking interference as the image distortion. Consequently, the receiver planning will be done to deliver the least possible image distortion on top of the desired band at lower frequencies.

The frequency planning of this architecture is a complex task in comparison with the previous architectures. It is due to the fact that several signals and interferes are replicating at the multiples of sampling frequency. A novel interfering profile is proposed to realize the most optimum frequency plan of the receiver based on the appropriate selection of the sampling frequency.

In summary, this thesis provides an in-depth overview of the RF sub-sampling receivers as a viable choice for the multi-standard applications. Effects of different component on its multi-frequency performance is investigated. The drawbacks of the architecture are studied and new techniques are proposed to tackle some of the major drawbacks of this type of architecture.

List of Acronyms

VTU   danish ministry of science, technology and innovation

SNR   signal to noise ratio

SDR   software defined radio

UMTS   universal mobile telecommunications system

WLAN   wireless local area network

GPS   global positioning system

DAB   digital audio broadcasting

DVB   digital video broadcasting

DVB-H   digital video broadcasting - handheld

WIMAX   worldwide interoperability for microwave access

ADC   Analog to digital converter

UL   uplink

DL   downlink

FDD   frequency Division Duplex

TDD   time division duplex

OFDM   orthogonal frequency division multiplexing

BPSK   binary phase shift keying

QAM   quadrature amplitude modulation

RF   radio frequency

IF   intermediate frequency

UE   user equipment

LNA   low noise amplifier

IR   image-rejection

SAW   surface acoustic wave

LO   local oscillator

PGA   programmable-gain amplifier

BB   baseband

I   in-phase

Q   quadrature phase

IQ   in/quadrature phase

LPF   low pass filter

BER   bit error rate

QDC   quadrature down conversion

CDMA   Code division multiple access

ACI   adjacent channel interference

NF   noise figure

QPSK   quadrature phase shift keying

SR   Software Radio

FPGA   field-programmable gate array

DSP   digital signal processing

PSD   power spectral density

S/H   sample and hold

EVM   error vector magnitude

IL   insertion loss

IFFT   inverse fast fourier transformation

RMS   root mean square

PDA   personal digital assistants

GSM   global system for mobile telecommunications

PCG   programmable clock generator

PG   processing gain

FIR   Finite Input Response

ASIC   application specific integrated circuits

DAC   digital to analog converter

Bibliography

[1] M. Brandolini, P. Rossi, D. Manstretta, and F. Svelto, "Toward multistandard mobile terminals - fully integrated receivers requirements and architectures," *IEEE Trans. Microwave Theory Tech.*, vol. 33, no. 10, pp. 1462–1469, Oct. 1998.

[2] D. M. Akos, M. Stockmaster, J. B. Y. Tsui, and J. Caschera, "Direct bandpass sampling of multiple distinct rf signals," *IEEE Trans. Commun.*, vol. 47, no. 7, pp. 983–988, 1999.

[3] M. L. Psiaki, S. P. Powell, H. Jung, and P. M. Kintner, "Design and Practical Implementation of Multi-frequency RF Front Ends Using Direct RF Sampling," *IEEE Trans. Microwave Theory Tech.*, vol. 53, no. 10, pp. 3082–3089, Oct. 2005.

[4] J. Mitola and Z. Zvonar, *Software Radio Technologies: Selected Readings.* New York, USA: Wiley-IEEE Press, 2001.

[5] *Universal Mobile Telecommunications Systems (UMTS); User Equipment (UE) radio transmission and reception (FDD)*, 3rd Generation Partnership Project (3GPP) Std. TS 25.101, Rev. version 7.8.0 Release 7, June 2006.

[6] *Universal Mobile Telecommunications Systems (UMTS); User Equipment (UE) radio transmission and reception (TDD)*, 3rd Generation Partnership Project (3GPP) Std. TS 25.102, Rev. version 7.7.0 Release 7, June 2006.

[7] *Wireless LAN Medium Access Control (MAC) and Physical Layer (PHY) specifications-Further Higher-Speed Physical Layer Extension in the 2.4 GHz Band, IEEE Standard 802.11g*, IEEE 802.11g Std., Rev. R2003, 2003.

[8] *Radio Acess Network; Radio transmission and reception*, 3rd Generation Partnership Project (3GPP);Technical Specification Group GSM/EDGE Std. TS 45.005, Rev. version 7.1.0 Release 7, June 2005.

[9] *Digital Video Broadcasting (DVB); Framing structure, channel coding and modulation for digitial terrestrial television*, European Standard (Telecommunication series), ETSI Std. EN 300 744, Rev. version 1.5.1, Nov. 2004.

[10] *Digital Video Broadcasting (DVB); Transmission System for Handhel Terminals (DVB-H)*, European Standard (Telecommunication series), ETSI Std. EN 302 304, Rev. version 1.1.1, Nov. 2004.

[11] *Radio Broadcasting Systems; Digital Audio Broadcasting (DAB) to mobile, portable and fixed receivers*, European Standard (Telecommunication series), ETSI Std. EN 300 401, Rev. version 1.3.3, May 2001.

[12] *IEEE Standard for local and metropolitan area networks; Part 16: Air Interface for Fixed Broadband Wireless Access Systems*, IEEE 802.16 Std. C.S0002, Rev. R2004, Oct. 2004.

[13] J. Heiskala and J. Terry. (2001, Dec.) OFDM wireless LANs: A theoretical and practical guide. [Online]. Available: http://www.samspublishing.com/bookstore/product.asp?isbn=0672321572&rl=1#

[14] X. Li and M. Ismail, *Multi-standard CMOS wireless receivers : analysis and design.* Hingham, MA, USA: KLUWER ACADEMIC PUBLISHERS, 2002.

[15] S. Cripps, *RF power amplifier for wireless communications*, 2nd ed. London, UK: Artech House Publishers, 2004.

[16] D. M. Pozar, *Microwave and RF Design of Wireless Systems.* New York, USA: John Wiley & Sons, 2001.

[17] B. Razavi, *RF Microelectronics.* Upper Saddle River NJ, USA: Prentice Hall PTR, 1998.

[18] Z. Shi and et al., "A 2.7 v mixed signal processor for cdma/amps cellular phones," in *IEEE RFIC Digest of Papers*, June 1999, pp. 29–32.

[19] K. L. Fong, "Dual-band high-linearity variable-gain low-noise amplifiers for wireless applications," in *IEEE ISSCC Digest of Technical Papers*, Feb. 1999, pp. 224–225.

[20] M. Ismail and D. R. de Llera Gonzlez, *Radio Design in Nanometer Technologies.* Dordrecht, Netherlands: Springer, 2007.

[21] M. Pui-In, U. Seng-Pan, and R. P. Martins, "Transceiver Architecture Selection: Review, State-of-the-Art Survey and Case Study," *IEEE Circuits Syst. Mag.*, vol. 7, no. 2, pp. 6–25, 2007.

[22] J. W. M. . Rogers and et al., "A fully integrated multi-band MIMO WLAN transceiver RFIC," in *IEEE Symposium on VLSI Circuits, Digest of Technical Papers*, June 2005, pp. 290–293.

[23] D. Zito, B. Neri, and R. Massini, "54 dB Image Rejection Fully Integrated Receiver for Multi-standard 5-GHz WLANs," in *The 1st European Microwave Integrated Circuits Conference*, Sept. 2006, pp. 187–189.

[24] R. Hartley, *Modulation System.* U.S.Patent 1,666,206, Apr. 1928.

[25] V. Vidojkovic and et al., "Analysis of an 1.8 - 2.5 GHz multi-standard high image-reject front-end," in *9th International Conference on Electronics, Circuits and Systems*, vol. 1, Sept. 2002, pp. 73–76.

[26] D. Zito and et al., "5-GHz WLAN Standards Compliant Image Reject Radio Receiver on Low-cost SiGe-CMOS Technology," in *Bipolar/BiCMOS Circuits and Technology Meeting*, Oct. 2006, pp. 1–4.

[27] S. Wu and B. Razavi, "A 900-MHz/1.8-GHz CMOS receiver for dual-band applications," *IEEE J. Solid-State Circuits*, vol. 33, no. 12, pp. 2178–2185, Dec. 1998.

[28] S. Cipriani and et al, "Fully integrated zero if transceiver for gprs/gsm/dcs/pcs application," in *European Solid-State Circuits Conference*, Sept. 2002, pp. 439–442.

[29] E. Duvivier and et al, "A fully integrated zero-if transceiver for gsm-gprs quad band application," in *IEEE International Solid-State Circuits Conference, Digest of Technical Papers*, Feb. 2003, pp. 274–275.

[30] R. Ahola and et al., "A single-chip CMOS transceiver for 802.11a/b/g wireless LANs," in *IEEE International Solid-State Circuits Conference (ISSCC)*, Feb. 2004, pp. 92–93.

[31] M. Zargari and et al., "A Single-Chip Dual-Band Tri-Mode CMOS Transceiver for IEEE 802.11a/b/g Wireless LAN," *IEEE J. Solid-State Circuits*, vol. 39, no. 12, pp. 2239–2249, Dec. 2004.

[32] H. Hashemi and A. Hajimiri, "Concurrent multiband low-noise amplifiers-theory, design, and applications," *IEEE Trans. Microwave Theory Tech.*, vol. 50, no. 1, pp. 288–301, Jan. 2002.

[33] Z. Xu and et al., "A compact dual-band direct-conversion CMOS transceiver for 802.11a/b/g WLAN," in *IEEE International Solid-State Circuits Conference*, vol. 1, Feb. 2005, pp. 98–586.

[34] E. Gotz and et al., "A quad-band low power single chip direct conversion CMOS transceiver with $\Sigma\Delta$-modulation loop for GSM," in *Proceedings of the 29th European Solid-State Circuits Conference, (ESSCIRC '03)*, Sept. 2003, pp. 217–220.

[35] Z. Pengfei and et al, "A single-chip dual-band direct-conversion IEEE 802.11a/b/g WLAN transceiver in 0.18 μm CMOS," *IEEE J. Solid-State Circuits*, vol. 40, no. 9, pp. 1932 – 1939, Sept. 2005.

[36] T. Ruhlicke and et al., "A Highly Integrated, Dual-Band, Multi-Mode Wireless LAN Transceiver," in *Proceedings of the 29th European Solid-State Circuits Conference (ESSCIRC '03)*, Sept. 2003, pp. 229–232.

[37] P. Quinlan and et al., "A multi-mode 0.3-128 kb/s transceiver for the 433/868/915 MHz ISM bands in 0.25 μm CMOS," in *IEEE International Solid-State Circuits Conference, Digest of Technical Papers (ISSCC)*, vol. 1, Feb. 2004, pp. 274–528.

[38] V. Vidojkovic and et al., "A DECT/Bluetooth multi-standard front-end with adaptive image rejection in 0.18 μm CMOS," in *International Symposium on Circuits and Systems (ISCAS '04)*, vol. 1, May 2004, pp. 573–576.

[39] T. Ching-Hsiang and C. Sun-Chung, "Direct downconversion of multiband RF signals using bandpass sampling," *IEEE Trans. Wireless Commun.*, vol. 5, no. 1, pp. 72–76, Jan. 2006.

[40] K. Borre, D. M. Akos, N. Bertelsen, P. Rinder, and S. H. Jensen, *A Software-Defined GPS and Galileo Receiver-A Single-Frequency Approach*. Boston, USA: Birkhuser, 2007.

[41] Vanu inc. [Online]. Available: http://www.vanu.com/technology/softwareradio.html.

[42] Terocelo. [Online]. Available: http://www.terocelo.com/

[43] J. A. Kilpatrick and et al., "New SDR architecture enables ubiquitous data connectivity," in *RFDesign*, Jan. 2006, pp. 32–38.

[44] K. Morris and et al., "Redefining Software Defined Radio- BitWave's SDR for the Masses," in *Embedded Technology Journal*, Nov. 2005, pp. 1–4.

[45] Maxim Integrated Products. [Online]. Available: http://www.maxim-ic.com

[46] National Semiconductor. [Online]. Available: http://www.national.com

[47] Texas Instruments. [Online]. Available: http://www.ti.com

[48] R. G. Vaughan, N. L. Scott, and D. R. White, "The theory of bandpass sampling," *IEEE Trans. Signal Processing*, vol. 39, no. 9, pp. 1973–1984, Sept. 1991.

[49] D. Jakonis, K. Folkesson, J. Dbrowski, P. Eriksson, and C. Svensson, "A 2.4-GHz RF sampling receiver front-end in 0.18 μm CMOS," *IEEE J. Solid-State Circuits*, vol. 40, no. 6, pp. 1265–1277, June 2005.

[50] Mathworks. matlab. [Online]. Available: http://www.mathworks.com/products/matlab/

[51] A. J. Jerri, "The shannon sampling theory Its various extensions and applications: A tutorial review," *Proc. of the IEEE*, vol. 65, no. 11, pp. 1565–1598, 1977.

[52] Y. R. Sun and S. Signell, "Algorithms for nonuniform bandpass sampling in radio receiver," in *Proc. of ISCAS*, vol. 1, 2003, pp. 1–4.

[53] Y. P. Lin and P. P. Vaidyanathan, "Periodically nonuniform sampling of bandpass signals," *IEEE Trans. Circuits Syst. II*, vol. 45, no. 3, p. 340351, 1998.

[54] A. V. Oppenheim, R. W. Schafer, and J. R. Buck, *Discrete-Time Signal Processing*. Upper Saddle River NJ, USA: Prentice Hall, 1999.

[55] S. J. Orfanidis, *Introduction to signal Processing*. USA: Prentice Hall, 1996.

[56] C. E. Shannon, "Communication in the presence of noise," in *Proc. IRE*, 1949, pp. 10–21.

[57] S. Andersson and C. Svensson, "A 750 MHz to 3 GHz tunable narrowband low-noise amplifier," in *23rd NORCHIP Conference*, Nov. 2005, pp. 8–11.

[58] S. Hori, T. Maeda, N. Matsuno, and H. Hida, "Low-power widely tunable Gm-C filter with an adaptive DC-blocking, triode-biased MOSFET transconductor," in *Proc. of ESSCIRC*, Sept. 2004, pp. 99–102.

[59] G. Bollati, S. Marchese, R. Castello, and M. Demicheli, "An eighthorder CMOS lowpass filter with 30120 MHz tuning range and programmable boost," in *Proc. of ESSCIRC*, Sept. 2000, pp. 164–167.

[60] A. Molnar, R. Magoon, G. Hatcher, J. Zachan, W. Rhee, M. Damgaard, W. Domino, and N. Vakilian, "A single-chip quad-band (850/900/1800/ 1900 MHz) direct-conversion GSM/GPRS RF transceiver with integrated VCOs and fractional-N synthesizer," in *IEEE International Solid-State Circuits Conf. (ISSCC) Dig. Tech. Papers*, vol. 1, Feb. 2002, pp. 232–462.

[61] K. Vavelidis and et al., "A single-chip, 5.15GHz-5.35GHz, 2.4GHz-2.5GHz, 0.18/spl μm CMOS RF transceiver for 802.11a/b/g wireless LAN," in *Proceedings of the 29th European Solid-State Circuits Conference (ESSCIRC)*, Sept. 2003, pp. 221–224.

[62] D. H. Shen, H. Chien-Meen, B. B. Lusignan, and B. A. Wooley, "A 900-MHz RF front-end with integrated discrete-time filtering," *IEEE J. Solid-State Circuits*, vol. 31, no. 12, pp. 1945–1954, Dec. 1996.

[63] D. Jakonis, "Direct RF Sampling Receivers for Wireless Systems in CMOS Technology," Ph.D. dissertation, Linköping University, 2004.

[64] K. Muhammad and et al., "Digital RF processing: Toward low-cost reconfigurable radios," *IEEE Commun. Mag.*, vol. 43, no. 8, p. 105113, 2005.

[65] K. Muhammad and et al, "A discrete-time bluetooth receiver in a 0.13 μm digital CMOS process," in *IEEE International Solid-State Circuits Conference (ISSCC)*, vol. 1, Feb. 2004, pp. 268–269.

[66] S. Karvonen, T. Riley, and J. Kostamovaara, "A low noise quadrature subsampling mixer," in *IEEE International on Circuits and Systems (ISCAS)*, vol. 4, May 2001, pp. 790–793.

[67] K. Muhammad and R. B. Staszewski, "Direct RF sampling mixer with recursive filtering in charge domain," in *IEEE International on Circuits and Systems (ISCAS)*, May 2004, p. 577580.

[68] E. Cijvat, P. Eriksson, T. Nianxiong, and H. Tenhunen, "A 1.8 GHz subsampling CMOS downconversion circuit for integrated radio circuits," in *IEEE International on Circuits and Systems (ISCAS)*, May 1998, pp. 65–68.

[69] H. Pekau and J. W. Haslett, "A 2.4 GHz CMOS sub-sampling mixer with integrated filtering," *IEEE J. Solid-State Circuits*, vol. 40, no. 11, pp. 2159–2166, 2005.

[70] D. Jakonis, K. Folkesson, J. Dabrowski, and C. Svensson, "Downconversion Sampling Mixer for wideband Low-IF Receiver," in *Proc. of MIXDES*, Lodz, Poland, June 2003.

[71] R. Gregorian and G. C. Temes, *Analog MOS Integrated Circuits For Signal Processing*. United Kingdom: John Wiley & Sons, 1986.

[72] J. H. Fischer, "Noise sources and calculation techniques for switched capacitor filters," *IEEE J. Solid-State Circuits*, vol. 17, no. 4, pp. 742 – 752, Aug. 1982.

[73] M. R. Spiegel, J. J. Schiller, and R. A. Srinivasan, *Schaumś Outline of Probability and Statistics*. USA: McGraw-Hill, 1971.

[74] G. Xu and J. Juan, "Accurate sample-and-hold circuit model," *Electronics Letter*, vol. 41, no. 9, Apr. 2005.

[75] V. W. Leung, L. E. Larson, and P. Gudem, "An improved digital-IF transmitter architecture for highly-integrated W-CDMA mobile terminals," in *The 57th IEEE Semiannual Vehicular Technology Conference (VTC)*, vol. 2, Apr. 2003, pp. 1335–1339.

[76] M. Shinagawa, Y. Akazawa, and T. Wakimoto, "Jitter analysis of high-speed sampling systems," *IEEE J. Solid-State Circuits*, vol. 25, no. 1, pp. 220–224, Feb. 1990.

[77] M. L. P. and D. Akos and J. Thor, " comparison of direct RF sampling and down-convert & sampling GNSS receiver architectures,," in *Proc. 16th International Satellite Division of the Institute of Navigation Technology*, 2003, pp. 1335–1339.

[78] S. S. Awad, "Analysis of accumulated timing-jitter in the time domain," *IEEE Trans. Instrum. Meas.*, vol. 47, no. 1, p. 6973, 1998.

[79] H. Kobayashi and et al., "Aperture jitter effects in wideband sampling systems," *Proc. of 16th IEEE Instrumentation and Measurement Technology Conference*, vol. 2, pp. 880–885, 1999.

[80] Y. R. Sun and S. Signell, "Effects of noise and jitter in bandpass sampling," *Journal of Analog Integrated Circuits and Signal Processing Special Issue of Norchip*, vol. 42, p. 8597, Jan. 2005.

[81] S. Lindfors, A. Parssinen, and K. A. I. Halonen, "A 3-V 230-MHz CMOS decimation subsampler," *IEEE Trans. Circuits Syst. II*, vol. 50, no. 3, pp. 105 – 117, Mar. 2003.

[82] S. Lindfors, "CMOS Baseband Integrated Circuit Techniques for Radio Receivers," Ph.D. dissertation, Helsinki University of Technology, 2000.

[83] Q. Gu, *RF System Design of Transceivers for Wireless Communications.* New York, USA: Springer, 2006.

[84] *MS Receiver Sensitivity in UTRA FDD Mode*, TSG-RAN Working Group 4; Nokia Mobile Phones Std. Document TSGW4 #1(99)005, Jan. 1999.

[85] O. K. Jensen and et al, "RF Receiver Requirements for 3G W-CDMA Mobile Equipment," *Microwave Journal*, Feb. 2000.

[86] N. Behjou, B. E. Priyanto, O. K. Jensen, and T. Larsen, "Interference Issues between UMTS & WLAN in a Multi-Standard RF Receiver," in *IST Mobile Summit Proceedings*, Mykonos, Greece, June 2006.

[87] Y. S. Poberezhskiy, "On Dynamic Range of Digital Receivers," in *IEEE Aerospace Conference*, Mar. 2007, pp. 1–17.

[88] Y. S. Poberezhskiy and G. Y. Poberezhskiy, "Influence of novel sampling and reconstruction on the architecture of software defined radios," in *IEEE Aerospace Conference*, Mar. 2005, pp. 1455–1474.

[89] G. Stepfenson, "Digitizing Multiple RF Signals Requires an Optimum Sampling Rate," in *Electronics*, Mar. 1972, pp. 106–110.

[90] R. G. Vaughan, N. L. Scott, and D. R. White, "The theorem of bandpass sampling," *IEEE Trans. Signal Processing*, vol. 39, p. 19731984, Sept. 1991.

[91] S. Haykin, *Communication Systems.* NY, USA: Wiley, 1978.

[92] P. F. Panter, *Modulation Noise and Spectral Analysis.* NY, USA: Mc. Graw Hill, 1965.

[93] K. S. Shanmugam, *Digital and Analogue Communication Systems.* NY, USA: Wiley, 1979.

[94] C. B. Feldman and W. R. Bennett, "Band width and transmission performance," *Bell System Tech. Journal*, vol. 28, p. 490595, 1949.

[95] Cypress semiconductor corporation. [Online]. Available: http://www.cypress.com/

[96] Rambus inc. [Online]. Available: http://www.rambus.com/us/products/xdr_xdr2/xdr_clock_generator.h

[97] Murata manufacturing Co., ltd. [Online]. Available: http://www.murata.com/DFYHA1G95HFHAA

[98] P. M. and O. K. Jensen and T. Amtoft and R. V. Reynisson and J. H. Mikkelsen and S. Laursen and C. R. Iversen and T. E. Kolding and T. Larsen and M. B. Jenner, "RF Requirements for UTRA/FDD Transceivers," in *Conf. Proc. WPMC 01*, vol. 1.

[99] Murata Manufacturing Co., Ltd. [Online]. Available: http://www.murata.com/SAFEB2G14FA0F00

[100] Murata manufacturing co., ltd.

[101] Rohde & Schwarz. SMIQ. [Online]. Available: http://www2.rohde-schwarz.com/product/smiq.html

[102] Rohde & Schwarz. AMIQ. [Online]. Available: http://www2.rohde-schwarz.com/product/AMIQ.html

[103] Rohde & Schwarz. WinIQSim. [Online]. Available: http://www2.rohde-schwarz.com/product/winiqsim.html

[104] C. E. Shannon, "A mathematical theory of communication," *Bell System Tech. Journal*, vol. 27, p. 623656, 1948.

[105] E. T. Whittaker, "On the functions which are represented by the expansions of the interpolation theory," in *Proc. Royal Soc. Edinburgh*, 1915, pp. 181–194.

[106] S. J. Orfanidis, *Optimum signal processing: An introduction*. USA: Collier Macmillan, 1988.